Investigating the role of species differences and subunit isoforms in sensitivity towards drugs that target nematode ligand-gated ion channels

Mark D. Kaji

Institute of Parasitology

McGill University, Montreal

July 27, 2020

A thesis submitted to McGill University in partial fulfillment of the requirements of the degree of Doctor of Philosophy

Abstract

Anthelmintic drugs are important tools for controlling the spread and intensity of parasitic nematode infections. Many classes of these drugs target pentameric ligand-gated ion channels (pLGICs), causing paralysis and inhibition of vital biological processes through perturbation or cessation of neurotransmission. Specificity of pharmacodynamics protect the host from toxicity against anthelmintics, but also acts as a variable in parasite susceptibility and thus warrant further investigation to explain treatment failure and to identify potential novel drug target candidates. In this thesis, I investigated species- and subunit type-related aspects of amino acid sequence variance as they pertain to pharmacodynamics of anthelmintics that target pLGICs. Comparing the structure and function of a cholinergic ionotropic receptor (ACR-16) from two of the major species of hookworms that infect *Homo sapiens*, I found that even closely related orthologs may possess distinct pharmacological profiles which can affect anthelmintic efficacy and I used *in silico* homology modelling to identify putative structural determinants for these differences. I next used *Caenorhabditis elegans* as a model to describe how the anthelmintic ivermectin and the related compound, moxidectin, activate glutamate-gated chloride channels (GluCls). One GluCl subunit, Cel-GLC-2, is not susceptible to these drugs and I identified 2 residues in Cel-GLC-2 that dictate moxidectin activity and distinguish these responses from ivermectin, previously believed to act using the same mechanism. This thesis sheds light on genetic factors of anthelmintic susceptibility, cautioning against extrapolating pharmacological data from one species to another. I provide much needed information on pharmacodynamic differences between the ivermectin and moxidectin and provide a rationale for differences in therapeutic effect.

Resumé

Les anthelminthiques sont des outils de contrôle de la propagation et de l'intensité des infections parasitaires causées par des nématodes. De nombreuses classes de ces médicaments ciblent les canaux ioniques ligand-dépendants pentamères, provoquant la paralysie et l'inhibition des processus biologiques vitaux par perturbation ou arrêt de la neurotransmission. Bien que la spécificité de la pharmacodynamie des anthelminthiques les rende non toxique pour l'hôte, la sensibilité aux antihelminthiques varie selon les parasites. Cela justifie par conséquent une enquête plus approfondie visant à expliquer les échecs thérapeutiques et identifier de nouvelles cibles médicamenteuses. Dans cette thèse, j'ai étudié les aspects de la variance des séquences d'acides aminés liés à l'espèce et au type de sous-unité vue que la pharmacodynamique des anthelminthiques qui ciblent les canaux ioniques ligand-dépendants pentamères en dépend. En comparant la structure et la fonction d'un récepteur ionotrope cholinergique (ACR-16) entre les deux espèces principales d'ankylostomes qui infectent les humains, j'ai trouvé que même les orthologues étroitement apparentés peuvent posséder des profils pharmacologiques distincts ce qui en conséquence peut affecter leurs efficacité anthelminthique. De plus, j'ai utilisé une approche in silico, basé sur la modélisation par homologie, pour identifier les déterminants structurels putatifs de ces différences. J'ai ensuite utilisé Caenorhabditis elegans comme modèle pour décrire comment l'ivermectine anthelminthique et le composé associé, la moxidectine, activent les canaux chlorure glutamate-dépendants (GluCls). Une sous-unité GluCl, Cel-GLC-2, n'est pas sensible à ces médicaments et j'ai identifié 2 résidus dans Cel-GLC-2 qui dictent l'activité de la moxidectine et distinguent ces réponses de celles évoquées par l'ivermectine, que l'on croyait auparavant agir en utilisant le même mécanisme. Cette thèse expose les facteurs génétiques de la sensibilité aux anthelminthiques, mettant en garde contre l'extrapolation des données pharmacologiques d'une espèce à l'autre. Je fournis des informations cruciales sur les différences pharmacodynamiques

entre l'ivermectine et la moxidectine, en proposant également une explication pour les différences d'effet thérapeutique observées pour ces deux molécules.

Acknowledgements

I would like to first deeply thank my supervisors Dr. Tim Geary and Dr. Robin Beech for helping me realize and achieve this thesis. Everything from funding, advice, editing, sharing experiences, and giving me the opportunities to expand my own ideas, I truly appreciate all that I have learned from you, and your continued support and mentorship.

I would like to thank and all the professors at the Institute of Parasitology for your valuable input, openness and academic discussions. Thank you Dr. Salavati, for your advice, and for facilitating all my radioactivity experiments.

Special thanks to my supervisory committee members Dr. Prichard and Dr. Dent, particularly for your support for my radioactivity experiments. Thank you, Dr. Dent for your invaluable advice and discussions of glutamate receptors; the discoveries in the GLC-2 chapter could not have been made without you.

Dr. Thomas Duguet, Dr. Georgia Limniatis and soon to be Dr. Jennifer Noonan, you have invaluable helped me throughout the best and the worst of my PhD and will always be my gold standards for being a scientist and a human being.

I find it impossible to express my gratitude to everyone that has helped me throughout my thesis. Thank you to all my friends and colleagues at the Institute of Parasitology, you helped create some of the most positive experiences of my life and I wish all of you the very best in life.

Thank you to my family for absolutely everything.

Contribution of Authors

Unless otherwise stated, funding for all experiments in this thesis was provided by the Canada Research Chairs (Dr. Tim Geary) or the NSERC (Dr. Tim Geary and Dr. Robin Beech).

The following section states the contribution that this thesis provides for original research and knowledge. All experiments and data presented in this thesis were performed, collected, analyzed and written by Mark Kaji under the supervision of Dr. Tim Geary and Dr. Robin Beech. This includes all cloning, PCR, electrophysiology, *in silico* modelling, and *in silico* docking, All submitted manuscripts and this thesis were edited by Dr. Tim Geary and Dr. Robin Beech.

Chapter 2 and 3 are based on the content of the following manuscript, which represents my own body of work, edited by Dr. Tim Geary and Dr. Robin Beech:

> A functional comparison of ACR-16 receptors from *Necator americanus* and *Ancylostoma ceylanicum*. Kaji, M.D., Geary, T.G., Beech, R.N.

The experimentally validated cDNA sequences of *acr-16* from *Necator americanus* and *Ancylostoma ceylanicum* are both novel contributions to science. These chapters present original electrophysiological functional characterizations and *in silico* analysis of hookworm ligand-gated ion channels and the subsequent bioinformatics-based analysis of their sequence and structure are also novel and contribute to hookworm nematode biology. This is also an original contribution to science because these receptors were not previously characterized and their existence was only predicted. The original idea of these studies included the functional expression of the ACR-16 receptors from *Ancylostoma ceylanicum* and *Necator americanus.* The original idea leading to the discovery of this research was that drug targets from hookworm species would possess different pharmacological profiles and that these profiles would contribute to differential drug sensitivity.

Chapter 4 is based on the content of the following manuscript, which represents my own body of work, edited by Dr. Tim Geary and Dr. Robin Beech:

> Structural mechanism underlying the differential pharmacology of ivermectin and moxidectin on the *C. elegans* glutamate-gated chloride channel GLC-2.

In this chapter I describe original findings that the drug moxidectin acts as an antagonist of a previously characterized glutamate-gated chloride channel. I was the first to use site-directed mutagenesis to identify and characterize two residues involved in the mechanism of antagonism and elucidated their role in determining whether moxidectin and related drugs act as agonists or antagonists.

Figures presented from these manuscripts have been taken with permission from the authors.

All other results presented in this thesis should be considered original contributions to the field of research and have not yet been submitted for publication.

• The pTD2 plasmid used to express nAChRs was designed by Dr. Thomas Duguet at the Institute of Parasitology (Duguet et al., 2016) and was derived from the original pTB207 plasmid gifted to the Dr. Beech lab from Dr. Thomas Boulin (Boulin et al., 2008).

• The Hco-Glc-5 receptor in the pT7TS plasmid was a gift from Dr. Sean Forrester (Forrester et al., 2003).

•The SmGluCl2.1 receptor was cloned by Dr. Vanessa Dufour at the Institute of Parasitology (Dufour et al., 2013).

• An original *C. elegans glc-2* cRNA was a gift from Dr. Joseph Dent, but all GLC-2 data presented in this thesis was derived from *C. elegans* cDNA obtained by Mark Kaji.

• Tritiated ivermectin was synthesized by Moravek, Inc. from a grant written by Dr. Tim Geary and Dr. Roger Prichard designed for Mark Kaji to perform under the radioactivity license of Dr. Reza Salavati

•Adult *A. ceylanicum* cDNA was generously provided by Dr. John Hawdon (George Washington University School of Medicine & Health Sciences, Washington, DC). Adult *A. ceylanicum* and *N. americanus* were provided by the Dr. Raffi Aroian lab (University of Massachusetts Medical School, Worchester, MA).

•The SP1735 *dyf-7* mutant strain of *C. elegans* was provided by Dr. Joseph Dent

• The IVR10 and MOX4R strains of *C. elegans* were provided by Dr. Prichard from the Lespine lab (Ménez et al., 2016).

List of abbreviations

• ^{3}H = tritium

• ^{3}H-IVM = [22,23 -tritiated] ivermectin

• 5-HT = serotonin

• 5-HT_3 = ionotropic serotonin receptor

• AAD = amino-acetonitrile derivatives

• ACC- 1-4 = acetylcholine-gated chloride channel

• Ace-ACR-16 = *Ancylostoma ceylanicum* ACR-16 receptor

• ACh = acetylcholine

•AChBP = acetylcholine binding protein

• ACR-16 = acetylcholine receptor subunit alpha-type acr-16

•BAPTA-AM=1,2-bis(2-aminophenoxy)ethane-N,N,N′,N′-tetraacetic acid tetrakis(acetoxymethyl ester)

• BZD = benzimidazole

• cDNA = complementary deoxyribonucleic acid

• Cel-GLC-2 = *Caenorhabditis elegans* GLC-2 receptor

• CLM = cutaneous larva migrans

• cRNA = copy ribonucleic acid

• DALY = disability-adjusted life year

• DEG-3 = DEGeneration of certain neurons subfamily 3

• EC_{50} = half maximal effect concentration

• epg = eggs per gram

• ECD = extracellular domain

• ELIC = *Erwinia* ligand-gated ion channel

• EXP-1 = GABA receptor Expulsion defective protein 3

• GABA = γ-aminobutyric acid

• GLC-2 = glutamate-gated chloride channel subunit β

• GLIC = *Gloeobacter* ligand-gated ion channel

• GI = gastrointestinal

• GluCl / GLC = glutamate-gated chloride channel

• GlyR = ionotropic glycine receptor

• GPCR = G-protein coupled receptor

• IC_{50} = half maximal inhibitory concentration

• IVM = ivermectin

• L1-L4 = larval stages 1-4

• LD_{50} = half maximal lethal dose

• LSC = liquid scintillation cocktail

• mAChR = metabotropic muscarinic acetylcholine receptor

• MDA = mass drug administration

• mdr1 = the multiple drug resistance gene 1

• ML = macrocyclic lactone

• MOX = moxidectin

• nAChR = ionotropic nicotinic acetylcholine receptor

• Nam-ACR-16 = *Necator americanus* ACR-16 receptor

• ND96 = normal oocyte saline buffer

• PCR = polymerase chain reaction

• pLGIC = pentameric ligand-gated ion channel

• RIC = resistance to inhibitors of cholinesterase

• SLO-1 = calcium-activated potassium channel slo-1

• STH = soil-transmitted helminths

• TEVC = two-electrode voltage clamp

• TM = transmembrane domain

• WHO = World Health Organization

TABLE OF CONTENTS

Chapter 1: General introduction & Literature review

GENERAL INTRODUCTION

Pentameric ligand-gated ion channels (pLGICs) are the operational units of fast ionotropic synaptic signal transduction. Because of their important physiological roles, many drugs have been developed that target these proteins in humans, animals, and parasitic nematodes. However, there is limited information of how these drugs interact with their target proteins, and there are many factors that allow targeting of some species but not others. Two important classes of pLGIC that are targets of anthelmintics are the glutamate-gated chloride channels (GluCls) targeted by the macrocyclic lactones (MLs) ivermectin (IVM) and moxidectin (MOX), and the ionotropic acetylcholine receptor, composed of the acetylcholine receptor subunit alpha-type acr-16 (ACR-16) targeted by oxantel, and to a lesser extent, pyrantel. These proteins are generalized as being homogenous among different parasites, but there is reason to suspect that species differences contribute to treatment failure or lower efficacy. For instance, IVM is not used for human hookworm infections because *Necator americanus* is 50-fold less susceptible than *Ancylostoma* spp. (Behnke et al., 1993; Richards et al., 1995). These hookworms are targeted by pyrantel, but not the structurally similar compound, oxantel, and this sensitivity profile is reversed for whipworms (Keiser et al., 2013). The goal of this thesis was to investigate the role of amino acid differences associated with species differences and subunit type that determine susceptibility to anthelmintics. I hypothesize that minor differences in amino acid composition of orthologous or related pLGICs are responsible for differences in anthelmintic efficacy, and that this can be tested using electrophysiology and *in silico* modeling to compare pharmacologies of pLGICs.

To achieve these goals, in Chapter 2 I compared the function of homomeric ACR-16 receptors from *N. americanus* and *A. ceylanicum*, two closely related hookworm species that infect humans. This receptor is formed from the assembly of 5 identical ACR-16 subunits, permitting the direct comparison of function of a receptor between species in the absence of multiple subunit interfaces. To investigate potential structural determinants of the functional differences in *N. americanus* and *A. ceylanicum* ACR-16 receptors, I next used *in silico* homology modeling and ligand docking of agonists into the predicted ligand-binding domain.

IVM and other MLs pseudo-irreversibly activate GluCls, but one GluCl subunit, the glutamate-gated chloride channel subunit β (GLC-2), forms channels that are insensitive to these drugs. Furthermore, there are 2 structurally distinct classes of ML, avermectins (including IVM) and milbemycins (including MOX) that are believed to act on the same receptors, but the pharmacological functions of MOX on GLC-2 have not been reported. The objective of Chapter 4 was to express GLC-2 from the free-living nematode *Caenorhabditis elegans* as a model of hookworm receptors to measure the ability of MOX to interact with this GLC-2 and to identify residues of *C. elegans* GLC-2 that are responsible for IVM-insensitivity and use site-directed mutagenesis to probe their contribution to the ML response.

C. elegans is an important organism for the study parasitic nematode biology and anthelmintic targets, but as described in Chapter 2, even small differences in the sequence of receptors between species can have large effects, with important implications for the study of nematode physiology and pharmacology. In the following literature review, I begin with *C. elegans* as a model organism and highlight important attributes useful for the study of parasite biology.

1.0 LITERATURE REVIEW

1.1 *Caenorhabditis elegans*

Caenorhabditis elegans, named for the elegance of its movements, is a free-living, soil-dwelling roundworm in the phylum Nematoda that is ubiquitously used as a model organism. Originating from efforts by Dr. Sydney Brenner in the 1960s to "tame a small metazoan organism to study development directly", *C. elegans* has since become a vital tool for drug discovery and is used as a eukaryotic system for the study of nearly every fundamental process in biology, including neurotransmission (Brenner, 1974; Strange, 2006). Several important characteristics make *C. elegans* well-suited for this role, including the availability of a large body of knowledge and technical platforms, ease of genomic-level manipulation, a completely mapped nervous system and a rapid and simple life-cycle. These characteristics will be elaborated upon, with specific examples, in the following sections to rationalize why *C. elegans* was used as a model in this thesis.

1.2 *C. elegans* life-cycle

These entirely free-living worms complete their full life-cycle in two weeks; maturation from eggs to larval stages (L1-L4) to adults occurs rapidly within 3 days, after which an adult hermaphrodite can self-fertilize with a fecundity of > 300 eggs in ideal conditions (Aprison and Ruvinsky, 2014). *C. elegans* are androdioecious, and infrequently produce male offspring, which combined with a rapid life-cycle, allows researchers the ability to grow large numbers of progeny in a short period of time, while permitting control over self- or cross-fertilization for genetics studies.

C. elegans is an important model to study parasitic nematode biology, but many genetic differences set parasitic nematodes apart from each other and their free-living relatives. For instance, like *C. elegans,* the sheep parasite *Haemonchus contortus* also possess 5 pairs of autosomal chromosomes, but instead of self-fertilizing hermaphrodites, has male and female individuals that are obligate sexual organisms (Redman et al., 2008). Understanding species differences is important for understanding the usefulness and limitation of *C. elegans* as a model for parasitic nematodes. This will be exemplified in Chapters 2 and 3 in which I characterize orthologous of ion channels from hookworm nematodes and compare them with that of *C. elegans*.

1.3 *C. elegans* is easily grown and manipulated in a laboratory setting

C. elegans can be grown inexpensively at room temperature (ideally 20 °C) in liquid or solid media, requiring only *Escherichia coli* as a food source, and can be grown to high density in a laboratory setting (Byerly et al., 1976). Adult hermaphrodites measure roughly 1-2 mm in length and are readily distinguished from the smaller males and larval stages by simple stereomicroscopy. These features allow large numbers to be grown on a single plate, while still facilitating facile methods for observing feeding, behaviour, and movement phenotypes, of particular relevance for high-throughput pharmacological screening assays. Furthermore*, C. elegans* is transparent, which allows the use of proteins modified with green fluorescent proteins as probes to study cellular processes *in situ*, as well as visual discrimination of internal structures. For instance, researchers can express fluorescently-labelled ion channels cloned from parasitic nematodes (Glendinning et al., 2011), or even human proteins (Link, 1995) in wild-type or orthologous knockout strains of *C. elegans* by microinjecting plasmid DNA directly into the visible gonad and assaying for functional expression in progeny. This technique is made more powerful because the genome of *C. elegans*

encodes proteins that often share high sequence similarity with proteins from parasitic nematodes (Bird and Opperman, 1998; Gilleard, 2004; and to be further discussed in this thesis), and contains many genes with orthologs in humans, as indicated by the database Ortholist 2: http://ortholist.shaye-lab.org/ (Kim et al., 2018; Shaye and Greenwald, 2011). These techniques are relevant to this thesis because I study the function of ion channels from nematodes, and knowledge of their tissue expression provides important information on their physiological roles. As will be discussed later, like their function, the tissue expression patterns of the ion channels studied in this thesis vary in a species-dependent manner.

1.4 *C. elegans*: large body of resources, tools and knowledge

As previously noted, *C. elegans* is often used as a model, including in this thesis, because a large body of resources, tools and knowledge is available for studying its biology. *C. elegans* was the first multicellular organism to have its genome fully sequenced, occurring over 20 years ago (The *C. elegans* Sequencing Consortium, 1998). Since this initial study, multiple whole organism sequencing efforts, using more modern and sophisticated technologies, have independently improved, validated and updated this genome to exceptionally high quality (Hillier et al., 2008; Yoshimura et al., 2019). Collectively, these studies have determined that *C. elegans* contains 1 sex chromosome (diploid in hermaphrodites and haploid in males) and 5 pairs of holocentric (lacking a predefined site for the protection of cohesion in meiosis I) autosomal chromosomes containing ~100 million base pairs encoding ~21,000 genes (Hillier et al., 2008; The *C. elegans* Sequencing Consortium, 1998; Yoshimura et al., 2019). Availability of these genomics datasets, in combination with the readily available vast libraries of mutant strains of *C. elegans* (Thompson et al., 2013; https://cgc.umn.edu/), has created an extremely manipulatable system for the study of

an entire organism. Since the original sequencing efforts in the 1990s, very large amounts of "omics" data have been published and, as illustrated by the Ortholist 2 database, scientists have used bioinformatics to build easily accessible high-resolution databases and tools for the study of *C. elegans*. These databases include transcriptomics (Hillier et al., 2009; Reboul et al., 2001; Roach et al., 2020), a European nucleotide archive (https://www.ebi.ac.uk/ena), RNAi libraries (Ashrafi et al., 2003; Kamath et al., 2003; Kamath and Ahringer, 2003), proteomics (Costanzo et al., 2000; Waterston et al., 1992; https://www.uniprot.org/proteomes/UP000001940) and protein-protein interactions (Simonis et al., 2009), numerous commercially available antibody libraries (https://www.novusbio.com/celegansantibodies.html), gene ontology knowledgebase for the information of function of genes (Ashburner et al., 2000; http://geneontology.org/), lipidomics (Witting et al., 2017; Witting and Schmitt-Kopplin, 2016; Yang and Han, 2016), metabolomics (Copes et al., 2015; Von Reuss et al., 2012), phenomics (McDiarmid et al., 2018) and behavioural phenotypes (http://www.wormatlas.org/). In this thesis I use the knowledge resources described in this section to mine the genome of *C. elegans* and other nematode species for the cloning and analysis of pLGICs

1.5 *C. elegans* nervous system

Dr. Brenner originally proposed *C. elegans* as a model organism to study the biological development of a nervous system (Brenner, 1974). In realization of this goal, *C. elegans* was the first and still the only organism to have a complete map of the connectome of the nervous system for both sexes generated (Cook et al., 2019). The adult hermaphrodite contains 302 neurons, whereas males, which comprise a small portion of a given population, have 383 (Hodgkin and Doniach, 1997; Ward and Carrel, 1979). In hermaphrodites, these neurons synapse at 4887

locations, of which 2000 represent chemical neuromuscular junctions (NMJ), and 1447 are gap junctions. In addition to possessing more neurons, males also have a greater number of synapses (5315), with 1755 gap junctions (Cook et al., 2019; White et al., 1986). A major reason for the greater number of neurons and synapses in males is the presence of a highly innervated copulatory apparatus in the posterior tail region (Garcia et al., 2001; Liu and Sternberg, 1995).

Because the architecture of its nervous system is known, *C. elegans* is used as a model to study neurodegenerative disorders of humans, such as Alzheimer's disease (Link et al., 2003) and Parkinson's disease (Braungart et al., 2004), and is used to screen for and characterize drugs that target the nervous system of parasitic nematodes. This is especially relevant among nematodes possessing orthologous protein drug targets that share high sequence identity with *C. elegans*, such as hookworms and the important trichostrongyloid parasite of ruminants, *H. contortus.*

1.6 Parasitic nematodes

Parasites are eukaryotic organisms that have at least one obligate life stage in which they must live inside (endo) or on (ecto) a living host organism from which they obtain food energy and metabolites (Actor, 2011). This definition was originally meant to distinguish parasitic animals from predacious organisms and bacteria, and as such distinguishes the noun "parasite" from the verb "parasitic", which can describe the behaviour of parasites and infective bacteria (Swellengrebel, 1940). As this thesis is a study of parasitic nematode ion channels and how they compare to those of *C. elegans*, I begin with a broad description of parasites as a group to give the necessary context for these comparisons. Parasites are broadly classified as protozoa (e.g., trypanosomes, *Plasmodium* spp., etc.), ectoparasites (ticks, lice, flies, mites), or helminths. Helminths, or parasitic worms, include a wide range of species, especially amongst the phyla

Platyhelminthes and Nematoda, that parasitize plants (Baldwin et al., 2004), humans (Chandy et al., 2011; Norhayati et al., 2003; Whittington, 1997) and animals (Hrckova and Velebny, 2013). Nematodes are further categorized into 5 major clades (I-V) based on evolutionary relatedness (Figure 1.1) (Blaxter, 2011; Meldal et al., 2007), of which clade V contains *C. elegans* and some of the most socio-economically important parasitic nematodes including hookworms, which are a focus of study in this thesis (Jourdan et al., 2018).

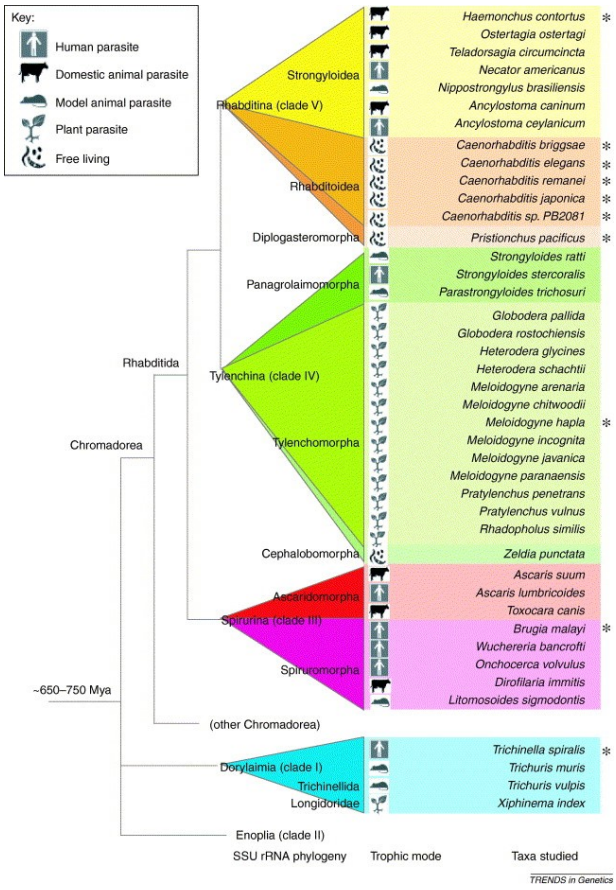

Figure 1.1 Visualization of the clades of nematodes showing evolutionary relatedness *relates to genome projects completed or underway as of 2005. *Adapted with permission from Elsevier [Trends in Genetics]* (Mitreva et al., 2005)*, copyright (2020)*.

Hookworms also belong to an important mixed-clade group of parasites called soil-transmitted helminths (STH), which have a direct life-cycle not involving an intermediate host, and infect an estimated 25% of all humans and are associated with significant morbidity worldwide (Jourdan et al., 2018). This group of intestinal-dwelling parasites is comprised of the clade III *Ascaris lumbricoides* and *A. suum*, clade I whipworm (*T. trichiura*), Clade IV *Strongyloides* spp., and clade V hookworms (*N. americanus*, *Ancylostoma duodenale*, and to a lesser extent, *Ancylostoma ceylanicum*). Of these, hookworms are considered the most pathologically significant.

1.7 Hookworms

Hookworms are blood-feeding intestinal parasitic nematodes that are found throughout the world, primarily proximal to the equator. Hookworm species can infect a vast array of fauna, from Arctic seals, North American bears, dingoes, to African and Asian elephants (Seguel and Gottdenker, 2017)**.** Seguel and Gottdenker (2017) identified at least 68 different species of hookworms, which infect > 111 different animals. In human and veterinary medicine, parasites in the genus *Ancylostoma* are of most importance for causing disease and morbidity, estimated to have a worldwide prevalence of roughly 230 million human infections (Dull et al., 2019).

Three main species of hookworms of veterinary importance are capable of zoonosis in humans, namely the dog hookworm *A. caninum,* the cat hookworm *A. braziliense*, and *A. ceylanicum*, which infects dogs, cats, hamsters and humans; the European dog hookworm *Uncinaria stenocephala* and the cattle hookworm *Bunostomum phlebotomum* are more rarely seen in humans (Blackwell and Vega-Lopez, 2001; Loukas and Prociv, 2001; Prociv, 1998; Prociv and Croese, 1996; Traub, 2013; Traub et al., 2008). Of these, only *A. ceylanicum* is considered capable of achieving a patent infection in humans in which eggs are produced, but a recent study suggests

that *A. caninum* may also have this ability (Furtado et al., 2020). Larvae of the other species can penetrate the skin of humans but are incapable of invading the basal membrane and transiently cause as a syndrome known as cutaneous larva migrans (CLM), a local inflammatory response to migrating larvae in the epidermis, which may also be caused by human hookworms (Feldmeier and Schuster, 2012; Gillespie, 2004). This clinically presents as wavy line lesions under the skin (representing the path of migrating larvae) that are red, extremely itchy, uncomfortable, and can persist for months if left untreated (Blackwell and Vega-Lopez, 2001; Feldmeier and Schuster, 2012). Even a single larva can cause CLM (Sandground, 1939), and in large numbers these parasites can cause significant pathology (Caumes et al., 1995; Hochedez and Caumes, 2007). Presentation of CLM is primarily localized to the lower extremities resulting from barefoot exposure to unsanitary soil or sand harbouring infective larvae shed in the feces of infected animals, and for this reason is commonly called ground itch. As such, its incidence is most highly associated with impoverished regions of developing countries (Heukelbach et al., 2003; McCrindle et al., 1996; Reichert et al., 2018), and tourism in tropical regions where these species of hookworm are endemic (Bouchaud et al., 2000; Heukelbach and Feldmeier, 2008; Sow et al., 2017). In rare cases, *A. caninum* may infiltrate the gastrointestinal (GI) tract of humans and cause eosinophilic enteritis (Croese et al., 1994).

Only 3 species of hookworm fulfill their life-cycle in humans: *A. duodenale*, *N. americanus*, and the zoonotic *A. ceylanicum*. Eggs are shed in the feces excreted from an infected host and hatch in a process that takes 1-2 days (Bowman et al., 2010). Egg hatching and survival of the emerging L1 larvae optimally occurs at a temperature range of 22-28 °C and with relative humidity > 80% (Tandon et al., 1998). These rhabditiform larvae are non-parasitic and feed on microbes in the soil for up to 2 weeks until they moult to the infective L3 stage (Hawdon and

Hotez, 1996). L3 are highly mobile and actively search for a host in the soil, surviving up to 4 weeks in ideal conditions. Infective larvae enter their host percutaneously by puncturing the skin, then secrete proteases and hyaluronidases, allowing them to migrate into blood vessels through which they travel to the lungs (Hotez et al., 1994, 1990). From the lungs, they migrate into the upper airway to be swallowed, passing into the small intestine as their final destination where they molt to L4 and then again to sexually dimorphic adult life stages. Here, *N. americanus* are capable of living up to 10 years inside a host, whereas *A. duodenale* can achieve one-third that lifespan (Hoagland and Schad, 1978). L3 larvae of some hookworm species, such as *A. duodenale*, are also capable of full development after entering the host by being swallowed, while others, such as *N. americanus*, cannot (Prociv, 1998). Adults orally latch onto mucosa of the intestinal villi where they reproduce, lay eggs, and feed on blood and mucosa (Bowman et al., 2010). Another alternative means of transmission is through the mother-child transplacental or transmammary route during newborn breastfeeding in humans and canines (Budhathoki et al., 2008; Prociv, 1998).

Globally, human hookworm infections are found mostly in Asia, South America, and sub-Saharan Africa (Figure 1.2).

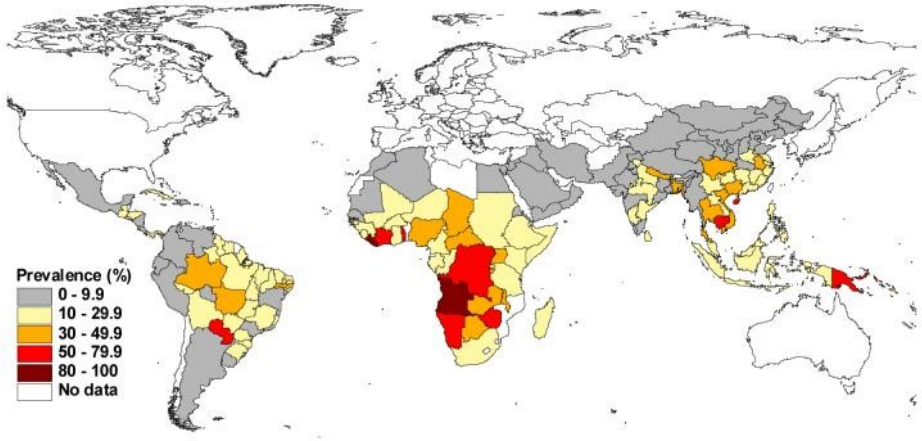

Figure 1.2 Global distribution and prevalence of human hookworm. *With permission from ELSEVIER [Advances in Parasitology]* (Brooker et al., 2004)*, copyright (2020).*

Hookworm infections are most commonly heterogenous, with the predominant species being highly region-specific (Adenusi and Ogunyomi, 2003; Labiano-Abello et al., 1999); recent studies indicate that *A. ceylanicum* constitutes a significant portion of the global hookworm burden, and is more common than previously considered (Inpankaew et al., 2014; O'Connell et al., 2018; Traub, 2013).

N. americanus is the most widespread of these species, concentrated primarily in Southern China, India, Southeast Asia, sub-Saharan Africa and South America (Brooker et al., 2004). In comparison, *A. duodenale* is more geographically restricted than *N. americanus*, but this species is more resilient because it can be found in colder and drier climates. Adults may undergo hypobiosis inside their host, becoming dormant during unfavorable seasons, and their eggs can hatch at temperatures roughly 10 °C lower than those required by *N. americanus* (25-35°C) and are more resistant to desiccation (Hoagland and Schad, 1978).

One challenge in identifying the composition of hookworm infections from field studies is that the eggs from different species are indistinguishable and positive identification requires the use of polymerase chain reaction (PCR) or hatching eggs and cultivating infective larvae (Verweij et al., 2007). In contrast to the eggs, larvae exhibit very species-specific behaviour (reviewed by Haas et al., 2005) and adults are easily distinguished, as *A. duodenale* has 4 visible teeth used for latching onto the intestine, whereas *A. ceylanicum* only has 2, and *N. americanus* possesses 2 cutting plates; adult *Ancylostoma* spp. and *N. americanus* also differ in the location of the female genital opening (Mehlhorn, 2016).

Positive species identification is important because susceptibility to drug targeting is highly species-dependent and the intensity of an infection is directly related to egg count in feces. The World Health Organization (WHO) has defined low intensity infection as < 2,000 eggs per gram

(epg) of feces, moderate levels as 2,000-4,000 epg and heavy intensity as > 4,000 epg (Montresor et al., 2002). This relates to species identification because adult female *A. duodenale* may produce > 30,000 eggs per day, whereas *N. americanus* releases 9,000 eggs per day (Stoll, 1923; Soper, 1927). Additionally, not all hookworms cause equal degrees of blood loss; *N. americanus* are the least voracious human blood feeders, while *A. ceylanicum*, whose contribution to human blood loss have been previously discounted due to perceived rarity of infection, is potentially as severe in this regard as *A. duodenale* (Albonico et al., 1998; Traub, 2013).

In moderate to heavy infections, hookworms cause severe and chronic iron-deficiency related anemia, protein deficiency and malnutrition directly proportional to the number of worms in the host. These symptoms are a result of the feeding activity of adult worms, which secrete protease inhibitors that inhibit host coagulation factors, causing additional bleeding (Diemert et al., 2008; Harrison et al., 2002; Lee and Vlasuk, 2003). These effects become magnified because worms often change the site of adherence and feeding, which increases the surface area of damaged, bleeding, and inflamed intestine (Wei et al., 2017). Persistent inflammation and damage to intestinal lining results in malabsorption of nutrients (Kilby et al., 2019), and wreaks havoc for impoverished regions of the world where hookworm is endemic and anemia has been estimated to affect half of all school-aged children (Stoltzfus et al., 1997). Infection in children can have serious long-term health issues stemming from stunted growth and development. These children can have lower body weight, muscle mass, physical activity, and reduced mental capacity (Adams et al., 1994; Drake et al., 2000; Sakti et al., 1999). It has been estimated that 44 million pregnant women are infected with hookworms; not only does this speak of the relative risk of infection for their children, but pregnant women are among the highest risk group for hookworm-associated anemia due to lower stores of iron (Bundy et al., 1995; Crompton, 2000; Montresor et al., 2002). As

hookworm infection is rarely directly fatal (Lee et al., 2011), the true impact of the disease is often expressed in term of disability-adjusted life year (DALYs) lost (Anand and Hanson, 1997), which is an estimate of the sum of the total and productive number of years of life lost due to impaired health. From these metrics, researchers estimate that hookworms cause a loss of over 4 million DALYs and are responsible for tens to hundreds of billions of dollars in lost productivity (Bartsch et al., 2016). By comparison, all filariases combined impose a reported burden of 2.78 to 5.09 million DALYs (Ton et al., 2015). One challenge in determining the impact of hookworm infections is that most infected individuals are also host to multiple other parasites and pathogens, especially among low socio-economic groups in developing countries (Akinbo et al., 2011; Ndyomugyenyi et al., 2008). As such, monitoring programs are of utmost importance to determine effective drug treatment plans (Giardina et al., 2019) as recommended by the WHO strategic plan for STH (World Health Organization, 2012).

Programs designed to control hookworm prevalence are two-pronged, targeting the parasite inside the host using mass drug administration (MDA) of anthelmintics, and in the environment though improvement of sanitation and public awareness. This is exemplified by the Rockefeller Sanitary Commission for the Eradication of Hookworm Disease campaigns, which effectively eradicated hookworms in the Southern USA in the early 1900s by treating 400,000 individuals, heightening awareness, and improving sanitation (Bleakley, 2007). This region is no longer endemic for hookworms, although some indications suggest a potential re-emergence (Sanders and Goraleski, 2017). A factor limiting the effectiveness of MDA is that different species of hookworm are differentially sensitive to anthelmintics. The next section discusses the mechanism of action of different groups of anthelmintics and their effectiveness in the treatment of hookworm disease, vital for understanding the rationale for studying the drugs and drug targets

presented in this thesis. There are a limited number of chemotherapeutics for treating parasitic nematode infections, and describing drug resistance and treatment failure in hookworms impresses upon the reader the importance of understanding the reasons for the mixed success and failure of drugs that share a common mechanism of action, or a common drug target.

1.8 Anthelmintic drugs

The primary means by which hookworm infection is controlled is through the administration of anthelmintics, drugs that kill or remove worms from a host. To this end, in 2001 the WHO enacted resolution 54.19 with the goal of reducing prevalence by treating 75% of all school-aged children in regions at risk for hookworm through MDA of albendazole or mebendazole (Montresor et al., 2002; World Health Organization, 2012); this goal was pushed back to 2020, and again more recently to 2030 with the inclusion of IVM for treatment of *Strongyloides stercoralis* (World Health Organization, 2020).

One rather large hurdle for the laboratory study of human hookworms is the ethical and scalability considerations for infecting human volunteers in order to passage the worms and test novel drug treatments (Carroll and Grove, 1986; Cline et al., 1984; Maxwell et al., 1987). In lieu of mass human testing, scientists use the golden hamster, *Mesocricetus auratus*, as a model host for *N. americanus* and *A. ceylanicum* to assess morbidity, drug activity, and treatment plans for pre-clinical trials (Garside and Behnke, 1989; Rajasekariah et al., 1985).

Two classes of drugs approved by the WHO for the treatment of hookworms are benzimidazoles (BZDs; albendazole and mebendazole) and nicotinic acetylcholine receptor (nAChR) agonists (pyrantel and levamisole), but only the BZDs are used for MDA (Keiser and

Utzinger, 2008). This is because few drugs have efficacy against all species of human hookworm and other STH species. IVM and other MLs can clear *Ancylostoma* spp., but studies in hamsters show that *N. americanus* is 300 times less sensitive (Behnke et al., 1993) and, *in vitro*, 40-50 times less sensitive to paralysis than *Ancylostoma* spp. (Richards et al., 1995). Given the limited options in the chemotherapeutic arsenal against hookworms, a better understanding of the mechanisms of action of available anthelmintics and the limitations of their use is essential to meet the WHO 2030 goals and beyond. As such, in the next sections I list the classes of anthelmintics available, their mechanisms of action and limitations of use.

1.9 Drugs: Benzimidazoles (BZDs)

As a drug class BZDs are characterized by the presence of a dicyclic moiety formed from the fusion of an imidazole and a benzine ring (McKellar and Scott, 1990) and are currently the front-line treatment for STH infections, including hookworms. The prototype BZD, thiabendazole, was originally developed as an antifungal treatment before its adoption as an anthelmintic in human and veterinary medicine; since then, subsequent BZD derivatives have been used extensively for a wide range of ailments, including as proton pump inhibitors for gastroesophageal reflux disease, antiviral, anticancer, as well as antiparasitic agents against protozoa and helminths (Yadav and Ganguly, 2015).

By binding to β-tubulin, BZDs cause a local unfolding of the tubulin structure and inhibit polymerization, which disrupts numerous essential microtubule-associated cellular functions, including development of the mitotic spindle for cellular replication and glucose absorption (Borgers and De Nollin, 1975; Lacey, 1988; Van den Bossche and De Nollin, 1973; Wood, 1982). Loss of microtubule networks also results in loss of motility, causing paralysis and expulsion from

hosts (Sutherland and Lee, 1990). BZDs bind to parasite β-tubulin with greater affinity than to mammalian tubulin, contributing to a large therapeutic window for safety (Lacey, 1988; McKellar and Scott, 1990). As a corollary, overdose toxicity usually presents in rapidly dividing cells, including intestinal epithelia and hair follicles, causing stomach issues and hair loss (McKellar and Scott, 1990). BZDs are not generally administered to children under two years of age and some are also associated with teratogenicity (Bradley and Horton, 2001).

The first BZD anthelmintic for humans was thiabendazole, produced in the early 1960s and used for the treatment of strongyloidiasis, CLM, and trichinosis, but it had limited efficacy against adult hookworms (Cuckler, 1961; Gourgiotou et al., 2001; Harland et al., 1977; Huang and Brown, 1963; Ishizaki et al., 1963). Thiabendazole has since been discontinued due to a relatively high frequency of side effects (Grove, 1982; Huang and Brown, 1963) and potential teratogenicity (Ogata et al., 1984). The primary BZD anthelmintics used today are carbamate derivatives, notably albendazole, mebendazole and fenbendazole, the latter of which is approved for treatment of *A. caninum* and *U. stenocephala* infections in dogs (Wiebe et al., 2015).

In humans, 400 mg albendazole or 500 mg mebendazole are the front-line therapy for acute infections as well as MDA programs against STH, with albendazole generally showing better efficacy (Steinmann et al., 2011). In MDA programs, a single dose of either drug annually or biannually is provided in regions that meet endemicity thresholds for school children up to 12 years of age. Unfortunately, single dose treatment may be associated with low clearance of worms, including hookworms (for reviews see Clarke et al., 2019; Keiser and Utzinger, 2008) and the CDC recommendation for acute infection is a 3-day course of treatment with mebendazole; albendazole is not FDA approved for treating hookworms in humans.

Resistance to BZDs in veterinary parasites appeared shortly after their introduction (Conway, 1964; Drudge et al., 1964) and has since become widespread in livestock (reviewed by Kaplan, 2004). Definitive BZD resistance has not been reported in humans, despite long term and intensive use, although few studies have been designed specifically to detect it. Resistance to BZDs is a continuing and growing concern across the field of parasitology, with reports of resistance in veterinary medicine rising, and is a looming threat over human control programs, where treatment failure is becoming increasingly common (Albonico et al., 2004; De Clercq et al., 1997; Flohr et al., 2007; Speich et al., 2016). Recent work has also identified an alarming increase in treatment failure of hookworms of dogs in the United States and alternative pharmacological control measures need to be explored (Castro et al., 2019).

1.10 Drugs: Anthelmintics that target pentameric ligand-gated ion channels (pLGICs)

Several drug families target ion channels in the nematode neuromuscular system (ion channels to be discussed in section 1.11). Most of these drugs can be divided into those that target excitatory signalling and those which target inhibitory signalling pathways. Unfortunately, these drugs generally possess varying capabilities to target different species of parasites or are limited in use due to acquired drug resistance. The largest group of drugs available for treatment of hookworm infections are those that target receptors for the neurotransmitter acetylcholine, which induces muscle contraction in nematodes and other organisms. Early electrophysiological studies identified 3 distinct populations of nAChRs in the nematode body wall muscle, which are distinguishable by drug sensitivity (Robertson et al., 2002) and are composed of different combinations of nAChR subunits (Holden-Dye et al., 2013). One subclass was sensitive to nicotine (in this thesis called the N-type or N-nAChR), but others are insensitive to nicotine and

preferentially activated by levamisole (L-nAChR) (Boulin et al., 2008), morantel (M-nAChR) (Courtot et al., 2015) or bephenium (B-nAChR) (Qian et al., 2006).

1.10.1 Imidazothiazoles

Levamisole is an agonist of a subset of excitatory acetylcholine-gated ion channels (L-nAChRs) found in the somatic muscle of nematodes, and causes contractile paralysis and elimination from hosts (Atchison et al., 1992). First introduced in the early 1960s by Janssen Pharmaceutica, levamisole showed broad spectrum anthelmintic activity, especially against ascariasis (Lionel et al., 1969; Miller, 1980) and microfilaria of *Wuchereria bancrofti* and *Brugia malayi* (McMahon, 1979; Zaman and Lal, 1973), and completely cleared hookworm infections of humans (Farid et al., 1977; Kilpatrick et al., 1981; Miller, 1980; Page, 2008). Levamisole has since been withdrawn from human use due to significant adverse effects including agranulocytosis and vasculitis (Caldwell et al., 2012; Mouzakis et al., 2011). Despite adverse effects and the presence of drug resistance (Giménez-Pardo et al., 2003), it is still used in veterinary medicine for treating hookworms in cats and dogs (Caldwell et al., 2012; Page, 2008) (Caldwell et al., 2012; Page, 2008), and increasingly, for cattle infected with macrocyclic lactone resistant *Cooperia oncophora* (Leathwick et al., 2016).

1.10.2 Tetrahydropyrimidines: pyrantel, oxantel, morantel

Tetrahydropyrimidines are an old class of broad-spectrum anthelmintics discovered in the 1950s at Pfizer as cyclic amidines derived from lead compounds identified in a large screening assay in a mouse model of multiple helminth infections (McFarland, 1982). Tetrahydropyrimidines activate nematode neuromuscular acetylcholine receptors with 100-fold greater potency than acetylcholine,

causing contractile paralysis (Harrow and Gration, 1985; Martin et al., 1996). This mechanism of action is very similar to that of levamisole, and indeed these compounds share the same general binding site; however, tetrahydropyrimidines interact with different residues of the binding pocket and activate different subtypes of nematode nAChRs (Rayes et al., 2004; Martin et al., 2004; Bartos et al., 2006, 2009).

A single dose of 10 mg/kg pyrantel, the prototype of this class (Figure 1.3A), has high efficacy and prolonged activity against a broad range of nematodes, including *Ascaris* spp. and hookworms of humans and animals (Becskei et al., 2020; Behnke et al., 1993; De Clercq et al., 1997; McFarland, 1982), but lacks activity against whipworms (McFarland, 1982). Drug resistance has been reported in hookworms in dogs (Castro et al., 2019; Kopp et al., 2007, 2008), and although rarely used in humans, drug resistance remains a continuous threat due to the limited options of efficacious alternative treatments (Reynoldson et al., 1997).

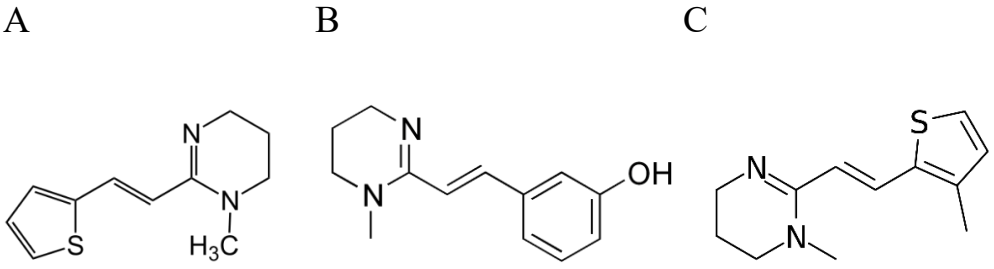

Figure 1.3 Chemical structure of pyrantel (A) oxantel (B) and morantel (C).

Oxantel was developed as a consequence of the lack of activity of pyrantel in whipworm infections. This drug was synthesized by an m-oxyphenol substitution of the thiophenol ring of pyrantel, and is highly efficacious against whipworm infections (Figure 1.3B) (Barda et al., 2018; Garcia, 1976; Howes Jr, 1972; McFarland, 1982), but lacks efficacy against hookworm (Bhopale

and Bhatnagar, 1988; Keiser et al., 2013; Speich et al., 2014). Interestingly, oxantel appears to show preference towards N-type nAChRs, in contrast to the L- and M-type targeted by pyrantel, which might account for differences in resistance and spectrum of activity (Martin et al., 2004).

Morantel is an analog of pyrantel containing a 3-(ortho position)-methylation of the thiophenol ring (Figure 1.3C). Although similar in structure to pyrantel (Courtot et al., 2015), it is primarily used against helminths of sheep and goats for its potent larvicidal activity (McFarland, 1982), but is not generally used in humans or dogs and cats because of first pass metabolism and poor GI absorption (Baggot, 2007). Morantel and pyrantel activate M-type nAChR composed of ACR-26 and ACR-27 subunits (Courtot et al., 2015). Deviating from the pyrantel pharmacological profile, morantel may also act as a channel blocker of N-nAChRs (Abongwa et al., 2016a; Evans and Martin, 1996), and because it differs from pyrantel only by the presence of a methyl group, is a useful tool to probe structure-function relationships at the level of drug targets.

1.10.3 Tribendimidine

The development of new anthelmintics is a rare event. As such, tribendimidine, which reached the Chinese market in 2004, was met with great acclaim because of its very broad spectrum of activity, efficacy with a single 300 mg dose, and safety profile in children (Coulibaly et al., 2019; Xiao et al., 2005). Tribendimidine is unstable in aqueous solution and is a prodrug of amidantel, which was released in the 1970s and showed great efficacy in canine hookworm infections, but lacked efficacy against *N. americanus* and whipworm in humans (Thomas, 1979; Wollweber et al., 1979). Concern was also raised about the potential carcinogenicity and mutagenicity of the aniline-containing metabolite of the drug (Epe and Kaminsky, 2013). The National Institute of Parasitic Diseases branch of the Chinese Center for Disease Control and Prevention undertook a large

screening assay of synthetic derivativities of amidantel, to produce tribendimidine as a treatment for human hookworm infections. It has efficacy against some trematodes, cestodes and numerous nematodes that infect humans, including all species of hookworm as well as *A. caninum* in dogs (Kulke et al., 2012; Moser et al., 2017; Steinmann et al., 2011; Tritten et al., 2012b; Xiao et al., 2005). By generating amidantel in the host, tribendimidine belongs to the class of anthelmintics that activate excitatory cholinergic receptors to cause contractile paralysis; these results are seen even in the presence of levamisole resistance, suggesting receptor subtype specificity (Robertson et al., 2015). Paralysis of worms is achieved *in vitro* within 1 hr of exposure (Ren et al., 1988) and worsening physical degradation of internal organs and body muscle of adult hookworms is seen from 6 hr onwards (Yang et al., 1988).

1.10.4 Spiroindoles: derquantel & paraherquamide

Derquantel (2-desoxoparaherquamide) is a cholinergic ion channel antagonist clinically used in combination therapy with the macrocyclic lactone abamectin due to synergy in causing flaccid paralysis of intestinal nematodes (Robertson et al., 2002; Zinser et al., 2002). Derquantel is used the treatment of nematode infections in sheep, in which it possesses a wide safety profile, while the related compound paraherquamide had poor efficacy and high adverse toxicity against dog hookworms (Shoop et al., 1991).

1.10.5 Thiazolide: nitazoxanide

Nitazoxanide is notable for its activity against both intestinal protozoa, including *Cryptosporidium* spp. in children, and STH, including *A. duodenale* (Abaza et al., 1998), but requires administrating

500 mg doses to adults (200 mg or less to children) twice daily for more than 3 days (Fox and Saravolatz, 2005), which creates issues of compliance; no data are available on its efficacy against *N. americanus*. The proposed mechanism of action is by inhibition of pyruvate ferredoxin oxidoreductase in protozoa and other microorganisms (Anderson and Curran, 2007). It has also been proposed that, in nematodes, nitazoxanide activity relies on glutamate-gated chloride channels (GluCls; Somvanshi et al., 2014) based on efficacy studies in mutant strains of *C. elegans;* in these experiments, nitazoxanide demonstrated additional benefits when combined with albendazole and pyrantel.

1.10.6 Cyclooctadepsipeptides: emodepside

Emodepside, a semisynthetic analog of a natural product derived from a fungal fermentation, was released to market in the 1990s (Sasaki et al., 1992) and is used to treat GI nematodes, including *A. tubaeforme*, in cats, and has also shown efficacy against *N. americanus* and *A. ceylanicum* in laboratory animal models of human hookworm infection (Karpstein et al., 2019). The emodepside/praziquantel combination product Profender® is approved for use for treatment of parasites in dogs in Europe (Schimmel et al., 2009) and cats globally (Böhm et al., 2015). Emodepside activates inhibitory potassium channels, specifically the Ca^{2+}-activated potassium channel slo-1 (SLO-1) of nematodes, causing paralysis (Martin et al., 2012).

1.10.7 Amino-acetonitrile derivatives (AADs): monepantel

Monepantel was discovered in a screen of over 600 synthetic AAD compounds for efficacy in a mouse model of nematode infection and then in sheep (Kaminsky et al., 2008). Monepantel

paralyzes worms by acting as a positive allosteric modulator of the DEG-3 (DEGeneration of certain neurons subfamily 3) subfamily of ionotropic acetylcholine receptors, distinct from the targets of spiroindoles, imidazothiazoles and tetrahydropyrimidines (Baur et al., 2015; Rufener et al., 2013, 2010). These drugs display a large safety window and are administered as an oral drench in sheep at a dose of 2.5 mg/kg for treatment of intestinal nematode infections (Kaminsky et al., 2008). Tritten et al. (2011) identified *in vitro* efficacy against adult *A. ceylanicum* as well as worm clearance in an *in vivo* model of hookworm infection. However, no effect against *N. americanus* was seen up to a dose of 10 mg/kg, nor were infective larvae of either species affected. Furthermore, trials for *Trichuris suis* and *A. suum* in swine, which are models of human STH, also showed no efficacy, limiting its clinical use in humans or companion animals.

1.10.8 Macrocyclic lactones

Macrocyclic lactones (MLs) are a class of very potent, safe, broad-spectrum endectocides. The prototype, IVM, was discovered at Merck in the 1970s in an assay of fermentation products; the active fermentation was from *Streptomyces avermitilis* which was found in a Japanese golf course sand bunker (Õmura and Crump, 2004). This drug screen led to a Nobel Prize as a result of the collaboration between Satoshi Õmura of the Kitasato Institute and William Campbell and colleagues of the Merck Institute for Therapeutic Research, who screened novel natural products exhibiting anthelmintic activity in a *Nematospiroides dubius* mouse model (Burg et al., 1979). One product, avermectin B1, was found to have potent anthelmintic activity (Egerton et al., 1979), and the 22,23 dihydroavermectin derivative, IVM, was synthesized as a result (Campbell et al., 1983; Õmura & Crump, 2004). IVM was introduced in 1981 as having broad spectrum activity against nematodes and ectoparasites of animals (Chabala et al., 1980) at low doses (6 to 200 µg/kg) and

has since been used extensively in human and veterinary medicine (Campbell et al., 1983; spectrum of activity reviewed by Crump and Omura, 2011).

The IVM molecular structure is characterized by a disaccharide attached to a spiroketal and a cyclohexene (benzofuran) in a 80:20 mixture of avermectin B1a:B1b which differ by the presence of a methyl group at carbon 25 proximal to the 23,24 dihydrogenated site created during drug optimization for dosage form and spectrum of activity (Figure 1.4A) (Chabala et al., 1980). Another class of MLs, derived from *Streptomyces cyaneogriseus*, is the milbemycins, including MOX, which differ from the avermectins by the lack of a sugar moiety, may lack the C5 cyclohexene hydroxyl or replacement with a ketoxime (the oxime in milbemycin oxime), and have an alkane or alkene modified C23 and C25 (C23 methoxime and a branched 6 carbon alkene at position C25 in MOX). MOX generally has a longer biological half-life, and is used predominantly in veterinary medicine (Figure 1.4B) (Shoop et al., 1995; Takiguchi et al., 1980), but has recently been approved for the treatment of onchocerciasis in humans (de la Torre and Albericio, 2019). All MLs share a common mechanism of action: targeting an invertebrate-specific class of GluCls (Cully and Paress, 1991; Dent et al., 1997; Geary and Moreno, 2012).

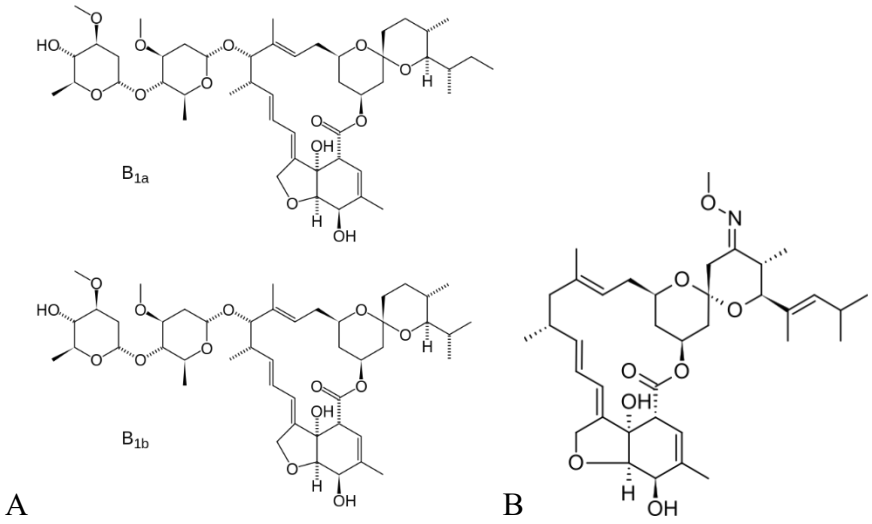

Figure 1.4. Molecular structure of (A) the two compounds that make up IVM and (B) MOX

One important characteristic of MLs is their wide therapeutic index in humans. This is a result of two factors: the targeting of invertebrate-specific ion channels, and being a substrate for p-glycoprotein (Pgp) efflux proteins in the host blood-brain barrier, protecting neurotransmission (Schinkel et al., 1994). In mammals, adverse drug reactions are caused by off-target effects primarily on GABA receptors (Ménez et al., 2012) and glycine receptors (GlyR) (Shan et al., 2001). Active efflux across the blood-brain barrier is the more significant protector, illustrated by the textbook example of IVM toxicity in collie breeds of dogs. IVM is used to prevent heartworm (*D. immitis*) infections in companion animals, but certain breeds of dog, especially collies, have a 4 base pair deletion loss-of-function mutation in the multiple drug resistance gene *mdr1a* that encodes a Pgp, causing the accumulation of IVM in the brain (Mealey et al., 2001). These animals can exhibit signs of toxicity at an oral dose of 100 µg/kg, whereas in beagles the LD_{50} is 80 mg/kg and they can safely tolerate doses up to 2.5 mg/kg (approved oral dose = 0.006 mg/kg) (Mealey, 2013). Neurotoxicity manifests as central nervous system depression including mydriasis, ataxia, blindness, and comas, and in high concentrations MLs can cause death (Barbet et al., 2009; Neff

et al., 2004). In the human *mdr-1* gene, most single nucleotide polymorphisms are silent, and mutations are not thought to play a role in IVM entry into the brain (Chandler, 2018). However, the treatment of IVM for onchocerciasis co-infected with a large *Loa loa* microfilaremic burden can cause serious neurological reactions including encephalopathy, coma and even death (Turner et al., 2010). It is believed that serious adverse reactions involve an immune response to IVM-induced killing of *L. loa* microfilaria that have invaded the central nervous system (Mackenzie et al., 2003), and therefore, IVM is not used to treat onchocerciasis in regions endemic for *L. loa*. This highlights the importance of pharmacokinetics in the safety of IVM, but it also likely plays an important role in IVM exposure and efficacy in the worm, as target tissue concentrations in the host are related to the concentrations found in the parasite *H. contortus* (Lloberas et al., 2013, 2012).

IVM has a plasma half-life of ~18 hr in humans, with peak plasma concentration achieved 4 hr after oral administration (the only approved route in humans) (Canga et al., 2008). IVM is extensively metabolized in the liver and almost exclusively eliminated by the fecal route (Chiu et al., 1990). Attributable to its strong lipophilicity, IVM has a large volume of distribution (Canga et al., 2008) but also binds avidly to plasma proteins (Krishna and Klotz, 1993), and can diffuse across capillary endothelium into tissues inhabited by parasites. High concentrations of IVM are detectable in fat tissue, skin, and the GI including the intestinal mucosa, greatly aiding targeting of intestinal nematodes such as hookworms (Baraka et al., 1996; Lifschitz et al., 2000).

In comparison to the pharmacokinetics of IVM inside the infected host, very little is known about how it is handled by parasites. IVM inhibits pharyngeal pumping, rapidly blocking feeding behaviours in intestinal blood feeding helminths (Geary et al., 1993; Richards et al., 1995), causes flaccid paralysis of somatic body muscles (Turner and Schaeffer, 1989), and persistently reduce

egg counts of parasites, including hookworms (Awadzi et al., 1985; Wang et al., 1989). Disruption of parasite Pgp activity by mutation or drug antagonism enhances sensitivity to IVM (Ardelli and Prichard, 2013; Heckler et al., 2014), indicating a role in direct efflux. Nematodes possess a greater diversity of Pgps than mammals, and multiple subtypes have been reported to be upregulated upon exposure to IVM (Raza et al., 2016). Consequently, altered drug sensitivity has been associated with allelic variation of Pgps in *H. contortus* and other important parasites (De Graef et al., 2013; Maté et al., 2018; Sangster et al., 1999; Williamson et al., 2011) associated with the emergence of high levels of drug resistance (Demeler et al., 2009; Fiel et al., 2001). The genetic basis for IVM resistance is not completely known, and is likely multigenic, including modification in expression or even the function of drug targets (Amanzougaghene et al., 2018; Blackhall et al., 1998; Feng et al., 2002; Njue et al., 2004). Backcrossing two different IVM-resistant field isolates of *H. contortus* with an IVM-sensitive strain showed a lower proportion of resistance in their progeny, suggesting multiple independent loci contributing to resistance (Redman et al., 2012). In this thesis I analyze the pharmacology of IVM drug targets and identify amino acid residues related to drug sensitivity and insensitivity.

Like the tetrahydropyrimidines, MLs target nematode pLGICs. However, MLs target inhibitory, not excitatory, receptors called GluCls. The high lipophilicity of MLs allows them to bind to their drug targets proximal to the cell membrane in a pseudo-irreversible manner, essentially causing permanent activation of these inhibitory channels and inducing flaccid paralysis in the parasite (GluCls reviewed in section 1.13). Despite having broad-spectrum activity, there are species-related limitations of ML use. As noted, *N. americanus* is one of the few parasitic nematode species insensitive to the paralytic effects of MLs. This is especially notable in light of the fact that the closely related *Ancylostoma* spp. are 50-fold more sensitive (Behnke et al., 1993;

Richards et al., 1995). IVM is not effective in paralyzing microfilariae or adult filariids at pharmacologically relevant concentrations (Wolstenholme et al., 2016), but single doses of IVM cause prolonged sterilization of adult filariids, greatly reducing microfilarial levels for many months (Kläger et al., 1993; Li et al., 2014). Interestingly, schistosomes or other flukes express a family of GluCl that are non-orthologous and phylogenetically distinct from those of nematodes that do not respond to IVM, and these species are not susceptible to the drug (Dufour et al., 2013; Lynagh et al., 2014).

A common theme in many anthelmintics is the targeting of the nematode nervous system. These organisms have evolved complex neurotransmission mechanisms sufficiently divergent from those of their hosts to enable selective chemotherapy. The most important functional units of the nematode neuromuscular system are ligand-gated ion channels.

1.11 Ligand-gated ion channels

Ligand-gated ion channels are a superfamily of membrane-spanning proteins that form a central pore through the cell membrane, and when activated by a ligand, facilitate the selective movement of ions down their electrochemical gradient (Thompson et al., 2010)**.** These are represented by trimeric ATP receptors (Dubyak, 2007; Valera et al., 1994), tetrameric excitatory glutamate receptors (Rosenmund et al., 1998), and the large family of cys-loop pLGICs, which are the focus of this thesis.

pLGICs are responsible for fast ionotropic synaptic neurotransmission in humans and animals, but have also recently been discovered in prokaryotes, instead playing roles in pH and environmental sensing (Tasneem et al., 2005). Only 3 prokaryotic pLGICs have been discovered,

the pH-sensing proton channel, *Gloeobacter* ligand-gated ion channel (GLIC) (Bocquet et al., 2007), the *Erwinia* ligand-gated ion channel (ELIC) receptor, activated by small molecules containing a primary amine (such as GABA) (Zimmermann and Dutzler, 2011), and the recently published DeCLIC from a *Desulfofustis* deltaproteobacterium which is inhibited by Ca^{2+} (Hu et al., 2020). This is highly implicative of an evolutionary lineage vital for success of biological fitness and represents a model for studying and comparing pLGIC structure and function.

Much of our knowledge of the function of pLGICs comes from heterologous expression studies in mammalian cells and oocytes of *Xenopus laevis*. These systems allow channel over-expression for radiolabelled, fluorometric and electrophysiological assessment of their pharmacology (Wagner et al., 2000; Yu et al., 2016). The crystal structures of ELIC (Hilf and Dutzler, 2008) and GLIC (Bocquet et al., 2009; Hilf and Dutzler, 2009) were instrumental in the advancement of structure-function relationship studies of pLGICs, and also indicated that prokaryotic receptors are very similar to eukaryotic receptors in topology of quaternary structures, despite low amino acid sequence similarity and the absence of the characteristic and highly conserved 13 amino acid cys-loop (Hu et al., 2020; Limapichat et al., 2010).

The earliest X-ray crystal structure of pLGICs was not from a pLGIC at all, but rather of an acetylcholine binding protein (AChBP), which is representative of the extracellular domain (ECD) of pLGICs (Brejc et al., 2001). This was followed by two highly influential publications of an entire pLGIC at 4 Å resolution from the electric organ of *Torpedo marmorata* (Miyazawa et al., 2003; Unwin, 2005). These discoveries were important because obtaining crystal structures of transmembrane proteins is notoriously difficult (Torres et al., 2003), and previous knowledge of the structure of pLGICs relied on mutagenesis (Backus et al., 1993) and other indirect (Langosch et al., 1988) or low resolution techniques (Kubalek et al., 1987). Modern structural analysis of

novel pLGICs often use these crystals as a template for 3-dimensional homology modeling (Šali and Blundell, 1993), a technique utilized in this thesis.

pLGICs are composed of 5 individually translated subunits, each containing a large N-terminal ECD, 4 transmembrane (TM) domains and a short C-terminal in the ECD. These subunits assemble in membranes into ~300 kDa pLGICs in a ring-like structure around a central pore formed by the TM2 of each subunit. Receptors can exist as homopentamers formed from 5 identical copies of a single gene product, or as heteropentamers containing subunits encoded by multiple different genes. Different receptor stoichiometry resulting from different combinations of subunits yields unique channel properties including ion conductance, and agonist affinity and efficacy. Agonists bind in the orthosteric ligand binding pocket located at the ECD interface between two adjacent subunits (termed the (+) principal and the (-) complementary subunits). Agonist binding causes conformational changes that allow ion conductance controlled by residues that line the hydrated pore formed by TM2 (Figure 1.5).

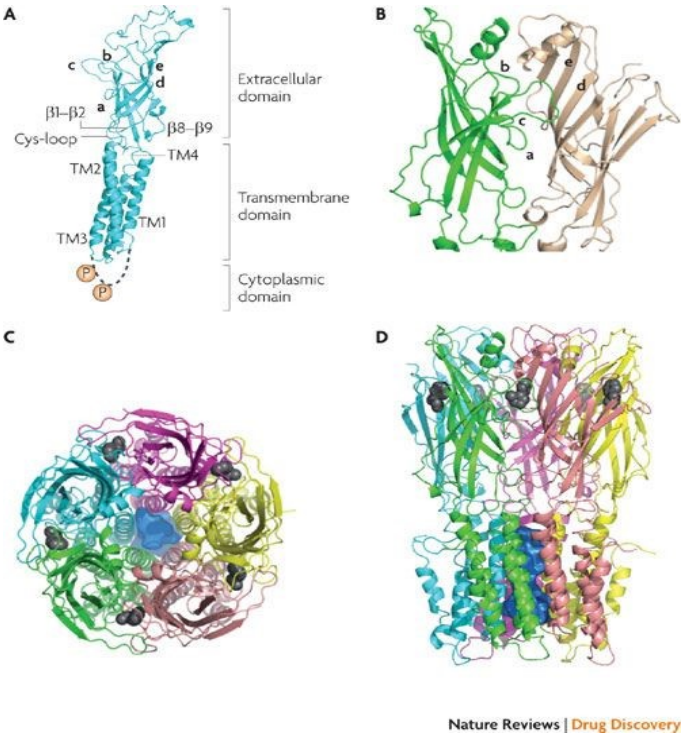

Nature Reviews | Drug Discovery

Figure 1.5 Homology model of a homopentamer of α7 nAChR model shows (A) an individual subunit (B) the extracellular ligand binding domain with loops A-C and D-F contributed by the green principal (+) subunit and the tan complementary (-) subunit respectively (C) view looking "down" into the pore (Blue) from the ECD (D) membrane cross-section side view profile of a pLGIC. *With permission from Springer Nature [Nature Reviews Drug Discovery]* (Taly et al., 2009)*, copyright (2020).*

Viewed from the side perpendicular to the pore of the channel in a closed inactive state the pore-lining TM2 domains assemble in an hourglass-like shape with the narrowest point forming the gate, or more accurately a girdle of hydrophobic residues roughly 3 Å in diameter composed primarily of Leu or Val residues (Beckstein and Sansom, 2006; Miyazawa et al., 2003).

In general, channel activation involves a series of conformational changes initiated when a small molecule occupies the orthosteric ligand binding site. This binding site is commonly called the aromatic box, a region enriched with aromatic amino acids donated by loop regions A-C contributed by the (+) principal subunit and loops D-F (and sometimes G) contributed by an adjacent (-) complementary subunit (Figure 1.5B). These "loops" are short segments of ß-strands, which protrude into a cleft formed by the principal and complementary subunit faces. Ligand binding occurs by formation of hydrogen bonds and characteristic π-cation interactions of an aromatic group with a positively charged ion. Upon ligand binding, these charged interactions contract the binding cleft, like a clamping jaw, forcing a conformational wave that propagates throughout the ECD of all subunits, increasing the affinity of the other binding sites for agonists in a phenomenon called positive cooperative binding (Stefan and Le Novère, 2013). In contrast, competitive antagonists bind to the orthosteric pocket without inducing closure of the binding cleft

and block agonist binding, and inverse agonists bind and stabilize the inactive state, reducing spontaneous activity (Kletke et al., 2013).

There are 5 identical binding pockets in a homopentamer, whereas in a heteropentamer, agonist binding is controlled by the composition of the subunit interfaces. For instance, in human ionotropic acetylcholine receptors, the binding site is located at the interface between adjacent α and non- α subunits (Tapia et al., 2007); there are 10 different α and 4 β subunits, as well as γ, δ and ε subunits, each with differing ligand affinities and biophysical properties (Millar and Gotti, 2009).

When sufficient orthosteric sites are occupied (typically 2-3 agonist molecules; Baumann et al., 2003), the ECD of each subunit experiences a rotational twisting conformational change propagating into the cys-loop which pulls the TM2-TM3 extracellular loop like a lever, causing the top half of the TM2 to twist and tilt outward away from the pore (Hung et al., 2005). This outward tilting/bending transiently opens the pore in less than a millisecond, increasing the diameter of the gate from 3 Å to ~7.5-8.5 Å in cation-conducting channels (Beckstein and Sansom, 2004; Wang and Imoto, 1992; Yang, 1990) and ~5.2-6.2 Å in anion-conducting channels (Baumann et al., 2003; Fatima-Shad and Barry, 1993; Wotring et al., 1999).

Cation- and anion-selective pLGICs facilitate excitatory and inhibitory neurotransmission, respectively, required for basic brain function and muscle contraction. These channels are generally named after the neurotransmitter that gates them. In mammals, nAChRs and serotonin receptors (5-HT_3) propagate excitatory signaling, whereas $GABA_A$ and GlyRs carry inhibitory signals (Baer et al., 2009; Kozuska and Paulsen, 2012). Upon activation, these receptors induce excitatory or inhibitory post-synaptic potentials which cumulatively increase or reduce the probability of an action potential. Once an action potential reaches the synaptic cleft,

neurotransmitters are released from vesicles of the presynaptic cell and bind their specific receptors on effector cells, mediating inhibition or excitation in the post-synaptic cell.

Because these receptors are critical for physiological function, they are implicated in numerous important pathologies. For example, nAChRs play a direct role in the progression of neurodegenerative disorders, including Alzheimer's disease, Parkinson's disease, and schizophrenia (O'Neill et al., 2002; Posadas et al., 2013). As a consequence of their role in physiology and disease, they are the targets of many drugs used for therapy or recreation. For instance, $GABA_A$ receptors are the target of ethanol and anesthetics (Hemmings Jr et al., 2005; Söderpalm et al., 2017), and benzodiazepines, which also target these receptors, are used to treat seizures and anxiety and sleep disorders (Pritchett et al., 1989).

The fundamental property of normal pLGIC function is the selective passage of a certain type and number of ions gated by each class of receptor. As determined by mutational and computational studies of closed versus open receptor conformations, ion selectivity and conductance are controlled by residues lining and adjacent to the TM2 pore in a direct but complex multifactorial role; no consensus on a unifying mechanism has been achieved (Cymes and Grosman, 2016).

Excitatory pLGICs preferentially gate smaller monovalent cations, specifically Na^+ and K^+ (Huang et al., 1978), while some nAChRs are also capable of passing Ca^{2+} (Bertrand et al., 1993). Charge selectivity is most strongly determined by the presence of a negatively charged Glu just below the hydrophobic girdle, proximal to the cytoplasm. This region is called the intermediate ring, and contains a highly conserved GEK/R motif in cation channels (Figure 1.6) (Corringer et al., 1999; Jensen et al., 2005), and an equally conserved PAR motif in anion channels in which the analogous Glu residue is a neutral Ala (Keramidas et al., 2002; Wotring and Weiss, 2008).

Intriguingly, one of the anionic pLGICs studied in this thesis lacks this PAR motif, which has implications for ion conductivity.

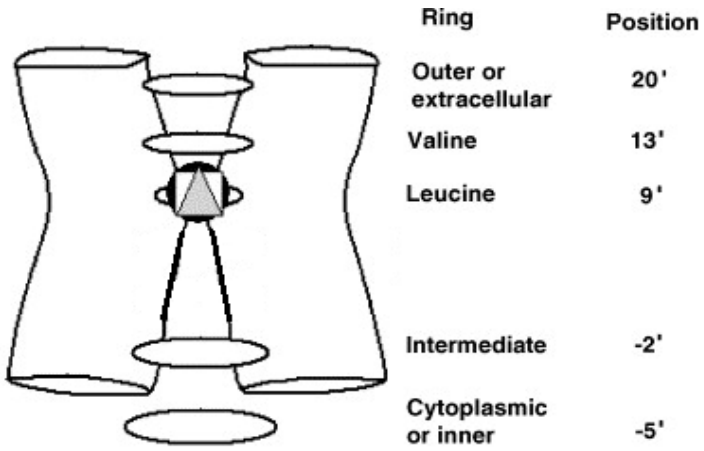

Figure 1.6 Cartoon representation of important residues that line the pore of an nAChR. Two subunits in a closed, desensitized state are shown for simplicity. *Adapted with permission from Elsevier [The International Journal of Biochemistry & Cell Biology]* (Arias et al., 2006)*, copyright (2020).*

Two additional rings of charged residues contribute to cation selectivity, one near the opening of the pore, called the extracellular ring, and one at the end of the pore, called the cytoplasmic ring (Thompson and Lummis, 2003). Cation-selective receptors also contain a pore-facing Val between the extracellular ring and the hydrophobic girdle, whereas anionic receptors contain an analogous polar Ser/Thr and a V→S/T mutation converts cation to anion gating (Corringer et al., 1999). Interestingly, like cation channels, anionic channels possess negatively charged residues in the cytoplasmic ring. Together with the presence of Pro in the PAR motif, this suggests that charge selectivity not only involves ionic interactions, but also spatial constraints, and that anion passage is more permissive whereas cation gating requires additional selectivity.

Mammals and invertebrates share numerous orthologous pLGIC subunits, including those that form inhibitory $GABA_A$ receptors and excitatory nAChRs. However, the evolutionary histories of these groups diverged over 600 million years ago (Ayala et al., 1998), long enough that their orthologs share low sequence similarity, and for the helminth nervous system to evolve pLGICs distinct from humans and other mammals. Indeed, in comparison to humans which possess 45 genes encoding pLGICs, the *C. elegans* genome encodes over 100, resulting in the existence of pLGICs unique to nematodes (Jones and Sattelle, 2008). For instance, nematodes possess inhibitory acetylcholine-gated chloride channels (formed by acetylcholine-gated chloride channel subunit, ACC- 1-4; Putrenko et al., 2005), and inhibitory GluCls (Cully et al., 1994), whereas these neurotransmitters exclusively gate the transmission of cations in vertebrates. Likewise, the nematode GABA receptor Expulsion defective protein 3 (EXP-1) is an excitatory GABA-gated channel that gates cations, whereas in the vertebrate nervous system, this neurotransmitter exclusively gates anion channels (Beg and Jorgensen, 2003). Furthermore, nematodes contain pLGICs activated by completely different ligands, including channels gated by the biogenic amines dopamine (Rao et al., 2009) and tyramine (Pirri et al., 2009). These differences in ligand activation and the large divergence of function, coupled with the lack of a protective blood-brain barrier, allow for the safe use of anthelmintics and pesticides that selectively target invertebrates outside and inside a human host with minimal side effects from off-target binding to host pLGICs. Two groups of ion channels of significance for anthelmintic activity and central to this thesis are the GluCls and the nAChRs.

1.12 Glutamate-gated chloride channels (GluCls)

1.12.1 Glutamate is a neurotransmitter

Glutamate, a non-essential amino acid, is the anionized zwitterion form of glutamic acid and can be biosynthesized from glutamine, α-ketoglutarate and 5-oxoproline (Chen et al., 1998; Cho et al., 2001; Hu et al., 2010). In the 1930s, high concentrations of glutamate were discovered in the mammalian central nervous system, eventually leading to the elucidation of glutamate as a neurotransmitter (Curtis and Johnston, 1974). Since then, ionotropic tetrameric glutamate receptors have been shown to be some of the most important excitatory ion channels in humans (Madden, 2002; Rosenmund et al., 1998). Orthologs play a similar role in invertebrates (Schuster et al., 1991; Tikhonov and Magazanik, 2009), having existed before the divergence of animals and plants (Chiu et al., 1999).

By contrast, inhibitory glutamate receptors do not exist in vertebrates; the closest human ortholog is the α1 GlyR, which shares roughly 34% sequence identity with the first GluCl discovered from nematodes. (Daeffler et al., 2014). The existence of hyperpolarizing GluCls was first discovered, and distinguished from their excitatory depolarizing counterparts, in extrasynaptic locust membranes by altering ion composition and measuring conductance associated with the applications of glutamate and its structural analog, ibotenate (Cull-Candy, 1976; Lea and Usherwood, 1973a, 1973b). In one of the first uses of *X. laevis* oocytes as a heterologous expression system for invertebrate ion channels, Fraser et al. (1990) injected locust mRNA into oocytes to functionally express and measure the activity of GluCls. cDNAs encoding GluCls were cloned from *C. elegans* in the early 1990s, in an attempt to identify the target of IVM and other MLs (Cully et al., 1994). Before this, IVM was thought to act on GABA receptors (Turner and Schaeffer, 1989).

1.12.2 The GluCls

When GluCl characterization was still in its infancy, IVM was suspected to act on ligand-gated chloride channels, but a high affinity (Vassilatis et al., 1997) primary drug target was not identified until Cully et al. (1991; 1994) isolated and expressed the *C. elegans* GLC-1 (GluClα) and GLC-2 (GluClβ) GluCl subunits in *X. laevis* oocytes. Starting with these subunits was fortuitous because homomeric Cel-GLC-1 receptors respond to IVM (indicated by α denotation) but not glutamate, whereas homomeric Cel-GLC-2 receptors do the opposite (lack of IVM sensitivity, denoted by β), and heteromeric Cel-GLC-1/GLC-2 receptors respond to both. Of the 8 nematode GluCl subunits now characterized, only Cel-GLC-1 forms functional homomeric receptors insensitive to glutamate, and only Cel-GLC-2 forms homomeric receptors insensitive to IVM. This specific combination of Cel-GLC-1 and -2 delineated glutamate versus IVM activation, highly suggestive of distinct binding sites. Interestingly Cel-GLC-1 does bind glutamate, but only after previous exposure to IVM (Hibbs and Gouaux, 2011). In this thesis, I analyzed 2 residues that differentiate Cel-GLC-2 and α-type IVM-sensitive subunits to ascertain their role in glutamate activity and ML susceptibility, and created a mutant Cel-GLC-2 that, like Cel-GLC-1, responds to glutamate only after previous exposure to IVM.

In *Xenopus* oocytes, prototypical pLGIC orthosteric agonist exposure, such as mM concentrations of glutamate on GluCls, quickly activates receptors (1 ms) to produce a peak current across the membrane, followed by a slower desensitization state and a rapid return to baseline equilibrium after drug washout (Figure 1.7). In contrast, IVM activation requires much lower concentrations (nM to low μM) and produces slow but irreversible activation of GluCls, thereby preventing depolarization, which causes flaccid paralysis of the organism. These agonist

concentrations and response profiles appear to be consistent across different GluCl subunit types from different species of nematode that are susceptible to IVM.

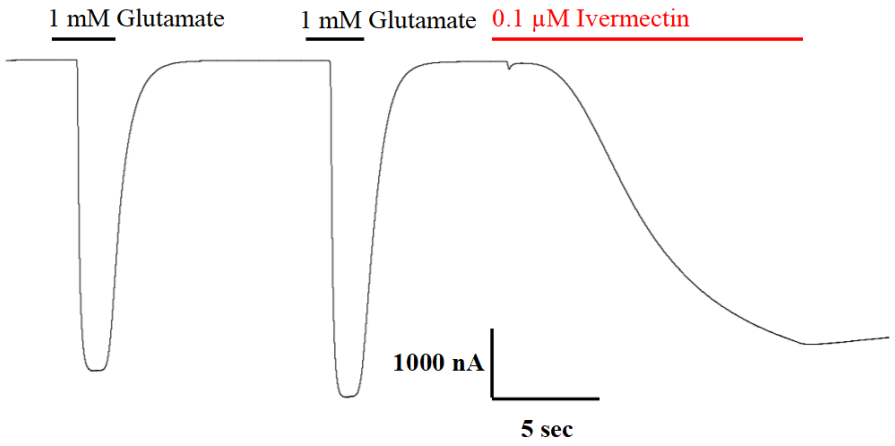

Figure 1.7 Representative tracing of IVM and glutamate activation of a GluCl (Hco-GLC-5 used in this thesis) expressed in *X. laevis* oocytes. Downward deflections represent current (expressed in nanoamperes) passing through a membrane due to activation of the ion channel. Note the rapid activation and return to baseline for glutamate applications in contrast to the slow, irreversible activation profile from IVM.

The family of GluCl subunits is summarized below (Table 1.1). Of these, GLC-1 is only found in *C. elegans* and is absent even from clade V nematodes closely related to *C. elegans,* such as *H. contortus* (Laing et al., 2013), *Ancylostoma* spp., (Schwarz et al., 2015) and *N. americanus* (Tang et al., 2014). Important highlights from this table include the fact that homopentameric GLC-2 receptors are the only nematode GluCls not activated by IVM; they are instead antagonized (Degani-Katzav et al., 2017b). This fact is significant for this thesis because certain drug-resistant nematode isolates may exploit this feature by decreasing expression of GluCl genes encoding IVM-targeted subunits (α-type encoding functional subunits that, when expressed as a pLGIC, are sensitive to activation by IVM), and increasing expression of *glc-2* (El-Abdellati et al., 2011).

Furthermore, the incorporation of GLC-2 into an α-type receptor significantly reduced potency and maximal effect of IVM (Atif et al., 2019). However, another study found no association between levels of *glc-2* and drug-resistance (Njue and Prichard, 2004).

C. elegans GLC-2 subunits are expressed in metacorpus and isthmus pharyngeal muscles, which are innervated by fast inhibitory M3 motor neurons. Laser ablation of M3 neurons increases the duration of pharyngeal contractility and impairs feeding behaviour (Avery, 1993). This tissue distribution appears to be species-specific, as expression of GLC-2 in *H. contortus* is limited to body motor neuron commissures and is absent from the pharynx (Figure 1.8). (Delany et al., 1998; Portillo et al., 2003).

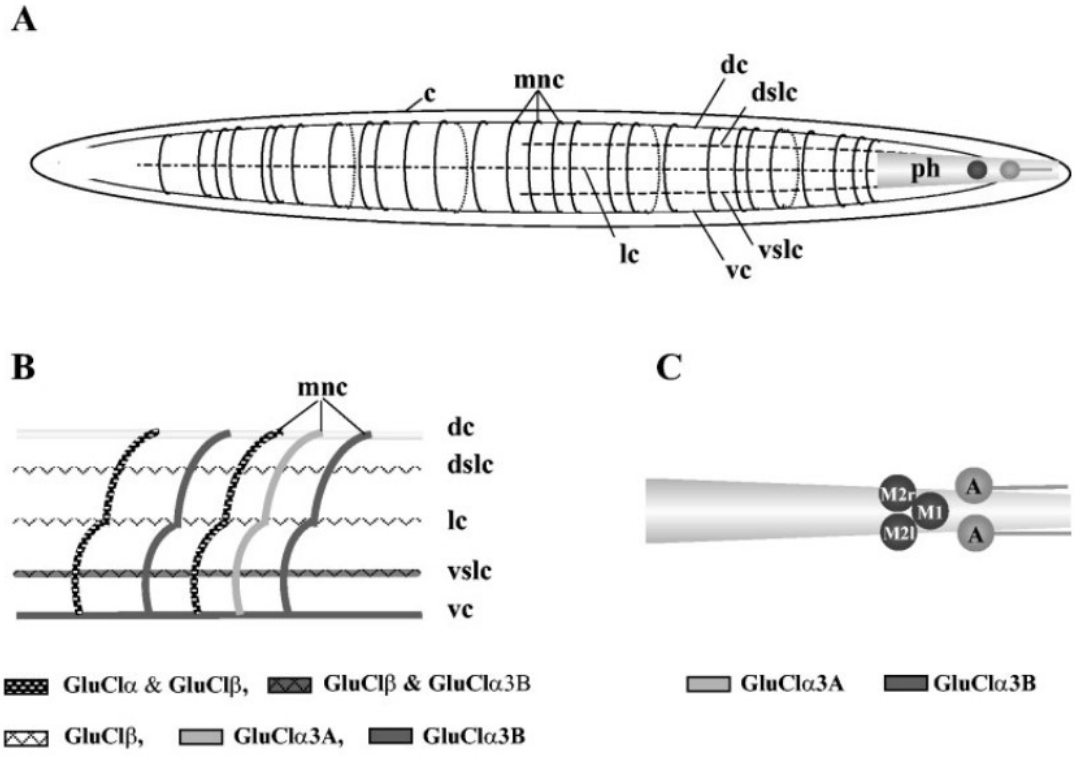

Figure 1.8 Expression of GluCls subunits in *H. contortus; nota bene, In this figure H. contortus* GluClα = Glc-5 ≠ Cel-GluClα. *With permission from John Wiley and Sons [Journal of Comparative Neurology]* (Portillo et al., 2003)*, copyright (2020).*

Tissue distribution plays a significant role in the organism-level effects of IVM. There is still controversy whether paralysis of pharyngeal pumping (Brownlee et al., 1997; Geary et al., 1993), or somatic body wall muscles (Kotze et al., 2004; Sheriff et al., 2005) is the primary means of worm killing. MLs also act on GluCls expressed in the secretory-excretory apparatus of *B. malayi* (Moreno et al., 2010) and cause long-term inhibition of egg laying and sterilization of adult worms (Walker et al., 2017).

Table 1.1 List of GluCl subunits and their properties

Subunit	**Glutamate Sensitivity**	**ML Sensitivity**	**Tissue location**
GLC-1 (GluClα) (Cully et al., 1994)	Only after exposure to IVM (Hibbs and Gouaux, 2011)	None	N/A
GLC-2 (GluClβ) (Cully et al., 1994)	Yes	IVM antagonist (Degani-Katzav et al., 2017b) MOX not tested	*C. elegans* (Dent et al., 1997; Laughton et al., 1997) →Pharynx (metacorpus, isthmus; same pattern as Avr-15) *H. contortus* (Delany et al., 1998; Portillo et al., 2003) → NOT pharynx (same body muscle pattern as Glc-5)
GLC-3 (Horoszok et al., 2001)	Yes	Yes	N/A
GLC-4	Yes	Yes	N/A

(Glendinning et al., 2011)			
GLC-5 (Hco-GluClα) (Forrester et al., 2003, 1999)	Yes	Yes	*H. contortus* (Portillo et al., 2003) →motor neuron commissures Non-pharyngeal (same distribution of Hco-Glc-2)
GLC-6 (Glendinning et al., 2011)	Yes	Yes	N/A
AVR-14 GluClα3 Gbr-2 (Dent et al., 2000; Yates and Wolstenholme, 2004)	Yes *14a not functional as homopentamer	Yes	*C. elegans* (Dent et al., 2000) → body wall muscle motor neurons and mechanosensory neurons *H. contortus* (Jagannathan et al., 1999; Portillo et al., 2003; Yates et al., 2003) → body wall muscle motor neurons and mechanosensory neurons. Avr-14B also found in pharyngeal neurons *B. malayi* (Moreno et al., 2010) →oral opening, nerve ring, the excretory-secretory apparatus, the inner body, and anal pore
AVR-15 GluClα2 (Dent et al., 1997)	Yes	Yes	*C. elegans* (Dent et al., 1997; Laughton et al., 1997) →Pharynx (metacorpus, isthmus; same pattern as Avr-15)
SmGluCl2.1 (Dufour et al., 2013) ** **flatworm**	Yes	No *phylogenetically distinct from nematode GluCls	N/A

1.12.3 IVM binding site

The second biggest discovery that advanced the study of IVM pharmacodynamics was the publication of a high resolution (3.3 Å) crystal structure of a GluCl (Cel-GLC-1) in an open state, bound to IVM and glutamate (Figure 1.9) (Hibbs and Gouaux, 2011). IVM allosterically binds in the plasma membrane proximal to the extracellular domain at the interface between a (+)TM3 and a (-)TM1 subunit, inserting its cyclohexene group in toward the TM2 domains (Figure 1.10). By wedging between these subunits, the cyclohexene carbon-5 hydroxyl group has space to contact a Ser residue of TM2. This residue is present in receptors activated by IVM, but in the IVM-insensitive Cel-GLC-2 receptor it is a bulkier Gln, likely acting as a physical barrier for IVM to penetrate deep enough into TM2 to cause activation.

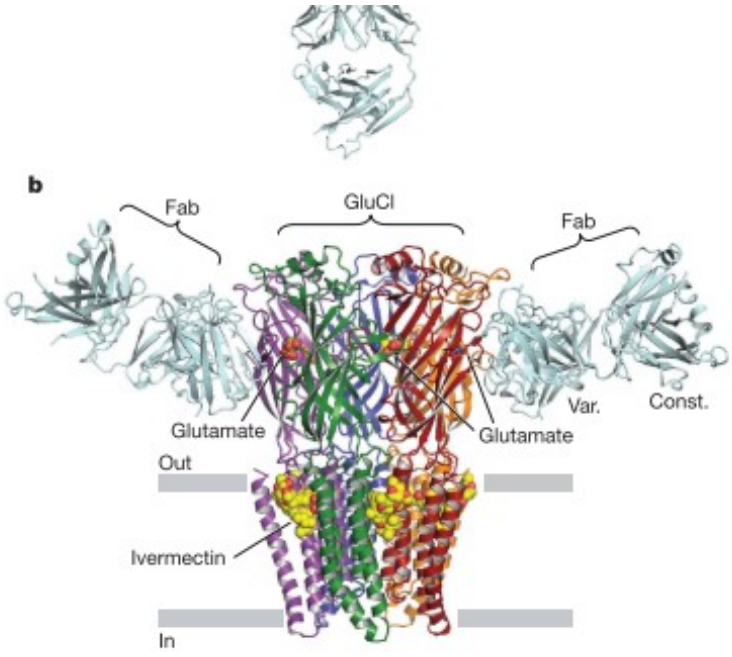

Figure 1.9 Crystal structure of the *C. elegans* GLC-1 receptor bound to glutamate and IVM. Each subunit coloured for distinction. Sites of IVM and glutamate binding are indicated *Adapted with permission from Springer Nature [Nature]* (Hibbs and Gouaux, 2011)*, copyright (2020).*

The authors also suggested that residues of the first sugar of the disaccharide were important for contact with the TM2-TM3 loop, an integral hinge in alleviating rigidity of the TM2 and instrumental in opening the receptor. However, MOX and other milbemycins lack this sugar moiety, and the biological relevance of each contact point/bond identified from the crystal structure is uncertain.

It is likely that IVM activates GluCls in a mechanism dissimilar and downstream from the ECD involvement required by glutamate activation, and that the cyclohexene positioning proximal to the M2 Ser is critical for this direct agonism. Lynagh et al. (2011) screened a series of mutations in the human GlyR, assaying for functional changes in IVM responses. They found that many single mutations of residues predicted to be important for binding by the Hibbs & Gouaux model increased, decreased, or abolished IVM responses, or even converted the drug into an antagonist. These results indicate that even a single amino acid difference between GluCl subunits or in the same subunit in different species may have a large role in dictating IVM sensitivity; unfortunately, they only tested IVM, and it remains to be seen if all MLs interact with the same residues to elicit anthelmintic activity. To date, no binding differences or direct effects of differential binding have been found for MOX and IVM. In this thesis, I provide evidence of such a difference.

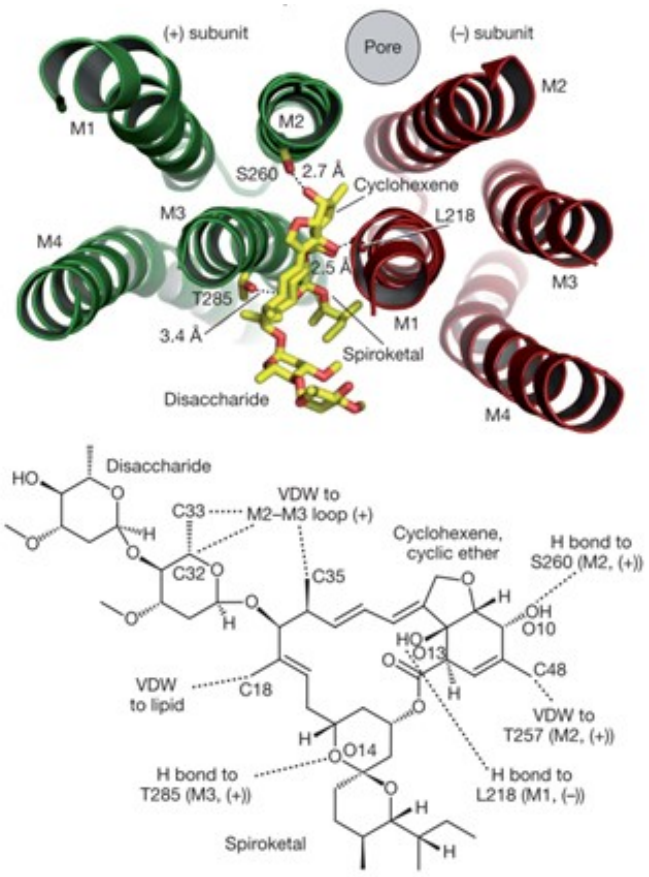

Figure 1.10 (top) A yellow IVM molecule inside its binding site between adjacent subunits coloured green and red (bottom) functional groups of IVM predicted to bind to Cel-GLC-1. *With permission from Springer Nature [Nature]* (Hibbs and Gouaux, 2011)*, copyright (2020).*

1.13 Excitatory nAChRs

Nematode acetylcholine receptors are responsible for a range of essential physiological functions, including movement (Touroutine et al., 2005), feeding (McKay et al., 2004), and egg laying (Duerr et al., 2001) via regulation of muscle contraction. Acetylcholine receptors are a very large group of proteins that are broadly divided into G-protein coupled receptors (GPCRs) and pLGICs. By convention, the distinction between acetylcholine GPCRs and pLGICs is denoted by the agonist

used to originally characterize each receptor; namely the muscarinic GPCR type mAChR (Wess, 1996) and the nicotine-activated ionotropic nAChR (Holladay et al., 1997).

All subtypes of nAChR except for the ACCs are excitatory and gate cations by acetylcholine activation of the orthosteric aromatic box. Despite wide heterogeneity of nAChR subunits among humans and nematodes (Holden-Dye et al., 2013), acetylcholine binding generally requires two α-type subunits, which contain a conserved pair of adjacent Cys residues in loop C of the principal (+) subunit contributing to the binding pocket (Corringer et al., 1998). Some 27 different nematode nAChR subunits have been identified, all with different capacities to bind anthelmintics, and are classified by homology as DEG-3-like, ACR-16-like, ACR-8-like, UNC-38-like and UNC-29-like (Jones and Sattelle, 2004; Martin et al., 2005). As previously noted in section 1.10, nematode nAChR subunits can form multiple populations of receptors, distinguishable by their susceptibility to different anthelmintics (Figure 1.11).

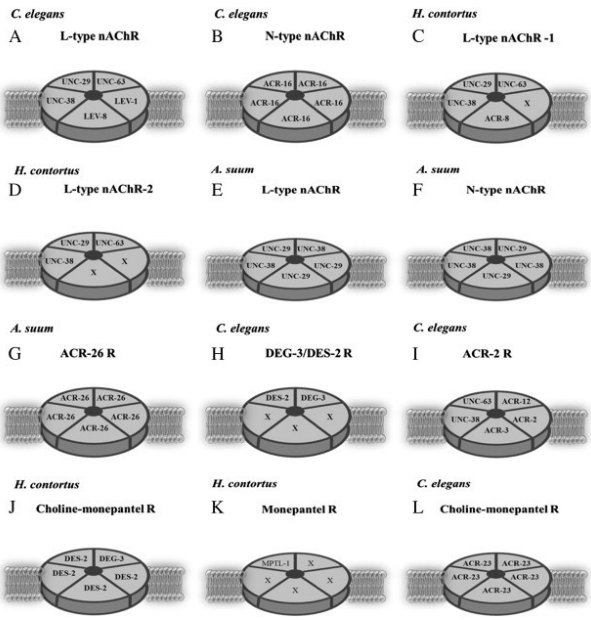

Figure 1.11 Examples of different subunit stoichiometry that defines receptor subtype in nematodes. (A-L) represents different subtypes of nematode nAChRs defined by the subunit composition, and interfaces of the receptor. *With permission from ELSEVIER [Parasitology Internatioal]* (Holden-Dye et al., 2013)*, copyright (2020).*

Despite the critical importance of conserving acetylcholine binding and gating, M- N- B- and L- nAChR subunits possess differences in their orthosteric agonist binding pocket permitting differential targeting by bephenium, morantel, levamisole, pyrantel and oxantel while maintaining function as a functional acetylcholine receptor. For instance, the presence of Glu 153 in loop B is necessary for the activity of levamisole (Rayes et al., 2004) and pyrantel (Bartos et al., 2006). However, pyrantel and morantel binding also requires the presence of a Gln 57 in loop D on the complementary subunit (Bartos et al., 2006, 2009).

Pyrantel is generally considered to be an agonist of L- and M-type receptors, but also weakly activates the homomeric N-type nAChR, ACR-16. This receptor is expressed in many tissues, including body wall muscles, motoneurons and head and tail neurons (Holden-Dye et al., 2013). ACR-16 is one of the easier nematode nAChRs to study, attributable to its wide physiological distribution, ability to form homomeric receptors, and requirement for only a single accessory protein, Resistance to Inhibitors of Cholinesterase 3 (RIC-3), for robust functional expression in *X. laevis* oocytes (Abongwa et al., 2016b). RIC-3 is an accessory protein embedded in endoplasmic reticulum membranes that is required for functional expression of the human α7 nAChR and the orthologous nematode ACR-16 (Vallés and Barrantes, 2012). ACR-16 is translated as individual subunits which are folded and integrated into the membrane of the endoplasmic reticulum where they subsequently oligomerize into pentamers (Treinin, 2008). It is believed that

RIC-3 directly interacts with nAChR subunits in the endoplasmic reticulum membrane and acts as a chaperone protein to facilitate receptor oligomerization (Castillo et al., 2005; Halevi et al., 2002) and may play a role in stoichiometry determinism for heteromeric nAChRs (Nelson et al., 2003).

Original studies of the *C. elegans* ACR-16 receptor (Cel-ACR-16) were performed in *Xenopus* oocytes in the absence of RIC-3, and these authors noted the difficulty of achieving functional expression (Ballivet et al., 1996; Raymond et al., 2000). Since then, ACR-16 has been characterized in the parasitic nematodes *A. suum* (Abongwa et al., 2016b), *Parascaris equorum* (Charvet et al., 2018) and *A. caninum* (Choudhary et al., 2019), but not from a human hookworm parasite until this thesis. Previous studies validated the agonist effects of nicotine and pyrantel and substantiated the insensitivity of levamisole on N-type receptors. Interestingly, oxantel is considered to be an N-type selective agonist (Martin et al., 2004), and ACR-16 receptors are not activated by oxantel in oxantel-insensitive parasites. This will be further addressed in the electrophysiological and *in silico* homology modelling experiments reported in this thesis.

Chapter 2: A Functional comparison of ACR-16 receptors from *Necator americanus* and *Ancylostoma ceylanicum*.

2.1 INTRODUCTION

Infection by hookworms in the family *Ancylostomidae* is a source of significant morbidity in humans and companion animals, with several species capable of invading the skin of human hosts and causing an inflammatory dermal syndrome known as CLM (Hochedez and Caumes, 2007). However, the vast majority of patent human infection is caused by *N. americanus* and *A. duodenale*, with a lesser contribution from the zoonotic parasite of dogs and cats, *A. ceylanicum* (Hoagland and Schad, 1978; Traub, 2013). These parasites are associated with low mortality rates, but a notable longevity of infection in the intestine of their host, where they feed on blood. Untreated hookworm infections account for anemia and malnutrition responsible for large economic productivity losses (Hotez, 2008) and over 4 million DALYs lost (Bartsch et al., 2016). Furthermore, these organisms are well-suited to adapt to and proliferate in the moderate increases in temperature associated with global climate change, and represent a continuing challenge for reducing the prevalence and spread of neglected tropical diseases (Blum and Hotez, 2018; Okulewicz, 2017; Weaver et al., 2010). The primary means used to reduce the severity of their social and economic impact is through the use of anthelmintics, drugs that remove helminths from their hosts. However, there are incongruities in susceptibility to anthelmintics among the different species of hookworm (Kotze et al., 2004). For instance, *Ancylostoma* spp. are highly sensitive to the ML IVM, while *N. americanus* is incompletely cleared by doses up to 25 mg/kg in hamsters

(Behnke et al., 1993; Tritten et al., 2012a). The extent to which differences in drug targets across hookworm species govern anthelmintic efficacy has not been fully investigated. This is especially important for drugs that target other STH but cannot be used against hookworm, as is the case for oxantel, used to treat *Trichuris* spp. (Keiser et al., 2013). To better understand the basis of differential species responses to anthelmintics, one must first characterize the drug targets and compare their function between closely related species; this is the purpose of this chapter.

Some of the most important classes of anthelmintic targets are the nAChRs. Nematode acetylcholine-gated cation channels are responsible for fast, excitatory ionotropic neurotransmission required for a range of essential physiological functions, including movement (Touroutine et al., 2005), feeding (McKay et al., 2004), and egg laying (Duerr et al., 2001) via regulation of muscle contractions. Nematode nAChRs are orthologous but pharmacologically distinct from their vertebrate host counterparts, providing specificity for drug targeting (Atchison et al., 1992); anthelmintics acting on nematode nAChRs induce paralysis and death and consequent expulsion from the host. Nematode nAChRs include 4 subtypes, B- L- M- and N-type nAChRs, characterized by their subunit composition and preferential sensitivity to bephenium, levamisole, morantel and nicotine, respectively (Courtot et al., 2015; Martin et al., 2005). The major N-type nAChR subunit is encoded by *acr-16*, which forms functional homopentameric receptors in the presence of the accessory protein RIC-3 (Bennett et al., 2012), and has been characterized from *C. elegans* (Ballivet et al., 1996; Raymond et al., 2000), *A. suum* (Abongwa et al., 2016b), *P. equorum* (Charvet et al., 2018) and the dog hookworm *A. caninum* (Choudhary et al., 2019). ACR-16 is ideal for the study of ion channels as drug targets because of the growing body of functional data from multiple parasitic species, the ease of expression in *Xenopus* oocytes with only a single accessory protein, and the presence of a single subunit interface type (the site of agonist binding)

since it is a homopentamer. In contrast, L-nAChRs exist as heteropentamers composed of 5 different subunits in *C. elegans* that are each required for functional expression, with different subunit combinations existing in different species of parasitic nematodes (Boulin et al., 2011; Buxton et al., 2014; Neveu et al., 2010; Williamson et al., 2009). This means that there are numerous possible interfaces in any given cell and each combination likely has distinct binding sites. These receptors also require multiple accessory proteins for functional expression (Boulin et al., 2011, 2008; Duguet et al., 2016).

The function of ACR-16 has not been reported in hookworms that infect humans, in which recent failure of treatment with the BZDs albendazole or mebendazole has been documented (Humphries et al., 2011; Soukhathammavong et al., 2012). This fact alone provides justification for research on the physiology of the hookworm nervous system. Characterizing these receptors also contributes to a growing body of literature on ACR-16 from different species and enables previously unavailable comparison of sequence and function from organisms that primarily infect humans. Furthermore, few alternative drugs are approved for treatment. Recent work has also identified an alarming increase in treatment failure of canine hookworm infections in the United States (Castro et al., 2019). The WHO put forth a goal of reducing morbidity of helminthiases by treating 75% of human childhood hookworm infections by 2030, extended from the original 2010 and 2020 deadlines (World Health Organization, 2020, 2012). However, this goal relies solely on the use of mebendazole or albendazole. Also approved for this indication, but little used in MDA campaigns for hookworm control, are pyrantel pamoate and levamisole, albeit with more limited reported success (Botero and Castano, 1973; Keiser and Utzinger, 2008; Krepel et al., 1993; Reynoldson et al., 1997). The increasingly intensive use of BZDs raises the threat of the selection and spread of drug-resistant hookworm populations. This, coupled with the fact that the global

prevalence of hookworm infection has only dropped by 9% since 1996 (Hotez, 2018) despite large scale deworming programs, illustrates the urgent need to identify new safe and effective treatments to minimize the risk of rising hookworm infection prevalence. By characterizing understudied nematode ion channels, we may better understand the mechanisms by which current anthelmintics work and discover new targets to aid in the discovery of novel anthelmintics.

Here I report the identification and cloning of cDNAs encoding *acr-16* from *A. ceylanicum* and *N. americanus*, the first pLGICs studied from hookworm species that infect humans. Using two-electrode voltage clamp electrophysiology, I characterized these receptors after heterologous expression in *Xenopus* oocytes and compared their pharmacological profiles. Despite high sequence similarity between these hookworm *acr-16*s and with previously characterized nematode *acr-16*s, our results identify key differences in their pharmacological profiles that emphasize the potential importance of species-specific drug discovery programs for hookworm infection, and perhaps for all parasitic nematodes. These data provide the first molecular rationalization for the lack of efficacy of oxantel for these species, and show weak but measurable effects from pyrantel and levamisole exposure.

2.2 RESULTS

2.2.1 Cloning

Nested PCR of *ace-* (accession # MT163735) and *nam-acr-16* (accession # MT163736) each generated transcripts encoding 498 amino acid polypeptides. The sequence alignment (Figure 2.1) illustrates that both subunits contain signature pLGIC cation characteristics, including a motif for

cation selectivity, presence of a predicted cys-loop, 4 transmembrane domain regions, and a predicted signal peptide cleavage site after residue 21.

The amino acid sequences of Nam- and Ace-ACR-16 share 75-78% identity with ACR-16 from the clade III nematodes *A. suum* and *P. equorum*, as well as the clade V free-living nematode *C. elegans* (Meldal et al., 2007). The greatest degree of shared identity was among the hookworm ACR-16 receptors (95-98%) and the closely related *H. contortus* receptor Hco-ACR-16 (84-88%). Ace- and Nam-ACR-16 differ in amino acids at 22 residues, primarily within the putative signal peptide, and in the C-terminal region. The *A. ceylanicum* and *A. caninum* receptors differ in 8 residues, half of which are located in the signal peptide. Regions of highest similarity include the transmembrane domains and the large extracellular domain; however, some differences exist in the aromatic loop regions that comprise the orthosteric ligand binding domain and could play a role in differential ligand specificity.

A

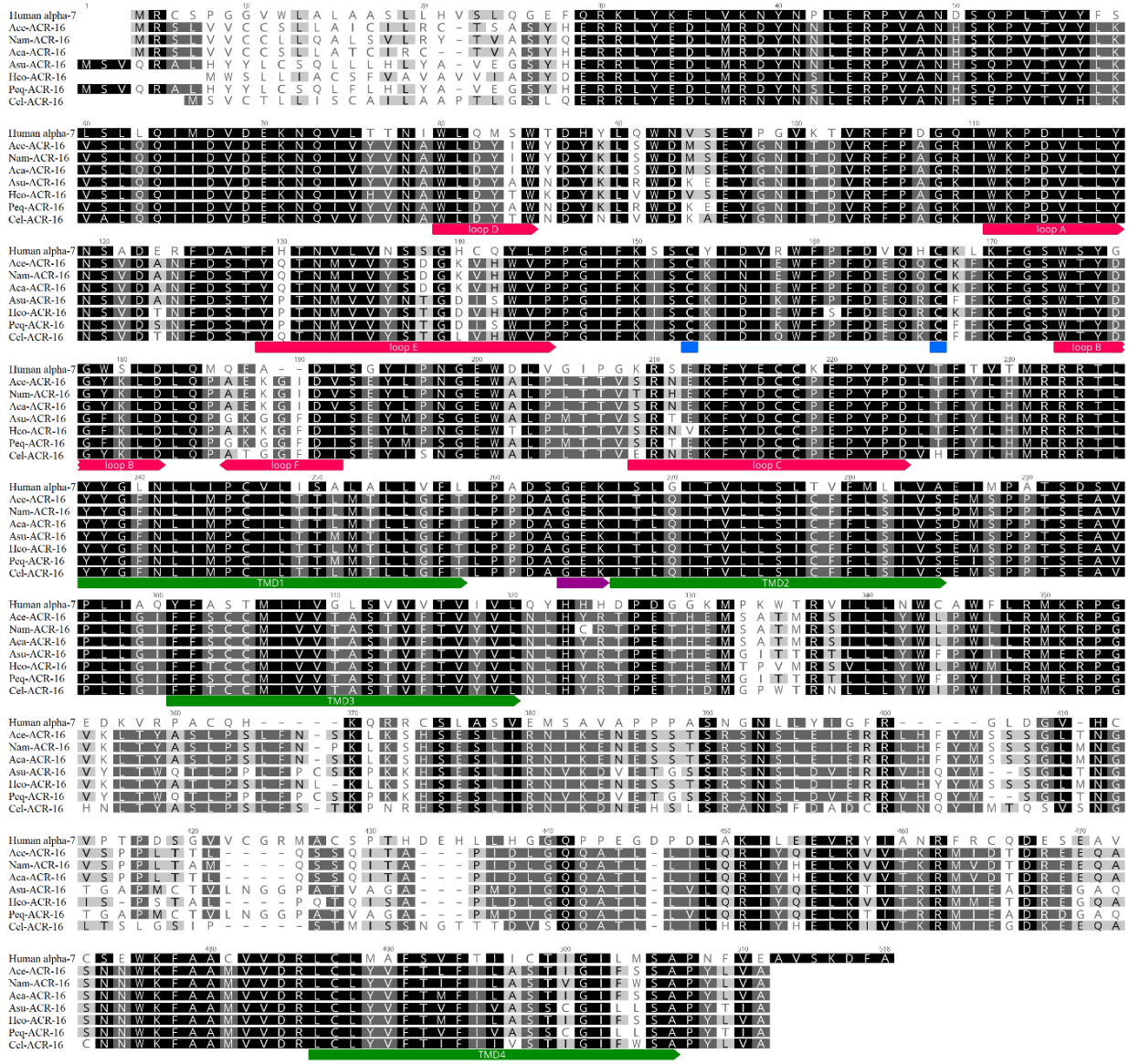
Human alpha-7
Ace-ACR-16
Nam-ACR-16
Aca-ACR-16
Asu-ACR-16
Hco-ACR-16
Peq-ACR-16
Cel-ACR-16
loop D
loop A
loop E
loop B
loop B
loop F
loop C
TMD1
TMD2
TMD3
TMD4

B

	Human α-7	Ace-ACR-16	Nam-ACR-16	Aca-ACR-16	Asu-ACR-16	Hco-ACR-16	Peq-ACR-16	Cel-ACR-16
Human α-7		44.4	43.8	44.0	43.5	43.7	43.5	44.2
Ace-ACR-16	44.4		95.4	98.0	77.5	87.5	76.9	78.0
Nam-ACR-16	43.8	95.4		96.0	75.7	86.3	75.0	77.8
Aca-ACR-16	44.0	98.0	96.0		76.5	87.5	75.9	77.6
Asu-ACR-16	43.5	77.5	75.7	76.5		78.4	99.2	73.4
Hco-ACR-16	43.7	87.5	86.3	87.5	78.4		78.4	77.6
Peq-ACR-16	43.5	76.9	75.0	75.9	99.2	78.4		73.0
Cel-ACR-16	44.2	78.0	77.8	77.6	73.4	77.6	73.0	

Figure 2.1 (A) Sequence alignment of ACR-16 from *A. ceylanicum* (accession # MT163735), *N. americanus* (accession # MT163736) *A. caninum* (accession # QEM53385.1), *C. elegans* (accession # CCD64102.1), *H. contortus* (accession # AZS27833.1), *A. suum* (accession # KP756901), *P. equorum* (accession # AZS27834.1), and the human α7 acetylcholine receptor subunit (accession # P36544.5). Amino acids are shaded by consensus sequence similarity; black is most, and white is least similar. The ECD ligand binding loops A-E are denoted in red, the characteristics cys-loop is indicated in blue, the cation selectivity motif is shown in purple and the transmembrane domains are in green. (B) % Identity matrix of the polypeptide sequences for comparison.

2.2.2 Functional expression of hookworm ACR-16

The human hookworm ACR-16 receptors expressed relatively quickly in *Xenopus* oocytes, producing currents on a timescale and magnitude similar to those reported for other ACR-16s (Abongwa et al., 2016b; Charvet et al., 2018; Choudhary et al., 2019; Raymond et al., 2000). Maximal responses were detected 48 hr post-cRNA injection and currents were detectable until oocyte quality degraded to the point of loss of membrane integrity, roughly 4-5 days after injection. Oocytes expressing Ace-ACR-16 alone elicited very small but detectable current responses upon an initial 1 mM acetylcholine application, used to screen for functional expression (Figure 2.2A).

Oocytes co-injected with *ace-acr-16* and *H. contortus ric-3* elicited large concentration-dependent currents in response to acetylcholine as early as 24 hr after injection (Figure 2.2B), while oocytes injected with water produced no response. In comparison, formation of any functional Nam-ACR-16 receptors required the presence of Hco-RIC-3 (Figure 2.2A), but with some notable and surprising differences. Nam-ACR-16 required 48 hr for functional expression, the magnitude of the acetylcholine response was significantly smaller than for Ace-ACR-16, and the signal from repeated exposures to acetylcholine diminished over time (Figure 2.2C), in contrast to responses in *ace-acr-16* injected oocytes, which remained constant. These differences were consistent regardless of the amount of *nam-acr-16* cRNA injected.

A

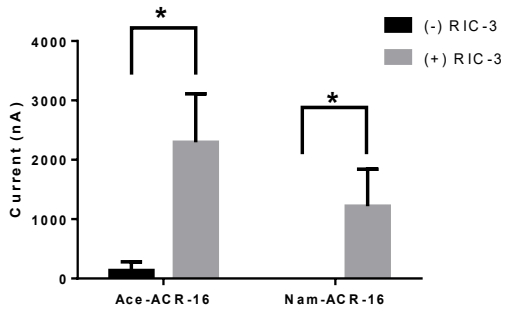

B

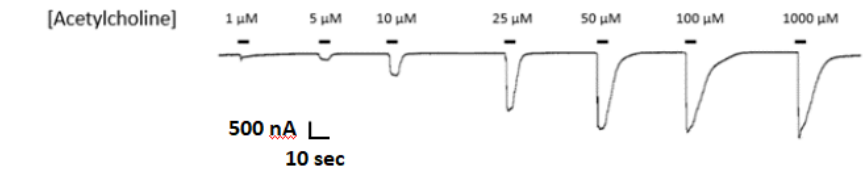

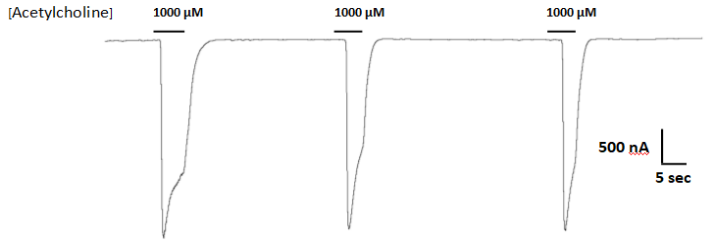

C

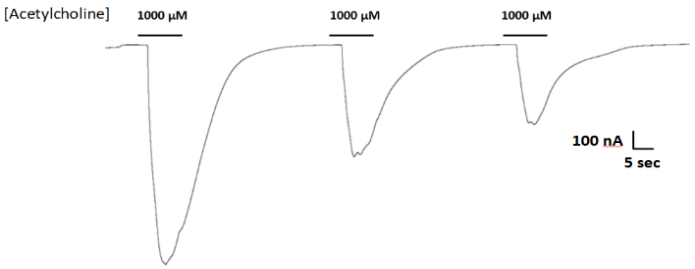

Figure 2.2 Functional expression of hookworm ACR-16 receptors. (A) amplitude of current response to 1 mM acetylcholine in the presence or absence of the accessory protein Hco-RIC-3 measured 48 hr after injection. Nam-ACR-16 (+) Ric-3 n= 9 all else n = 7; *t-test, $p < .05$. (B) Ace-ACR-16 response profile to increasing (top) and repeated (bottom) concentrations of acetylcholine. (C) Nam-ACR-16 response profile to repeated concentrations of acetylcholine. Repeated acetylcholine exposures produce decreasing current responses.

2.2.3 Effect of time between agonist exposures on maximal responses

To investigate the reduction in Nam-ACR-16 signal from repeated exposures to a single concentration of acetylcholine, we measured the change in current amplitude as a function of time

between exposures to 1 mM acetylcholine (Figure 2.3). Oocytes were allowed to recover from voltage clamp and equilibrate in ND96 buffer for 1 min before recording initial responses. Incubation time prior to first exposure to acetylcholine did not influence the magnitude of the initial response.

A

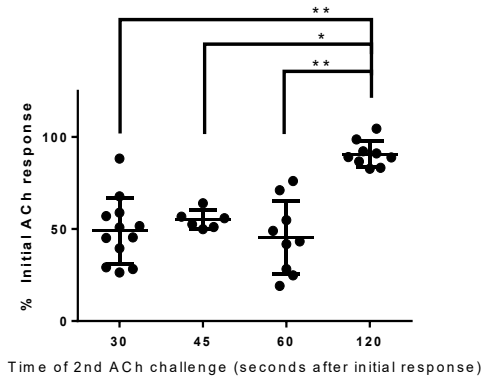

B

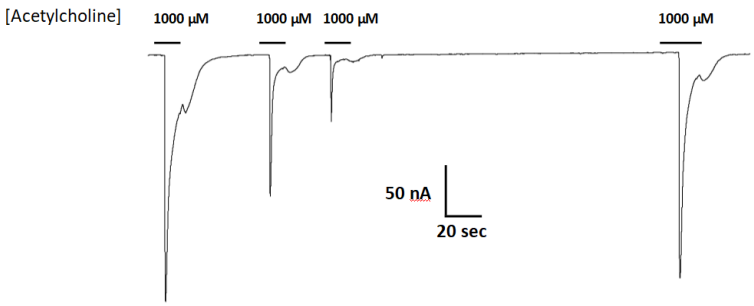

Figure 2.3 (A) The effect of time between subsequent applications of 1 mM acetylcholine on the magnitude of current elicited from Nam-ACR-16. Oocytes given 2 min recovery time from an initial acetylcholine exposure produced significantly larger currents than any other timepoint. Data at each time point were derived from experiments conducted on oocytes from at least two different frogs. n > 6, *ANOVA, p =

.0004, **p < .0001. (B) Representative tracing of current responses induced by varying time between exposures to acetylcholine.

If agonist exposure generated a refractory desensitized state in Nam-ACR-16, then lengthening the recovery time between exposures should reproduce maximal responses once a greater proportion of receptors was again primed for activation. Up to 1 min after an initial response to acetylcholine, subsequent applications generated attenuated responses, and a third application sometimes failed to generate a response. Only after 2 min continual washout with ND96 solution did we see rescue of maximal amplitude, indicating a very slow but completely reversible desensitization period.

2.2.4 Pharmacology of hookworm ACR-16

In addition to the differences reported above, we found that acetylcholine was more potent on Ace-ACR-16 (EC_{50} = 20.64 ± 0.32 μM; Hill slope = 1.55 ± 0.13) than on Nam-ACR-16 (EC_{50} = 170.1 ± 1 9.23 μM; Hill slope = 1.11 ± 0.37) (Figure 2.4). The lower sensitivity of Nam-ACR-16 was magnified in response to nicotine, which acted as a weak partial agonist for this receptor (EC_{50} = 597.9 ± 59.12 μM; Hill slope = 6.19 ± 1.43; maximal ACh response = 30.4 ± 7.4%). Initial Nam-ACR-16 nicotine trials produced such small currents that we originally suspected degradation of the drug. However, Ace-ACR-16 receptors injected in the same week produced large and reproducible responses to nicotine, comparable to those elicited from acetylcholine (EC_{50} = 24.37 ± 2.89 μM; Hill slope = 1.43 ± 0.15) (Figure 2.4B).

A

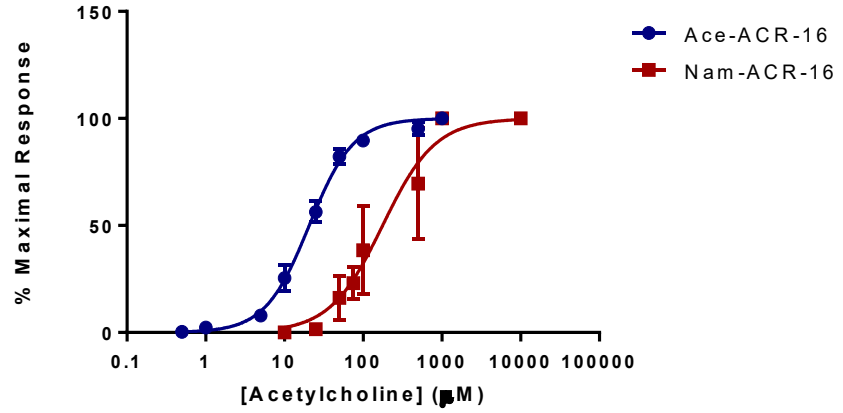

B

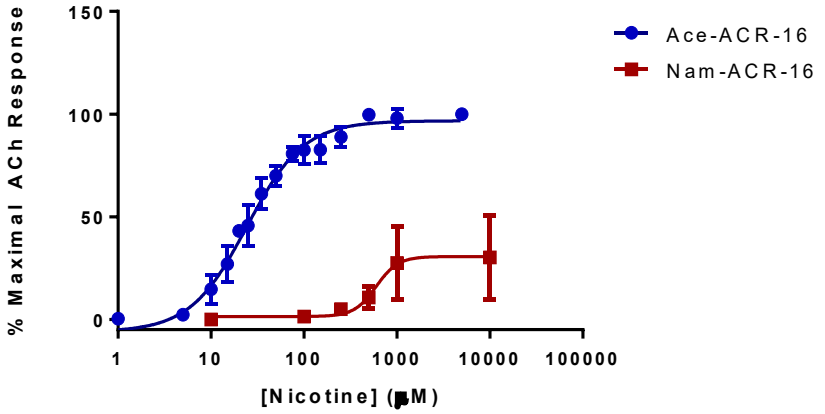

Figure 2.4 Concentration-response curves for acetylcholine (A) and nicotine (B) on Ace- and Nam-ACR-16. Individual oocytes were exposed to increasing concentrations of acetylcholine and all responses were standardized to the maximal current achieved within each oocyte. n>6. Individual oocytes were exposed to repeated maximal concentrations of acetylcholine to determine stability of response, and to serve as a maximal effect reference to standardize all nicotine current responses. Nicotine acts as a full agonist on Ace-ACR-16 but as a weak partial agonist of Nam-ACR-16 n >6.

2.2.5 Current voltage trials

ACR-16 gates Na^+ and Ca^{2+} ions into the cell, which in turn can activate endogenous intracellular Ca^{2+}-gated Cl^- channels in *X. laevis* oocytes (Miledi and Parker, 1984). To ensure that receptor activation measurements were not influenced by this cascading Ca^{2+} signalling, we incubated oocytes expressing Ace-ACR-16 with the intracellular Ca^{2+} ion chelator BAPTA-AM (100 µM) for 1 hr. Following incubation, oocytes were washed in ND96 and voltage clamp measurements made immediately after. This receptor was chosen because the stability and reproducibility of tracings provided better accuracy than Nam-ACR-16 for comparing BAPTA-treated versus untreated oocytes. Figure 2.5A shows that BAPTA-AM treatment did not affect the sensitivity or activation profile of Ace-ACR-16. However, it did alter the reversal potential ((+)BAPTA-AM = 13.55 mV; (-)BAPTA-AM = -8.53 mV) and slope ((+)BAPTA-AM = 34.6 ± 2.4; (-)BAPTA-AM = 67.7 ± 2.6) of the current-voltage relationship, indicating an altered population of ions transported across the membrane (Fig. 5B). Because of the variable pharmacology of ACR-16 receptors reported in the literature, we sought to validate the gating of Na^+ and Ca^{2+} ions by completely replacing the buffer ion composition with sodium gluconate (96 mM) as an anion replacement, glucosamine HCl (96 mM) as a cation replacement or $CaCl_2$ (1.8 mM). Reversal potential values from these ion replacement curves are consistent with the values indicative of a, primarily Na^+, cation-gated nAChR (Harrow and Gration, 1985). In the absence of Na^+ and Ca^{2+} ions in solution, no current was detected when acetylcholine was applied (Fig. 5C, glucosamine HCl).

A

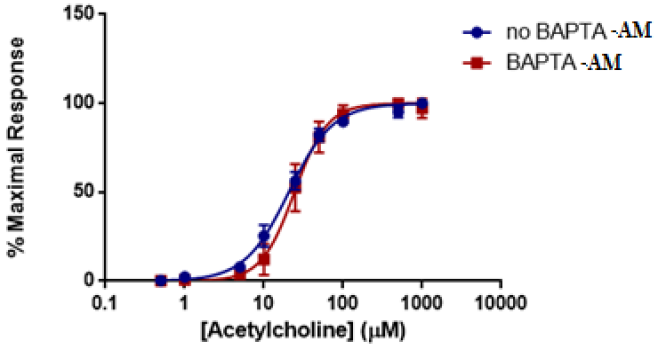

No BAPTA-AM	EC50 = 20.64 ± 1.06 µM	Hill = 1.55 ± 0.13
BAPTA-AM	EC50 = 24.32 ± 1.04 µM	Hill = 2.1 ± 0.16

B

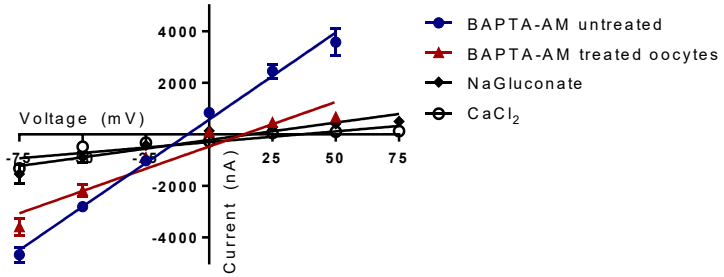

C

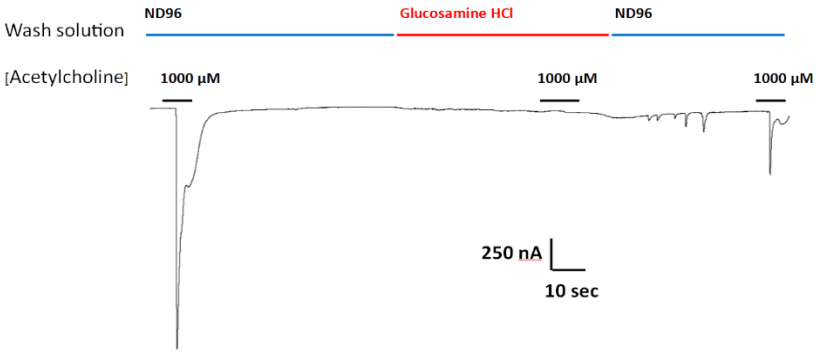

Figure 2.5 (A) BAPTA-AM was used to examine the role of activating intrinsic Ca^{2+} sensing Cl^- channels induced by Ca^{2+} influx from Ace-ACR-16 activation. BAPTA-AM treatment had no effect on the ability of acetylcholine to activate Ace-ACR-16 in oocytes. n>5; Vc = -60 mV (B) Current-voltage relationship of ACR-16 induced by 100 μM acetylcholine in ND96 (reversal potential = -8.5 mV), ND96 with BAPTA-treatment (reversal potential = 13.6 mV), 96 mM sodium gluconate (reversal potential = 15.9 mV), 1.8 mM $CaCl_2$ (reversal potential = 35.8 mV). BAPTA-associated inhibition of Ca^{2+} gated Cl^- channels altered the conductance from activating ACR-16. Ion replacement with either sodium gluconate, or $CaCl_2$ altered conductance in a manner predicted by theoretical values attributable to Na^+ and Ca^{2+} ions. Oocytes were exposed to 100 μM acetylcholine at holding potentials beginning at -75 mV and increasing by 25 mV steps to +50 mV. (C) 100 μM acetylcholine produced no current responses in 96 mM glucosamine HCl solution. Channel activity in response to acetylcholine was restored when this solution was replaced with ND96.

2.2.6 Activity of anthelmintics and classic cholinergics against the ACR-16 receptors

Previous studies indicate that *Ancylostoma* spp. and *N. americanus* respond differently to some anthelmintics (Behnke et al., 1993; Richards et al., 1995; Tritten et al., 2011). To investigate differences in anthelmintic sensitivity between these receptors, we tested them against a panel of drugs, including cholinergic anthelmintics.

A

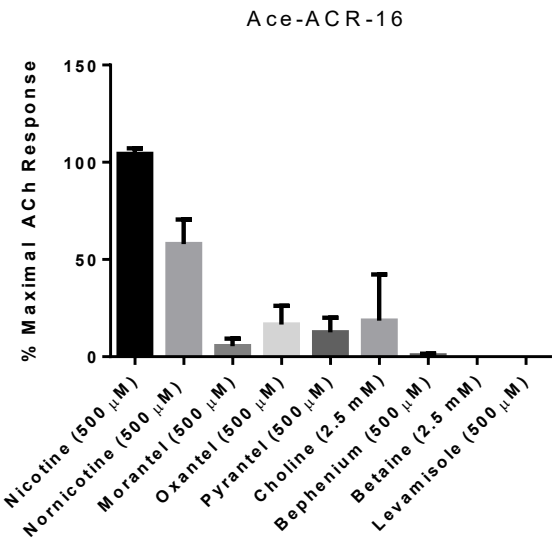

B

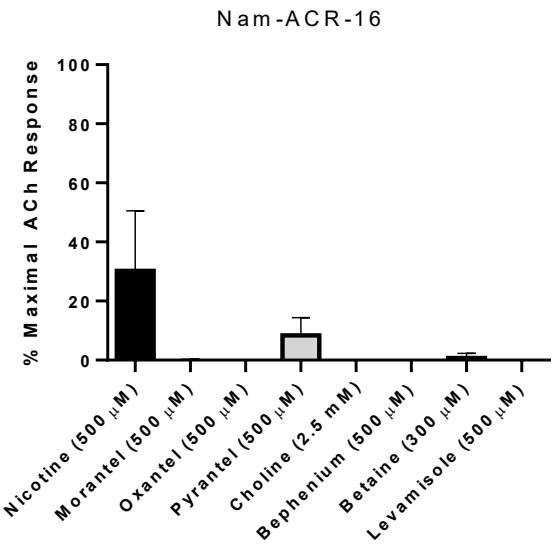

C

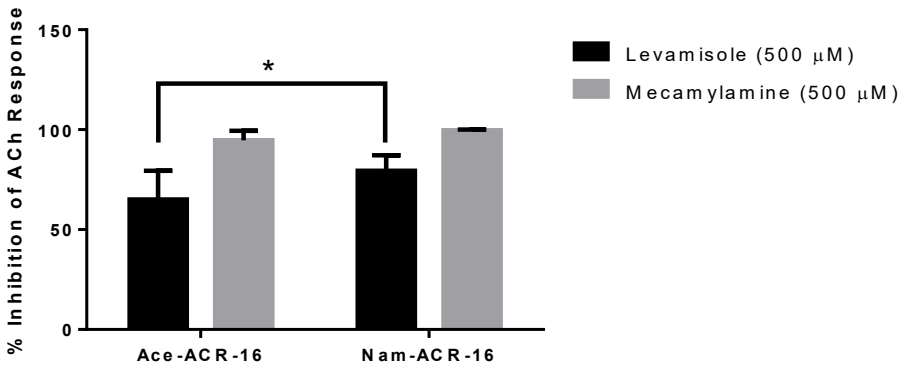

Figure 2.6 (A) Ace-ACR-16 and (B) Nam-ACR-16 agonist response profiles to classical cholinergics and anthelmintics. All current responses are standardized relative to that of a maximal 1 mM acetylcholine response; n = 5 (C) inhibition of EC_{50} acetylcholine-induced responses in Ace- and Nam-ACR-16 by levamisole and the nAChR antagonist mecamylamine; $n \geq 4$; *t-test, p=.0419.

Nematodes possess 4 subtypes of nAChRs: nicotine- (N-type), levamisole- (L-type), morantel- (M-type) and bephenium-sensitive (B-type). As expected for an N-type nAChR, neither receptor was activated by levamisole or bephenium. Ace-ACR-16 was only weakly activated by the tetrahydropyrimidines oxantel (15.6 ± 9.6% maximal acetylcholine response), pyrantel (12.5 ± 7.5%) and morantel (5.5 ± 3.9%), while Nam-ACR-16 was only activated by pyrantel (8.3 ± 6.0%) (Figure 2.6A). Raymond et al. (2000) showed that *C. elegans* ACR-16 is antagonized by levamisole. To further characterize the hookworm ACR-16s, we assayed compounds and anthelmintics known to modulate the activity of pLGICs. Supporting the findings of Raymond et al. (2000), we observed significant inhibition of acetylcholine-induced channel activation by levamisole for Ace-ACR-16 (65.1 ± 14.3% inhibition) and Nam-ACR-16 (79.5 ± 7.7% inhibition) (Figure 2.6B).

The classical non-competitive cholinergic antagonist mecamylamine was also inhibitory, with comparable inhibition of acetylcholine responses for Ace-ACR-16 (94.7 ± 4.7% inhibition) and Nam-ACR-16 (99.7 ± 0.4% inhibition) (Figure 2.6B). Up to 10 μM IVM had no effect on acetylcholine-induced currents after either pre-treatment or simultaneous exposure of oocytes.

2.3 DISCUSSION

2.3.1 Expression and agonist activity of acetylcholine and nicotine

Our results indicate that the ACR-16 sequence is highly conserved across nematode species, especially in the ligand-binding and transmembrane domains. With such high similarity, especially in the ligand-binding domain, one would predict very similar pharmacological profiles, but there are surprising differences. Acetylcholine was a full agonist for both receptors, but nicotine was a

weak partial agonist on the Nam-ACR-16 receptor and a full and potent agonist of the Ace-ACR-16. Agonist binding is determined by interactions with residues in the orthosteric binding pocket, which differ between these species, and these differences are analyzed in detail in Chapter 3.

Another unexpected difference is that Ace-ACR-16 responses were in the large microamp range, whereas the Nam-ACR-16 receptor generated currents in the nanoamp to small microamp range. This was unexpected because the amplitude of *A. caninum* ACR-16 responses reported by Choudhary et al. (2019) better match with those from *N. americanus*, rather than *A. ceylanicum*, which is in the same genus. Ion selectivity and conductance are determined by residues that line and are proximal to the TM2 pore of the channel (Thompson et al., 2010), but the three hookworm ACR-16 receptors have identical sequences spanning the region of TM1-TM3. Differences in magnitude of responses could be attributable to differences in expression levels resulting from the signal peptide sequence. Signal peptide function relies on the presence of hydrophobic and charged residues (Von Heijne, 1985) to embed pLGICs into endoplasmic reticulum membranes for direction into the plasma membrane (Walter and Blobel, 1980). The Nam-ACR-16 signal sequence possesses polar and non-polar residues that differ from those in Ace-ACR-16, and both these receptors also differ from Aca-ACR-16 in the position of an Arg in the signal peptide. This level of regulation can control the rate at which a protein exits the endoplasmic reticulum (Li et al., 1996), which may explain why Nam-ACR-16 took longer to reach maximal functional expression. Additional mutagenesis and signal peptide swapping experiments are necessary to determine the extent, if any, to which signal peptide differences influence the functional expression of ACR-16 receptors in oocytes.

2.3.2 Desensitization of Nam-ACR-16

The mechanisms previously mentioned, however, do not explain the decreased Nam-ACR-16 responses after repeated agonist exposure. Agonist binding increases the likelihood of ACR-16 entering an open ion conducting conformational state, but once closed again, those receptors that are still agonist-bound represent a desensitized population unable to gate ions. Using single channel patch-clamp electrophysiology to determine desensitization rate constants may resolve whether altered desensitization is responsible for this phenomenon (Granfeldt et al., 2006).

One possible source of Nam-ACR-16 desensitization is the sequence of the intracellular TM3-TM4 variable loop, which is known to affect channel expression, agonist EC_{50} values and desensitization (Hu et al., 2006; Kelley et al., 2003; Kracun et al., 2008). Residues of this loop that are proximal to the TM3 and TM4 domains may be involved in conformational changes associated with desensitization and alter activation of the receptor (McKinnon et al., 2012). In the region proximal to TM3, Nam-ACR-16 possesses a Cys320 compared to a Tyr in the other hookworm receptors, a difference that warrants further investigation into potential functional consequences.

The TM3-TM4 loop is also a site of phosphorylation-related regulation of pLGICs. Phosphorylation significantly increases recovery from both rapid (msec) desensitization (Hoffman et al., 1994) and slower (sec-min), Protein Kinase A-dependent, long-term desensitization of nAChRs expressed in *Xenopus* oocytes (Paradiso and Brehm, 1998). Kinases also induce internalization of pLGICs (Velázquez-Flores and Salceda, 2011), and chronic nicotine exposure causes desensitization of mammalian nAChR (Fenster et al., 1999). Of relevance to kinase regulation, Nam-ACR-16 has a Pro364 in place of a Ser or Thr present in all other published nematode ACR-16s.

Functional expression also relies on the presence of other key residues. The recently published *H. contortus* ACR-16 was not successfully functionally expressed, despite having high sequence identity with known functional ACR-16s (Charvet et al., 2018). An important caveat is that this protein (accession code # AZS27833.1) differs from an earlier published sequence (accession code # ABW07339.1) by a single amino acid in the cys-loop (Ser versus Pro in ABW07339.1). This Pro residue has been reported to be of critical importance for ligand-activation in the pLGIC family (Lummis et al., 2005; Rienzo et al., 2016), and highlights the role that a single residue can play in receptor activation and expression.

2.3.3 Levamisole inhibition of ACR-16: does this play a role in its anthelmintic activity?

In line with all published ACR-16 data, neither Ace- nor Nam-ACR-16 was activated by levamisole, the anthelmintic activity of which is strongly associated with L-type nAChRs (Lewis et al., 1980). Of note, the first report of ACR-16 function indicated that levamisole was an antagonist of this receptor (Ballivet et al., 1996). Our results also show strong inhibition of acetylcholine responses by levamisole. The effect of levamisole exposure in ACR-16 knockout strains of *C. elegans* was slightly smaller, but not significantly so, than in wild-type worms. (Touroutine et al., 2005); these authors did not rule out the possibility that ACR-16 sensitivity to levamisole is redundant to, and masked by, the presence of L-nAChRs. When the *C. elegans* L-type nAChR was abolished by replacement with a null *unc*-29 allele, roughly 10% of worms were still paralyzed by exposure to levamisole (Duguet et al., 2016), suggesting a small but detectable contribution of a subset of levamisole-sensitive secondary targets. The significance of this interaction for the therapeutic properties of levamisole is unclear, and we cannot discount the possibility that inhibition of ACR-16 receptors plays a role in its anthelmintic action.

2.4 CONCLUSION

Our aim was to characterize ACR-16s from human hookworms and determine differences in pharmacology attributable to basic physiology and species-specificity in anthelmintic effects. This is important because there is a complete lack of information regarding pharmacodynamics of ionotropic-acting anthelmintics on the species of hookworms that infection humans. These data are important to provide information on the pharmacophore of current anthelmintics which is important for the informed use of these drugs, and to monitor for sequence changes related to drug resistance. There is also a large gap in knowledge of the basic biology of the nervous system of *N. americanus* and *A. ceylanicum* and this thesis provides novel insights into differences in excitatory synaptic transmission in these species.

These receptors were activated by acetylcholine and nicotine, the defining features of N-type nAChRs, and differed in sensitivity to the anthelmintic oxantel, which warrants further investigation. Together with existing data on ACR-16s of other nematode species, our data suggest a high degree of variability in response profiles to anthelmintics even among closely related nematode species. These implications caution against generalizing functional results obtained on ion channel drug targets from one nematode to another and highlight the importance of relating therapeutic outcomes to the unique nature of each drug target. These observations were explicitly not clear for ACR-16 before the presentation of this thesis. One way to analyze structural differences in anthelmintic binding to pLGICs is the use of *in silico* homology modelling, as described in the next chapter of this thesis.

Chapter 3: *in silico* homology modelling of the ACR-16 orthosteric binding site from *Necator americanus* and *Ancylostoma ceylanicum*

3.1 INTRODUCTION

In the previous Chapter, I presented functional data of ACR-16 from two closely related hookworm species. Results from this study showed that pyrantel had similar effects on the receptors from both species, in support of findings that it paralyzes worms of both species roughly equally (Richards et al., 1995). However, we also identified a greater ability of nicotine and oxantel to activate Ace-ACR-16 compared to Nam-ACR-16. Oxantel is effective against whipworm infections (Barda et al., 2018; Garcia, 1976; Howes Jr, 1972; McFarland, 1982), but lacks efficacy against hookworms (Bhopale and Bhatnagar, 1988; Keiser et al., 2013; Moser et al., 2016; Speich et al., 2014), and unfortunately no information exists on the characterization of an oxantel-specific target in any of these species. A combination therapy of pyrantel and oxantel has been effective in treating STH infection (Grandemange et al., 2007; Rim et al., 1975), but high level of pyrantel resistance in *A. caninum* (Kopp et al., 2007) is indicative of the threat of drug resistance. Interestingly, at doses of 1 mg/kg, oxantel can kill L3 *A. ceylanicum* (9% killed compared to 100% survival of *N. americanus* L3) (Keiser et al., 2013) and in the previous chapter, I showed the ability of oxantel to partially activate Ace- but not Nam-ACR-16 receptors. Oxantel is believed to show preference for N-type nAChRs (Martin et al., 2004), and it remains to be seen whether ACR-16 from *Trichuris* spp. are more sensitive to oxantel than Ace-ACR-16, or why it fails to elicit currents from Nam-ACR-16. Functionally expressed Cel-ACR-16 also shows a lack of full agonist activity

by oxantel (Raymond et al., 2000) but no structural rationale exists to explain the lack of efficacy. Therefore, in this chapter I use the proram Modeller to perform predictive *in silico* homology modelling to attempt to fill in gaps of knowledge pertaining to the basis for species differences in pharmacology of the ACR-16 receptor.

Homology modelling is a very useful tool to study structure-activity relationships of pLGICs that lack crystal structures. High resolution electron microscopy of the *Torpedo marmorata* AChBP has been instrumental in studying the ECD of nAChRs (Unwin, 2005), and enables researchers to identify residues of interest for mutation (Ott et al., 1996) and predict inter-molecular interactions of ligands. These features are increasingly used to generate massive libraries of compounds (Wishart et al., 2006) which can be used in large-scale high throughput *in silico* drug screens to identify potential lead compounds (Ekins et al., 2007). Because these data are only predictive, it is vital to experimentally validate any *in silico* results (or in this thesis, backtrack to explain previous functional results), but they remain an important step in information gathering to design further experiments.

In this chapter, I address putative structural determinants for differential agonist function on ACR-16 from *N. americanus*, *A. ceylanicum C. elegans* and *T. muris* by using AutoDock Vina to predict binding energies. In doing so, my goal is to not only validate/explain my previously reported functional data, but also to identify residues of interest for future study, to aid in elucidating pharmacophores that underlie the mechanism of action of these anthelmintics and to compare results with the predicted structure of the receptor from a model organism. Furthermore, there remains an unanswered question: can the generally smaller magnitude of responses in Nam-ACR-16 compared Ace-ACR-16 be explained by generally lower agonist affinity?

The *in silico* analyses of the receptors studied in the previous chapter stand alone as Chapter 3, and do not specifically pertain to the pharmacological effects of the anthelmintics on Nam-ACR-16 and Ace-ACR-16 described in Chapter 2. Beyond ACR-16 from these species, Chapter 3 includes *in silico* experiments describing the features of ACR-16 from *C. elegans* and *Trichuris muris* and discusses the theme *of C. elegans* as a model (described in detail in the literature review). This chapter also focuses on a predicted rationale for the failure of oxantel to bind and elicit full activation on ACR-16 from *N. americanus*, *A. ceylanicum*, and *C. elegans*, compared to the *in vivo* effectiveness of oxantel on *Trichuris* spp. and our predictions of high affinity binding to a *T. muris* ACR-16. The mechanisms of drug success and failure are of key importance to guide clinical use. These results are further validated by *in vitro* data from a preprint manuscript released after the submission of this thesis, which found oxantel to act as a super-agonist on a Tsu-ACR-16 like receptor (Hansen et al., 2020).

3.2 RESULTS

3.2.1 Generation of homology models

To create *in silico* homology models of the ligand-binding domain of homomeric Ace-ACR-16 and Nam-ACR-16, I used a chimera of the ECD of the human homomeric α-7 nicotinic receptor and *Lymnaea stagnalis* AChBP at 2.80 Å bound to the agonist epibatidine as a template (PDB 3SQ6) (Li et al., 2011) as described in the Methods section 6. This chimera shares 40% sequence identity with both Ace- and Nam-ACR-16, which share 98% sequence identity between them in the ECD region used for modelling. Top Ace-ACR-16 models of dimers generated molpdf scores (representing the sum of restraints in building the models; i.e. the lower score the better) of 3140,

3159 and 3194 compared to scores of 3091, 3151 and 3174 for Nam-ACR-16. The best scoring of these models is shown in Figure 3.1.

A

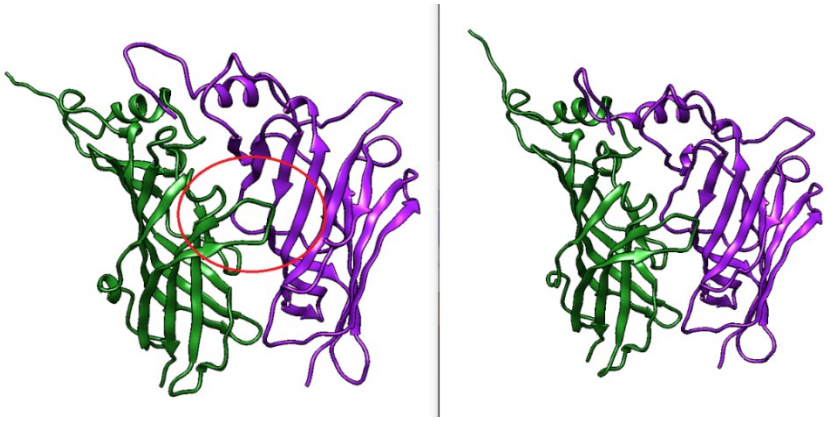

B

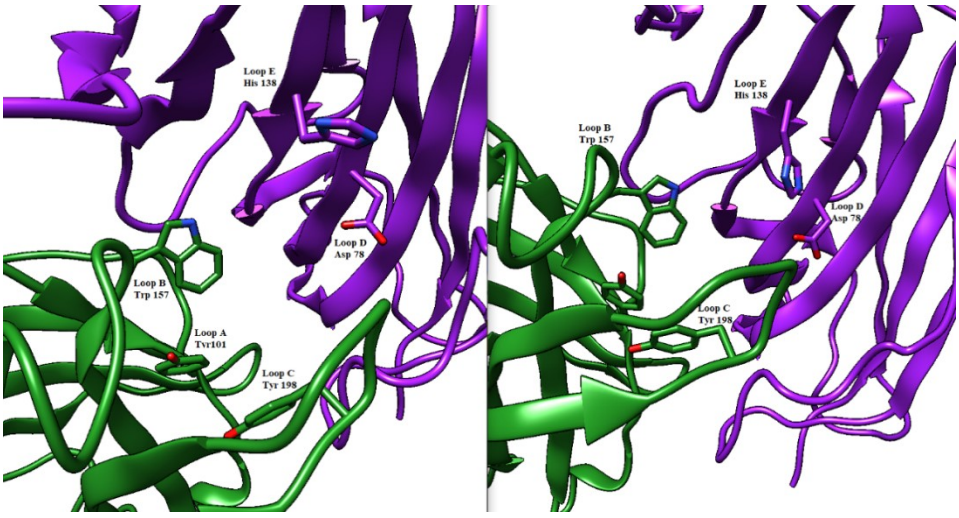

Figure 3.1 (A) Homology model of a dimer of the ECD from Ace-ACR-16 (left) and Nam-ACR-16 (right). The principal (+) subunit is coloured green, and the complementary (-) subunit is coloured purple. A red circle indicates the location of the orthosteric ligand binding domain (B) Zoom in of the binding site of Ace-ACR-16 (left) and Nam-ACR-16 (right). Aromatic residues of the (+) binding loops comprising the aromatic box are indicated along with important residues of the (-) subunit.

3.2.2 In silico docking: acetylcholine and nicotine

Homology modelling and *in silico* ligand docking predictions were used to investigate structural differences between the receptors that might underlie some of the differences in pharmacology. Acetylcholine and nicotine docked into the orthosteric binding pocket of both ACR-16 models with comparable predicted energies (acetylcholine: -4.3 kcal/mol Ace-ACR-16, -4.0 kcal/mol Nam-ACR-16; nicotine: -5.4 kcal/mol Ace-ACR-16, -4.6 kcal/mol Nam-ACR-16) (Figure 3.2). However, docking simulations simply place the ligand in a position to form bonds with the lowest predicted binding energies, and do not take into account hydrogen bonding and π-cation interactions required for activating pLGICs.

Both agonists oriented centrally into the binding pocket of Ace-ACR-16 with their cation nitrogens placed near aromatic residues of loops B and C, notable for forming important π-cation bonds with ligands (Dougherty, 2008). In comparison, acetylcholine and nicotine docked more peripherally into Nam-ACR-16, 4-5 Å closer to the transmembrane domain, placing their cation nitrogens further from the aromatic pocket than in Ace-ACR-16.

A B

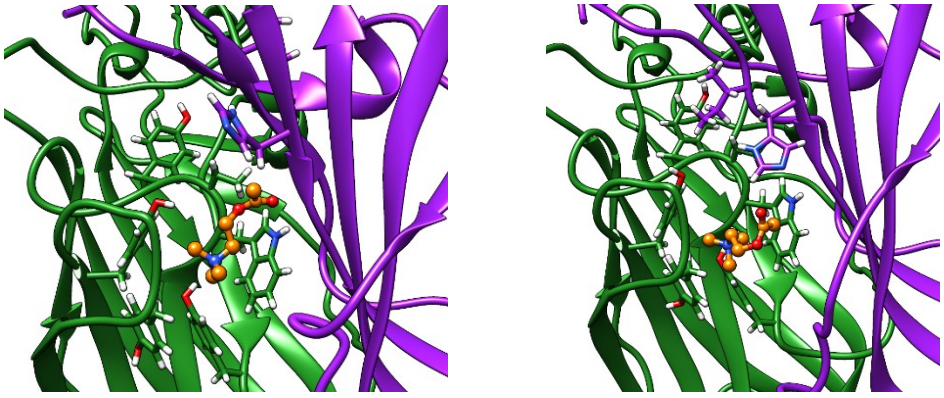

C D

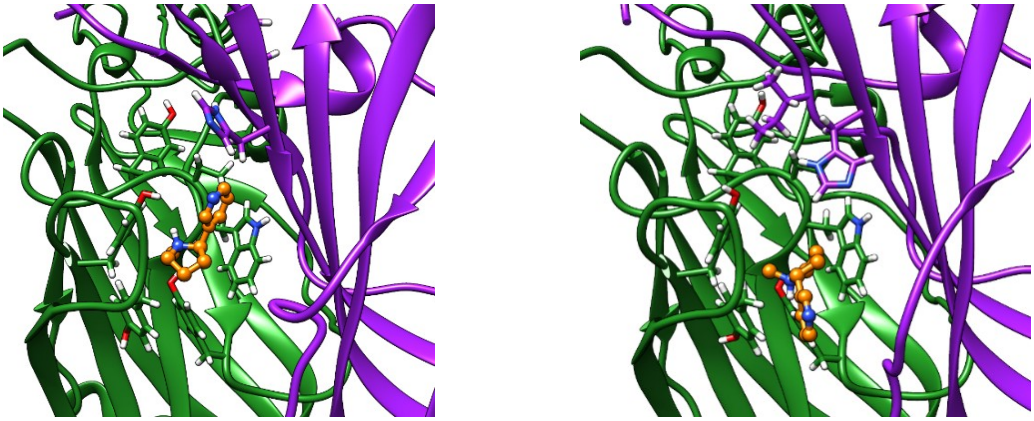

Figure 3.2 Homology models of the acetylcholine binding into (A) Ace-ACR-16 (-4.3 kcal/mol) and (B) Nam-ACR-16 (-4.0 kcal/mol), and nicotine docking into (C) Ace-ACR-16 (-5.4 kcal/mol) and (D) Nam-ACR-16 (-4.6 kcal/mol). The principal (+) subunit is coloured green, and the complementary (-) subunit is coloured purple. Carbons of the ball and stick acetylcholine and nicotine ligands are coloured orange, with oxygens and nitrogens coloured red and blue, respectively.

These differences in docking orientation could offer a structural explanation for the lower affinity for the site of activation in Nam-ACR-16, potentially explaining the higher EC_{50} values for this receptor. Furthermore, in the Nam-ACR-16 model, nicotine molecules did not dock with the pyridine group presenting to the complementary subunit, which is expected to hydrogen bond with a water molecule essential for agonist activation (Blum et al., 2010; Celie et al., 2004). Indeed, the best scoring docking simulation for Nam-ACR-16 flipped the nitrogenous ring of nicotine away from Loop D of the complementary subunit, roughly 9 Å further than in the Ace-ACR-16

docking model. This difference conceivably prevents the complete closure of the binding pocket and could explain why nicotine acted as a partial agonist on Nam-ACR-16.

3.2.3 *in silico* docking: anthelmintics

Interestingly, our model also predicts significant differences in tetrahydropyrimidine (oxantel, pyrantel, morantel) binding between these receptors. When constrained to bind in the Ace-ACR-16 orthosteric agonist binding pocket, oxantel (-6.4 kcal/mol), pyrantel (-5.5 kcal/mol) and morantel (-5.7 kcal/mol) all docked with similar energies, comparable to acetylcholine and nicotine (Figure 3.3). Using the same constraints for Nam-ACR-16, all three tetrahydropyrimidine docking simulations produced positive binding energies indicative of poor affinity (oxantel = +3.6 kcal/mol; pyrantel = +1.1 kcal/mol; morantel = +0.7 kcal/mol); only when binding parameters were extended to a large section of the ECD was oxantel able to dock with higher affinity, but still in a site and conformation peripheral to the main binding pocket.

A B

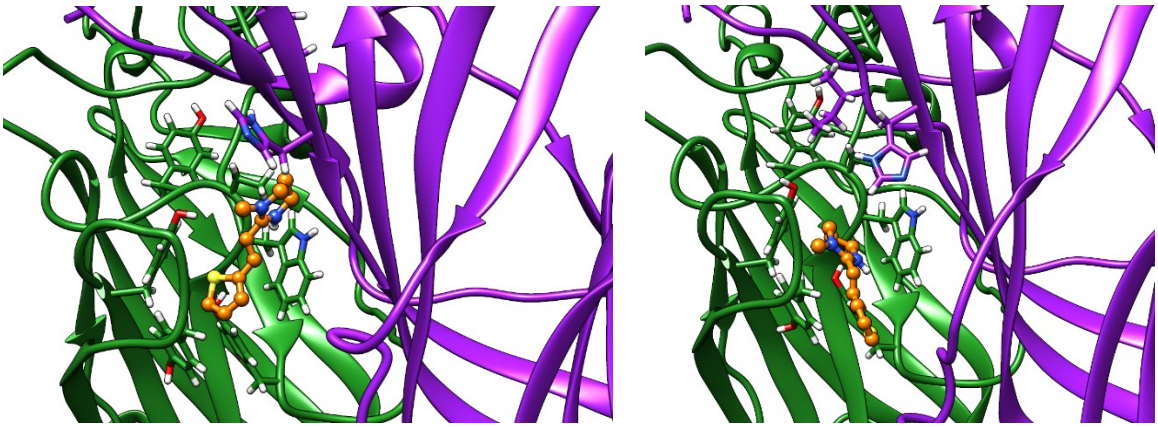

C

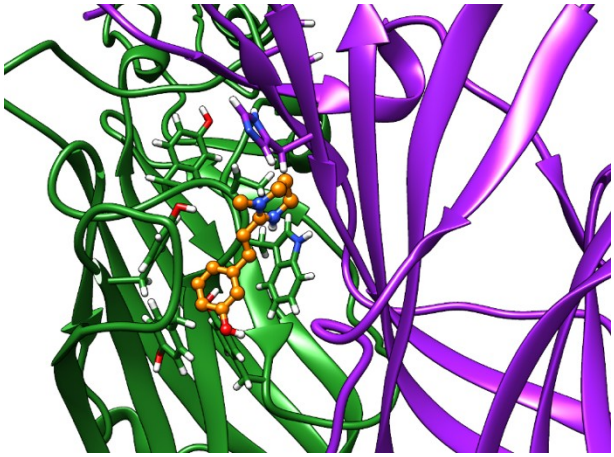

D

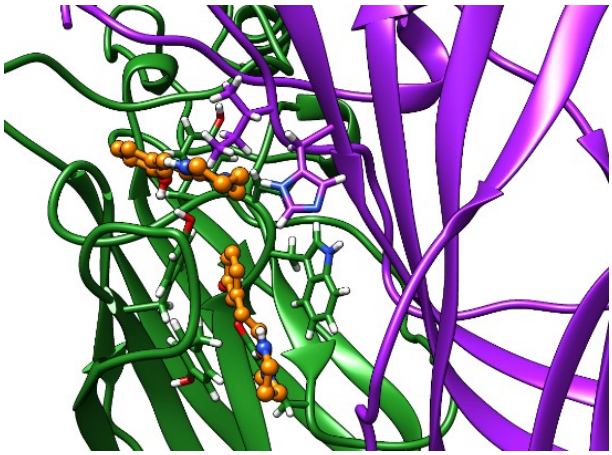

E

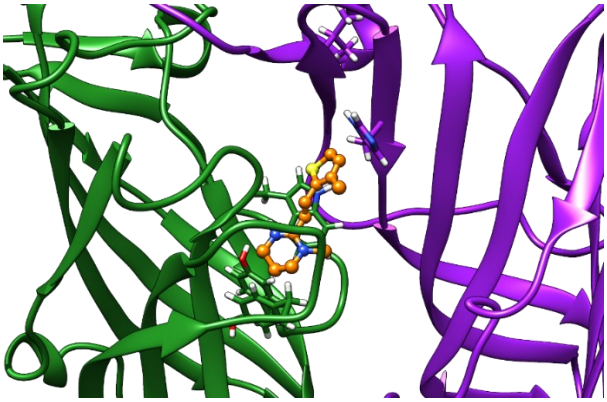

F

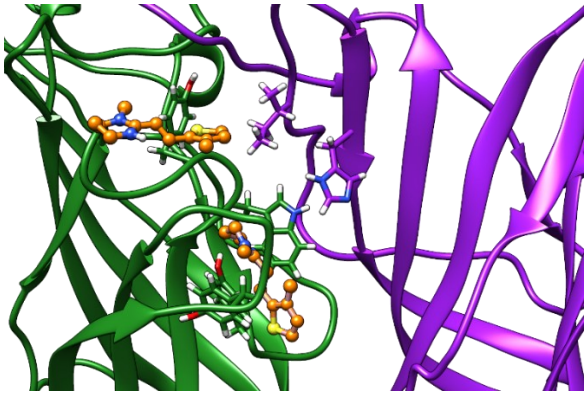

Figure 3.3 Homology models of the Ace-ACR-16 and Nam-ACR-16, docking: pyrantel (A, B,), oxantel (C, D) and morantel (E, F). Where docking produced multiple poses with equal binding energies, both poses are shown. The principal (+) subunit contributing to key residues of Loops A, B and C, is coloured green and the subunit contributing the complementary (-) face of the binding pocket contributing Loops D, E and F is coloured in purple ribbon. Carbon atoms of docked agonists are coloured in orange ball and stick. Red, blue and yellow molecules show oxygen, nitrogen and sulphur atoms, respectively.

3.2.4 Investigating the role of Ile130 in Nam-ACR-16

Only the oxantel-insensitive Cel-ACR-16 and Nam-ACR-16 sequences possess an Ile130 in the complementary subunit proximal to the binding pocket, compared to a Leu in the human α-7 receptor, and a Val in all other published ACR-16s. We modelled the Cel-ACR-16 receptor and also found an inability to dock oxantel (+2.5 kcal/mol), mirroring *in vitro* findings of very weak partial agonism (Raymond et al., 2000) (Figure 3.4). Interestingly, Ile130 in both Cel- and Nam-ACR-16 and Val130 of the oxantel-insensitive Aca-ACR-16 point inward into the agonist binding site, whereas the side chain points in the opposite direction in Ace- and Asu-ACR-16, which both respond to oxantel. To determine if more negative space in this position is associated with improved docking predictions, we changed the models of Nam- and Cel-ACR-16 from Ile130 to Val, which is one carbon side-chain shorter, or to Leu, which has the same length as Ile but the side chain of which branches in the opposite direction. We then repeated the docking simulations for acetylcholine and oxantel (Figure 3.4) and found I130V and I130L both allowed simulations to generate binding energies comparable to those of Ace-ACR-16 (Table 3.1), with oxantel better able to fit into the binding pocket. As expected, the reverse change of the analogous position in Ace-ACR-16 (Val130 to Ile) had no effect on predicted binding parameters because this residue branches away from the binding site.

A

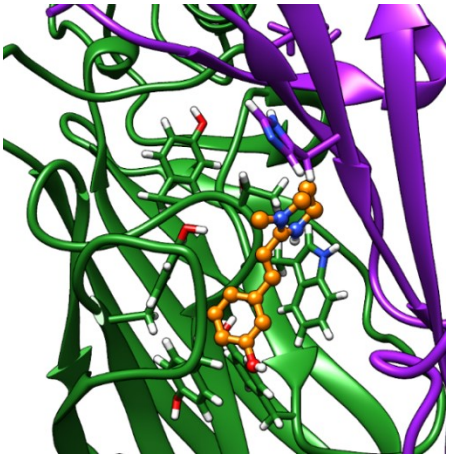

B

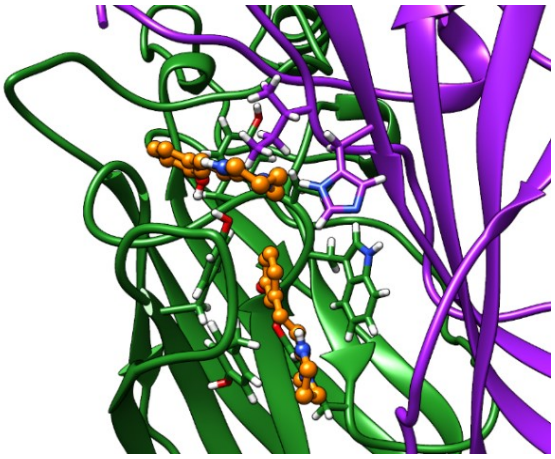

C

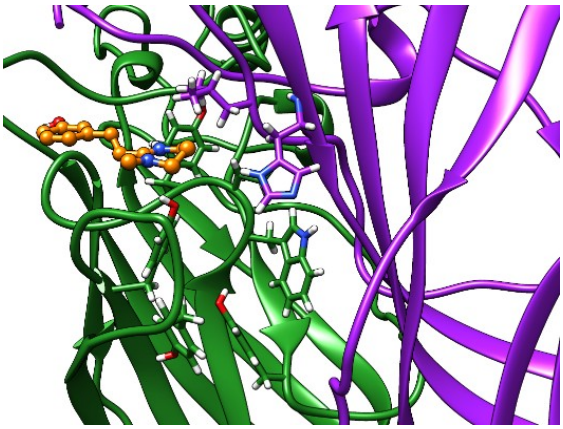

D

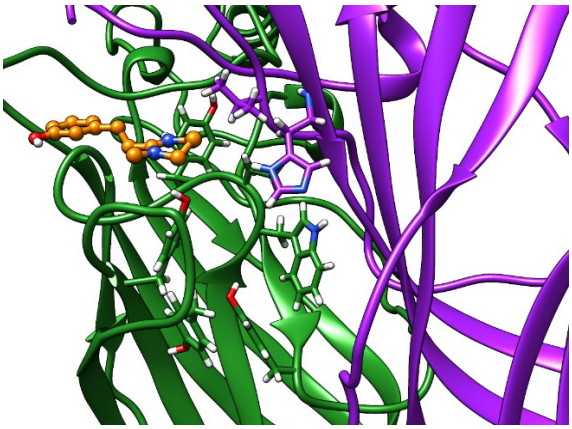

E F

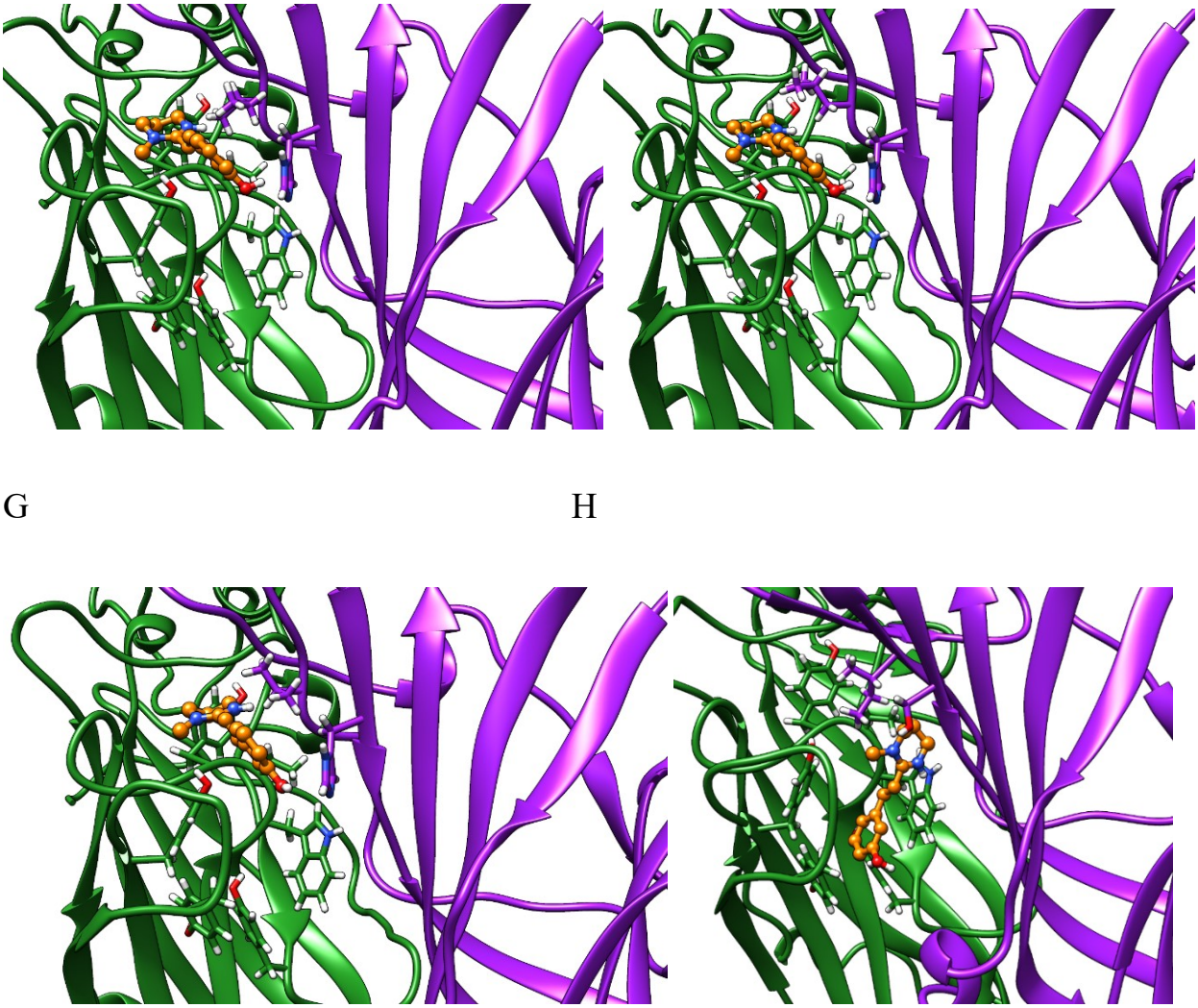

G H

Figure 3.4 Homology models of oxantel docking into: (A) Ace-ACR-16 V130I (B) Nam-ACR-16 (C) Nam-ACR-16 I130L (D) Nam-ACR-16 I130V (E) Cel-ACR-16 (F) Cel-ACR-16 I130L (G) Cel-ACR-16 I130V (H) Tmu-ACR-16. Colouration is the same as in Figure 3.3.

3.2.5 Predicted *T. muris* ACR-16 *in silico* docking

Oxantel does not clear hookworm infections in standard single-dose regimens, but is efficacious against *Trichuris* spp. We mined the genome of *Trichuris* spp. and, using a curated

gene annotation, obtained the predicted sequences of ACR-16 from *T. muris, T. trichiura,* and *T. suis*. Predicted sequences from all three species possess an analogous Ile130, and our homology modeling of *T. muris* indicates that this residue extends toward the binding pocket as in Cel- and Nam-ACR-16 (Figure 3.4). Remarkably, docking simulations of oxantel into *Trichuris* ACR-16 yielded strong predicted binding (-5.4 kcal/mol), and in orientations more central to the binding pocket, similar to poses in Ace-ACR-16. However, the sequence of *T. muris* is more divergent from the clade V nematodes and contains differences in the binding pocket.

Table 3.1 Calculated binding energies of *in silico* simulated agonist docking, highlighting residue 130

Dimer	acetylcholine	oxantel
	Binding energy (kcal/mol)	
Ace-ACR-16 V→I	-4.3	-6.4
Nam-ACR-16	-4	+4.3
Nam-ACR-16 I→L	-4.4	-3.3
Nam-ACR-16 I→V	-4.7	-4.4
Cel-ACR-16	-3.7	+2.5
Cel-ACR-16 I→L	-3.9	-1.5
Cel-ACR-16 I→V	-4.2	-2
Tmu-ACR-16	-4.9	-5.4

One unique characteristic of the predicted Tmu-ACR-16 binding pocket is the relative positioning of the vicinal Cys, two adjacent conserved Cys residues important for nAChR binding (Mongan et al., 2002). The Tmu-ACR-16 model positions these Cys residues roughly 1 Å further

away from the binding pocket than in all other models (Figure 3.5A), allowing greater space for ligand binding. This is illustrated by comparing the distance from the vicinal Cys to loop B Thr158, the position of which varies little from model to model (Figure 3.5B, Table 3.2).

A B

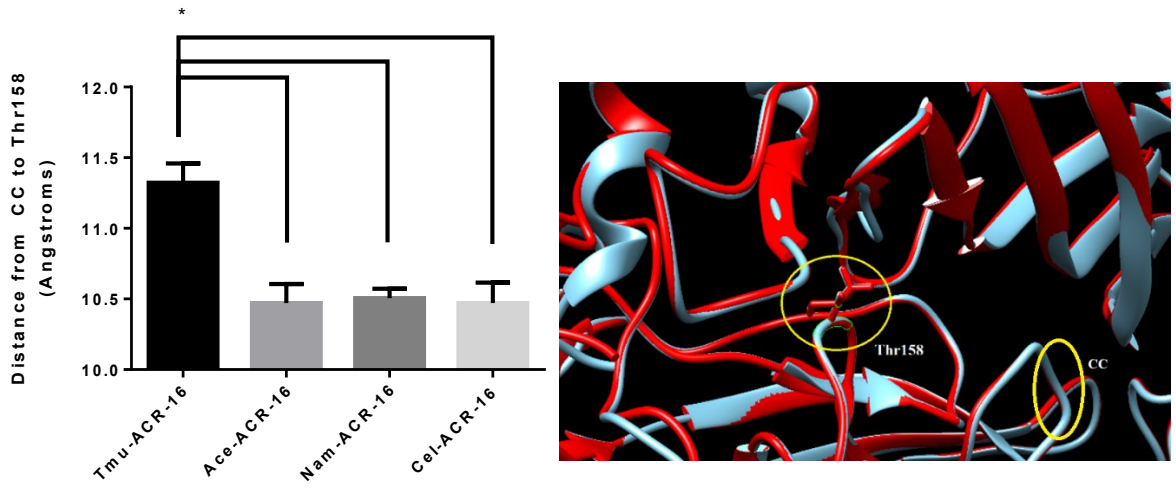

Figure 3.5 (A) Average distance from Thr158 to the vicinal Cys of the ACR-16s. Replicates represent the average from 4 model iterations. *ANOVA, $p < .05$. (B) Representative overlay of two receptors (Ace-ACR-16 in red and Nam-ACR-16 in teal) showing stability of position Thr158 as a reference point).

Table 3.2 Variance in the position of Thr158 between models

Dimer	Difference in Thr158 position of models overlaid with Ace-ACR-16 as reference (Å ± standard deviation)
Ace-ACR-16	0.06 ± 0.08
Nam-ACR-16	0.1 ± 0.04
Cel-ACR-16	0.17 ± 0.12
Tmu-ACR-16	0.67 ± 0.07

3.2.6 Homology modelling: Met129

Perhaps the most important characteristic of Tmu-ACR-16 oxantel binding is that this receptor lacks an inwardly directed Met129 that is present in the other ACR-16 receptors modelled (Figure 3.5). In the Ace-ACR-16 receptor, Met129 is positioned further away from the binding pocket than in the Nam- and Cel-ACR-16 receptors, allowing greater space for ligand binding (Figure 3.6).

A B

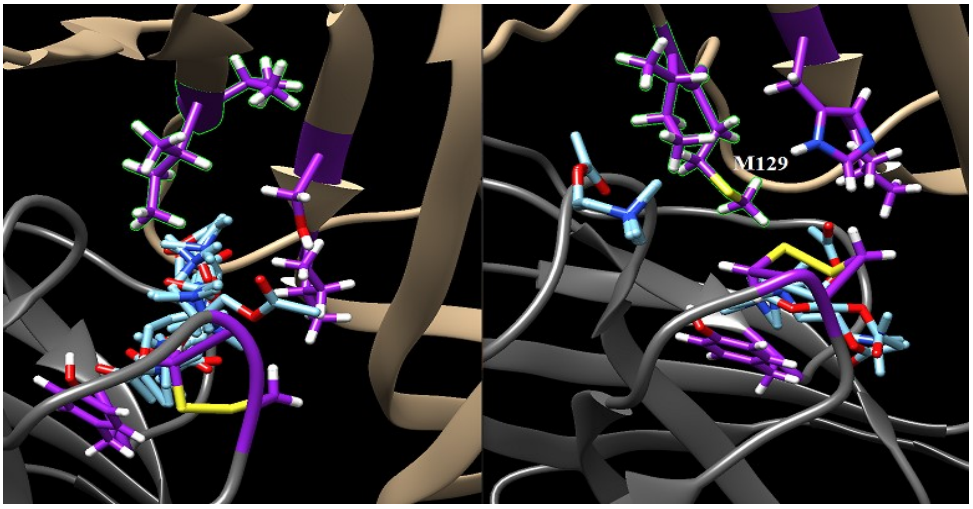

C D

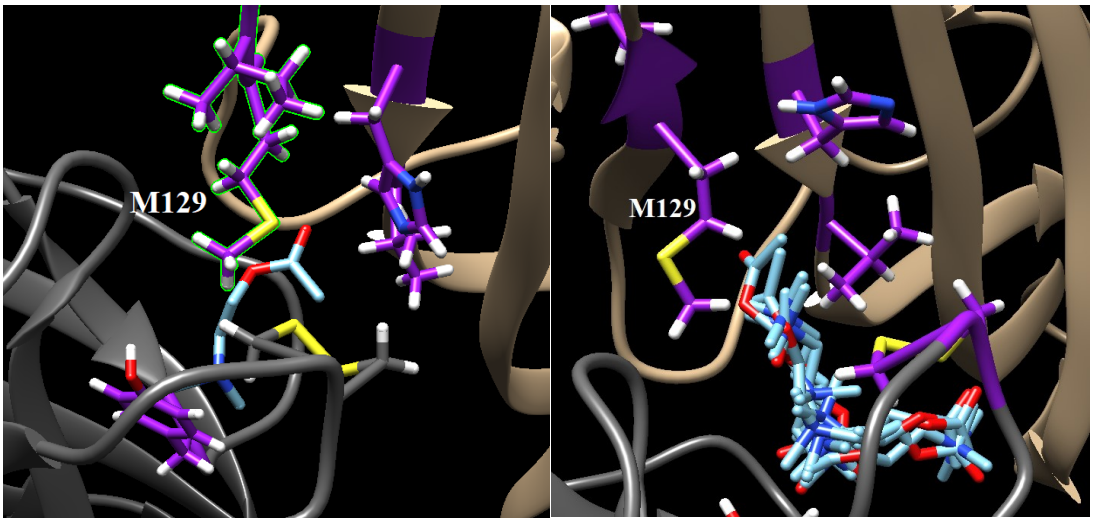

Figure 3.5 Clusters of teal acetylcholine molecules docked in the ACR-16 binding pocket of (A) Tmu-ACR-16 (B) Nam-ACR-16 (C) Cel-ACR-16 (D) Ace-ACR-16. Residue Met129 (M129), when present, is indicated on the complementary (-) subunit (coloured brown relative to grey (+) subunit. Red, blue, white and yellow colours indicate oxygen, nitrogen, hydrogen, and sulphur atoms.

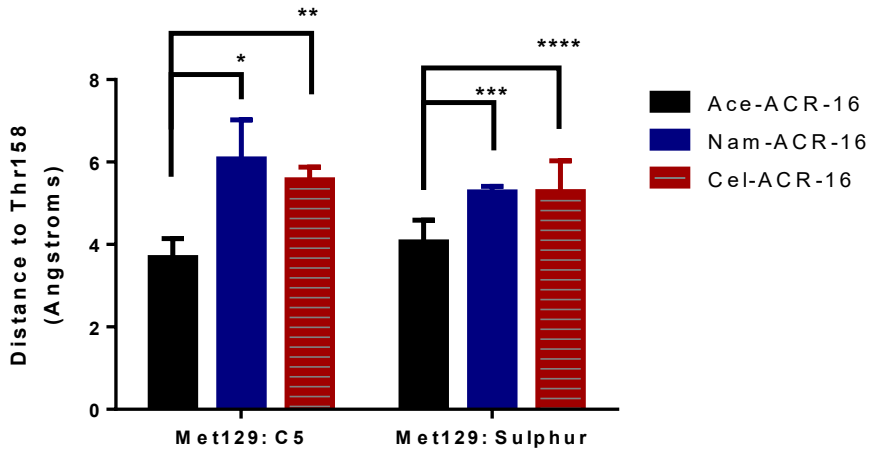

Figure 3.6 Distance from Thr158 to the sulphur or the terminal carbonyl of Met129. Tmu-ACR-16 lacks an analogous residue directed towards the binding site. Replicates represent the average from 4 model iterations. Significance was determined by ANOVA *p = .0012; **p =.0058; ***p =.026; ****p =.02555.

3.3 DISCUSSION

Homology modelling of proteins is often used prior to their *in vitro* expression to identify residues and interactions of importance for functional or mutagenesis analysis. In this thesis, I instead used homology modeling to rationalize results from *in vitro* experiments and suggest avenues for future research. We used homology modelling to determine if structural differences in the binding pocket may explain differences in the pharmacology of *A. ceylanicum* and *N. americanus* ACR-16. Some differences in binding positions, but not binding energies of nicotine and acetylcholine, were predictive of lower potency and efficacy on Nam-ACR-16. The inability of ligands to bind deeply

into the aromatic box and form hydrogen bonds with loop D of the complementary subunit has been associated with reduced channel activation for human nAChRs (Blum et al., 2010; Celie et al., 2004). It is possible that the inability to dock the pyrimidine of nicotine fully into the binding pocket is related to its inability to produce maximal current responses; *in vitro* mutagenesis studies will be required to define the binding partners involved.

3.3.1 Tetrahydropyrimidine docking

Significant differences in binding energies were predicted for tetrahydropyrimidine binding, expected to occupy the same pocket (Bartos et al., 2006; Martin and Robertson, 2007). Ace-ACR-16 responded to pyrantel and oxantel *in vitro*, and both drugs docked into our *in silico* model with similar predicted energies and orientations. In contrast, Nam-ACR-16 was much less responsive to pyrantel *in vitro*, and not at all to oxantel, and neither drug could be docked into the *in silico* model with a negative kcal/mol value (no bonds predicted to form).

3.3.2 Analysis of residue 130

Nam-ACR-16 has an Ile in position 130 of the (-) complementary subunit that contributes to the binding pocket. In all oxantel-insensitive ACR-16s, the analogous residue points inwards to the binding pocket, whereas it points away from the pocket in the oxantel-sensitive Ace- and Asu-ACR-16. This difference in orientation could reflect limitations of our models, but as a counterargument, it accurately predicted acetylcholine binding in the *A. suum* ACR-16 model (Zheng et al., 2016) as well as in crystallographic analyses of acetylcholine binding (Olsen et al., 2014; Pan et al., 2012). Changing this residue to a smaller Val in the model of either Nam- or Cel-

ACR-16 allowed more space for oxantel to bind and yielded stronger predicted binding energies. This position is Leu in the human α-7 nAChR, for which oxantel is a full agonist. Substitution of Ile130 with Leu in both Cel- and Nam-ACR-16 models also rescued predicted oxantel binding, albeit in a fashion comparable to changing Ile130 to Val. Yao et al. (2008) showed that loop E residues play a role in neonicotinoid selectivity and may rationalize differences in Ace- and Nam-ACR-16 anthelmintic binding in our models. One limitation to a putative role of a smaller residue in sensitivity to oxantel is that Aca-ACR-16 contains an inward facing Val130 and did not respond to oxantel. It is possible that oxantel responses are hidden by the small magnitude of currents generated by this receptor, or that this extra space allows binding but not gating.

3.3.3 Predicted *T. muris* ACR-16 analysis

Increased space in this position alone is not likely to be a sufficient condition for determining oxantel sensitivity, as the homology model of *Trichuris* spp. also indicated the presence of an inward facing Ile130 residue. *Trichuris* spp. are paralyzed by oxantel, and our model of a putative *Trichuris* ACR-16 sequence also predicted strong ligand binding, despite the bulky side chain. However, the clade I *Trichuris* spp. are phylogenetically divergent from hookworms, and contain other sequence differences, including the absence of an inward facing Met129 and a bulky His138 residue in loop E, which provides greater space for oxantel binding in our model. Interestingly, loop E His138 is also absent in the oxantel-sensitive Asu-ACR-16 (Abongwa et al., 2016b). This suggests that multiple species-specific residues play a role in selective oxantel sensitivity, and that Ile130 may play a secondary role in oxantel selectivity.

3.3.4 Linking *in silico* results with anthelmintic activity of tetrahydropyrimidines

The relevance of differential tetrahydropyrimidine activity on ACR-16s and its relationship to hookworm sensitivity to this drug class has intriguing implications. Richards et al. (1995) reported that *N. americanus* and *A. ceylanicum* are similarly paralyzed by pyrantel *in vitro*. Additionally, reports of pyrantel and oxantel combination therapy have shown mixed results in clearance of worms, and modest efficacy in reducing egg counts in human hookworm infections (Moser et al., 2017; Rim et al., 1975). When used alone, oxantel had minimal ability to clear *Ancylostoma* spp. or *N. americanus* infections *in vivo*, in contrast to high clearance levels against *Trichuris* spp. (Keiser et al., 2013). Interestingly, this study did find a greater ability of oxantel (1 µg/ml) to kill L3 A. *ceylanicum* (9%) compared to *N. americanus* (2.3%), but not at other concentrations. Oxantel has been suggested to directly target N-type nAChRs as the mechanism of anthelmintic activity (Martin et al., 2004), and it is therefore possible that ACR-16 played a role in the results from the Keiser et al. study (2013). If this is the case, then identifying a *Trichuris* spp. ACR-16 and determining its *in vitro* oxantel and pyrantel sensitivity profiles may be illuminating. In support of this, the preprint of a pharmacological profile of a *T. suis* ACR-16 receptor was made available on-line after the initial submission of this thesis, showing super-agonism by oxantel compared to acetylcholine and modest partial agonism by pyrantel (Hansen et al., 2020). Our preliminary modelling of the putative *T. muris* ACR-16 indicates that it contains the analogous Ile130 pointing inward toward the binding pocket, but that oxantel is still predicted to bind with high affinity.

Chapter 4: Structural mechanism underlying the differential pharmacology of ivermectin and moxidectin on the *C. elegans* glutamate-gated chloride channel GLC-2

4.1 INTRODUCTION

In the previous chapters, I focused on the effects of cholinergic compounds targeting hookworm nAChRs, but another important pLGIC family targeted by anthelmintics is the inhibitory glutamate-gated chloride channels (GluCls; Cully et al., 1994; Geary and Moreno, 2012; Wolstenholme and Rogers, 2005). These receptors are the targets of MLs, including IVM and MOX, which exert their anthelmintic activity by pseudo-irreversibly allosterically activating GluCls (Cully et al., 1994; Dent et al., 2000) causing flaccid paralysis of body wall muscles (Turner and Schaeffer, 1989), inhibition of pharyngeal pumping (Geary et al., 1993), inhibition of the secretory-excretory pore (Moreno et al., 2010), and persistent reduction in egg laying (Walker et al., 2017). MLs are an important class of well-tolerated, potent, broad-spectrum anthelmintics originally developed for use in veterinary medicine (Nolan and Lok, 2012), and now also used for treating human filariases (Cross et al., 1998; Taylor and Greene, 1989) and ectoparasitic infestations (Youssef et al., 1995); they also have activity against some GI nematodes (Ottesen and Campbell, 1994; Whitworth et al., 1991), but are not used for hookworm infections because of an unresolved lack of efficacy against *N. americanus* (Richards et al., 1995). To better understand the limitations of MLs, it is useful to characterize the pharmacodynamics of their interactions with drug targets in a model organism such as *C. elegans*.

A crystal structure of an IVM-bound GluCl (Cel-GLC-1) predicts that IVM binds in the upper transmembrane region at the interface between two adjacent subunits, inserting its cyclohexene group toward the pore-lining (+)TM2 of the principal subunit by wedging between the (+)TM1 helix and the (-)TM3 helix of the complementary subunit (Hibbs and Gouaux, 2011). All nematode GluCl subunits characterized to date are the IVM-sensitive α-type, except for the lone IVM-insensitive β-type, GLC-2 (Cully et al., 1994). Cel-GLC-2 is unusual because, unlike all other GluCls, it is antagonized by IVM (Degani-Katzav et al., 2017b). GLC-2 is unlikely to form homomeric channels *in vivo* (Degani-Katzav et al., 2017a) and inclusion of GLC-2 into heteromeric receptors significantly reduces the IVM activation response and shifts the concentration-response curve of glutamate left or right, depending on the EC_{50} of the partner subunit (Atif et al., 2019; Cully et al., 1994).

Despite the atypical GLC-2 responses to IVM, few studies have investigated the role β-type subunits play in *in vivo* susceptibility to MLs. Glendinning et al. (2011) showed that a triple α-type GluCl null mutant line of *C. elegans* was not paralyzed by IVM (DA1316:*avr-14*, *avr-15*, *glc-1*). Exogenous expression of GLC-2 under control of the *avr-14* promoter did not rescue IVM sensitivity in this line, suggesting that GLC-2 does not directly contribute to IVM-induced paralysis of worms. El-Abdellati et al. (2011) reported that IVM-resistant isolates of the trichostrongyloid parasite *Cooperia oncophora* have increased abundance of *glc-2* mRNA, whereas Njue and Prichard showed no such association (2004); α-type subunit expression has been reported to be up- or down-regulated as well (Martínez-Valladares et al., 2012; Williamson et al., 2011). SNPs have been found in GluCl subunits in some drug-resistant field isolates (Ghosh et al., 2012), but the functional significance of these alleles is unknown. One difficulty in correlating transcript level to resistance is that these genes show species-specific variation in sequence and

even tissue distribution. For instance, in *C. elegans*, GLC-2 is expressed in cells innervated by M3 neurons in the pharynx (Laughton et al., 1997), but in the phylogenetically related small ruminant parasite *H. contortus*, it is absent from the pharynx and instead localized to nerve cords and motor neuron commissures (Portillo et al., 2003); other species have not been investigated.

Further complicating matters is the fact that MLs encompass two structurally different classes of molecules: the avermectins (e.g., IVM) and milbemycins (e.g., MOX). Both contain a macrolide ring and were discovered as products of *Streptomyces* spp. fermentation, but milbemycins lack the sugar moiety found in avermectins, may lack the C5 cyclohexene hydroxyl or replace it with a ketoxime (milbemycin oxime), and have an alkane or alkene modified C23 and C25 (C23 methoxime and a branched 6 carbon alkene at position C25 in MOX). These differences lead to the milbemycins generally having longer half-lives and more persistent activity and a wider safety window in dogs (Paul et al., 2000; Shoop et al., 1995; Takiguchi et al., 1980). In *C. elegans*, IVM and MOX differently affect pharyngeal pumping and body wall contraction, but these differences were not seen in a *glc-2* deletion mutant (Ardelli et al., 2009). Furthermore, an IVM-resistant strain of *H. contortus* showed less clinical resistance to MOX, which suggest differences in pharmacokinetics and/or dynamics (Paiement et al., 1999). Studies with radiolabelled drugs showed that glutamate pre-exposure enhanced the binding of IVM more than MOX to *H. contortus* GLC-5 (Forrester et al., 2002). This suggests a difference in affinity for the binding site, but could also represent differences in lipophilicity (for further review of IVM and MOX see Prichard et al., 2012; Prichard and Geary, 2019). No mechanistic explanation has been advanced to explain the differential pharmacology of MOX and IVM on GluCls. Here, we sought to determine if MOX was inhibitory on Cel-GLC-2 like IVM, and to identify amino acid residues that might play a role in discriminating agonist vs. antagonist responses.

4.2 RESULTS

4.2.1 Wild-type Cel-GLC-2 function

To study interactions between Cel-GLC-2 and MLs, we initially confirmed previous *C. elegans* GLC-2 electrophysiology results (Cully et al., 1994) in our platform. Oocytes expressing our Cel-GLC-2 responded to glutamate with an EC_{50} of 70.8 ± 1.1 µM (Hill coefficient = 2.8 ± 0.16), compared to 380 ± 20 µM (Hill coefficient = 1.9 ± 0.2) reported by Cully et al. (1994). These channels were not directly activated by IVM or MOX and had a maximal response at roughly 350 µM glutamate (EC_{99}) (Figure 4.1).

A

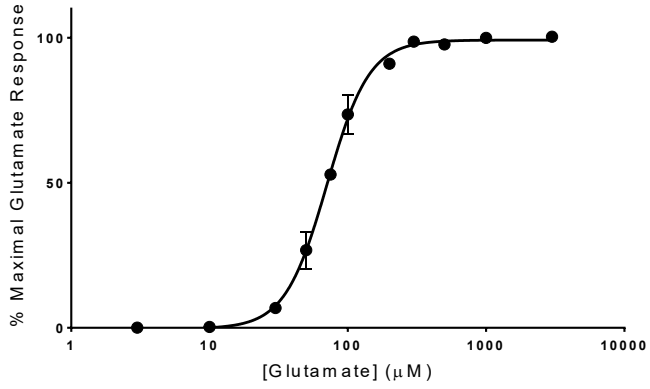

B

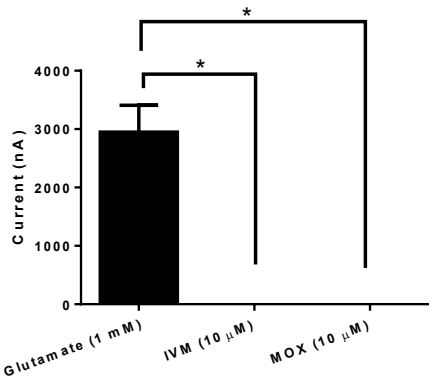

C

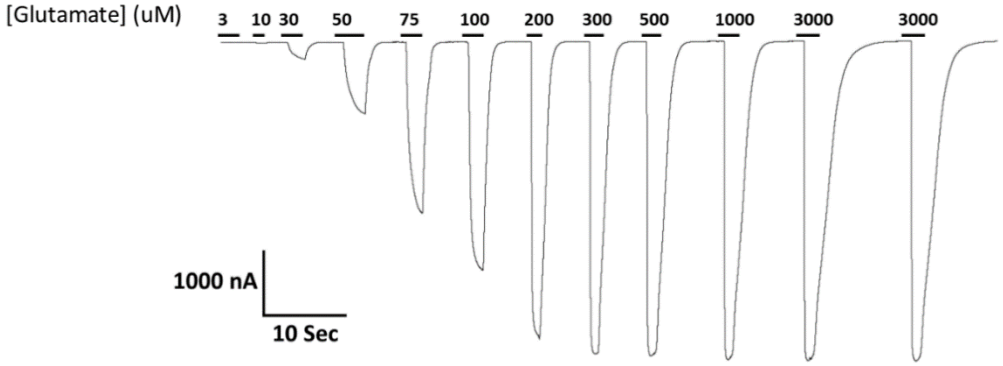

Figure 4.1 (A) Concentration-response curve for glutamate activation of Cel-GLC-2. EC_{50} = 70.8 ± 1.1 µM (Hill coefficient = 2.8 ± 0.16) n = 4. (B) Cel-GLC-2 is robustly activated by 1 mM glutamate but not by IVM or MOX (10 µM) n=4; *ANOVA, p<.05. (C) Representative tracing of a glutamate concentration-response for wild-type Cel-GLC-2.

Likewise, the IVM-insensitive *S. mansoni* GluCl2 responded robustly to glutamate but not to either ML (Figure 4.2A). As a control for ML sensitivity, the *H. contortus* GLC-5 receptor was directly activated by glutamate, IVM and MOX, with both ML responses exhibiting the characteristic slow and irreversible gating commonly associated with GluCl activation by IVM (Figure 4.2B; representative tracing in Figure 1.7).

A B

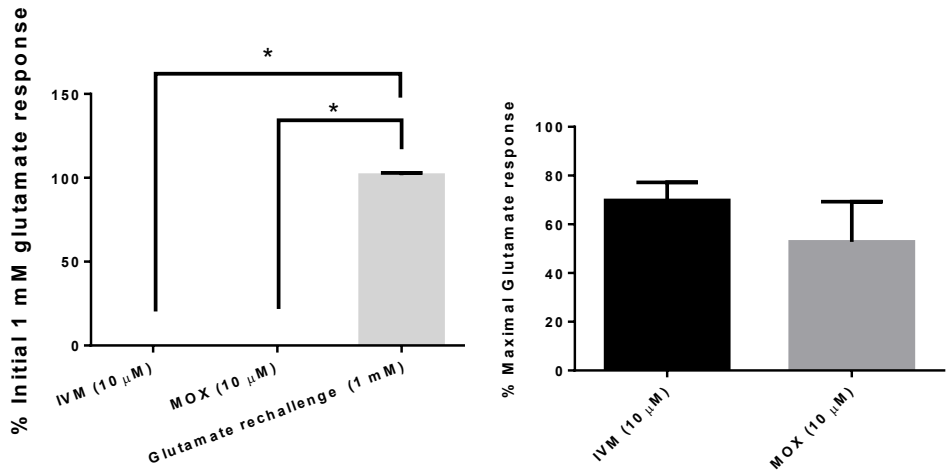

Figure 4.2 (A) The SmGluCl2 receptor is not activated or modulated by IVM or MOX n=3; *ANOVA, p<.05. (B) the Hco-GLC-5 receptor is directly activated by IVM and MOX; n=3.

4.2.2 Allosteric modulation of wild-type Cel-GLC-2

Having established functionality of Cel-GLC-2, we next sought to determine if MOX allosterically modulates glutamate responses, and to replicate IVM antagonism (Degani-Katzav et al., 2017b). Oocytes were first challenged with multiple applications of a maximal concentration of glutamate to establish stable amplitude of responses, then pre- and co-treated with 10 μM MOX or IVM with glutamate to measure changes in the glutamate-induced signal. In control oocytes, we re-applied glutamate in a similar time-course, but in the absence of ML exposure to rule out signal decay or desensitization. These drugs are very lipophilic and it was possible that exposure non-specifically altered membrane fluidity, causing channels to become leaky. To demonstrate specificity, we applied the same treatment regimen to the *S. mansoni* GluCl2 receptor (not to be confused with GLC-2, which does not exist in *S. mansoni*) (Accession code AGV21041.1) and saw no effect on the glutamate signal (Figure 4.2A). SmGluCl2 was chosen because flatworm GluCls are not activated by IVM (Lynagh et al., 2015) nor are they allosterically modulated. This simple test showed that IVM and MOX antagonized glutamate responses in Cel-GLC-2, but had no effect on the evolutionarily distinct IVM-insensitive SmGluCl2 receptor. These data support the conclusion that the MLs specifically antagonized the glutamate response of Cel-GLC-2.

To determine the extent of antagonism, we generated concentration-response curves measuring the inhibitory profile of IVM and MOX on Cel-GLC-2 by testing increasingly higher concentrations of IVM or MOX in the presence of the EC_{50} concentration of glutamate (Figure 4.3). These experiments were also conducted using individual oocytes for each concentration point, standardized as a percentage of the EC_{50} glutamate response to reduce drug carryover. The oocyte holding chamber was thoroughly washed between replicates as described in section 6.7.

Both drugs irreversibly inhibited glutamate-induced currents at low micromolar concentrations (IVM IC_{50} = 1.28 ± 0.78 µM; Hill slope = -1.74 ± 0.76; MOX IC_{50} = 0.11 ± 1.42 µM; Hill slope = -0.65 ± 0.14) with a maximal effect at 10 µM.

A

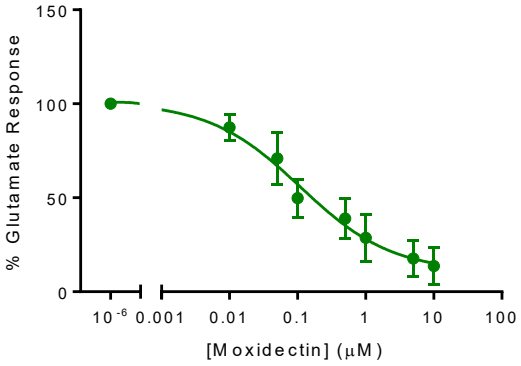

B

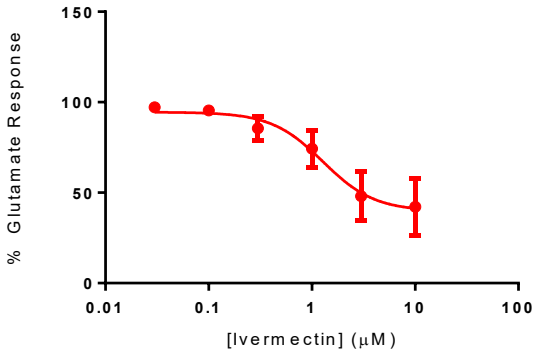

C

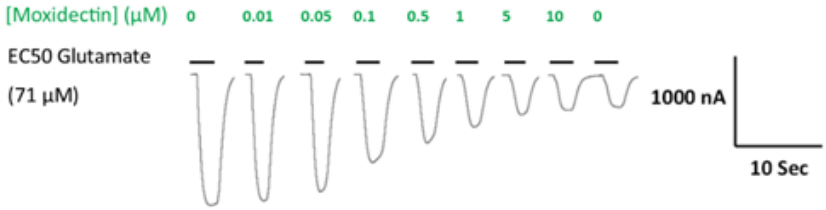

Figure 4.3: Glutamate responses are inhibited by increasing concentrations of MLs. Inhibitory response curves for (A) MOX and (B) IVM on wild-type *C. elegans* GLC-2 in the presence of EC_{50} glutamate (IVM IC_{50} = 1.28 ± 0.78 µM; Hill slope = -1.74 ± 0.76; MOX IC_{50} = 0.11 ± 1.42 µM; Hill slope = -0.65 ± 0.14) n ≥ 3. (C) Representative tracings of the MOX concentration-response inhibition profile. Irreversible inhibition is indicated by the inability of drug washout (10 µM MOX) to restore maximal responses to glutamate.

To minimize drug carryover after washout, we added 1% ethanol or 5% intralipid to ND96 as solvents to improve removal of drug to determine reversibility of inhibition, relying on the concept that a lipophilic sink for MLs could help remove them from surfaces and non-specific lipid membrane binding sites. After ML exposure, 5 min of continuous washout with ND96 in the presence or absence of 5% intralipid or 1% ethanol was unable to restore maximal glutamate activation. IVM cannot form covalent or strong ionic bonds, which together with the washout studies, suggests that these drugs very slowly exit the lipid environment of the binding site in the bilayer of the lipid membrane.

IVM and MOX are in the avermectin and milbemycin classes of anthelmintics, respectively. We next assayed for inhibition by milbemycin oxime and selamectin (another avermectin) and compared the responses with those of MOX and IVM to determine if other MLs have the same inhibitory effects (Figure 4.4). Co-treatment with any of the MLs (10 μM) produced > 50% inhibition of the glutamate response, with MOX having the greatest effect.

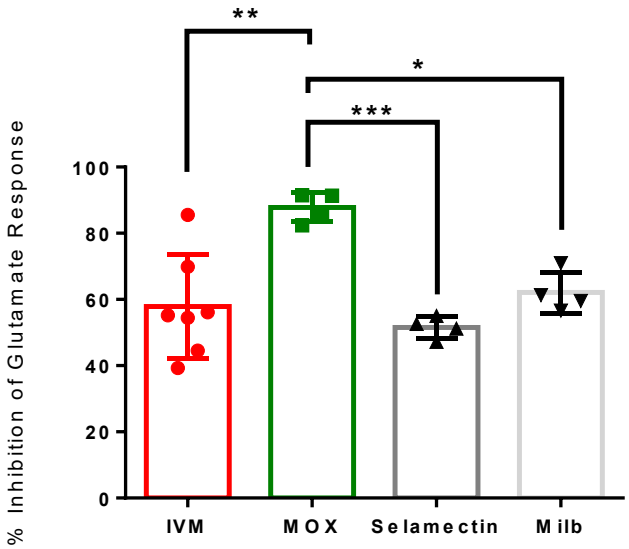

	IVM	MOX	Selamectin	Milbemycin oxime
n	7	4	4	4
Mean inhibition (%)	57.86	87.82	51.52	62.11
Standard error of mean	5.89	2.20	1.64	3.11

Figure 4.4 Comparison of ML (10 μM) inhibition of EC_{50} glutamate responses on Cel-GLC-2. n > 4. Significance was determined by ANOVA *p = .0167; **p = .002; ***p = .001.

4.2.3 Sequence analysis of Cel-GLC-2

We next investigated if specific amino acids in Cel-GLC-2 can explain the differences in IVM activity on α-type GluCls. Sequence alignment of *C. elegans* GluCls shows the presence of two adjacent residues, Met291 and Gln292, in the second transmembrane domain of Cel-GLC-2, proximal to the predicted IVM binding site (Figure 4.5A). In all GluCl subunits that are directly activated by IVM, these residues are Gln and Ser or Ala, respectively. We built a phylogenetic tree of nematode GLC-2 subunits and identified 3 main clusters with differing motifs in this position: MQ is present in nematodes closely related to *C. elegans* such as hookworms and *H. contortus*, whereas LT is present among parasitic filarial nematodes of human and animal significance, and LQ in *Ascaris suum, A. lumbricoides*, *Toxocara canis* and *Strongyloides stercoralis* (Figure 4.5B).

A

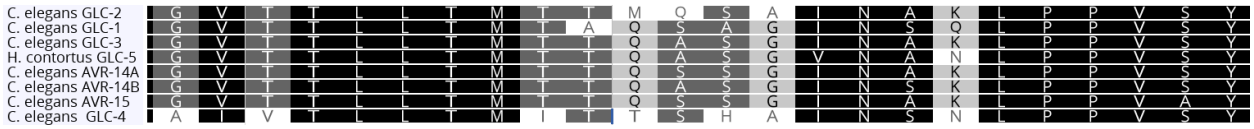

B

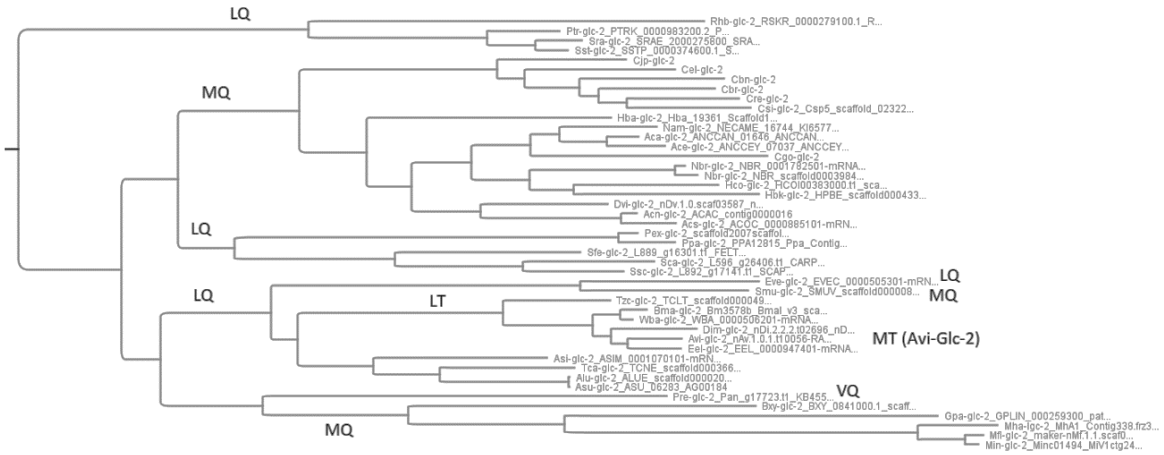

Figure 4.5 (A) Sequence alignment of *C. elegans* GluCl subunits in a highly conserved region of the second transmembrane domain that includes the predicted IVM binding site. AVR-14A (accession # AAC25481), AVR-14B (AAC25482), AVR-15 (CAA04170), GLC-2 (NP_491470), GLC-3 (CAB51708), and the *H. contortus* GLC-5 (AAG43233). Presence of a Met and Gln residue only in GLC-2 (positions 291 and 292). (B) Phylogenetic tree of *glc-2* subunits in nematodes highlighting the encoded conserved residues 291, 292 in different branches.

4.2.4 Homology models

To investigate the structural implications of these residues, we created *in silico* homology models of Cel-GLC-2 using a template of the crystal structure of a Cel-GLC-1 receptor in the holoprotein state bound to glutamate and IVM in an open channel conformation; PDB = 3RIF (Hibbs and Gouaux, 2011). As a quality control of our models, we performed docking simulations of IVM into the Cel-GLC-1 template to validate that it recreated the binding conformation in the crystal structure. Our models produced strong IVM binding energies (-10.6 kcal/mol) with orientations

placing the cyclohexene directed towards (+)TM2 Ser292, nearly identical to those found in the crystal structures, indicating the high quality of prediction; MOX also bound in this pose (-5.9 kcal/mol), but binding was strongest outside this pocket (-8.2 kcal/mol) (Figure 4.6A,C). In contrast, the Cel-GLC-2 model was unable to bind IVM with as high affinity (-7.0 kcal/mol) or in orientations positioning the cyclohexene group into the Gln292 residue of the principal subunit (Figure 4.6B,D).

A

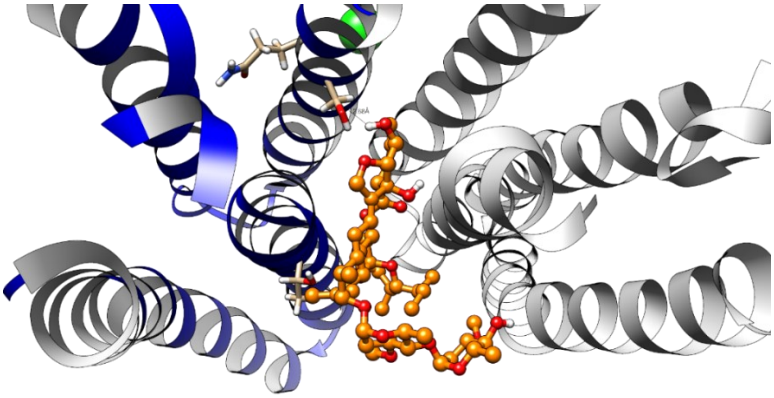

B

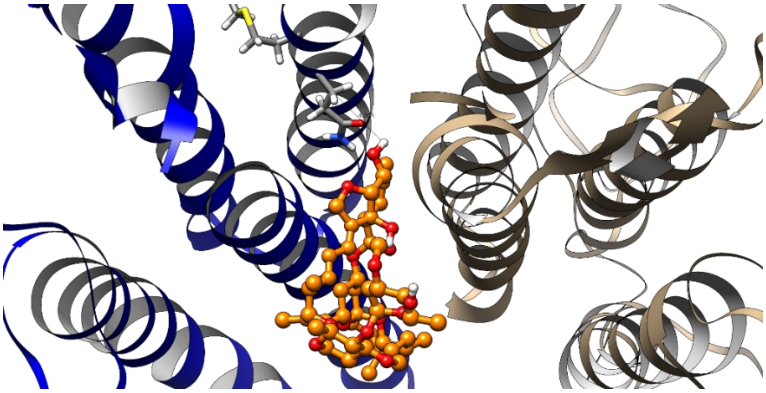

C

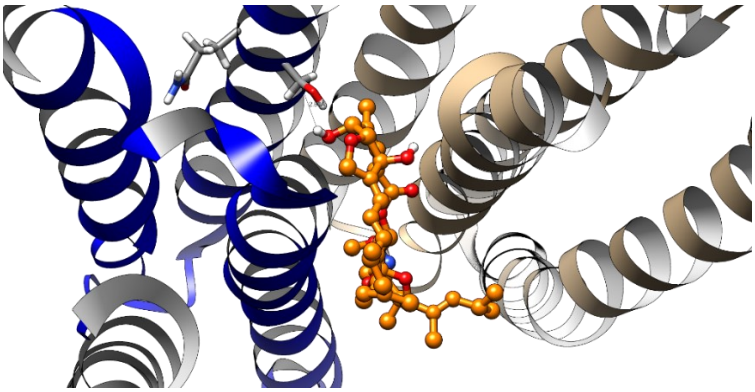

D

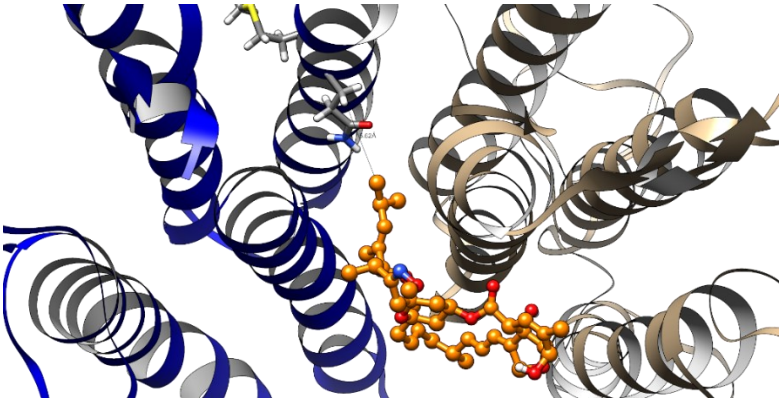

Figure 4.6 Homology model of the IVM (orange ball and stick molecule) binding site between adjacent (+) principal subunit (blue coils) and the (-) complementary subunit (grey coils). Side chains of residues 291 and 292 are indicated. Oxygen, nitrogen and sulphur atoms are coloured red, blue and yellow, respectively. Distance from closest atom of ligand to the R-group at position 291 is indicated. IVM: (A) Cel-GLC-1 (-10.6 kcal/mol). Green ball in the upper middle region denotes a Cl^- ion in the pore of the receptor for reference (B) Cel-GLC-2 (-7.6 kcal/mol). MOX: (C) Cel-GLC-1 (-5.9 kcal/mol) (D) Cel-GLC-2 (-8.4 kcal/mol).

We then changed the sequence of the Cel-GLC-2 model at positions Met291 and Gln292 individually or together to the residues present in α-type IVM-sensitive subunits to see if these changes could recapitulate the predicted IVM binding *in silico* (Figure 4.7). We also changed MQ→LT to represent the residues present at these positions in the filarial nematode GLC-2 subunit (see Table 4.1 for mutants generated).

Table 4.1 Creation of the Cel-Glc-2 mutants

Cel-Glc-2 mutants

Wild-type residues	Mutant products
Met291	Gln291
Gln292	Ser292
Met291 & Gln292	Gln291 & Ser292
Met291 & Gln292	Leu291 & Thr292

Interestingly, position 291 is not directed towards the pore of the channel, nor does it face it; this position is not expected to interact with an IVM molecule. However, in docking simulations of M291Q, IVM (-1.2 kcal/mol) and MOX (-7.8 kcal/mol) yielded attenuated binding energies and failed to present the cyclohexene to Gln292 (+)TM2; the disaccharide of IVM and the carbonyl of MOX were the closest structures to this position (Figure 4.7). In comparison, both the Q292S and the MQ→QS double mutant docked IVM and MOX with binding energies and orientations comparable to the Cel-GLC-1 model (Q292S: IVM = -9.2; MOX = -7.9 kcal/mol) (MQ→QS double mutant: IVM = -9.5; MOX = -9.2). In the MQ→LT double mutant model, even with the

presence of a smaller polar Thr, IVM only docked with an energy of -7.6 kcal/mol, albeit in a conformation with the cyclohexene directed into this residue. MOX was predicted to bind with -8.9 kcal/mol, but with the carbonyl group positioned towards Thr291. Modelling M291L alone produced the same binding as MQ→LT double mutants.

A

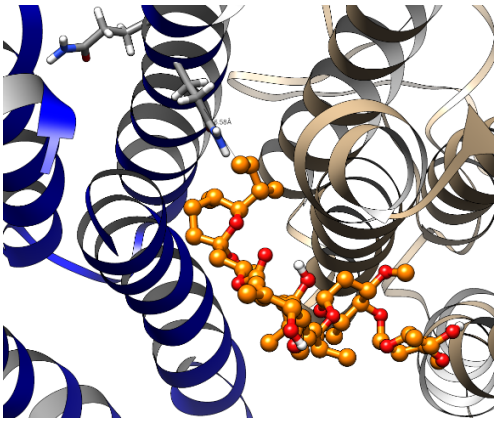

B

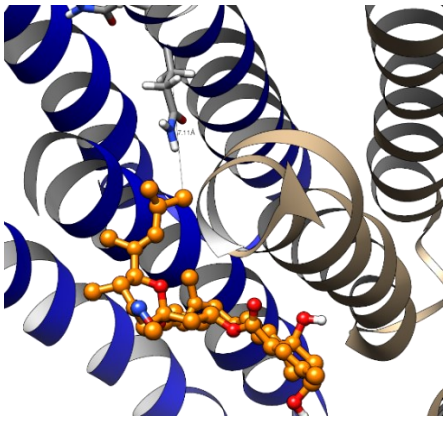

C

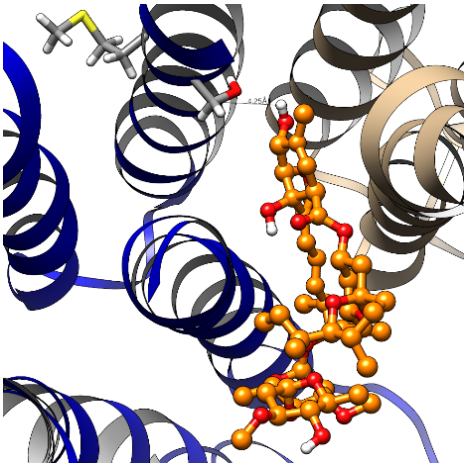

D

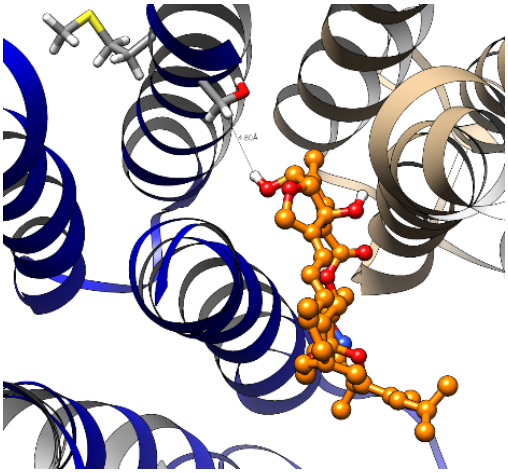

E F

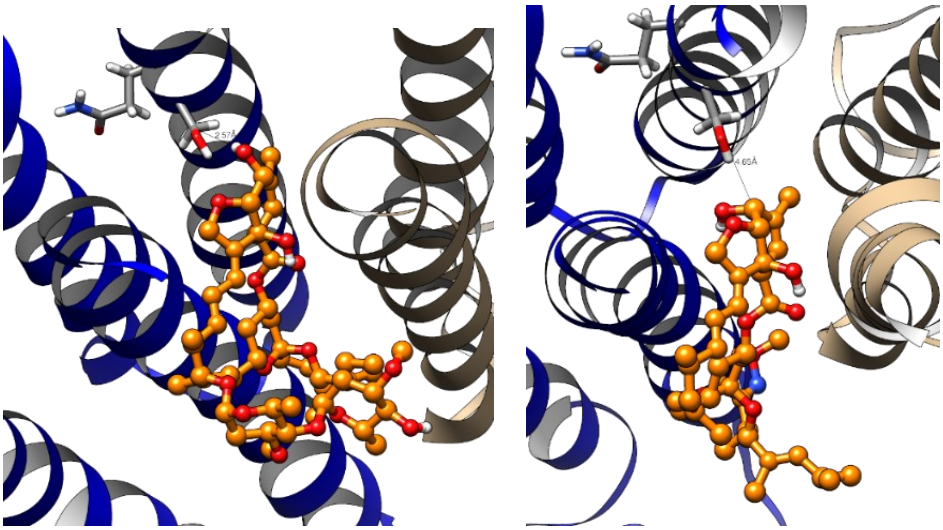

G H

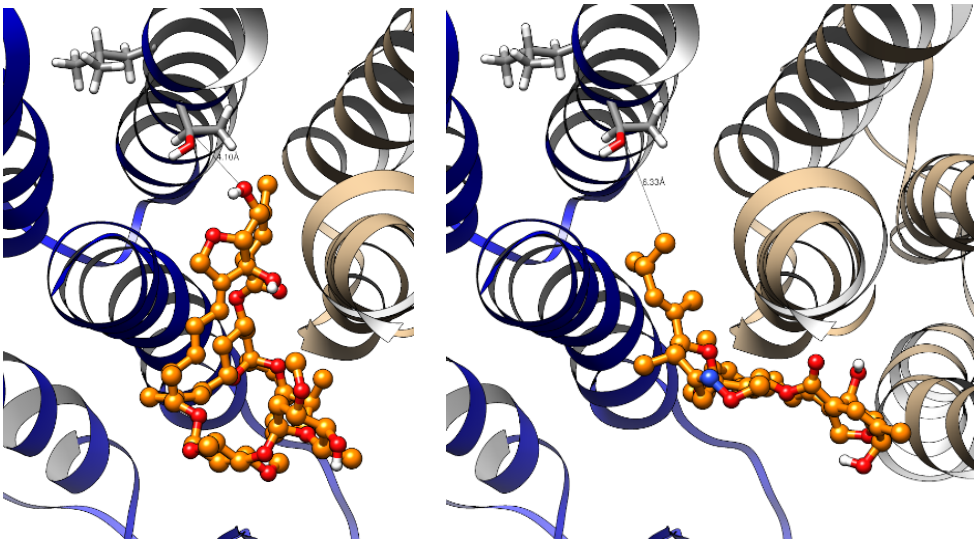

Figure 4.7 Homology models of the putative IVM and MOX (orange ball and stick molecule) binding site between adjacent (+) principal subunit (blue coils) and the (-) complementary subunit (grey coils). Side chains of residues 291 and 292 are indicated. Oxygen, nitrogen and sulphur atoms are coloured red, blue and yellow, respectively. Distance from closest atom of ligand to the R-group at position 291 is indicated. M291Q mutant (A) IVM (-1.2 kcal/mol) (B) MOX (-7.8 kcal/mol). Q292S (C) IVM (-9.2 kcal/mol) (D) MOX (-7.9 kcal/mol). MQ →QS double mutant (E) IVM (-9.5 kcal/mol) (F) MOX (-9.2 kcal/mol). MQ→LT double mutant (G) IVM (-7.6 kcal/mol) (H) MOX (-8.9 kcal/mol).

4.2.5 Mutagenesis pharmacology

To test the function of the residues studied in the *in silico* analysis, we performed site-directed mutagenesis on Cel-GLC-2 (Table 4.1). All mutants were directly activated by glutamate, but with concentration-response curves shifted to the right in the order of wild-type > Q292S > M291Q > MQ→QS double mutant, with the MQ→LT double mutant producing only a minimal response to 1 mM glutamate (Figure 4.8). The slope of the concentration-response curve of the Q292S mutant, the most sensitive of the mutants, was significantly shallower than that for wild-type or the M291Q Cel-GLC-2. This response was also present in the MQ→QS double mutant. A steeper slope suggests more cooperativity of binding between glutamate molecules; initial agonist binding greatly increases the affinity of binding of subsequent agonist molecules, leading to improved channel activation kinetics.

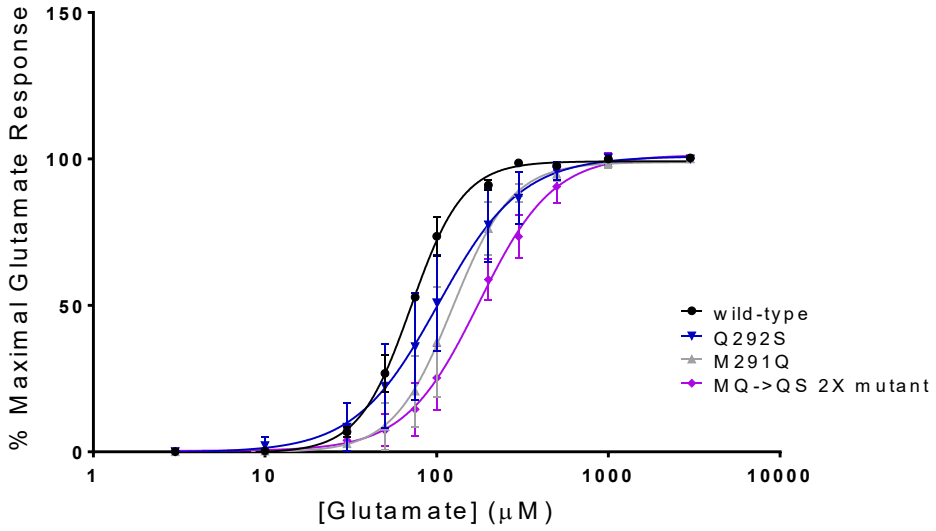

	wild-type	Q292S	M291Q	MQ→QS
EC_{50} (μM)	70.77	102.0	123.9	176.3

	± 3.88	± 24.83	± 18.72	± 17.55
Hill slope	2.844	1.793	2.498	2.015
	± 0.1642	± 0.2803	± 0.2939	± 0.1809

Figure 4.8. Concentration-response curves for glutamate activation of wild-type Cel-GLC-2 and the mutants M291Q, Q292S, and MQ→QS. The order of potency was wild-type > Q292S > M291Q > MQ→QS. In the presence of glutamate alone (1 mM), the LT double mutant had < 50 nA channel activation. n > 3.

4.2.6 M291L + Q292T double mutant

Oocytes expressing the MQ→LT doubly mutated Cel-GLC-2 responded to glutamate with much lower magnitude compared to wild-type Cel-GLC-2. This was surprising because the LT motif is found in filarial nematodes and, although published mutants of IVM receptors can alter Cl^- conductance, our residues do not line the channel pore and are not predicted to impact channel activation by glutamate. Interestingly, the LT double mutant was equally activated by MOX and IVM (Figure 4.9). Cully *et al.* (1994) reported that low concentrations of IVM potentiate glutamate responses in GluCls, and we exposed oocytes expressing the LT double mutant to a series of glutamate-IVM-glutamate exposures to determine whether it could potentiate subsequent glutamate responses. Indeed, compared to the initial glutamate response, incubation with 10 μM IVM or MOX caused a >10-fold increase in signal amplitude after re-challenge with glutamate. This enhancement of signal was concentration-dependent for both glutamate and MLs (Figure 4.9B,C). In the presence of 10 μM IVM, the glutamate EC_{50} was 174.3 ± 56.4 μM (Hill slope = 0.80 ± 0.32), placing it close to the MQ→QS double mutant in potency.

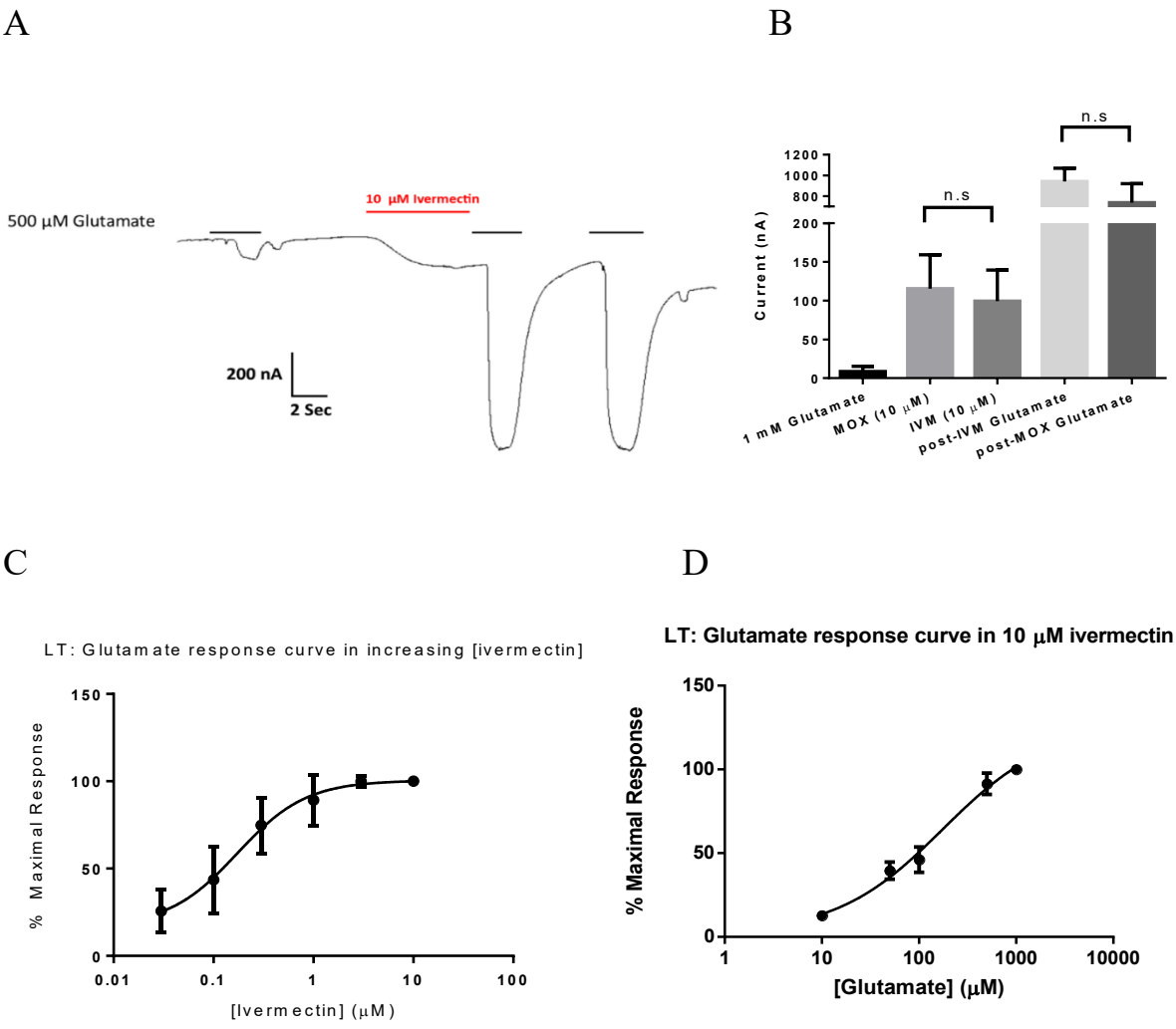

Figure 4.9. (A) Representative recording of the LT double mutant showing that IVM directly activates the channel and potentiates glutamate responses. (B) MOX and IVM (10 µM) similarly activated the LT double mutant, and enhanced glutamate signaling n>5. (C) IVM caused a concentration-dependent increase in the response to 1 mM glutamate. EC_{99} current produced with 6.6 µM IVM. (D) The IVM-induced glutamate response was concentration-dependent. Glutamate EC_{50} = 174.3 ± 56.4 µM (Hill slope = 0.7993 ± 0.3193). n=4.

4.2.7 α-type mutagenesis

We next sought to determine if amino acid substitutions associated with α-type GluCl residues also recreated the response of ML activation. Changing Gln292 to the smaller and polar Ser, which

has been shown to form a hydrogen bond with the cyclohexene of IVM, was strongly predicted to permit IVM and MOX binding. Indeed, in oocytes, Q292S Cel-GLC-2 was activated by IVM and MOX with the characteristic slow, irreversible hyperpolarization response seen with α-type GluCls (Figure 4.10A,B). Interestingly, in the M291Q homology model, IVM was predicted to have very low affinity and MOX was predicted to bind as it does to wild-type Cel-GLC-2. Oocytes expressing M291Q mutants responded to MOX in the same way as those expressing wild-type Cel-GLC-2: there was no direct activation and subsequent glutamate responses were strongly antagonized (Figure 4.10C). In contrast, IVM directly activated M291Q receptors (Figure 4.10D), albeit to a smaller extent than for Hco-GLC-5 or other α-type GluCls reported in the literature.

As no GluCl has been reported to exhibit differential activation by IVM and MOX, we tested if these drugs bound to the same site despite eliciting different responses. We applied 1 μM MOX onto M291Q-expressing oocytes already irreversibly activated by 1 μM IVM. MOX apparently competed for the IVM biding site, causing the current to return to baseline (Figure 4.10D). When the order of exposure was reversed, pre-treatment with 1 μM MOX for 15-20 sec delayed and reduced the activation induced by 1 μM IVM, suggesting that MOX molecules occupied the binding site and were slowly removed by competition with IVM (Figure 4.10E; Table 4.2).

A (Q292S)

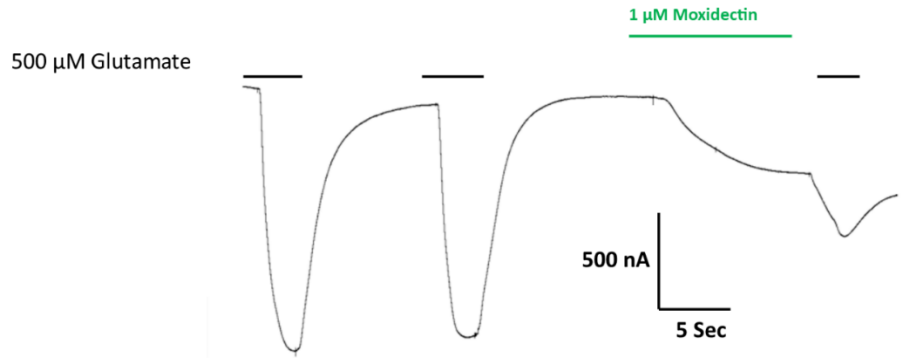

B (Q292S)

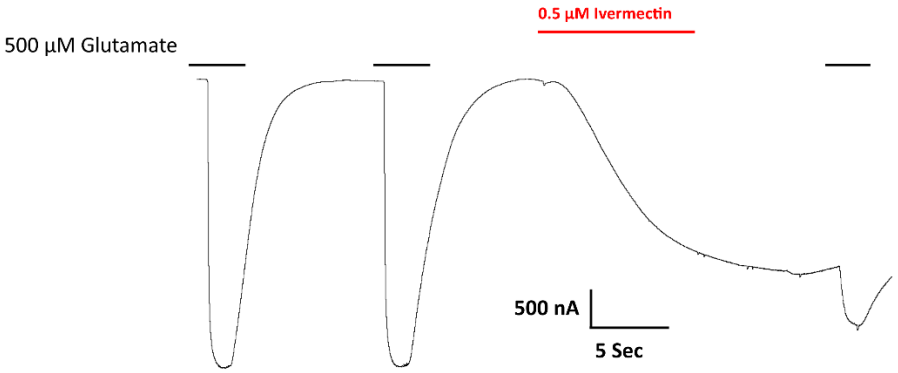

C (M291Q)

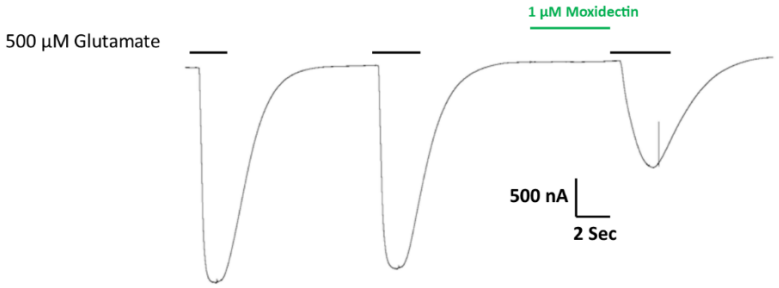

D (M291Q)

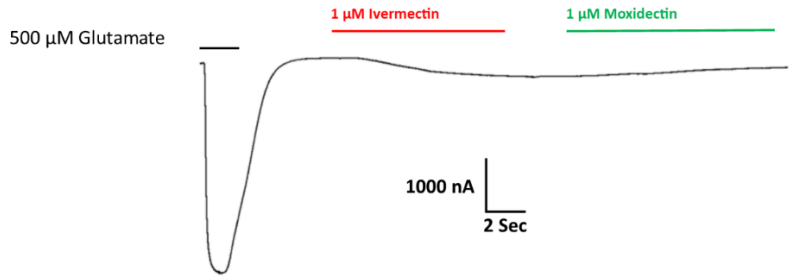

E (M291Q)

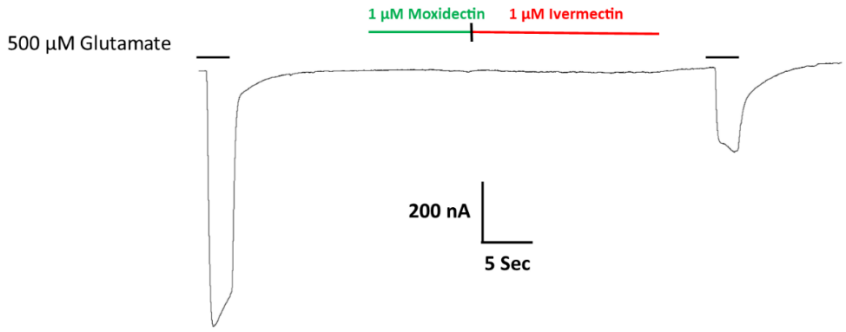

Figure 4.10. (A) Representative traces of the Q292S mutant activation by glutamate and MOX. (B) Representative traces of the Q292S mutant activation by glutamate and IVM. (C) Glutamate activation of the of M291Q mutant was antagonized by MOX. MOX did not activate M291Q (D) Activation of the M291Q mutant by IVM. Cessation of IVM exposure did not return to baseline, but activation was reversed by subsequent application of MOX. (E) Attenuation of the IVM response by pre-exposure to MOX. MOX did not activate the M291Q mutant.

Table 4.2: M291Q mutant responses to IVM and MOX

	Time to IVM response after application (sec ± SEM)	**IVM response (% initial glutamate response ± SEM)**	**Amplitude of IVM response (nA ± SEM)**
No MOX pre-treatment	*13.6 ± 2.1	**13.7 ± 2.2	***390.4 ± 125.9
15-20 sec MOX pre-treatment	*34.4 ± 4.9	**4.0 ± 2.8	***26.6 ± 11.4

n=5; Significance determined by t-test, *p=.0045; **p=.0261; ***p=.0206

We next assayed the MQ→QS double mutant to determine if the MOX agonist activity observed for Q292S was suppressed by the presence of the M291Q substitution. Oocytes expressing the MQ→QS double mutant were directly activated by both IVM and MOX, as predicted by the *in silico* model. Interestingly, the glutamate concentration-response curve was shifted further to the right for the MQ→QS double mutant than for either individual mutant. In contrast, this construct was most sensitive to the agonist activity of IVM (Figure 4.11); the presence of both substitutions greatly increased sensitivity to IVM.

A

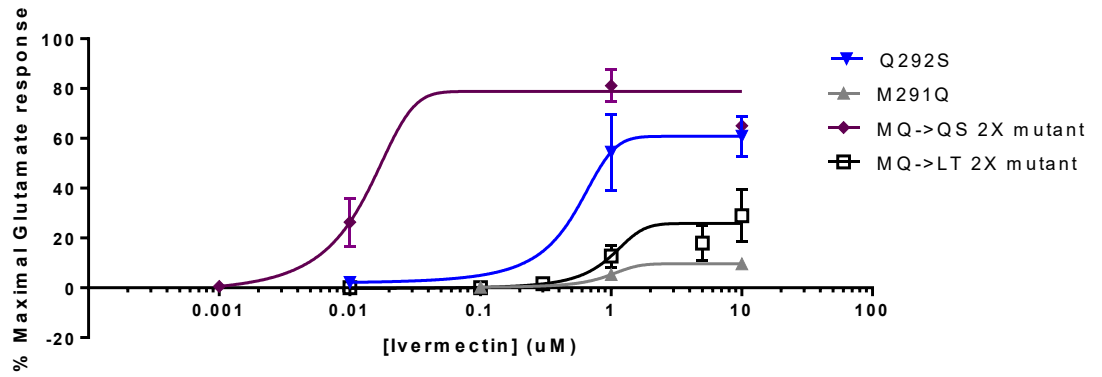

	Q292S	M291Q	MQ→QS	MQ→LT
EC_{50} (μM)	~3.15	~8.49	~1.03	~9.21
Hill slope	~1.9	~1.5	~59.5	~1.3

B

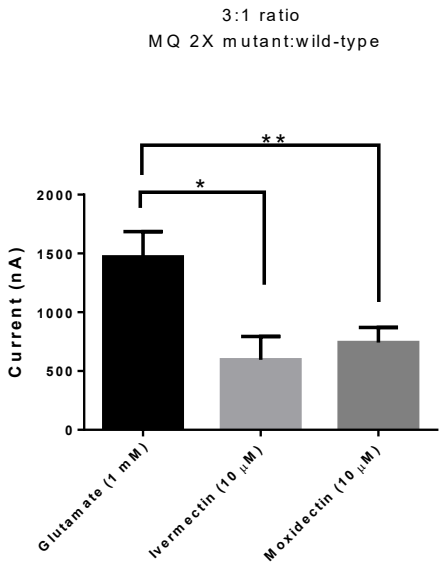

Figure 4.11 (A) Concentration-response curves of IVM activation for Cel-GLC-2 mutations. (B) Responses to IVM and MOX in oocytes co-expressing wild-type and MQ→QS double mutant subunits; n ≥ 6; Significance determined by ANOVA, *p=.0356; **p=.0457

Since IVM sensitivity was the dominant phenotype of the mutants, we next investigated whether co-injecting cRNA encoding the QS double mutant and wild-type Cel-GLC-2 would form receptors activated by IVM. Because Cel-GLC-2 subunits form homomeric receptors, we predicted that that wild-type and mutant subunits would form heteromeric receptors with each other. Co-expression of these subunits produced oocytes with MQ→QS type responses (smaller currents than wild-type Cel-GLC-2 with direct activation by IVM and MOX; Figure 4.11B). A caveat is that we could not differentiate oocytes expressing only heteromeric receptors from those expressing populations of both heteromeric and homomeric wild-type and mutant subunits. To partially address this, we altered the ratio of wild-type or mutant subunit cRNA injected from 1:1 to 1:3, and 3:1; however, this had no impact on the pharmacology (data not shown).

4.3 DISCUSSION

Recently, Degani-Katzav et al. (2017b) showed in a CHO cell expression system that the response of *C. elegans* Cel-GLC-2 to 100 mM glutamate is antagonized by IVM. Considering these findings and the diverse activities of MLs, we initially sought to determine if this inhibition could be replicated in oocytes at more physiological concentrations of glutamate and if Cel-GLC-2 is also allosterically modulated by MOX. We discovered two residues that convert antagonist into agonist activity, one of which distinguishes IVM from MOX. Our data corroborate previous findings that

IVM is an antagonist of Cel-GLC-2, showing in *Xenopus* oocytes that IVM inhibits glutamate responses and demonstrating that Cel-GLC-2 is also non-competitively antagonized by MOX, an ML in the milbemycin class. These results are summarized in Figure 5.1.

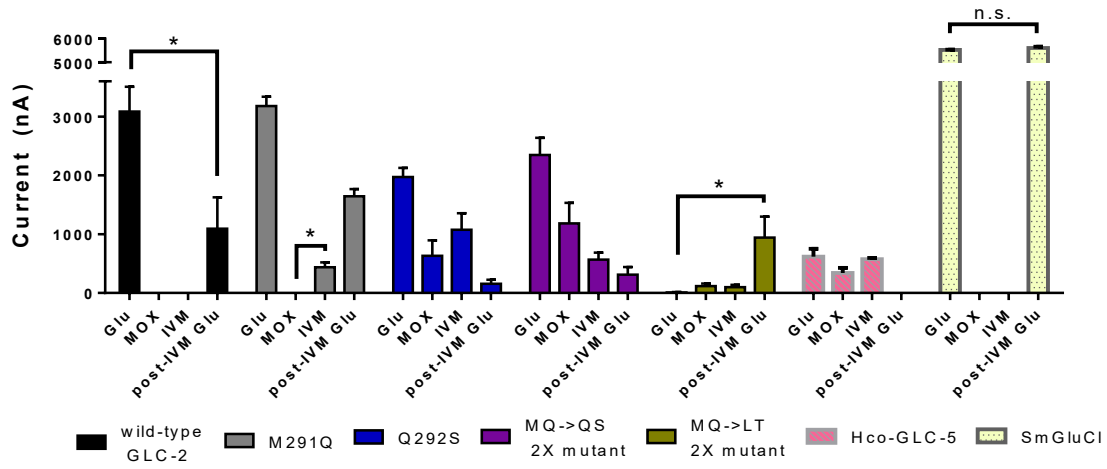

Figure 5.1. Maximal current activation by 1 mM glutamate, 10 µM IVM, 10 µM MOX, or a re-challenge of 1 mM glutamate after IVM. M291Q, Q292S and the double mutants MQ→QS and MQ→LT all responded to IVM, but only the M291Q mutation did not convert Cel-GLC-2 into a MOX responder. *H. contortus* GLC-5 and *S. mansoni* GluCl-2 were used as controls for IVM sensitivity and insensitivity, respectively, and were not challenged with MOX in this thesis; n ≥ 3; *t-test, p<.05.

4.3.1 General pharmacology

We generated individual and double Cel-GLC-2 mutants, M291Q and Q292S, corresponding to sequences found in α-type GluCl subunits, and a double MQ→LT mutant corresponding to the residues present in filarial parasitic nematodes, including *B. malayi*, *W. bancrofti*, and *D. immitis*. This region is just downstream of the pore-lining PAR anion selectivity motif typically found in

anion channels (Galzi et al., 1992). Instead of this motif, the homologous sequence in Cel-GLC-2 is AGR, yet this channel retains Cl^- specificity (Atif et al., 2019; Cully et al., 1994; Degani-Katzav et al., 2017b). Mutating cation-selective acetylcholine- (Corringer et al., 1999; Galzi et al., 1992) and 5-HT-gated (Gunthorpe and Lummis, 2001) channels ($5\text{-}HT_3$) to incorporate this Pro-containing motif, or mutating anion-selective channels to remove the Pro and substitute the Ala with a positively charged residue, switches ion selectivity (Keramidas et al., 2002, 2000). The Ala-to-Gly difference in Cel-GLC-2 may not greatly influence ion selectivity, but the lack of the Pro may partially explain the differential activity of glutamate on heteromeric αβ receptors containing the Cel-GLC-2 subunit compared to homomeric α-type channels (Atif et al., 2019; Cully et al., 1994).

We found that Cel-GLC-2 mutants were less sensitive to glutamate than wild-type Cel-GLC-2; these mutants do not vary in residues that line the channel pore. Many studies report using high mM concentrations of glutamate to activate receptors in oocytes, including homomeric AVR-14B (Dent et al., 2000; Yates and Wolstenholme, 2004), AVR-15 (Dent et al., 1997), and a heteromeric Cel-GLC-1 (Cully et al., 1994), which produce very small currents. In contrast, homomeric GLC-2 (Cully et al., 1994), -3 (Horoszok et al., 2001), and -5 (Forrester et al., 2004) respond to μM glutamate, suggesting that some stoichiometries are artefactual and that *in vivo* receptors are likely heteromeric and require the presence of additional subunits. It is possible that the absence of a PAR motif coupled with the presence of M291 and Q292 in Cel-GLC-2 contribute to greater sensitivity to glutamate in heteromeric receptors, but it is clear that agonist activity relies on many other factors (Degani-Katzav et al., 2016).

4.3.2 Mutagenesis: Q292S position

The cyclohexene hydroxyl of IVM is indicated to a hydrogen bond with Ser260 of the (+)TM2 (Gln292 of Cel-GLC-2 including signal peptide) in the crystal structure of Cel-GLC-1 bound to IVM; this relative residue position is denoted 15' in the literature (Hibbs and Gouaux, 2011). In the human GlyR, mutating the analogous Ser to Ile did not markedly affect IVM sensitivity (Lynagh et al., 2011). In comparison, the Cel-GLC-2 Q292S mutation converted IVM and MOX from antagonists to agonists in our study. Gln is slightly longer than Ile and this difference in length may exceed a threshold for IVM and MOX to be able to fit deep enough into the binding site to activate GluCls. Comparing the wild-type and Q292S channels in *in silico* models showed that IVM and MOX were positioned twice as far when a Gln rather than a Ser was present at 292. Furthermore, the M291L + Q292T double mutant was also activated by IVM and MOX in the presence of a Leu291. However, IVM responses are complex, and the role of size of the side chain at the analogous 292 position may be limited to the GluCls that are directly activated by IVM. IVM does not directly activate, but is a positive allosteric modulator of the α-7 nAChR in which the analogous 292 position is a Met. Substitution of this Met with (smaller) Leu converted IVM into a negative allosteric modulator instead of a direct activator (Collins and Millar, 2010). It should be noted that in the acetylcholine receptor model, IVM is predicted to bind in a different cleft, between (+)TM1 and (+)TM4, which may explain the different roles of these residues.

4.3.3 Mutagenesis: M291Q position

Whereas we anticipated that mutating Gln292 would influence activation of Cel-GLC-2 by MLs, an adjacent Met in the analogous Met291 position is not present in any receptor known to interact with MLs, and this residue points away from the pore and the ML binding site. In a series of GlyR

mutants, Lynagh et al. (2011) mutated the analogous 291 position from Gln to Trp and found little effect on IVM activity, but did not test other MLs. In stark comparison, we found that substituting Met for Gln (present in α-type GluCl subunits) transformed the IVM response from antagonism into activation, but MOX remained an antagonist. Superimposing the wild-type Cel-GLC-2 and M291Q mutant models showed that the Gln292 residue was positioned further from the IVM binding site in the M291Q mutant, but no other significant positional changes were present. Permission of IVM gating in M291Q may also be a result of changing local conformational flexibility. In the M291Q mutant, *in silico* analysis predicted the primary amine of the Gln to form a hydrogen bond with the backbone carbonyl oxygen of (+)TM1 Leu252 in the same subunit. The analogous hydrogen bond is also present in the IVM-sensitive Cel-GLC-1 model (Leu220) and may play a role in the ability of IVM to induce the conformational changes required for channel activation, unlike the wild-type Met291 Cel-GLC-2. Furthermore, Met interacts with aromatic residues of α-helices (Cregut and Serrano, 1999; Viguera and Serrano, 1995) as strong as salt bridges and up to ~6 Å apart (Valley et al., 2012) in a 1:1 ratio (Bodner et al., 1980). Two aromatic residues in our model fit this criteria: (+)TM1 Tyr247 and (+)TM3 Trp311. It is possible that increased or altered steric hindrance in this location may result in reduced capacity of MLs to perturb local residues, preventing activation of wild-type Cel-GLC-2 receptors. Weak M291Q induction of IVM but not MOX agonism is indicative of a dual role of the 291 and 292 positions, and suggests that, compared to MOX, IVM better fits into the binding pocket to induce activation.

4.3.4 Mutagenesis: M291L + Q292T positions

Filarial nematode GLC-2 subunits possess an LT motif at the positions analogous to the MQ residues discussed thus far. IVM is a potent microfilaricide and causes prolonged sterilization of

adults of some filariids, but lacks strong macrofilaricidal activity, requiring repeated high doses to clear infection (Bazzocchi et al., 2008; Dreyer et al., 1995; McCall et al., 2001). The MQ→LT substitution in Cel-GLC-2 nearly abolished glutamate responses, but converted IVM and MOX into weak partial agonists. Cel-GLC-1 binds glutamate only after previous exposure to IVM, but even then, glutamate only elicits very small currents (Etter et al., 1996). We found that IVM also facilitated glutamate-induced responses in the LT double mutant, but unlike in Cel-GLC-1, these were comparable in amplitude to wild-type Cel-GLC-2 responses (Figure 5.1). Characterization of wild-type filarial GLC-2 will be required to determine the profile of sensitivity to avermectins and milbemycins, and whether different levels of expression and/or tissue localization can explain the different responses observed in these parasites.

A limitation of our study was that we did not investigate a mutant in which the 291 or 292 residues are LQ, which is the sequence in multiple nematode clades. Our rationale was that the LT mutation is more relevant to the important filarial nematodes. Additionally, we separately tested each residue in the presence of Gln in position 292 in wild-type and the M291Q mutant Cel-GLC-2, and the Leu in position 291 was tested in the LT double mutant.

4.3.5 Conclusion

We provided clear evidence of differential pharmacology of avermectins and milbemycins on a GluCl and show milbemycin antagonism of wild-type *C. elegans* homomeric Cel-GLC-2 receptors. We corroborate that Cel-GLC-2 is antagonized by IVM and suggest that avermectins and milbemycins bind to the same pocket, and that agonist and antagonist activities of the two classes of MLs rely on different residues that are not directly related to those lining the IVM

binding pocket. Cel-GLC-2 has different ML-selection motifs in different species, with implications for species differences in drug sensitivity.

Chapter 5: General discussion & conclusions

When new drugs are discovered, they are often tested against a single model of parasitic infection, and testing is gradually expanded to other species to determine the spectrum of activity. A limitation of this process is that no mechanism for treatment failure is determined if the spectrum is suboptimal, and there is a gap in our knowledge about how variation in drug-receptor interactions influences species differences in anthelmintic sensitivity. Amino acid sequences of drug targets can be highly similar between closely related parasites and homogeneity of drug targets and responses is often accepted by generalization, but understanding the physiological effects of these differences and their role in determining efficacy is important for their therapeutic use. The goal of this thesis was to assess factors that affect susceptibility to anthelmintics that target pLGICs. How do species-specific differences in the sequence of ion channel subunits affect drug efficacy?

5.1 ACR-16

Much of our understanding of anthelmintic targets and their function is derived from studies of the free-living nematode, *C. elegans* (reviewed by Geary and Thompson, 2001), including the levamisole (Boulin et al., 2008) and IVM receptors (Cully and Paress, 1991). However, large differences in drug sensitivity have been reported between closely related parasitic nematodes, even those in which the drug targets show high levels of sequence homology (Behnke et al., 1993; Schwarz et al., 2015; Tang et al., 2014). This suggests that model organisms are an appropriate starting point, but drug effects and drug targets must be studied individually in each

species of parasitic nematode to assess differences in pharmacodynamics. ACR-16 is one such drug target relevant for hookworms of humans and animals.

I began my thesis by comparing the pharmacology of cholinergic anthelmintics on the pLGIC, ACR-16, from two closely related species of hookworm, *N. americanus* and *A. ceylanicum*. Table 5.1 summarizes the current state of knowledge for ACR-16s. As a general trend, a functional ACR-16 take 2-3 days to reach maximal expression in *Xenopus* oocytes, requires co-expression of the RIC-3 accessory protein, and responds to acetylcholine and nicotine at low μM EC_{50} values. They are antagonized by the classic nAChR antagonist mecamylamine and are not activated by levamisole or bephenium.

I found that, despite the very high sequence identity between Ace- and Nam-ACR-16 (95%), these receptors exhibit different pharmacology that could not have been predicted by comparison with a model organism or ACR-16 receptors from other parasites. For instance, despite being phylogenetically closer to *N. americanus* and *A. caninum*, *A. ceylanicum* ACR-16 pharmacology more closely resembles that of ACR-16 from the clade III nematode *A. suum* (Meldal et al., 2007). This is highlighted by large evoked current amplitudes, greater potency of nicotine than acetylcholine, and weak activation by oxantel on Ace- and Asu-ACR-16, but not on Nam- and Aca-ACR-16 (Abongwa et al., 2016b).

Table 5.2 Comparison of ACR-16 pharmacology

Species	Acetylcholine response (μM EC_{50})	Maximal response (current)	Nicotine response (μM EC_{50})	Response to oxantel?	Research group
A. ceylanicum	20.64	nA-µA	24.33	Yes	Present study
N. americanus	170.1	nA	570.7 *Partial agonist	No	Present study
A. caninum	50	~100nA	*Partial agonist	No	(Choudhary et al., 2019)
H. contortus	Non-functional	Non-functional	Non-functional	Non-functional	(Charvet et al., 2018)
C. elegans	15.85	62.5 ± 10 nA	n/a	Very weak	(Raymond et al., 2000)
C. elegans	55.4	nA-µA	12.6 *Partial agonist	n/a	(Ballivet et al., 1996)
Parascaris equorum	6.4	µA	2.9	n/a	(Charvet et al., 2018)

A. suum	5.9	nA-µA	3.9	Yes	(Abongwa et al., 2016b)

Interestingly, *N. americanus* ACR-16 failed to achieve maximal channel activation with nicotine (similar to Aca- and Cel-ACR-16, but unlike Ace-, Peq- and Asu-ACR-16), and nicotine was roughly 5-fold less potent than acetylcholine, in contrast to the situation in other published ACR-16s. *N. americanus* and *A. ceylanicum* exhibit different thermogenic profiles at rest and in response to levamisole (Flores et al., 2016), which may indicate that ACR-16 has different functional roles in these organisms. In *C. elegans,* L-type nAChR subunits are encoded by several genes (*unc-63, unc-38, unc-29, lev-1* and *lev-8*) and comprise receptors distinct from ACR-16 receptors, but serve a partially redundant role in muscle contraction, as only disruption of both receptor populations results in paralysis (Francis et al., 2005; Touroutine et al., 2005). Therefore, functional differences in Ace- and Nam-ACR-16 must be viewed in the context of a whole-organism setting, and further research is required to investigate the function of hookworm L-type nAChRs and their *in vivo* interplay with ACR-16.

Compared to acetylcholine and nicotine, less is known about the intermolecular interactions required for tetrahydropyrimidine efficacy on AChRs. Pyrantel-induced activation is strongly associated with the presence of a glutamic acid in loop B (Bartos et al. 2006) (Rayes et al. 2004) and a glutamine in loop D (Bartos et al. 2006). This loop D glutamine is also required for morantel, but not acetylcholine or oxantel binding to the α7 receptor (Bartos et al. 2009). Interestingly, all characterized ACR-16 subunits lack these residues, and instead possess an analogous loop D aspartic acid and loop B glycine. These differences in amino acid composition may explain the lack of efficacy of pyrantel and morantel, but do not explain differences between

ACR-16 receptors. Together with the electrophysiological data, our homology model predictions suggest that there are separate mechanisms of binding for nicotine and acetylcholine compared to tetrahydropyrimidines, and that the Nam-ACR-16 agonist binding pocket strongly discriminates between these two classes of molecules. These studies are important to understand which amino acids are vital for drug sensitivity and to build a database that allows comparison of pharmacodynamic parameters from numerous species to aid in future rational drug design and high through-put *in silico* drug screening. A caveat to the interpretation of these homology modelling results is the observation of a pyrantel-induced signal in oocytes expressing Nam-ACR-16, but no signal in response to oxantel or morantel, a difference in efficacy inconsistent with predicted binding. It is possible that the smaller and decaying nature of Nam-ACR-16 responses to agonists, compared to Ace-ACR-16, could prevent detection of low proportions of activated receptors.

5.2 GLC-2

Having characterized differences in anthelmintic efficacy on N-type nAChRs, I next used *C. elegans* to investigate the relationship between MLs and Cel-GLC-2, the only GluCl subunit not directly activated by this class of anthelmintic. I used *C. elegans* because the tissue location and basic pharmacology of Cel-GLC-2 is known (Laughton et al., 1997; Cully et al., 1994; Degani-Katzav et al., 2017b), whereas no functional hookworm GluCls have been characterized. I discovered that MOX, like IVM, is a Cel-GLC-2 antagonist, and identified a mutation, Q292S, that converts both drugs into agonists. I also discovered that the mutation M291Q converted IVM into an agonist while retaining antagonistic properties of MOX.

Many studies have shown that variations in the structure of MLs, including the absence of the disaccharide motif in MOX, play vital roles in pharmacokinetics and efficacy (Gopal et al., 2001; Ménez et al., 2012; Michael et al., 2001), but to date, no other study has shown differential responses at the level of drug target. The pharmacodynamic significance of the Met291 and Gln292 residues for *in vivo* sensitivity to IVM or MOX is unknown, but there are clear differences in Cel-GLC-2 function when these residues are changed to represent α-type subunits or filarial β-type subunits. Interestingly, both changes cause Cel-GLC-2 to be directly activated by IVM and MOX, even though these drugs are not macrofilaricidal (Richard-Lenoble et al., 2003). However, they do paralyze adults at high concentrations (Strote et al., 1990; Tompkins et al., 2010), posing the question whether filarial GLC-2 subunits fit the IVM-insensitive β-type category. Future studies comparing the function of heterologously expressed GLC-2 and other GluCls between IVM-sensitive parasites and filarial nematodes should be prioritized to identify differences in function and pharmacology. The GluCl AVR-14 from *D. immiti*s showed IVM-sensitivity in *Xenopus* oocytes, but required a very high concentration of glutamate (10 mM) to elicit very small (100 nA) responses (Yates and Wolstenholme, 2004). This is suggestive of either the wrong ligand, or that missing pieces are required to reconstitute expression of receptors found *in vivo*. This is demonstrative of the usefulness of *Xenopus* oocytes as a system to assay pLGIC function, but also demonstrates its limitations if the *in vivo* stoichiometry of receptors is not known.

Another area that requires further investigation is determining the GLC-2 tissue location in different species of parasitic nematodes. In *C. elegans*, Cel-GLC-2 is expressed in the pharynx (Laughton et al., 1997) and MOX and IVM inhibit pharyngeal pumping (Pemberton et al., 2001), but at different concentrations (Ardelli et al., 2009). In comparison, pharyngeal activity is also inhibited in *H. contortus* (Geary et al., 1993), but Hco-GLC-2 is expressed in motor neuron

commissures and nerve cords, and not in the pharynx (Portillo et al., 2003). As such, determining GLC-2 tissue location in different species of parasitic nematode, and identifying the subunit partners of recombinantly expressed and native receptors using techniques such as crystallography or immunoprecipitation (Fasoli et al., 2016), are important areas for future research.

These studies and ours highlight the importance of species-specific effects of ML targeting and the possibility of species differences in the manifestation of drug resistance. I show that human hookworm ACR-16 receptors are pharmacologically distinct from each other, and suggest structural roles for the mechanism of oxantel targetability. I further show that subunit- and species-specific differences in a single amino acid in Cel-GLC-2 can dictate ML sensitivity, and even distinguish IVM and MOX responses. Taken together, this thesis fills in important gaps in knowledge of the use of anthelmintics and highlights the strengths and weaknesses of using model organisms in the study of parasitology.

Chapter 6: Materials and methods

6.1 Ethics statement

All experiments complied with McGill University and Canadian Council on Animal Care animal protocols. All surgical procedures and animal care were performed by trained personnel as outlined in AUP 2015-7758 issued by the McGill Animal Care Committee.

6.2 Animals used

The wild-type N2 Bristol strains of *C. elegans* was originally obtained from the *Caenorhabditis* Genetics Center (CGC), funded by the National Institute of Health National Center for Research Resources. Worms were maintained on nematode growth medium (NGM) plates (17 g/L agar, 51.3 mM NaCl, 2.5 g/L peptone, 1mM $CaCl_2$, 1 mM $MgSO_4$, 5.11 mM K_2HPO_4, 20 mM KH_2PO_4) supplemented with 1 mL of 5 mg/ml cholesterol (in 100% ethanol), grown at 20 °C , and seeded with *Escherichia coli* OP50 according to standard culture methods (Brenner, 1974). Plates used for IVM resistant worms were supplemented with 11.4 nM IVM and plates used for MOX resistant worms were supplemented with 4.6 nM MOX to maintain selectin of resistant worms (Ménez et al., 2016).

Frozen, adult *A. ceylanicum* and *N. americanus* were provided by the Dr. Raffi Aroian lab (University of Massachusetts Medical School, Worchester, MA).

Xenopus laevis

All experiments using *X. laevis* complied with McGill University and Canadian Council on Animal Care animal protocols. All surgical procedures and animal care were performed by trained personnel as outlined in AUP 2015-7758 issued by the McGill Animal Care Committee. Adult female *X. laevis* were purchased from Xenopus1 (http://www.xenopus1.com).

6.3 Cloning

6.3.1 RNA extraction

Total RNA was isolated from 20-30 adult hookworms, or two 100 mm NGM plates of wild-type *C. elegans* washed with M9 minimal salt buffer (33.9 g/L Na_2HPO_4, 15 g/L KH_2PO_4, 5g/L NH_4Cl, 2.5g/L NaCl) and collected in a conical tube. Worms were crushed with a mortar and pestle and kept cold with liquid N_2 until ground into a fine powder and suspended in TRIzol. RNA was isolated using Phenol TRIzol purification reagents and column purified with a Qiagen RNeasy MiniElute Cleanup Kit (Qiagen, Toronto, ON). Quality of RNA was validated by optical density and visual inspection following electrophoresis though a denaturing agarose gel.

First strand cDNA was synthesized using a Maxima H Minus First Strand cDNA Synthesis Kit, and double-stranded DNase-treated to remove genomic DNA (Thermo Fisher Scientific, Waltham, MA).

A. ceylanicum cDNA was also generously provided by Dr. John Hawdon (George Washington University School of Medicine & Health Sciences, Washington, DC), and cloning was performed on both cDNA libraries to validate presence of genes.

A partial sequence of *N. americanus* ACR-16, NECAME_12789, was obtained by BLASTP search. A primer specific for the common nematode 5' trans-splice leader 1 (SL1) was used to amplify the 5' end and a poly-A primer was used to amplify the 3' end of the *acr-16.* Cloned amplicons were verified Sanger sequencing (at Genome Quebec). For other PCR, full length sequences were obtained from NCBI and primers were designed to amplify the full coding sequences flanked by a 5' *NotI* and 3'*ApaI* restriction site. All PCR was performed using primers designed by Primer3 (Rozen and Skaletsky, 2000) and amplified genes are listed Table 6.1.

Table 6.1 cDNAs amplified and the primers used

Gene	**Forward**	**Reverse**	**Accession Code**
A. ceylanicum acr-16	Outer primer: 5'-GATGGAAAAGTGCACTGGGTG -3' Inner primer: 5'-GCGGCCGCATGTGATGCGTTCGCTGGTC-3'	Outer primer: 5'-GAGAGGAATAAGAAGAACAGACGAC -3' Inner primer: 5'-GGGCCCCACAAGGGTTAGGCGACGAG-3'	accession # MT163735

N. americanus acr-16	Outer primer: 5'-GCGGTTTAATTACCCAAGTTTGAG-3' Inner primer: 5'-ATATAGCGGCCGCATGCGTTCGTTGGTCGTCT-3'	Outer primer: 5'-CCTCAAAAATGTCTAGAGAGTTCG-3' Inner primer: 5'-GGGCCCAGAGTTCGATCTAGGCGACA-3'	accession # MT163736
C. elegans glc-2	5' – ATTTGCGGCCGCATGACTACACCTAGTTCATTTTC -3'	5' – ATTTGGGCCCCTAAACGAGAGACTCTGGAGTGG-3'	NM_059069.4

PCR amplicons roughly 1.5 kb in size were gel purified using a Zymoclean Gel DNA Recovery Kit (Cedarlane Laboratories, Ltd. Burlington, Ontario) for column purification and then double digested with *NotI* and *ApaI* for T4 ligation into the pGEMT-Easy subcloning vector (Invitrogen, Waltham, MA). Plasmid was transformed into DH-5α competent cells (ThermoFisher Scientific, Waltham, MA), extracted using a BioBasic alkaline lysis miniprep kit (Cedarlane Laboratories, Ltd. Burlington, Ontario), and sent to Genome Quebec for Sanger sequencing.

Confirmed clones were digested out of pGEMT-Easy with *NotI* and *ApaI* and inserted into the pTD2 *X. laevis* oocyte expression plasmid with a T4 ligase (Duguet et al., 2016). pTD2 contains

the 5' and 3' UTR of *X. laevis* β-globin designed to stabilize exogenous genes injected into oocytes and increase translation efficiency.

6.3.2 Site-directed mutagenesis

To investigate the role of residues suspected to convey ML insensitivity in Cel-GLC-2, we created 4 different mutants outlined in Table 6.2. Overlapping mutagenesis primers were designed using the online Agilent QuikChange Primer Design tool software (https://www.agilent.com/store/primerDesignProgram.jsp). Primer pairs are designed to contain base pair mismatches in the sense and antisense target site, flanked by long regions of base pairing to maximize efficiency of amplification. In lieu of the Agilent QuikChange II mutagenesis kit (ThermoFisher Scientific, Waltham, MA) we employed the high-fidelity Q5 proofreading DNA polymerase (New England Biolabs) to synthesize mutant copies of the entire pTD2 plasmid with Cel-GLC-2 insert and used *DpnI* to eliminate wild-type parental methylated DNA grown in DH-5α. This polymerase has been reported to be unable to generate full length circular mutant plasmid using the QuikChange complementary primers protocol (Xia et al., 2015). As Q5 generates blunt ended PCR products, I hypothesized that ligase treatment of the resulting amplicons would permit generation of plasmid and allow subsequent bacterial transformation. Resulting plasmids were re-grown in DH-5α and sent for sequencing to Genome Quebec for verification of mutagenesis.

Table 6.2 Primers used to generate *Cel-glc-2* mutations. Codons encoding positions 291 and 292 are highlighted green and yellow respectively.

	Forward primer (5'-3')	Reverse Primer (5'-3')
M291Q	GGCGTTGATTGCAGATTGC TGTGTAGTCATTGTAAGAA GCGTAG	CTACGCTTCTTACAATGACTACACAGC AATCTGCAATCAACGCC
Q292S	AAGCTTGGCGTTGATTGAA GATGACATTGTAGTCATTG TAAGAAGC	GCTTCTTACAATGACTACAATGTCATC TGCAATCAACGCCAAGCTT
MQ→QS (double mutant)	GGAAGCTTGGCGTTGATTG CAGATGACTGTGTAGTCAT TGTAAGAAGCGTAGT	ACTACGCTTCTTACAATGACTACACAG TCATCTGCAATCAACGCCAAGCTTCC
MQ→LT (double mutant)	GGAAGCTTGGCGTTGATTG CAGATGTAAGTGTAGTCAT TGTAAGAAGCGTA	TACGCTTCTTACAATGACTACACTTAC ATCTGCAATCAACGCCAAGCTTCC

6.4 RNA synthesis

NheI-linearized pTD2 was column purified and used as a template for *in vitro* transcription of copy RNA (cRNA) using a mMESSAGE mMACHINE T7 Transcription kit (Ambion, Burlington, ON). Parental plasmid was removed by DNase treatment and the newly synthesized capped cRNA was precipitated using LiCl, then resuspended in nuclease free water and stored at -80 °C.

6.5 *Xenopus laevis* oocytes and microinjection

Ovaries of *X. laevis* were surgically extracted from adult female frogs under 0.15% MS-222 tricaine methanesulphonate anaesthesia (Sigma-Aldrich, Oakville, ON), neutralized to pH 7 with sodium bicarbonate. Ovary segments were cut into roughly 15 oocytes and treated with collagenase type II from *Clostridium* (Sigma-Aldrich, Oakville, ON) in Ca^{2+}-free oocyte ringer solution (82 mM NaCl, 2 mM KCl, 1 mM $MgCl_2$, 5 mM HEPES buffer, $NaHCO_3$ to pH 7.3) to defolliculate and dissolve the tissue connecting individual oocytes. Oocytes were washed in ringer solution to remove leftover collagenase and allowed to recover at 19 °C for 1-2 hr in the saline solution ND96 (96 mM NaCl, 3 mM KCl, 1 mM $MgCl_2$, 1.8 mM $CaCl_2$, 5 mM HEPES buffer) supplemented with pyruvate (2.5 mM) as a carbon source and penicillin (100 U/ml) and streptomycin (100 μg/ml).

6.6. Oocyte injections

To form homopentameric receptors 25-50 ng of cRNA in 50 nl was injected into the cytoplasm of stage V or VI oocytes using a Nanoject II (Drummond Scientific Company, Broomall, Pennsylvania). Borosilicate glass injection needles were pulled from a P-1000 Flaming/Brown micropipette puller (Sutter Instrument Co, Novato, CA). Homomeric ACR-16 receptors require the presence of the endoplasmic reticulum membrane-associated accessory protein RIC-3 for maximal functional expression (Boulin et al., 2008). To express these receptors, oocytes were co-injected with equal amounts of ACR-16 and Hco-RIC-3 cRNA in 50 nl. ACR-16 is a cation channel that gates Na^+ and Ca^{2+} ions, which can in turn activate intracellular Ca^{2+}-gated Cl^- channels endogenous to *X. laevis* oocytes. To counteract the activity of these endogenous chloride

channels, selected oocytes were incubated with 100 µM of the Ca^{2+} chelator BAPTA-AM (Sigma-Aldrich, Oakville, ON), for 1 hr, then washed in ND96 immediately prior to experiments.

To form functional heteromeric receptors of wild-type and mutant GLC-2, oocytes were injected with equal amounts of cRNA in 50 nl. Hco-GLC-5 (generously provided by Dr. Sean Forrester, UOIT) and Sma-GluCl-2.1 (Dufour et al., 2013) served as controls for IVM sensitive and insensitive receptors respectively. Water-injected oocytes acted as a negative control for membrane integrity and activity of endogenous *Xenopus* receptors. Oocytes were allowed a minimum of 24 hr to synthesize and express the receptors, then were assayed daily afterwards.

6.7 Electrophysiology

Two-electrode voltage clamp (TEVC) electrophysiology was used to measure the activity of expressed ion channels. Briefly, oocytes were placed in a RC-1Z perfusion chamber (Harvard Apparatus, Saint-Laurent, QC) and pierced by two 1-5 MΩ glass microelectrodes backfilled with 3 M KCl and connected to HS-9A headstages (Axon Instruments, Foster City, CA) by Ag|AgCl wires feeding into a GeneClamp 500B operational amplifier (Axon Instruments); user-defined holding potentials allow the measurement of changes in current across the oocyte membrane. The current passing headstage had a gain (h) of 1 and the voltage sensing headstage had a gain of 0.1. Oocytes expressing GluCls were clamped at -80mV and those expressing ACR-16 were clamped at -60mV. For current-voltage studies oocytes were subject to repeated exposure to 100 µM acetylcholine at holding potentials ranging from -75 mV to +50 mV, increasing by increments of 25 mV. For those current-voltage studies a final 100 µM acetylcholine was prepared in the following solutions: ND96, 96 mM sodium gluconate, 96 mM glucosamine HCl, 1.8 mM $CaCl_2$.

Normal oocyte saline buffer (ND96 +0.1% DMSO) or drug solutions were constantly gravity-perfused into the oocyte chamber and washed out with a peristatic pump. Drugs were applied until a maximal current was achieved, or after a maximum of 20 sec exposure, followed by restoration of saline, unless specifically noted. All agonist responses on ACR-16 were normalized to a maximal acetylcholine response by exposing individual replicate oocytes to acetylcholine before agonist exposure. To test antagonism, compounds at indicated concentrations were co-applied to oocytes with an EC_{50} concentration of acetylcholine. Recordings were digitized using Digidata 1322A (Axon Instruments). Electrophysiological recordings were analyzed using the pClamp software package ClampFit (Molecular Devices, San Jose, CA).

MLs can have non-specific binding to tubes and laboratory apparatuses. For electrophysiological studies using MLs, the RC-1Z oocyte chamber was removed between every recording and thoroughly washed with 70% ethanol followed by distilled water. Failure to do so yielded cross-contamination between replicates, and those oocytes were excluded from data analysis, as were oocytes of poor membrane integrity (Current injection >1000 nA required to maintain Vc holding potential).

6.8. Drug solutions

Unless otherwise stated, each compound was purchased from Sigma-Aldrich and dissolved in ND96 at a mM stock concentration. Where noted, compounds were dissolved in pure DMSO and diluted in ND96 to a final concentration containing < 0.1 % DMSO: acetylcholine chloride, choline, betaine, (-)-nicotine hydrogen tartrate, glucosamine HCl, sodium gluconate, L-glutamate, bephenium hydroxynaphthoate (DMSO), nornicotine, mecamylamine hydrochloride (DMSO), levamisole - (-)-tetramisole hydrochloride, pyrantel citrate (DMSO), oxantel pamoate (DMSO),

morantel citrate (DMSO), ivermectin (IVM) (DMSO), moxidectin (MOX) (DMSO), milbemycin oxime (DMSO), selamectin (DMSO), ethanol, BAPTA-AM (DMSO).

6.9 Sequence Analysis

Signal peptide prediction was performed using the web-based program SignalP 5.0 (Nielsen and Krogh 1998) and by sequence alignment homology using Geneious 7.17 (https://www.geneious.com). Geneious was used for all primer design (Primer3 plugin (Rozen and Skaletsky 2000)), transmembrane domain predictions, sequence alignment and analysis (Kearse et al. 2012). Primers were synthesized by Thermo Fisher Scientific.

6.10 Phylogenetic Tree

A phylogenetic tree of 194 nematode GluCl subunits including 45 unique *glc-2* sequences was originally created by Dr. RN Beech using Geneious quick build.

6.11 *in silico* homology modeling

Modeller 9.23 was used to generate a homology model of the ECD of ACR-16 from *A. ceylanicum* and *N. americanus*, *C. elegans*, and *Trichuris muris* (Šali and Blundell, 1993). The crystallized chimeric human α-7 extracellular domain/*Lymnaea stagnalis* AChBP bound to epibatidine in an open conformation (protein data bank 3SQ6) served as a template for homology modelling.

The Hibbs & Gouaux (2011) open channel holoprotein of Cel-GLC-1 crystal structure (protein data bank 3RIF) in complex with glutamate and ivermectin served as a template to model Cel-

GLC-2 and associated mutants. To reduce processing time and for conciseness, only models of dimers were created to represent the orthosteric or ML binding sites between adjacent subunits.

Fifty models were generated for each receptor, and the best were chosen for docking simulations based on Molpdf score and Ramachandran plot analysis calculated by Modeller.

Resulting models were used to prepare *in silico* ligand binding analysis of a single binding site, implemented by AutoDock Vina (Trott and Olson, 2010). Ligands were downloaded from ZINC database (Sterling and Irwin, 2015) and prepped using AutoDock. Molecules were instructed to bind within volume of a 15 x 15 x 15Å box encompassing the orthosteric, and 20 x 20 x 20 Å ML binding site.

Fifty binding orientations were generated per root mean square from best fit, with a default exhaustiveness value of 8, and the best binding poses were chosen according to predicted binding energies. All imaging was performed using USCF Chimera (Pettersen et al., 2004).

6.12 Statistical analysis

Semi-log concentration-response curves were generated using Prism 6.0 (GraphPad Software, San Diego, CA). Data were fit to non-linear regression defined as: Imax=1/ [1+ (EC_{50}/[D])h], where Imax is the maximal current response, [D] is the concentration of drug, EC_{50} is the value of [D] at 50% maximal response, and h is the Hill slope which was used to gauge positive cooperativity for agonist binding. Microsoft Excel and Prism 6.0 were used to generate graphs and all other statistical analyses.

Appendix

^{3}H-IVM STUDIES IN *C. ELEGANS*

The ability of a drug to affect its target is predicated on the ability of the drug to reach that target. In keeping with the theme of differential drug susceptibility, an important associated question is how anthelmintics reach their drug targets inside the nematode, and does differential drug accumulation contribute to differences in drug susceptibility between different species of parasite? Many studies have described the pharmacokinetics of anthelmintics in the host organism (for example, Lifschitz et al., 2017), but few have investigated drug pharmacokinetics in the parasite itself. Studies controlling for oral ingestion of chemicals and anthelmintics have shown that uptake across the cuticle is the primary means by which anthelmintics enter nematodes (Ho et al., 1992), and that more lipophilic drugs, such as IVM, more easily cross the cuticle (Thompson et al., 1993). In *C. elegans*, IVM binds with high specificity to isolated membranes (Schaeffer and Haines, 1989), but how IVM interacts with a live, intact nematode, and to what extent acquired drug resistance affects this interaction have not been adequately explored. As such, drug absorption needs to first be characterized in whole nematodes.

In this appendix, I present preliminary data from an investigation of the ability of [22,23 ^{3}H]-ivermectin (^{3}H-IVM), to associate with the model organism *C. elegans*, in which pharyngeal pumping is inhibited by 5 nM IVM (Avery and Horvitz, 1990; Ardelli et al., 2009) and total body paralysis achieved at 20 nM after 2.5 hr exposure (Arena et al., 1995; Ardelli et al., 2009). I hypothesized that strains of *C. elegans* selected for drug resistance will exhibit differences in the accumulation and dissociation of ^{3}H-IVM from exposure in solution. We used an IVM-resistant strain (IVR10), a MOX-resistant strain (MOX4R) to determine cross-resistance to MOX and live

and heat-killed wild-type N2 Bristol as controls. We also used an amphid dye-filling mutant (*dyf-7*) strain to probe the role of amphid structure (SP1735), known to be associated with low levels of IVM resistance (Dent et al., 2000).

Among the numerous mutations present in the IVR10 and MOX4R strains of *C. elegans* they are also dye-filling defective (Ménez et al., 2016). As such, it was of interest to compare ^{3}H-IVM association between IVR10 and SP1735 to determine the extent of the contribution from *dyf* mutants.

Since no standard methodology exists to measure drug uptake in *C. elegans*, I compared three independent techniques to estimate ^{3}H-IVM accumulation in worms: a) indirectly, by measuring the disappearance of radioactivity in the supernatant of tubes containing worms incubated with a solution of ^{3}H-IVM; b) directly, by vacuum-filtration of worms through a fiberglass filter (GF/B) after exposure to ^{3}H-IVM; and c) directly by centrifugation of worms though modified GF/B spin columns after exposure to the labelled drug. Radioactivity associated with worms may be a result of internalized ^{3}H-IVM or drug adherence to the surface of worms. This appendix relates to the thesis of "Investigating species, and subunit composition differences in sensitivity towards drugs that target ligand-gated ion channels" because it is uncertain if, or to what extent IVM-resistant phenotypes in *C. elegans* alter the drug concentration that a given receptor receives. The main goals of this appendix were to compare the three methods to determine if drug association and dissociation are reliably measurable in *C. elegans*, and if so, to determine the role, if any, that drug resistance plays in these processes.

APPENDIX METHODS

The *dyf-7* mutant SP1735 was obtained from Dr. Joseph Dent (McGill University), IVR10, and MOX4R were provided by Dr. Prichard (McGill University) from the laboratory of Dr. Lespine (French National Institute for Agricultural Research. Toulouse, France). Worms were maintained as in Methods section 6.2.

All radioactivity experiments were conducted under the Internal Radioisotope Permit #R-00313 for Dr. Reza Salavati. Experiments were performed in a designated radioactivity space under McGill radioactivity protocols. A 16.6 Ci/mmol stock of tritiated ^{3}H-IVM [22,23 -^{3}H] (in 100% ethanol) was synthesized by Moravek, Inc (Brea, CA). All radioactive decay events were measured by transferring samples into scintillation vials containing 7 ml of liquid scintillation cocktail (LSC) (ScintiVerse™ BD Cocktail, Thermo Fisher Scientific) for liquid scintillation counting in a Tri-carb 4810-TR (PerkinElmer). Initial experiments were conducted to determine the appropriate volume of LSC for efficient detection (Appendix Figure 1). Briefly, 5 µl of a 1 µM ^{3}H-IVM aliquot (total disintegrations per minute (dpm) = 285,000) was transferred into 500 µl of M9 buffer (22 mM KH_2PO_4, 42 mM Na_2HPO_4, 85.5 mM NaCl, 1 mM $MgSO_4$) in a 1.5 ml centrifuge tube, and the entire volume subsequently transferred into scintillation vials containing 3, 7, or 10 ml of LSC for counting. For low energy β-particles such as ^{3}H, liquid scintillation detectors detect dpm with efficiency of 61% (termed counts per minute; cpm), and further signal loss is expected from ^{3}H IVM binding to tubes and pipette tips as well as experimental error. The 7 ml LSC volume was selected for all radioactivity experiments.

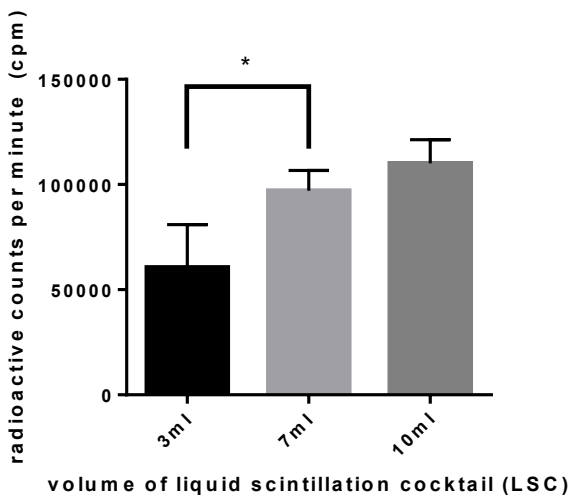

Appendix Figure 1. Efficiency of detecting ^{3}H-IVM in 500 µl M9 buffer using different volumes of LSC. 5 µl of a 1 µM ^{3}H-IVM aliquot were transferred into 500 µl of M9 buffer in 1.5 ml centrifuge tube (total cpm = 174,000), and loaded directly into 3, 7, or 10 ml of LSC for counting., n = 4, *t-test, p=.0177

i) Harvesting *C. elegans*

To study whether ML-resistant strains of *C. elegans* differentially accumulate ^{3}H-IVM, wild-type N2 Bristol, MOX4R, IVR10, and SP1735 strains of *C. elegans* were maintained on 88 mm NGM plates at 20 °C seeded with *E. coli* OP50 as a food source. Worms were synchronized 4-6 days before experimentation using standard bleach treatment (Porta-de-la-Riva et al., 2012) and washed eggs were re-plated onto four 88 mm NGM plates per strain and allowed to grow for 48 hr before collection. Worm were washed off the plates with M9 buffer into a conical tube and gently centrifuged at 1000 x g for 5 min X3 to wash and pellet worms which were then resuspended in 10 ml M9 buffer.

ii) Worm counting

Worm counting was performed as previously described (Scanlan et al., 2018). Briefly, 2 µl droplets of worms in M9 were pipetted onto a microscope slide in 9 replicates and the number of worms per droplet was counted to estimate the average number of worms in the originating tube. Worms were also visually assessed for homogeneity of life-stage and viability. A subset of wild-type *C. elegans* were heat-killed by exposure to 55 °C for 10 min to serve as a negative control for passive adsorption of ^{3}H-IVM.

iii) Association Assay Method 1: Association by supernatant disappearance

In these experiments 10,000 worms of each strain were added to 1.5 microcentrifuge tubes pre-treated with 1% BSA to reduce adherence of ^{3}H-IVM to the tubes, then gently mixed with 0.5 µCi ^{3}H-IVM in 500 µl M9 buffer (60 nM IVM) and allowed 2 hr to reach maximal association. Tubes were centrifuged for 30 sec at 100 x g to pellet worms and duplicate 100 µl samples of supernatant were transferred into LSC for scintillation counting. Silanized glass tubes were not used because of the necessity for centrifugation to separate suspended worms from supernatant.

iv) Dissociation Assay Method 1: Dissociation by supernatant appearance

To determine the dissociation of ^{3}H-IVM from worms, tubes from the final step of iii) were washed 5X by adding and gently mixing 1 ml M9 wash solution (plus 0.25% Triton X-100), centrifuging for 30 sec at 100 x g to pellet worms then removing the supernatant without disturbing the worm

pellet. After 5 washes worms were resuspended in 350 µl M9 buffer supplemented with 5% intralipid solution to act as a lipid sink to help capture free ^{3}H-IVM released from worms back into the supernatant. Immediately after resuspension, 10 µl samples of supernatant were taken for time = 0 timepoints, and the supernatant was resampled (10 µl) at subsequent timepoints to measure the rate of increase in ^{3}H-IVM found in the supernatant.

v) Association Assay Method 2: Association by vacuum-filtration through GF/B filters

Worms were incubated with ^{3}H-IVM for 2 hr as described above in iii). After incubation, the supernatant and worm pellet were applied to a modified 500 ml Nalgene® vacuum filtration system (Sigma-Aldrich), in which the 0.2 µm pore filter was replaced with a 25 mm Whatman GF/B fiberglass filter (Sigma-Aldrich). Filters were presoaked with M9 buffer containing 0.15% polyethylimine and 0.5% Triton X-100 to reduce non-specific binding of ^{3}H-IVM. Worms bound to GF/B filters were washed 3X with 5 ml of cold M9 buffer (containing 0.25% Triton X-100). Filters were then transferred to LSC for scintillation counting.

vi) Dissociation Assay Method 2: Dissociation by vacuum-filtration through GF/B filters

These studies were performed as described in iv). In addition to sampling supernatants, the remaining contents of tubes were transferred onto GF/B filters presoaked with M9 buffer (containing 0.15% polyethylimine and 0.5% Triton X-100) and vacuum-filtered using the procedure described in v).

vii) Association Assay Method 3: Association by centrifugation filtration through GF/B filters

GF/B filters were cut to fit into empty, unassembled 1.5 ml spin columns from BioBasic (Cedarlane, Burlington, ON). Filters were packed into columns and loosely fixed in position using plastic O rings with roughly $1/10^{th}$ sections of circumference removed to reduce pressure on filters and for ease of disassembly in subsequent steps.

Association experiments were performed as described in v) but instead of applying worms to 500 ml Nalgene® vacuum filtration systems, they were transferred into the modified spin columns presoaked with M9 buffer (containing 0.15% polyethylimine and 0.5% Triton X-100). Columns were centrifuged for 15 sec at 500 x g to terminate experiments and washed 3X with 1 ml M9 buffer (0.25% Triton X-100); total flow-through was collected for scintillation counting. Spin columns were carefully disassembled using forceps and GF/B filters removed for scintillation counting. Samples from the eluate of control tubes without radioactive material were used and analyzed by microscopy to confirm that worms were retained in the filter.

v) Data analysis

All data analysis and statistics was performed using Prism 6.0 (GraphPad Software, San Diego, CA) or Microsoft Excel.

APPENDIX RESULTS

i) Worm Studies: Measuring disappearance of ^{3}H-IVM from supernatant

In these experiments, I attempted to indirectly compare how much ^{3}H-IVM was associated, passively or actively, with wild-type or mutant strains of *C. elegans* to test whether selection for IVM or MOX resistance altered the kinetics of association. Drug association with worms was indirectly measured by sampling the supernatant after various periods of exposure; changes in the concentration of ^{3}H-IVM in the media has been previously shown to be representative of differences in drug association or accumulation with worms (Ho et al., 1992). As such, I first incubated worms with 0.5 µCi (60 nM) ^{3}H-IVM with gentle mixing for up to 2 hr and sampled the supernatant at time intervals to estimate maximal association by disappearance from media (Appendix Figure 2).

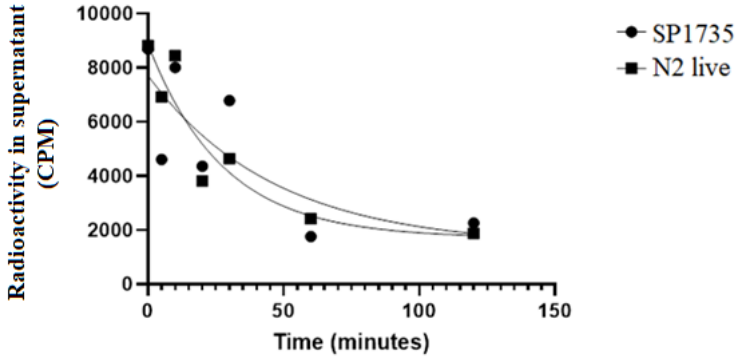

Appendix Figure 2. Time-course of ^{3}H-IVM disappearance from supernatant of tubes containing wild-type or SP1735 *C. elegans*. Worms (10,000) were incubated with 0.5 µCi ^{3}H-IVM in 500 µl M9 buffer. Aliquots of 10 µl were sampled at indicated timepoints to determine when a maximal disappearance from solution was achieved.

I next compared relative amounts of supernatant radioactivity after 2 hr incubation of ^{3}H-IVM with wild-type, heat-killed, IVR10, MOX4R or SP1735 strains of *C. elegans* to determine if differences in drug resistance status would affect drug accumulation in worms. After incubation, tubes were gently centrifuged to pellet worms and 100 µl aliquots of supernatant collected in LSC for scintillation counting (Appendix Figure 3). Data in Appendix Figure 3 shows the inverse of free ^{3}H-IVM in solution and can be used to proportionally approximate how much drug had associated with worms; relative association was standardized as a percentage of heat-killed N2 worms, which should represent passive association. The rank order relative amount of ^{3}H-IVM depleted from the media by worms is IVR10 > N2 dead +/- MOX4R +/- N2 live > SP1735, and indicates that drug-resistance status specifically may play a role in differential drug accumulation.

A

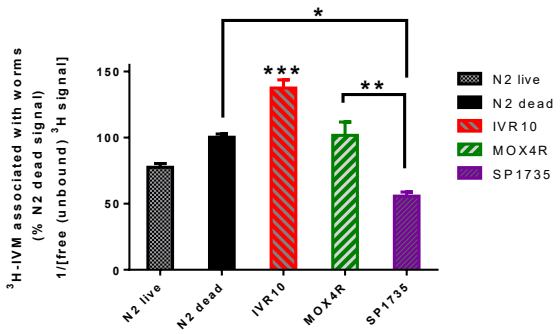

B

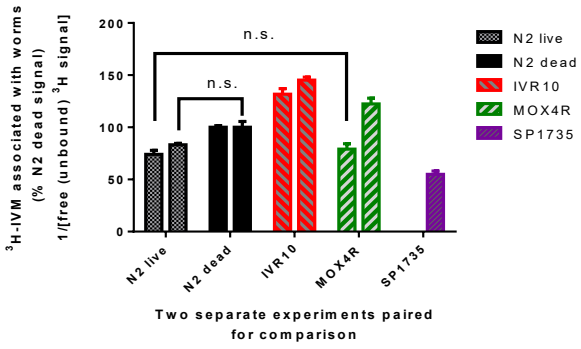

Appendix Figure 3 Relative amounts of ^{3}H-IVM disappearance from solution. Worm-associated ^{3}H-IVM is indirectly inferred from the disappearance of radioactivity in supernatant determined by the inverse of supernatant [^{3}H-IVM]. (A) Combined data from two separate experiments (SP1735 n=3 all else n=6) Significance determined by ANOVA, *p=.0025 **p=.0018 ***IVR10 is significantly different from all other strains p<.0029 (B) Two separate experiments using different aliquots of ^{3}H-IVM are shown side-by-side (experiment #1 on the left and experiment #2 on the right), n=3 for each experiment; only 1 experiment (n=3) was performed for SP1735. Significance determined by ANOVA. Within each experiment, all strains were significantly different ($p < .05$) except where noted by n.s. N2 = wild-type, IVR10 = IVM resistant, MOX4R = MOX resistant. SP1735 = dye-filling mutant.

ii) Dissociation assay: Supernatant

Having measured association levels, I next sought to determine if the rate of ^{3}H-IVM dissociation from worms back into media is correlated with drug resistance status. After the 2 hr incubation, worms were washed 5X with 1 ml M9 wash solution (with 0.25% Triton X-100) and immediately placed into fresh 350 µl M9 solution containing 5% intralipids to act as a lipid sink and better capture ^{3}H-IVM in the supernatant. Dissociation was determined by measuring the appearance of ^{3}H in the supernatant over time. Samples of supernatant taken immediately after washing were denoted as t = 0 and all samples were standardized as a percent of the total ^{3}H associated with worms after 2 hr to account for differences in starting cpm between tubes (Appendix Figure 4).

A Experiment #1

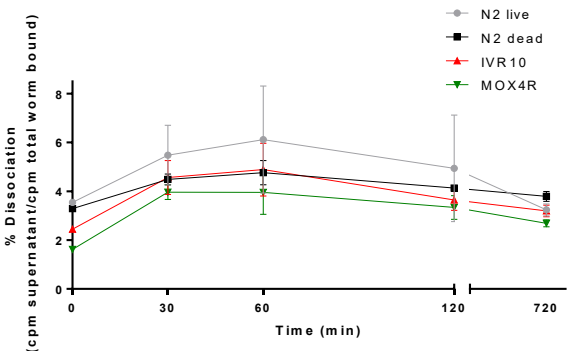

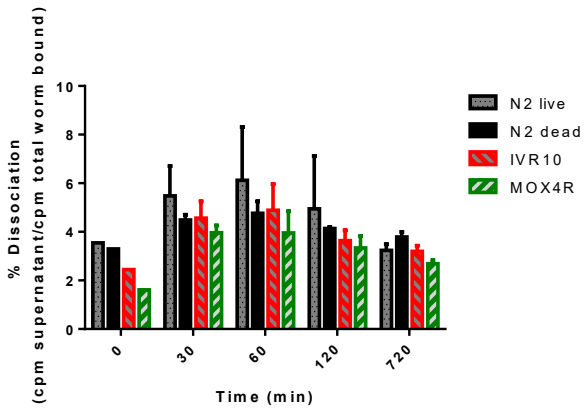

B Experiment #2

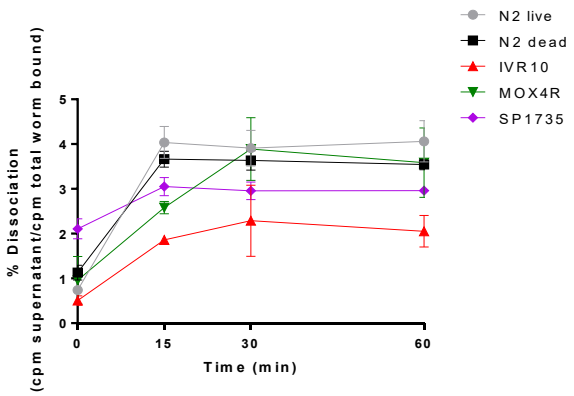

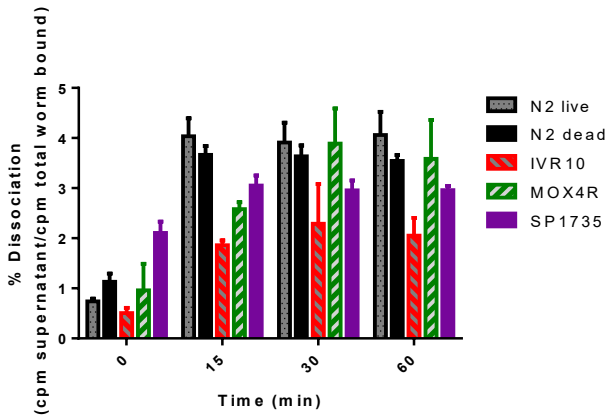

Appendix Figure 4 Time course of ^{3}H-IVM dissociation from wild-type N2 (live and dead), IVM-resistant worms (IVR10), MOX-resistant worms (MOX4R), and a *dyf-7* mutant (SP1735). After 2 hr incubation with 0.5 µCi ^{3}H-IVM, worms were washed and transferred into fresh M9 plus 5% intralipid solution containing no radioactivity to measure the appearance of ^{3}H-IVM in solution over time. Dissociation is expressed as a percent of total drug associated after 2 hr. Two separate experiments (A, B) (no replicates available for (A) t = 0), n = 3. ANOVA for each timepoint included in Appendix Table 1.

Appendix Table 1. ANOVA comparing strains of *C. elegans* at different timepoints of dissociation

Tukey's multiple comparisons test	Mean Diff.	95% CI of diff.	Significant?	Summary
0				
N2 live vs. N2 dead	-0.3912	-1.283 to 0.5002	No	ns
N2 live vs. IVR10	0.2315	-0.6599 to 1.123	No	ns
N2 live vs. MOX4R	-0.2224	-1.114 to 0.6690	No	ns
N2 live vs. SP1735	-1.370	-2.262 to -0.4787	Yes	***
N2 dead vs. IVR10	0.6227	-0.2687 to 1.514	No	ns
N2 dead vs. MOX4R	0.1687	-0.7227 to 1.060	No	ns
N2 dead vs. SP1735	-0.9790	-1.870 to -0.08758	Yes	*
IVR10 vs. MOX4R	-0.4539	-1.345 to 0.4375	No	ns
IVR10 vs. SP1735	-1.602	-2.493 to -0.7102	Yes	****
MOX4R vs. SP1735	-1.148	-2.039 to -0.2563	Yes	**
15				
N2 live vs. N2 dead	0.3741	-0.5173 to 1.266	No	ns
N2 live vs. IVR10	2.177	1.286 to 3.069	Yes	****
N2 live vs. MOX4R	1.456	0.5649 to 2.348	Yes	***
N2 live vs. SP1735	0.9861	0.09466 to 1.877	Yes	*
N2 dead vs. IVR10	1.803	0.9117 to 2.694	Yes	****
N2 dead vs. MOX4R	1.082	0.1907 to 1.974	Yes	*
N2 dead vs. SP1735	0.6119	-0.2795 to 1.503	No	ns
IVR10 vs. MOX4R	-0.7209	-1.612 to 0.1705	No	ns
IVR10 vs. SP1735	-1.191	-2.083 to -0.2997	Yes	**
MOX4R vs. SP1735	-0.4702	-1.362 to 0.4212	No	ns
30				
N2 live vs. N2 dead	0.2716	-0.6198 to 1.163	No	ns
N2 live vs. IVR10	1.620	0.7283 to 2.511	Yes	****
N2 live vs. MOX4R	0.01923	-0.8722 to 0.9106	No	ns
N2 live vs. SP1735	0.9514	0.06000 to 1.843	Yes	*

N2 dead vs. IVR10	1.348	0.4567 to 2.240	Yes	***
N2 dead vs. MOX4R	-0.2523	-1.144 to 0.6391	No	ns
N2 dead vs. SP1735	0.6798	-0.2116 to 1.571	No	ns
IVR10 vs. MOX4R	-1.600	-2.492 to -0.7091	Yes	****
IVR10 vs. SP1735	-0.6683	-1.560 to 0.2231	No	ns
MOX4R vs. SP1735	0.9322	0.04077 to 1.824	Yes	*
60				
N2 live vs. N2 dead	0.5190	-0.3724 to 1.410	No	ns
N2 live vs. IVR10	2.009	1.118 to 2.900	Yes	****
N2 live vs. MOX4R	0.4774	-0.4140 to 1.369	No	ns
N2 live vs. SP1735	1.103	0.2120 to 1.995	Yes	**
N2 dead vs. IVR10	1.490	0.5986 to 2.381	Yes	***
N2 dead vs. MOX4R	-0.04166	-0.9331 to 0.8497	No	ns
N2 dead vs. SP1735	0.5844	-0.3070 to 1.476	No	ns
IVR10 vs. MOX4R	-1.532	-2.423 to -0.6402	Yes	***
IVR10 vs. SP1735	-0.9056	-1.797 to -0.01415	Yes	*
MOX4R vs. SP1735	0.6261	-0.2653 to 1.517	No	ns

Tukey's multiple comparisons test	Mean Diff.	95% CI of diff.	Significant?	Summary
30				
N2 live vs. N2 dead	0.9921	-1.113 to 3.097	No	ns
N2 live vs. IVR10	0.9158	-1.189 to 3.021	No	ns
N2 live vs. MOX4R	1.516	-0.5893 to 3.620	No	ns
N2 dead vs. IVR10	-0.07632	-2.181 to 2.029	No	ns
N2 dead vs. MOX4R	0.5235	-1.581 to 2.628	No	ns
IVR10 vs. MOX4R	0.5998	-1.505 to 2.705	No	ns
60				
N2 live vs. N2 dead	1.356	-0.7492 to 3.460	No	ns
N2 live vs. IVR10	1.231	-0.8738 to 3.336	No	ns
N2 live vs. MOX4R	2.166	0.06085 to 4.271	Yes	*
N2 dead vs. IVR10	-0.1246	-2.229 to 1.980	No	ns
N2 dead vs. MOX4R	0.8100	-1.295 to 2.915	No	ns
IVR10 vs. MOX4R	0.9346	-1.170 to 3.039	No	ns
120				
N2 live vs. N2 dead	0.8098	-1.295 to 2.915	No	ns
N2 live vs. IVR10	1.302	-0.8028 to 3.407	No	ns
N2 live vs. MOX4R	1.607	-0.4976 to 3.712	No	ns
N2 dead vs. IVR10	0.4922	-1.613 to 2.597	No	ns
N2 dead vs. MOX4R	0.7974	-1.307 to 2.902	No	ns
IVR10 vs. MOX4R	0.3052	-1.800 to 2.410	No	ns

720				
N2 live vs. N2 dead	-0.5527	-2.658 to 1.552	No	ns
N2 live vs. IVR10	0.04217	-2.063 to 2.147	No	ns
N2 live vs. MOX4R	0.5493	-1.555 to 2.654	No	ns
N2 dead vs. IVR10	0.5949	-1.510 to 2.700	No	ns
N2 dead vs. MOX4R	1.102	-1.003 to 3.207	No	ns
IVR10 vs. MOX4R	0.5072	-1.598 to 2.612	No	ns

Roughly 1-3% of the total bound ^{3}H-IVM signal appeared in fresh M9 after washing at t = 0, and reached a peak radioactive signal within 15 to 30 min, gradually decreasing to steady-state after 2 hr; only a small percent (maximum of 5%) of the total bound ^{3}H-IVM was detectable in solution. Interestingly, despite having the lowest initial ^{3}H-IVM worm association, SP1735 had the had the highest dissociation solution levels at t = 0, which may relate to the reduced ability of these worm to re-uptake drug from solution after washing. There was the least difference in free ^{3}H-IVM between strains after 12 hr.

The indirect disappearance assay above was performed first because we lacked an efficient method to directly measure ^{3}H activity in the worms. In an attempt to validate the indirect results from these experiments and control for passive cuticular drug binding, I compared two separate methods: vacuum-filtration and spin column filtration.

iii) Association Assay Method 2: Association by vacuum-filtration through GF/B filters

These experiments were conducted similar to Appendix Figure 3, but after 2 hr incubation with ^{3}H-IVM, the worm pellet and supernatant were transferred onto Whatman fiberglass filters (GF/B filters), and subjected to 5 washes with M9 buffer (0.25% Triton X-100) under rapid vacuum

filtration. The filters were then transferred into LSC for scintillation counting. Filters should retain worms and associated ^{3}H-IVM, but free ^{3}H-IVM should be washed through into a radioactive waste receptacle. Residual free ^{3}H-IVM detected on filters amounted to < 0.5% of total signal loaded.

Results from GF/B filter binding indicate that much less ^{3}H-IVM was associated with worms after 2 hr incubation compared to 30 min, which may represent experimental error or a greater proportion of ^{3}H-IVM binding to the outer cuticle after 2 hr and subsequently being washed off during vacuum filtration (Appendix Figure 5). These data suggest a contrasting trend of association compared to the results from the disappearance assays in Appendix Figure 3; after 2 hr, the rank order of relative amount of ^{3}H-IVM associated with worms from the GF/B filter experiment was N2 live = SP1735 > N2 dead = MOX4R > IVR10 (compared to Appendix Figure 3: IVR10 >> N2 dead ± MOX4R ± N2 live > SP1735).

A

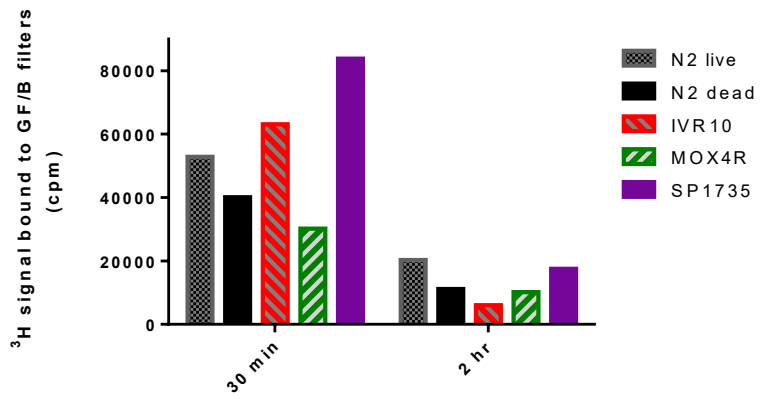

B

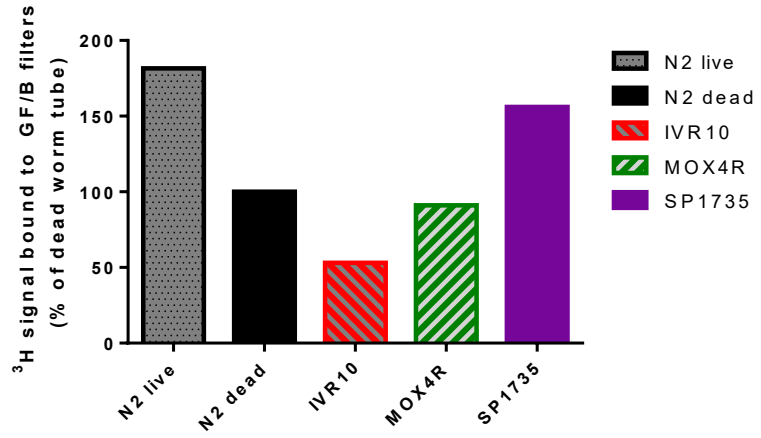

Appendix Figure 5 Amounts of ^{3}H-IVM bound/associating with *C. elegans* on GF/B filters after 30 min or 2 hr incubation with ^{3}H-IVM. No replicates available (A) comparing total radioactivity after 30 min and 2 hr (B) relative association after 2 hr.

iv) Dissociation: vacuum-filtration through GF/B filters

To measure dissociation parameters using GF/B filters, *C. elegans* were again incubated with ^{3}H-IVM for 2 hr, then washed 5X in M9 (0.25% Triton X-100) and placed in 5% intralipid M9 in the absence of IVM. After 30 min, worms were subjected to vacuum-filtration through GF/B filters

which were then transferred to LSC for scintillation counting to determine relative dissociation of ^{3}H-IVM during this period (Appendix Figure 6A). As it is prohibitively time consuming to test multiple timepoints using this method, 30 min was chosen to compare peak dissociation concentrations (determined from worms in Appendix Figure 3). In the single replicate trial, all living strains of *C. elegans* applied to GF/B filters had larger total radioactivity (~80,000-100,000 cpm) compared to heat-killed (56,000 cpm) (Appendix Figure 6A).

To determine the extent of ^{3}H-IVM dissociation, I compared radioactivity in worms on GF/B filters to that of their corresponding supernatant (Appendix Figure 6B). In heat-killed worms there was roughly an equal proportion (1:1.05) of free ^{3}H-IVM detected in supernatant to ^{3}H-IVM on GF/B filters, suggesting that, in the absence of active processes, the concentration in worms and solution reaches equal equilibrium. The IVM-resistant IVR10 strain of *C. elegans* had the next highest fraction of free ^{3}H-IVM (0.95). In comparison, wild-type, MOX4R and SP1735 all had ratios of 0.74-0.77 (with identical ratios in the one replicate of wild-type). Higher proportions of free ^{3}H-IVM might be expected if active efflux plays a significant role in drug resistance, or if worms are dead and lack active uptake capacity.

An important caveat to the interpretation of these results is that experiments measuring the association of radioactivity in worms incubated 30 min or 2 hr with ^{3}H-IVM (Appendix Figure 5A) was lower than in worms which were subsequently thoroughly washed to remove unbound ^{3}H-IVM and given 30 min to allow additional ^{3}H-IVM to dissociate (Appendix Figure 6). As such, when expressed as percent retention of maximal signal, the radioactivity after washing and 30 min of dissociation (from experiments in Appendix Figure 6A) was roughly 3-fold greater. Theoretically, there should be a stronger signal associated with worms after 2 hr of incubation compared to worms subsequently washed and allowed to passively diffuse or efflux additional

signal. Rather, these data show a roughly 3-fold greater signal after these steps, indicative of large variation in absolute radioactivity between experiments (i.e., variability between radioactivity detected on GF/B filters for 30 min or 2 hr association and 30 min dissociation).

A

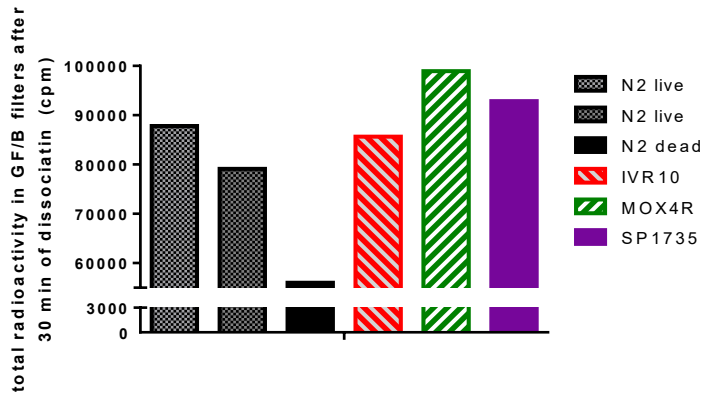

B

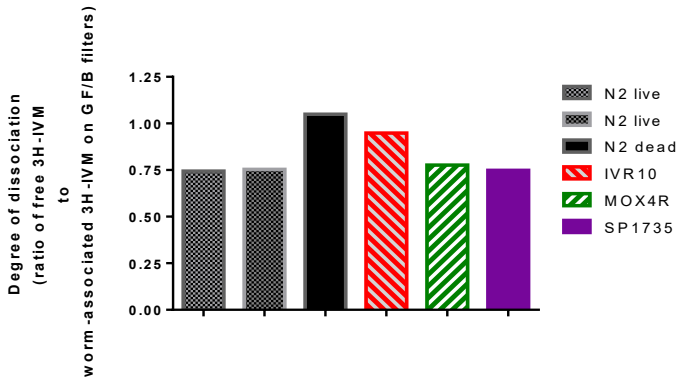

C

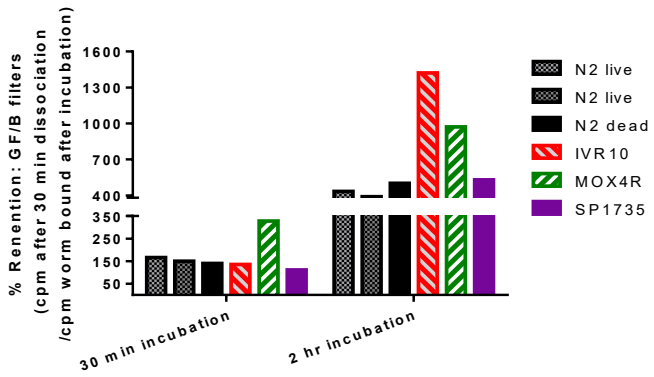

Appendix Figure 6. Radioactivity associated with *C. elegans* in GF/B filters after 30 min of dissociation. (A) Total radioactivity of ^{3}H-IVM in worms that have been washed and allowed 30 min to lose drug after an initial 2 hr incubation with ^{3}H-IVM. After 2 hr incubation with 0.5 µCi ^{3}H-IVM, worms were washed and transferred into fresh M9 with 5% intralipid solution containing no radioactivity to measure the associated signal loss after 30 min. (B) Ratio of free ^{3}H-IVM in solution to ^{3}H-IVM in worms bound to GF/B filters. (C) Associated signal "retention" as percent of "total binding" after initial 30 min or 2 hr incubation with ^{3}H-IVM. Quotations marks are used to highlight that total detected ^{3}H-IVM bound after initial incubation with ^{3}H-IVM was lower than the amount after subsequent washing and dissociation.

v) Association: Spin-column filtration

In an attempt to address some of the limitations using a home-made system for vacuum-filtration of GF/B filter to measure radioactivity, commercially available spin columns from BioBasic were assembled using GF/B filters in place of DNA binding filters. Preliminary experiments were performed to determine the reproducibility and viability of this setup in the absence of worms by applying 0.5 µCi ^{3}H-IVM in 500 µl M9 solution to columns. In contrast to the GF/B vacuum-filtration protocol, experiments using spin columns were terminated and subsequently washed using centrifugation. Control experiments in the absence of radioactive material indicate that no

worm, intact or debris, are detected in the flow-through under these conditions. To track the ^{3}H-IVM signal, the following were placed in LSC for scintillation counting: the 1.5 ml microcentrifuge tubes used for incubation, pipette tips used to transfer solution to the spin column, eluate, and the spin column itself (Appendix Figure 7). Results indicate that spin column filters retain minimal residual ^{3}H-IVM label with low tube-to-tube variability. A significant proportion of the signal is retained in tube and pipette tip binding. However, these values are relatively consistent for use in worm association assays, and final background noise of free ^{3}H-IVM binding to columns is comparable to GF/B filtration (< 0.5% of input).

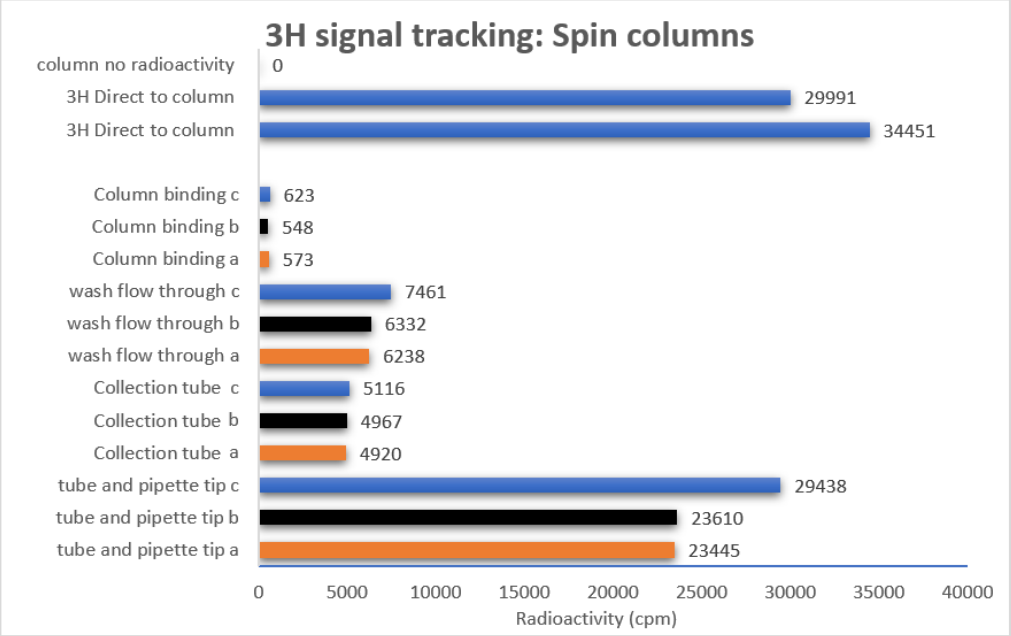

Appendix Figure 7 Preliminary control experiments tracking the fate of ^{3}H-IVM in spin column experiments. Replicates are shown individually by colour (orange, black, blue) to track the fate of ^{3}H-IVM for each sample.

When filtered using spin columns, < 20, 000 cpm of radioactivity was associated with worms (Appendix Figure 8). From both centrifugation and vacuum-filtration, the order of ^{3}H-IVM

association was N2 > MOX4R = heat-killed N2. Insufficient numbers of IVR10 and SP1735 worms prevented their inclusion in these experiments.

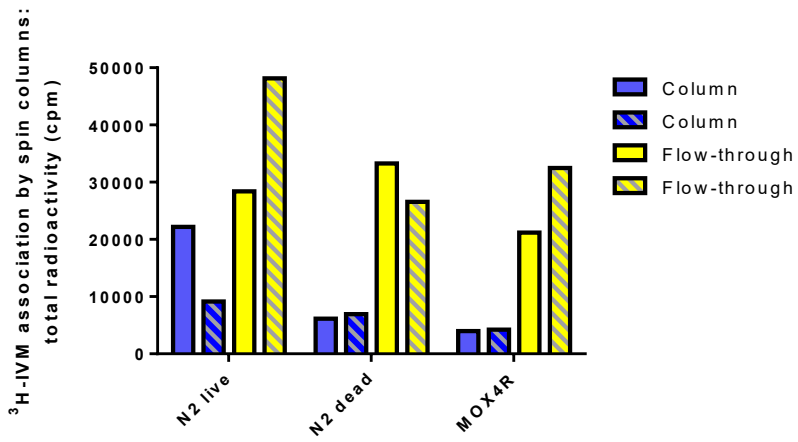

Appendix Figure 8. Amounts of ^{3}H-IVM bound/associating with *C. elegans* in modified spin columns containing GF/B filters after 2 hr incubation with ^{3}H-IVM. Experiments performed in duplicates.

The goal of this appendix was to ascertain if different strains of *C. elegans* with different susceptibilities to IVM would show different patterns of accumulation or dissociation of ^{3}H-IVM. Briefly, I have shown evidence, using multiple techniques, that drug resistance status does affect the amount of ^{3}H-IVM that associates with worms and that maximal ^{3}H-IVM dissociation from worms occurs within 15 min of drug removal. Acquired drug resistance in *C. elegans* is the result of the alternative expression of many genes, but studying the significance of changes to these genes in IVM resistance is primarily limited to paralysis studies. The data presented in this appendix provides a method to relate pharmacokinetic properties to the phenotype of IVM-resistance in *C. elegans* and could be adapted for the study of parasitic nematodes.

References

Abaza, H., El-Zayadi, A.R., Kabil, S.M., Rizk, H., 1998. Nitazoxanide in the treatment of patients with intestinal protozoan and helminthic infections: a report on 546 patients in Egypt. Curr. Ther. Res. 59, 116–121.

Abongwa, M., Baber, K.E., Martin, R.J., Robertson, A.P., 2016a. The cholinomimetic morantel as an open channel blocker of the *Ascaris suum* ACR-16 nAChR. Invertebr. Neurosci. 16, 10.

Abongwa, M., Buxton, S.K., Courtot, E., Charvet, C.L., Neveu, C., McCoy, C.J., Verma, S., Robertson, A.P., Martin, R.J., 2016b. Pharmacological profile of *Ascaris suum* ACR-16, a new homomeric nicotinic acetylcholine receptor widely distributed in *Ascaris* tissues. Br. J. Pharmacol. 173, 2463–2477.

Actor, J.K., 2011. Parasitology, in: Elsevier's Integrated Review Immunology and Microbiology E-Book: With STUDENT CONSULT Online Access. Elsevier Health Sciences, p. 147.

Adams, E.J., Stephenson, L.S., Latham, M.C., Kinoti, S.N., 1994. Physical activity and growth of Kenyan school children with hookworm, *Trichuris trichiura* and *Ascaris lumbricoides* infections are improved after treatment with albendazole. J. Nutr. 124, 1199–1206.

Adenusi, A.A., Ogunyomi, E.O.A., 2003. Relative prevalence of the human hookworm species, *Necator americanus* and *Ancylostoma duodenale* in an urban community in Ogun State, Nigeria. African J. Biotechnol. 2, 470–473.

Akinbo, F.O., Okaka, C.E., Omoregie, R., 2011. Prevalence of intestinal parasites in relation to CD4 counts and anaemia among HIV-infected patients in Benin City, Edo State, Nigeria. Tanzan. J. Health Res. 13, 8–13.

Albonico, M., Stoltzfus, R.J., Savioli, L., Tielsch, J.M., Chwaya, H.M., Ercole, E., Cancrini, G.,

1998. Epidemiological evidence for a differential effect of hookworm species, *Ancylostoma duodenale* or *Necator americanus*, on iron status of children. Int. J. Epidemiol. 27, 530–537.

Albonico, M., Wright, V., Bickle, Q., 2004. Molecular analysis of the β-tubulin gene of human hookworms as a basis for possible benzimidazole resistance on Pemba Island. Mol. Biochem. Parasitol. 134, 281–284.

Amanzougaghene, N., Fenollar, F., Diatta, G., Sokhna, C., Raoult, D., Mediannikov, O., 2018. Mutations in GluCl associated with field ivermectin-resistant head lice from Senegal. Int. J. Antimicrob. Agents 52, 593–598.

Anand, S., Hanson, K., 1997. Disability-adjusted life years: a critical review. J. Health Econ. 16.

Anderson, V.R., Curran, M.P., 2007. Nitazoxanide. Drugs 67, 1947–1967.

Aprison, E.Z., Ruvinsky, I., 2014. Balanced trade-offs between alternative strategies shape the response of *C. elegans* reproduction to chronic heat stress. PLoS One. 9, e105513

Ardelli, B.F., Prichard, R.K., 2013. Inhibition of P-glycoprotein enhances sensitivity of *Caenorhabditis elegans* to ivermectin. Vet. Parasitol. 191, 264–275.

Ardelli, B.F., Stitt, L.E., Tompkins, J.B., Prichard, R.K., 2009. A comparison of the effects of ivermectin and moxidectin on the nematode *Caenorhabditis elegans*. Vet. Parasitol. 165, 96–108.

Arias, H.R., Bhumireddy, P., Bouzat, C., 2006. Molecular mechanisms and binding site locations for noncompetitive antagonists of nicotinic acetylcholine receptors. Int. J. Biochem. Cell Biol. 38, 1254–1276.

Ashburner, M., Ball, C.A., Blake, J.A., Botstein, D., Butler, H., Cherry, J.M., Davis, A.P.,

Dolinski, K., Dwight, S.S., Eppig, J.T., 2000. Gene ontology: tool for the unification of biology. Nat. Genet. 25, 25–29.

Ashrafi, K., Chang, F.Y., Watts, J.L., Fraser, A.G., Kamath, R.S., Ahringer, J., Ruvkun, G., 2003. Genome-wide RNAi analysis of *Caenorhabditis elegans* fat regulatory genes. Nature 421, 268–272.

Atchison, W.D., Geary, T.G., Manning, B., VandeWaa, E.A., Thompson, D.P., 1992. Comparative neuromuscular blocking actions of levamisole and pyrantel-type anthelmintics on rat and gastrointestinal nematode somatic muscle. Toxicol. Appl. Pharmacol. 112, 133–143.

Atif, M., Smith, J.J., Estrada-Mondragon, A., Xiao, X., Salim, A.A., Capon, R.J., Lynch, J.W., Keramidas, A., 2019. GluClR-mediated inhibitory postsynaptic currents reveal targets for ivermectin and potential mechanisms of ivermectin resistance. PLoS Pathog. 15, e1007570.

Avery, L., 1993. Motor neuron M3 controls pharyngeal muscle relaxation timing in *Caenorhabditis elegans*. J. Exp. Biol. 175, 283–297.

Awadzi, K., Dadzie, K.Y., Shulz-Key, H., Haddock, D.R.W., Gilles, H.M., Aziz, M.A., 1985. The chemotherapy of onchocerciasis X. An assessment of four single dose treatment regimes of MK-933 (ivermectin) in human onchocerciasis. Ann. Trop. Med. Parasitol. 79, 63–78.

Ayala, F.J., Rzhetsky, A., Ayala, F.J., 1998. Origin of the metazoan phyla: molecular clocks confirm paleontological estimates. Proc. Natl. Acad. Sci. 95, 606–611.

Backus, K.H., Arigoni, M., Drescher, U., Scheurer, L., Malherbe, P., Möhler, H., Benson, J.A., 1993. Stoichiometry of a recombinant $GABA_A$ receptor deduced from mutation-induced rectification. Neuroreport 5, 285–288.

Baer, K., Waldvogel, H.J., Faull, R.L.M., Rees, M.I., 2009. Localisation of glycine receptors in the human forebrain, brainstem, and cervical spinal cord: an immunohistochemical review. Front. Mol. Neurosci. 2, 25.

Baggot, J.D., 2007. Veterinary dosage forms, in: Swarbrick, J. (Ed.), Encyclopedia of Pharmaceutical Technology, Volume 6. Informa Healthcare, New York, p. 3951.

Baldwin, J.G., Nadler, S.A., Adams, B.J., 2004. Evolution of plant parasitism among nematodes. Annu. Rev. Phytopathol. 42, 83–105.

Ballivet, M., Alliod, C., Bertrand, S., Bertrand, D., 1996. Nicotinic acetylcholine receptors in the nematode *Caenorhabditis elegans*. J. Mol. Biol. 258, 261–269.

Baraka, O.Z., Mahmoud, B.M., Marschke, C.K., Geary, T.G., Homeida, M.M.A., Williams, J.F., 1996. Ivermectin distribution in the plasma and tissues of patients infected with *Onchocerca volvulus*. Eur. J. Clin. Pharmacol. 50, 407–410.

Barbet, J.L., Snook, T., Gay, J.M., Mealey, K.L., 2009. ABCB1-1Δ (MDR1-1Δ) genotype is associated with adverse reactions in dogs treated with milbemycin oxime for generalized demodicosis. Vet. Dermatol. 20, 111–114.

Barda, B., Ame, S.M., Ali, S.M., Albonico, M., Puchkov, M., Huwyler, J., Hattendorf, J., Keiser, J., 2018. Efficacy and tolerability of moxidectin alone and in co-administration with albendazole and tribendimidine versus albendazole plus oxantel pamoate against *Trichuris trichiura* infections: a randomised, non-inferiority, single-blind trial. Lancet Infect. Dis. 18, 864–873.

Bartos, M., Price, K.L., Lummis, S.C.R., Bouzat, C., 2009. Glutamine 57 at the complementary

binding site face is a key determinant of morantel selectivity for α7 nicotinic receptors. J. Biol. Chem. 284, 21478–21487.

Bartos, M., Rayes, D., Bouzat, C., 2006. Molecular determinants of pyrantel selectivity in nicotinic receptors. Mol. Pharmacol. 70, 1307–1318.

Bartsch, S.M., Hotez, P.J., Asti, L., Zapf, K.M., Bottazzi, M.E., Diemert, D.J., Lee, B.Y., 2016. The global economic and health burden of human hookworm infection. PLoS Negl. Trop. Dis. 10, e0004922.

Baumann, S.W., Baur, R., Sigel, E., 2003. Individual properties of the two functional agonist sites in $GABA_A$ receptors. J. Neurosci. 23, 11158–11166.

Baur, R., Beech, R., Sigel, E., Rufener, L., 2015. Monepantel irreversibly binds to and opens *Haemonchus contortus* MPTL-1 and *Caenorhabditis elegans* ACR-20 receptors. Mol. Pharmacol. 87, 96–102.

Bazzocchi, C., Mortarino, M., Grandi, G., Kramer, L.H., Genchi, C., Bandi, C., Genchi, M., Sacchi, L., McCall, J.W., 2008. Combined ivermectin and doxycycline treatment has microfilaricidal and adulticidal activity against *Dirofilaria immitis* in experimentally infected dogs. Int. J. Parasitol. 38, 1401–1410.

Beckstein, O., Sansom, M.S.P., 2006. A hydrophobic gate in an ion channel: the closed state of the nicotinic acetylcholine receptor. Phys. Biol. 3, 147.

Beckstein, O., Sansom, M.S.P., 2004. The influence of geometry, surface character, and flexibility on the permeation of ions and water through biological pores. Phys. Biol. 1, 42.

Becskei, C., Thys, M., Kryda, K., Meyer, L., Martorell, S., Geurden, T., Dreesen, L., Fernandes,

T., Mahabir, S.P., 2020. Efficacy of Simparica Trio™, a novel chewable tablet containing sarolaner, moxidectin and pyrantel, against induced hookworm infections in dogs. Parasit. Vectors 13, 1–8.

Beg, A.A., Jorgensen, E.M., 2003. EXP-1 is an excitatory GABA-gated cation channel. Nat. Neurosci. 6, 1145–1152.

Behnke, J.M., Rose, R., Garside, P., 1993. Sensitivity to ivermectin and pyrantel of *Ancylostoma ceylanicum* and *Necator americanus.* Int. J. Parasitol. 23, 945–952.

Bennett, H.M., Lees, K., Harper, K.M., Jones, A.K., Sattelle, D.B., Wonnacott, S., Wolstenholme, A.J., 2012. *Xenopus laevis* RIC-3 enhances the functional expression of the *C. elegans* homomeric nicotinic receptor, ACR-16, in *Xenopus* oocytes. J. Neurochem. 123, 911–918.

Bertrand, D., Galzi, J.L., Devillers-Thiery, A., Bertrand, S., Changeux, J.P., 1993. Mutations at two distinct sites within the channel domain M2 alter calcium permeability of neuronal alpha 7 nicotinic receptor. Proc. Natl. Acad. Sci. 90, 6971–6975.

Bhopale, G.M., Bhatnagar, B.S., 1988. Efficacy of various anthelmintics against third-stage larvae of *Ancylostoma caninum* in the brain of mice. J. Helminthol. 62, 40–44.

Bird, D.M., Opperman, C.H., 1998. *Caenorhabditis elegans*: a genetic guide to parasitic nematode biology. J. Nematol. 30, 299.

Blackhall, W.J., Pouliot, J.-F., Prichard, R.K., Beech, R.N., 1998. *Haemonchus contortus*: selection at a glutamate-gated chloride channel gene in ivermectin-and moxidectin-selected strains. Exp. Parasitol. 90, 42–48.

Blackwell, V., Vega-Lopez, F., 2001. Cutaneous larva migrans: clinical features and management

of 44 cases presenting in the returning traveller. Br. J. Dermatol. 145, 434–437.

Blaxter, M., 2011. Nematodes: the worm and its relatives. PLoS Biol 9, e1001050.

Bleakley, H., 2007. Disease and development: evidence from hookworm eradication in the American South. Q. J. Econ. 122, 73–117.

Blum, A.J., Hotez, P.J., 2018. Global "worming": Climate change and its projected general impact on human helminth infections. PLoS Negl. Trop. Dis. 12, e0006370.

Blum, A.P., Lester, H.A., Dougherty, D.A., 2010. Nicotinic pharmacophore: the pyridine N of nicotine and carbonyl of acetylcholine hydrogen bond across a subunit interface to a backbone NH. Proc. Natl. Acad. Sci. 107, 13206–13211.

Bocquet, N., de Carvalho, L.P., Cartaud, J., Neyton, J., Le Poupon, C., Taly, A., Grutter, T., Changeux, J.P., Corringer, P.J., 2007. A prokaryotic proton-gated ion channel from the nicotinic acetylcholine receptor family. Nature 445, 116–119.

Bocquet, N., Nury, H., Baaden, M., Le Poupon, C., Changeux, J.P., Delarue, M., Corringer, P.J., 2009. X-ray structure of a pentameric ligand-gated ion channel in an apparently open conformation. Nature 457, 111–114.

Bodner, B.L., Jackman, L.M., Morgan, R.S., 1980. NMR study of 1: 1 complexes between divalent sulfur and aromatic compounds: a model for interactions in globular proteins. Biochem. Biophys. Res. Commun. 94, 807–813.

Böhm, C., Wolken, S., Schnyder, M., Basso, W., Deplazes, P., Di Cesare, A., Deuster, K., Schaper, R., 2015. Efficacy of emodepside/praziquantel spot-on (Profender®) against adult *Aelurostrongylus abstrusus* nematodes in experimentally infected cats. Parasitol. Res. 114,

155–164.

Borgers, M., De Nollin, S., 1975. Ultrastructural changes in *Ascaris suum* intestine after mebendazole treatment *in vivo*. J. Parasitol. 1, 110–122.

Botero, D., Castano, A., 1973. Comparative study of pyrantel pamoate, bephenium hydroxynaphthoate, and tetrachlorethylene in the treatment of *Necator americanus* infections. Am. J. Trop. Med. Hyg. 22, 45–52.

Bouchaud, O., Houzé, S., Schiemann, R., Durand, R., Ralaimazava, P., Ruggeri, C., Coulaud, J.P., 2000. Cutaneous larva migrans in travelers: a prospective study, with assessment of therapy with ivermectin. Clin. Infect. Dis. 31, 493–498.

Boulin, T., Fauvin, A., Charvet, C.L., Cortet, J., Cabaret, J., Bessereau, J.L., Neveu, C., 2011. Functional reconstitution of *Haemonchus contortus* acetylcholine receptors in *Xenopus* oocytes provides mechanistic insights into levamisole resistance. Br. J. Pharmacol. 164, 1421–1432.

Boulin, T., Gielen, M., Richmond, J.E., Williams, D.C., Paoletti, P., Bessereau, J.L., 2008. Eight genes are required for functional reconstitution of the *Caenorhabditis elegans* levamisole-sensitive acetylcholine receptor. Proc. Natl. Acad. Sci. 105, 18590–18595.

Bowman, D.D., Montgomery, S.P., Zajac, A.M., Eberhard, M.L., Kazacos, K.R., 2010. Hookworms of dogs and cats as agents of cutaneous larva migrans. Trends Parasitol. 26, 162–167.

Bradley, M., Horton, J., 2001. Assessing the risk of benzimidazole therapy during pregnancy. Trans. R. Soc. Trop. Med. Hyg. 95, 72–73.

Braungart, E., Gerlach, M., Riederer, P., Baumeister, R., Hoener, M.C., 2004. *Caenorhabditis elegans* MPP+ model of Parkinson's disease for high-throughput drug screenings. Neurodegener. Dis. 1, 175–183.

Brejc, K., van Dijk, W.J., Klaassen, R. V, Schuurmans, M., van der Oost, J., Smit, A.B., Sixma, T.K., 2001. Crystal structure of an ACh-binding protein reveals the ligand-binding domain of nicotinic receptors. Nature 411, 269–276.

Brenner, S., 1974. The genetics of *Caenorhabditis elegans*. Genetics 77, 71-94.

Brooker, S., Bethony, J., Hotez, P.J., 2004. Human hookworm infection in the 21st century. Adv. Parasitol. 58, 197.

Brownlee, D.J.A., Holden-Dye, L., Walker, R.J., 1997. Actions of the anthelmintic ivermectin on the pharyngeal muscle of the parasitic nematode, *Ascaris suum*. Parasitology 115, 553–561.

Budhathoki, S., Shah, D., Bhurtyal, K.K., Amatya, R., Dutta, A.K., 2008. Hookworm causing melaena and severe anaemia in early infancy. Ann. Trop. Paediatr. 28, 293–296.

Bundy, D.A.P., Chan, M.S., Savioli, L., 1995. Hookworm infection in pregnancy. Trans. R. Soc. Trop. Med. Hyg. 89, 521–522.

Burg, R.W., Miller, B.M., Baker, E.E., Birnbaum, J., Currie, S.A., Hartman, R., Kong, Y.L., Monaghan, R.L., Olson, G., Putter, I., 1979. Avermectins, new family of potent anthelmintic agents: producing organism and fermentation. Antimicrob. Agents Chemother. 15, 361–367.

Buxton, S.K., Charvet, C.L., Neveu, C., Cabaret, J., Cortet, J., Peineau, N., Abongwa, M., Courtot, E., Robertson, A.P., Martin, R.J., 2014. Investigation of acetylcholine receptor diversity in a nematode parasite leads to characterization of tribendimidine-and derquantel-sensitive

nAChRs. PLoS Pathog. 10, e1003870.

Byerly, L., Cassada, R.C., Russell, R.L., 1976. The life cycle of the nematode *Caenorhabditis elegans*: I. Wild-type growth and reproduction. Dev. Biol. 51, 23–33.

Caldwell, K.B., Graham, O.Z., Arnold, J.J., 2012. Agranulocytosis from levamisole-adulterated cocaine. J. Am. Board Fam. Med. 25, 528–530.

Campbell, W.C., Fisher, M.H., Stapley, E.O., Albers-Schonberg, G., Jacob, T.A., 1983. Ivermectin: a potent new antiparasitic agent. Science. 221, 823–828.

Canga, A.G., Prieto, A.M.S., Liébana, M.J.D., Martínez, N.F., Vega, M.S., Vieitez, J.J.G., 2008. The pharmacokinetics and interactions of ivermectin in humans—a mini-review. AAPS J. 10, 42–46.

Carroll, S.M., Grove, D.I., 1986. Experimental infection of humans with *Ancylostoma ceylanicum*: clinical, parasitological, haematological and immunological findings. Trop. Geogr. Med. 38, 38–45.

Castillo, M., Mulet, J., Gutiérrez, L.M., Ortiz, J.A., Castelán, F., Gerber, S., Sala, S., Sala, F., Criado, M., 2005. Dual role of the RIC-3 protein in trafficking of serotonin and nicotinic acetylcholine receptors. J. Biol. Chem. 280, 27062–27068.

Castro, P.D.J., Howell, S.B., Schaefer, J.J., Avramenko, R.W., Gilleard, J.S., Kaplan, R.M., 2019. Multiple drug resistance in the canine hookworm *Ancylostoma caninum*: an emerging threat? Parasit. Vectors. 12, 576.

Caumes, E., Carrière, J., Guermonprez, G., Bricaire, F., Danis, M., Gentilini, M., 1995. Dermatoses associated with travel to tropical countries: a prospective study of the diagnosis

and management of 269 patients presenting to a tropical disease unit. Clin. Infect. Dis. 20, 542–548.

Celie, P.H.N., van Rossum-Fikkert, S.E., van Dijk, W.J., Brejc, K., Smit, A.B., Sixma, T.K., 2004. Nicotine and carbamylcholine binding to nicotinic acetylcholine receptors as studied in AChBP crystal structures. Neuron. 41, 907–914.

Chabala, J.C., Mrozik, H., Tolman, R.L., Eskola, P., Lusi, A., Peterson, L.H., Woods, M.F., Fisher, M.H., Campbell, W.C., 1980. Ivermectin, a new broad-spectrum antiparasitic agent. J. Med. Chem. 23, 1134–1136.

Chandler, R.E., 2018. Serious neurological adverse events after ivermectin—do they occur beyond the indication of onchocerciasis? Am. J. Trop. Med. Hyg. 98, 382–388.

Chandy, A., Thakur, A.S., Singh, M.P., Manigauha, A., 2011. A review of neglected tropical diseases: filariasis. Asian Pac. J. Trop. Med. 4, 581–586.

Charvet, C.L., Guégnard, F., Courtot, E., Cortet, J., Neveu, C., 2018. Nicotine-sensitive acetylcholine receptors are relevant pharmacological targets for the control of multidrug resistant parasitic nematodes. Int. J. Parasitol. Drugs Drug Resist. 8, 540–549.

Chen, X., Schecter, R.L., Griffith, O.W., Hayward, M.A., Alpert, L.C., Batist, G., 1998. Characterization of 5-oxo-L-prolinase in normal and tumor tissues of humans and rats: a potential new target for biochemical modulation of glutathione. Clin. Cancer Res. 4, 131–138.

Chiu, J., DeSalle, R., Lam, H.M., Meisel, L., Coruzzi, G., 1999. Molecular evolution of glutamate receptors: a primitive signaling mechanism that existed before plants and animals diverged.

Mol. Biol. Evol. 16, 826–838.

Chiu, S.H.L., Green, M.L., Baylis, F.P., Eline, D., Rosegay, A., Meriwether, H., Jacob, T.A., 1990. Absorption, tissue distribution, and excretion of tritium-labeled ivermectin in cattle, sheep, and rat. J. Agric. Food Chem. 38, 2072–2078.

Cho, S., Yoon, H., Ahn, J., Lee, E., Lee, J., 2001. Cassette mutagenesis of lysine 130 of human glutamate dehydrogenase: An essential residue in catalysis. Eur. J. Biochem. 268, 3205–3213.

Choudhary, S., Tipton, J.G., Abongwa, M., Brewer, M.T., Chelladurai, J.J., Musselman, N., Martin, R.J., Robertson, A.P., 2019. Pharmacological characterization of a homomeric nicotinic acetylcholine receptor formed by *Ancylostoma caninum* ACR-16. Invertebr. Neurosci. 19, 11.

Clarke, N.E., Doi, S.A.R., Wangdi, K., Chen, Y., Clements, A.C.A., Nery, S. V, 2019. Efficacy of anthelminthic drugs and drug combinations against soil-transmitted helminths: a systematic review and network meta-analysis. Clin. Infect. Dis. 68, 96–105.

Cline, B.L., Little, M.D., Bartholomew, R.K., Halsey, N.A., 1984. Larvicidal activity of albendazole against *Necator americanus* in human volunteers. Am. J. Trop. Med. Hyg. 33, 387–394.

Collins, T., Millar, N.S., 2010. Nicotinic acetylcholine receptor transmembrane mutations convert ivermectin from a positive to a negative allosteric modulator. Mol. Pharmacol. 78, 198–204.

Conway, D.P., 1964. Variance in the effectiveness of thiabendazole against *Haemonchus contortus* in sheep. Am. J. Vet. Res. 25, 844–846.

Cook, S.J., Jarrell, T.A., Brittin, C.A., Wang, Y., Bloniarz, A.E., Yakovlev, M.A., Nguyen,

K.C.Q., Tang, L.T.H., Bayer, E.A., Duerr, J.S., 2019. Whole-animal connectomes of both *Caenorhabditis elegans* sexes. Nature 571, 63–71.

Copes, N., Edwards, C., Chaput, D., Saifee, M., Barjuca, I., Nelson, D., Paraggio, A., Saad, P., Lipps, D., Stevens Jr, S.M., 2015. Metabolome and proteome changes with aging in *Caenorhabditis elegans*. Exp. Gerontol. 72, 67–84.

Corringer, P.J., Bertrand, S., Bohler, S., Edelstein, S.J., Changeux, J.P., Bertrand, D., 1998. Critical elements determining diversity in agonist binding and desensitization of neuronal nicotinic acetylcholine receptors. J. Neurosci. 18, 648–657.

Corringer, P.J., Bertrand, S., Galzi, J.L., Devillers-Thiéry, A., Changeux, J.P., Bertrand, D., 1999. Mutational analysis of the charge selectivity filter of the α7 nicotinic acetylcholine receptor. Neuron 22, 831–843.

Costanzo, M.C., Hogan, J.D., Cusick, M.E., Davis, B.P., Fancher, A.M., Hodges, P.E., Kondu, P., Lengieza, C., Lew-Smith, J.E., Lingner, C., 2000. The yeast proteome database (YPD) and *Caenorhabditis elegans* proteome database (WormPD): comprehensive resources for the organization and comparison of model organism protein information. Nucleic Acids Res. 28, 73–76.

Coulibaly, J.T., Hiroshige, N., N'Gbesso, Y.K., Hattendorf, J., Keiser, J., 2019. Efficacy and safety of ascending dosages of tribendimidine against hookworm infections in children: a randomized controlled trial. Clin. Infect. Dis. 69, 845–852.

Courtot, E., Charvet, C.L., Beech, R.N., Harmache, A., Wolstenholme, A.J., Holden-Dye, L., O'Connor, V., Peineau, N., Woods, D.J., Neveu, C., 2015. Functional characterization of a novel class of morantel-sensitive acetylcholine receptors in nematodes. PLoS Pathog. 11,

e1005267.

Cregut, D., Serrano, L., 1999. Molecular dynamics as a tool to detect protein foldability. A mutant of domain B1 of protein G with non-native secondary structure propensities. Protein Sci. 8, 271–282.

Croese, J., Loukas, A., Opdebeeck, J., Fairley, S., Prociv, P., 1994. Human enteric infection with canine hookworms. Ann. Intern. Med. 120, 369–374.

Crompton, D.W.T., 2000. The public health importance of hookworm disease. Parasitology 121, S39–S50.

Cross, H.F., Renz, A., Trees, A.J., 1998. *In vitro* uptake of ivermectin by adult male *Onchocerca ochengi*. Ann. Trop. Med. Parasitol. 92, 711–720.

Crump, A., Omura, S., 2011. Ivermectin,'wonder drug'from Japan: the human use perspective. Proc. Japan Acad. Ser. B 87, 13–28.

Cuckler, A.C., 1961. Thiabendazole, a new broad spectrum anthelmintic. J. Parasitol. 47, 36–37.

Cull-Candy, S.G., 1976. Two types of extrajunctional L-glutamate receptors in locust muscle fibres. J. Physiol. 255, 449–464.

Cully, D.F., Paress, P.S., 1991. Solubilization and characterization of a high affinity ivermectin binding site from *Caenorhabditis elegans*. Mol. Pharmacol. 40, 326–332.

Cully, D.F., Vassilatis, D.K., Liu, K.K., Paress, P.S., Van der Ploeg, L.H.T., Schaeffer, J.M., Arena, J.P., 1994. Cloning of an avermectin-sensitive glutamate-gated chloride channel from *Caenorhabditis elegans*. Nature 371, 707–711.

Curtis, D.R., Johnston, G.A.R., 1974. Amino acid transmitters in the mammalian central nervous

system, in: (Eds.) Ergebnisse Der Physiologie Reviews of Physiology, Volume 69. Springer, Berlin, Heidelberg, pp. 97–188.

Cymes, G.D., Grosman, C., 2016. Identifying the elusive link between amino acid sequence and charge selectivity in pentameric ligand-gated ion channels. Proc. Natl. Acad. Sci. 113, E7106–E7115.

Daeffler, K.N.M., Lester, H.A., Dougherty, D.A., 2014. Functional evaluation of key interactions evident in the structure of the eukaryotic Cys-loop receptor GluCl. ACS Chem. Biol. 9, 2283–2290.

De Clercq, D., Sacko, M., Behnke, J., Gilbert, F., Dorny, P., Vercruysse, J., 1997. Failure of mebendazole in treatment of human hookworm infections in the southern region of Mali. Am. J. Trop. Med. Hyg. 57, 25–30.

De Graef, J., Demeler, J., Skuce, P., Mitreva, M., Von Samson-Himmelstjerna, G., Vercruysse, J., Claerebout, E., Geldhof, P., 2013. Gene expression analysis of ABC transporters in a resistant *Cooperia oncophora* isolate following *in vivo* and *in vitro* exposure to macrocyclic lactones. Parasitology. 140, 499–508.

de la Torre, B.G., Albericio, F., 2019. The pharmaceutical industry in 2018. An analysis of FDA drug approvals from the perspective of molecules. Molecules 24, 809.

Degani-Katzav, N., Gortler, R., Gorodetzki, L., Paas, Y., 2016. Subunit stoichiometry and arrangement in a heteromeric glutamate-gated chloride channel. Proc. Natl. Acad. Sci. U. S. A. 113, E644–E653.

Degani-Katzav, N., Gortler, R., Weissman, M., Paas, Y., 2017a. Mutational analysis at intersubunit

interfaces of an anionic glutamate receptor reveals a key interaction important for channel gating by ivermectin. Front. Mol. Neurosci. 10, 92.

Degani-Katzav, N., Klein, M., Har-Even, M., Gortler, R., Tobi, R., Paas, Y., 2017b. Trapping of ivermectin by a pentameric ligand-gated ion channel upon open-to-closed isomerization. Sci. Rep. 7, 1–18.

Delany, N.S., Laughton, D.L., Wolstenholme, A.J., 1998. Cloning and localisation of an avermectin receptor-related subunit from *Haemonchus contortus*. Mol. Biochem. Parasitol. 97, 177–187.

Demeler, J., Van Zeveren, A.M.J., Kleinschmidt, N., Vercruysse, J., Höglund, J., Koopmann, R., Cabaret, J., Claerebout, E., Areskog, M., von Samson-Himmelstjerna, G., 2009. Monitoring the efficacy of ivermectin and albendazole against gastro intestinal nematodes of cattle in Northern Europe. Vet. Parasitol. 160, 109–115.

Dent, J.A., Davins, M., Avery, L., 1997. *avr-15* encodes a chloride channel subunit that mediates inhibitory glutamatergic neurotransmission and ivermectin sensitivity in *Caenorhabditis elegans*. EMBO J. 16, 5867–5879.

Dent, J.A., Smith, M.M., Vassilatis, D.K., Avery, L., 2000. The genetics of ivermectin resistance in *Caenorhabditis elegans*. Proc. Natl. Acad. Sci. U. S. A. 97, 2674–2679.

Diemert, D.J., Bethony, J.M., Hotez, P.J., 2008. Hookworm vaccines. Clin. Infect. Dis. 282–288.

Dougherty, D.A., 2008. Cys-loop neuroreceptors: structure to the rescue? Chem. Rev. 108, 1642–1653.

Drake, L.J., Jukes, M.C.H., Sternberg, R.J., Bundy, D.A.P., 2000. Geohelminth infections

(ascariasis, trichuriasis, and hookworm): cognitive and developmental impacts, in: Seminars in Pediatric Infectious Diseases. WB Saunders. pp. 245–251.

Dreyer, G., Noroes, J., Amaral, F., Nen, A., Medeiros, Z., Coutinho, A., Addiss, D., 1995. Direct assessment of the adulticidal efficacy of a single dose of ivermectin in bancroftian filariasis. Trans. R. Soc. Trop. Med. Hyg. 89, 441–443.

Drudge, J.H., Szanto, J., Wyant, Z.N., Elam, G., 1964. Field studies on parasite control in sheep: comparison of thiabendazole, ruelene, and phenothiazine. Am. J. Vet. Res. 25, 1512–1518.

Dubyak, G.R., 2007. Go it alone no more—P2X7 joins the society of heteromeric ATP-gated receptor channels. Mol. Pharmacol. 72, 1402–1405.

Duerr, J.S., Gaskin, J., Rand, J.B., 2001. Identified neurons in *C. elegans* coexpress vesicular transporters for acetylcholine and monoamines. Am. J. Physiol. Physiol. 280, C1616–C1622.

Dufour, V., Beech, R.N., Wever, C., Dent, J.A., Geary, T.G., 2013. Molecular cloning and characterization of novel glutamate-gated chloride channel subunits from *Schistosoma mansoni*. PLoS Pathog. 9, e1003586.

Duguet, T.B., Charvet, C.L., Forrester, S.G., Wever, C.M., Dent, J.A., Neveu, C., Beech, R.N., 2016. Recent duplication and functional divergence in parasitic nematode levamisole-sensitive acetylcholine receptors. PLoS Negl. Trop. Dis. 10, e0004826.

Dull, P., Friede, M., Hwang, A., Hall, B.F., 2019. Meeting report: Global vaccine and immunization research forum, 2018. Vaccine 37, 7519–7526.

Egerton, J.R., Ostlind, D.A., Blair, L.S., Eary, C.H., Suhayda, D., Cifelli, S., Riek, R.F., Campbell, W.C., 1979. Avermectins, new family of potent anthelmintic agents: Efficacy of the B1(a)

component. Antimicrob. Agents Chemother. 15, 372–378.

Ekins, S., Mestres, J., Testa, B., 2007. *In silico* pharmacology for drug discovery: methods for virtual ligand screening and profiling. Br. J. Pharmacol. 152, 9–20.

El-Abdellati, A., De Graef, J., Van Zeveren, A., Donnan, A., Skuce, P., Walsh, T., Wolstenholme, A., Tait, A., Vercruysse, J., Claerebout, E., 2011. Altered *avr-14B* gene transcription patterns in ivermectin-resistant isolates of the cattle parasites, *Cooperia oncophora* and *Ostertagia ostertagi*. Int. J. Parasitol. 41, 951–957.

Epe, C., Kaminsky, R., 2013. New advancement in anthelmintic drugs in veterinary medicine. Trends Parasitol. 29, 129–134.

Etter, A., Cully, D.F., Schaeffer, J.M., Liu, K.K., Arena, J.P., 1996. An amino acid substitution in the pore region of a glutamate-gated chloride channel enables the coupling of ligand binding to channel gating. J. Biol. Chem. 271, 16035–16039.

Evans, A.M., Martin, R.J., 1996. Activation and cooperative multi-ion block of single nicotinic-acetylcholine channel currents of *Ascaris* muscle by the tetrahydropyrimidine anthelmintic, morantel. Br. J. Pharmacol. 118, 1127–1140.

Farid, Z., Bassily, S., Miner, W.F., Hassan, A., Laughlin, L.W., 1977. Comparative single/dose treatment of hookworm and roundworm infections with levamisole, pyrantel and bephenium*. J. Trop. Med. Hyg. 80, 107–108.

Fasoli, F., Moretti, M., Zoli, M., Pistillo, F., Crespi, A., Clementi, F., Mc Clure-Begley, T., Marks, M.J., Gotti, C., 2016. *In vivo* chronic nicotine exposure differentially and reversibly affects upregulation and stoichiometry of α4β2 nicotinic receptors in cortex and thalamus.

Neuropharmacology 108, 324–331.

Fatima-Shad, K., Barry, P.H., 1993. Anion permeation in GABA-and glycine-gated channels of mammalian cultured hippocampal neurons. Proc. R. Soc. London. Ser. B Biol. Sci. 253, 69–75.

Feldmeier, H., Schuster, A., 2012. Mini review: hookworm-related cutaneous larva migrans. Eur. J. Clin. Microbiol. Infect. Dis. 31, 915–918.

Feng, X., Hayashi, J., Beech, R.N., Prichard, R.K., 2002. Study of the nematode putative GABA type-A receptor subunits: evidence for modulation by ivermectin. J. Neurochem. 83, 870–878.

Fenster, C.P., Whitworth, T.L., Sheffield, E.B., Quick, M.W., Lester, R.A.J., 1999. Upregulation of surface α4β2 nicotinic receptors is initiated by receptor desensitization after chronic exposure to nicotine. J. Neurosci. 19, 4804–4814.

Fiel, C.A., Saumell, C.A., Steffan, P.E., Rodriguez, E.M., 2001. Resistance of *Cooperia* to ivermectin treatments in grazing cattle of the Humid Pampa, Argentina. Vet. Parasitol. 97, 213–219.

Flohr, C., Tuyen, L.N., Lewis, S., Minh, T.T., Campbell, J., Britton, J., Williams, H., Hien, T.T., Farrar, J., Quinnell, R.J., 2007. Low efficacy of mebendazole against hookworm in Vietnam: two randomized controlled trials. Am. J. Trop. Med. Hyg. 76, 732–736.

Flores, D., Panic, G., Braissant, O., Keiser, J., 2016. A novel isothermal microcalorimetry tool to assess drug effects on *Ancylostoma ceylanicum* and *Necator americanus*. Appl. Microbiol. Biotechnol. 100, 837–846.

Forrester, S.G., Beech, R.N., Prichard, R.K., 2004. Agonist enhancement of macrocyclic lactone activity at a glutamate-gated chloride channel subunit from *Haemonchus contortus*. Biochem. Pharmacol. 67, 1019–1024.

Forrester, S.G., Hamdan, F.F., Prichard, R.K., Beech, R.N., 1999. Cloning, sequencing, and developmental expression levels of a novel glutamate-gated chloride channel homologue in the parasitic nematode *Haemonchus contortus*. Biochem. Biophys. Res. Commun. 254, 529–534.

Forrester, S.G., Prichard, R.K., Beech, R.N., 2002. A glutamate-gated chloride channel subunit from *Haemonchus contortus*:: Expression in a mammalian cell line, ligand binding, and modulation of anthelmintic binding by glutamate. Biochem. Pharmacol. 63, 1061–1068.

Forrester, S.G., Prichard, R.K., Dent, J.A., Beech, R.N., 2003. *Haemonchus contortus*: HcGluCla expressed in *Xenopus* oocytes forms a glutamate-gated ion channel that is activated by ibotenate and the antiparasitic drug ivermectin. Mol. Biochem. Parasitol. 129, 115–121.

Fox, L.M., Saravolatz, L.D., 2005. Nitazoxanide: a new thiazolide antiparasitic agent. Clin. Infect. Dis. 40, 1173–1180.

Francis, M.M., Evans, S.P., Jensen, M., Madsen, D.M., Mancuso, J., Norman, K.R., Maricq, A.V., 2005. The Ror receptor tyrosine kinase CAM-1 is required for ACR-16-mediated synaptic transmission at the *C. elegans* neuromuscular junction. Neuron. 46, 581-594.

Fraser, S.P., Djamgoz, M.B.A., Usherwood, P.N.R., O'brien, J., Darlison, M.G., Barnard, E.A., 1990. Amino acid receptors from insect muscle: electrophysiological characterization in *Xenopus* oocytes following expression by injection of mRNA. Mol. Brain Res. 8, 331–341.

Furtado, L.F.V., de Oliveira Dias, L.T., de Oliveira Rodrigues, T., da Silva, V.J., de Oliveira, V.N.G.M., Rabelo, É.M.L., 2020. Egg genotyping reveals the possibility of patent *Ancylostoma caninum* infection in human intestine. Sci. Rep. 10, 1–7.

Galzi, J.-L., Devillers-Thiery, A., Hussy, N., Bertrand, S., Changeux, J.-P., Bertrand, D., 1992. Mutations in the channel domain of a neuronal nicotinic receptor convert ion selectivity from cationic to anionic. Nature 359, 500–505.

Garcia, E.G., 1976. Treatment for trichuriasis with oxantel. Am. J. Trop. Med. Hyg. 25, 914–915.

Garcia, L.R., Mehta, P., Sternberg, P.W., 2001. Regulation of distinct muscle behaviors controls the *C. elegans* male's copulatory spicules during mating. Cell. 107, 777–788.

Garside, P., Behnke, J.M., 1989. *Ancylostoma ceylanicum* in the hamster: observations on the host—parasite relationship during primary infection. Parasitology. 98, 283–289.

Geary, T.G., Moreno, Y., 2012. Macrocyclic lactone anthelmintics: spectrum of activity and mechanism of action. Curr. Pharm. Biotechnol. 13, 866–872.

Geary, T.G., Sims, S.M., Thomas, E.M., Vanover, L., Davis, J.P., Winterrowd, C.A., Klein, R.D., Ho, N.F.H., Thompson, D.P., 1993. *Haemonchus contortus*: ivermectin-induced paralysis of the pharynx. Exp. Parasitol. 77, 88–96.

Geary, T.G., Thompson, D.P., 2001. *Caenorhabditis elegans*: how good a model for veterinary parasites? Vet. Parasitol. 101, 371–386.

Ghosh, R., Andersen, E.C., Shapiro, J.A., Gerke, J.P., Kruglyak, L., 2012. Natural variation in a chloride channel subunit confers avermectin resistance in *C. elegans*. Science. 335, 574–578.

Giardina, F., Coffeng, L.E., Farrell, S.H., Vegvari, C., Werkman, M., Truscott, J.E., Anderson,

R.M., de Vlas, S.J., 2019. Sampling strategies for monitoring and evaluation of morbidity targets for soil-transmitted helminths. PLoS Negl. Trop. Dis. 13, e0007514.

Gilleard, J.S., 2004. The use of *Caenorhabditis elegans* in parasitic nematode research. Parasitology. 128, S49–S70.

Gillespie, S.H., 2004. Cutaneous larva migrans. Curr. Infect. Dis. Rep. 6, 50–53.

Giménez-Pardo, C., Martínez-Grueiro, M.M., Gómez-Barrio, A., Rodríguez-Caabeiro, F., 2003. Cholinesterase and phosphatase activities in adults and infective-stage larvae of levamisole-resistant and levamisole-susceptible isolates of *Haemonchus contortus*. Vet. Res. Commun. 27, 611–623.

Glendinning, S.K., Buckingham, S.D., Sattelle, D.B., Wonnacott, S., Wolstenholme, A.J., 2011. Glutamate-gated chloride channels of *Haemonchus contortus* restore drug sensitivity to ivermectin resistant *Caenorhabditis elegans*. PLoS One 6, e22390.

Gopal, R.M., West, D.M., Pomroy, W.E., 2001. The difference in efficacy of ivermectin oral, moxidectin oral and moxidectin injectable formulations against an ivermectin-resistant strain of *Trichostrongylus colubriformis* in sheep. N. Z. Vet. J. 49, 133–137.

Gourgiotou, K., Nicolaidou, E., Panagiotopoulos, A., Hatziolou, E., Katsambas, A.D., 2001. Treatment of widespread cutaneous larva migrans with thiabendazole. J. Eur. Acad. Dermatology Venereol. 15, 578–580.

Grandemange, E., Claerebout, E., Genchi, C., Franc, M., 2007. Field evaluation of the efficacy and the safety of a combination of oxantel/pyrantel/praziquantel in the treatment of naturally acquired gastrointestinal nematode and/or cestode infestations in dogs in Europe. Vet.

Parasitol. 145, 94–99.

Granfeldt, D., Sinclair, J., Millingen, M., Farre, C., Lincoln, P., Orwar, O., 2006. Controlling desensitized states in ligand− receptor interaction studies with cyclic scanning patch-clamp protocols. Anal. Chem. 78, 7947–7953.

Grove, D.I., 1982. Treatment of strongyloidiasis with thiabendazole: an analysis of toxicity and effectiveness. Trans. R. Soc. Trop. Med. Hyg. 76, 114–118.

Gunthorpe, M.J., Lummis, S.C.R., 2001. Conversion of the ion selectivity of the 5-HT_{3A} receptor from cationic to anionic reveals a conserved feature of the ligand-gated ion channel superfamily. J. Biol. Chem. 276, 10977–10983.

Haas, W., Haberl, B., Idris, I., Kallert, D., Kersten, S., Stiegeler, P., 2005. Behavioural strategies used by the hookworms *Necator americanus* and *Ancylostoma duodenale* to find, recognize and invade the human host. Parasitol. Res. 95, 30–39.

Halevi, S., McKay, J., Palfreyman, M., Yassin, L., Eshel, M., Jorgensen, E., Treinin, M., 2002. The *C. elegans ric-3* gene is required for maturation of nicotinic acetylcholine receptors. EMBO J. 21, 1012–1020.

Hansen, T.V.A., Cirera, S., Neveu, C., Calloe, K., Klaerke, D.A. 2020. The narrow-spectrum anthelmintic oxantel is a potent agonist of a novel acetylcholine receptor subtype in whipworms. Preprint. bioRxiv. doi: https://doi.org/10.1101/2020.09.17.301192.

Harland, P.S., Meakins, R.H., Harland, R.H., 1977. Treatment of cutaneous larva migrans with local thiabendazole. Br. Med. J. 2, 772.

Harrison, L.M., Nerlinger, A., Bungiro, R.D., Córdova, J.L., Kuzmič, P., Cappello, M., 2002.

Molecular characterization of *Ancylostoma* inhibitors of coagulation factor Xa. Hookworm anticoagulant activity *in vitro* predicts parasite bloodfeeding *in vivo*. J. Biol. Chem. 277, 6223–6229.

Harrow, I.D., Gration, K.A.F., 1985. Mode of action of the anthelmintics morantel, pyrantel and levamisole on muscle cell membrane of the nematode *Ascaris suum*. Pestic. Sci. 16, 662–672.

Hawdon, J.M., Hotez, P.J., 1996. Hookworm: Developmental biology of the infectious process. Curr. Opin. Genet. Dev. 6, 618–623.

Heckler, R.P., Almeida, G.D., Santos, L.B., Borges, D.G.L., Neves, J.P.L., Onizuka, M.K. V, Borges, F.A., 2014. P-gp modulating drugs greatly potentiate the *in vitro* effect of ivermectin against resistant larvae of *Haemonchus placei*. Vet. Parasitol. 205, 638–645.

Hemmings Jr, H.C., Akabas, M.H., Goldstein, P.A., Trudell, J.R., Orser, B.A., Harrison, N.L., 2005. Emerging molecular mechanisms of general anesthetic action. Trends Pharmacol. Sci. 26, 503–510.

Heukelbach, J., Feldmeier, H., 2008. Epidemiological and clinical characteristics of hookworm-related cutaneous larva migrans. Lancet Infect. Dis. 8, 302–309.

Heukelbach, J., Wilcke, T., Meier, A., Moura, R.C.S., Feldmeier, H., 2003. A longitudinal study on cutaneous larva migrans in an impoverished Brazilian township. Travel Med. Infect. Dis. 1, 213–218.

Hibbs, R.E., Gouaux, E., 2011. Principles of activation and permeation in an anion-selective Cys-loop receptor. Nature. 474, 54–60.

Hilf, R.J.C., Dutzler, R., 2009. Structure of a potentially open state of a proton-activated

pentameric ligand-gated ion channel. Nature. 457, 115–118.

Hilf, R.J.C., Dutzler, R., 2008. X-ray structure of a prokaryotic pentameric ligand-gated ion channel. Nature. 452, 375–379.

Hillier, L.W., Marth, G.T., Quinlan, A.R., Dooling, D., Fewell, G., Barnett, D., Fox, P., Glasscock, J.I., Hickenbotham, M., Huang, W., 2008. Whole-genome sequencing and variant discovery in *C. elegans*. Nat. Methods 5, 183-188.

Hillier, L.W., Reinke, V., Green, P., Hirst, M., Marra, M.A., Waterston, R.H., 2009. Massively parallel sequencing of the polyadenylated transcriptome of *C. elegans*. Genome Res. 19, 657–666.

Ho, N.F.H., Geary, T.G., Barsuhn, C.L., Sims, S.M., Thompson, D.P., 1992. Mechanistic studies in the transcuticular delivery of antiparasitic drugs II: *ex vivo*/*in vitro* correlation of solute transport by *Ascaris suum*. Mol. Biochem. Parasitol. 52, 1–13.

Hoagland, K.E., Schad, G.A., 1978. *Necator americanus* and *Ancylostoma duodenale*: life history parameters and epidemiological implications of two sympatric hookworms of humans. Exp. Parasitol. 44, 36–49.

Hochedez, P., Caumes, E., 2007. Hookworm-related cutaneous larva migrans. J. Travel Med. 14, 326–333.

Hodgkin, J., Doniach, T., 1997. Natural variation and copulatory plug formation in *Caenorhabditis elegans*. Genetics. 146, 149–164.

Hoffman, P.W., Ravindran, A., Huganir, R.L., 1994. Role of phosphorylation in desensitization of acetylcholine receptors expressed in *Xenopus* oocytes. J. Neurosci. 14, 4185–4195.

Holden-Dye, L., Joyner, M., O'Connor, V., Walker, R.J., 2013. Nicotinic acetylcholine receptors: a comparison of the nAChRs of *Caenorhabditis elegans* and parasitic nematodes. Parasitol. Int. 62, 606–615.

Holladay, M.W., Dart, M.J., Lynch, J.K., 1997. Neuronal nicotinic acetylcholine receptors as targets for drug discovery. J. Med. Chem. 40, 4169–4194.

Horoszok, L., Raymond, V., Sattelle, D.B., Wolstenholme, A.J., 2001. GLC-3: A novel fipronil and BIDN-sensitive, but picrotoxinin-insensitive, L-glutamate-gated chloride channel subunit from *Caenorhabditis elegans*. Br. J. Pharmacol. 132, 1247–1254.

Hotez, P., 2008. Hookworm and poverty. Ann. N. Y. Acad. Sci. 1136, 38–44.

Hotez, P., Cappello, M., Hawdon, J., Beckers, C., Sakanari, J., 1994. Hyaluronidases of the gastrointestinal invasive nematodes *Ancylostoma caninum* and *Anisakis simplex*: Possible functions in the pathogenesis of human zoonoses. J. Infect. Dis. 170, 918–926.

Hotez, P., Haggerty, J., Hawdon, J., Milstone, L., Gamble, H.R., Schad, G., Richards, F., 1990. Metalloproteases of infective *Ancylostoma* hookworm larvae and their possible functions in tissue invasion and ecdysis. Infect. Immun. 58, 3883–3892.

Howes Jr, H.L., 1972. Trans-1, 4, 5, 6-tetrahydro-2-(3-hydroxystyryl)-1-methyl pyrimidine (CP-14,445), a new antiwhipworm agent. Proc. Soc. Exp. Biol. Med. 139, 394–398.

Hrckova, G., Velebny, S., 2013. Parasitic helminths of humans and animals: health impact and control, in: Pharmacological potential of selected natural compounds in the control of parasitic diseases. SpringerBriefs in pharmaceutical science & drug development. Springer, Vienna. pp. 29–99.

Hu, H., Howard, R.J., Bastolla, U., Lindahl, E., Delarue, M., 2020. Structural basis for allosteric transitions of a multidomain pentameric ligand-gated ion channel. Proc. Natl. Acad. Sci. 117, 13437-13446.

Hu, W., Zhang, C., Wu, R., Sun, Y., Levine, A., Feng, Z., 2010. Glutaminase 2, a novel p53 target gene regulating energy metabolism and antioxidant function. Proc. Natl. Acad. Sci. 107, 7455–7460.

Hu, X.Q., Sun, H., Peoples, R.W., Hong, R., Zhang, L., 2006. An interaction involving an arginine residue in the cytoplasmic domain of the 5-HT3A receptor contributes to receptor desensitization mechanism. J. Biol. Chem. 281, 21781–21788.

Huang, L.Y., Catterall, W.A., Ehrenstein, G., 1978. Selectivity of cations and nonelectrolytes for acetylcholine-activated channels in cultured muscle cells. J. Gen. Physiol. 71, 397–410.

Huang, W.H., Brown, H.W., 1963. The efficacy of thiabendazole against hookworm and *Ascaris* of man. J. Parasitol. 1014–1018.

Humphries, D., Mosites, E., Otchere, J., Twum, WA., Woo, L., Jones-Sanpei, H., Harrison, L.M., Bungiro, R.D., Benham-Pyle, B., Bimi, L., 2011. Epidemiology of hookworm infection in Kintampo North Municipality, Ghana: patterns of malaria coinfection, anemia, and albendazole treatment failure. Am. J. Trop. Med. Hyg. 84, 792–800.

Hung, A., Tai, K., Sansom, M.S.P., 2005. Molecular dynamics simulation of the M2 helices within the nicotinic acetylcholine receptor transmembrane domain: structure and collective motions. Biophys. J. 88, 3321–3333.

Inpankaew, T., Schär, F., Dalsgaard, A., Khieu, V., Chimnoi, W., Chhoun, C., Sok, D., Marti, H.,

Muth, S., Odermatt, P., 2014. High prevalence of *Ancylostoma ceylanicum* hookworm infections in humans, Cambodia, 2012. Emerg. Infect. Dis. 20, 976.

Ishizaki, T., Katsumi, H., Yasuraoka, K., Hosaka, Y., 1963. The anthelmintic effect of thiabendazole against *Ascaris*, *Trichuris* and hookworm infections in man. I. Japanese J. Parasitol. 12, 182–185.

Jagannathan, S., Laughton, D.L., Critten, C.L., Skinner, T.M., Horoszok, L., Wolstenholme, A.J., 1999. Ligand-gated chloride channel subunits encoded by the *Haemonchus contortus* and *Ascaris suum* orthologues of the *Caenorhabditis elegans gbr-2* (*avr-14*) gene. Mol. Biochem. Parasitol. 103, 129–140.

Jensen, M.L., Schousboe, A., Ahring, P.K., 2005. Charge selectivity of the Cys-loop family of ligand-gated ion channels. J. Neurochem. 92, 217–225.

Jones, A.K., Sattelle, D.B., 2004. Functional genomics of the nicotinic acetylcholine receptor gene family of the nematode, *Caenorhabditis elegans*. BioEssays 26, 39–49.

Jones, A.K., Sattelle, D.B., 2008. The cys-loop ligand-gated ion channel gene superfamilyof the nematode, *Caenorhabditis elegans*. Invert Neurosci. 8, 41-47.

Jourdan, P.M., Lamberton, P.H.L., Fenwick, A., Addiss, D.G., 2018. Soil-transmitted helminth infections. Lancet 391, 252–265.

Kamath, R.S., Ahringer, J., 2003. Genome-wide RNAi screening in *Caenorhabditis elegans*. Methods. 30, 313–321.

Kamath, R.S., Fraser, A.G., Dong, Y., Poulin, G., Durbin, R., Gotta, M., Kanapin, A., Le Bot, N., Moreno, S., Sohrmann, M., 2003. Systematic functional analysis of the *Caenorhabditis*

elegans genome using RNAi. Nature. 421, 231–237.

Kaminsky, R., Ducray, P., Jung, M., Clover, R., Rufener, L., Bouvier, J., Weber, S.S., Wenger, A., Wieland-Berghausen, S., Goebel, T., 2008. A new class of anthelmintics effective against drug-resistant nematodes. Nature. 452, 176–180.

Kaplan, R.M., 2004. Drug resistance in nematodes of veterinary importance: a status report. Trends Parasitol. 20, 477–481.

Karpstein, T., Pasche, V., Häberli, C., Scandale, I., Neodo, A., Keiser, J., 2019. Evaluation of emodepside in laboratory models of human intestinal nematode and schistosome infections. Parasit. Vectors 12, 226.

Keiser, J., Tritten, L., Silbereisen, A., Speich, B., Adelfio, R., Vargas, M., 2013. Activity of oxantel pamoate monotherapy and combination chemotherapy against *Trichuris muris* and hookworms: Revival of an old drug. PLoS Negl. Trop. Dis. 7.

Keiser, J., Utzinger, J., 2008. Efficacy of current drugs against soil-transmitted helminth infections: systematic review and meta-analysis. Jama. 299, 1937–1948.

Kelley, S.P., Dunlop, J.I., Kirkness, E.F., Lambert, J.J., Peters, J.A., 2003. A cytoplasmic region determines single-channel conductance in 5-HT_3 receptors. Nature. 424, 321–324.

Keramidas, A., Moorhouse, A.J., French, C.R., Schofield, P.R., Barry, P.H., 2000. M2 pore mutations convert the glycine receptor channel from being anion-to cation-selective. Biophys. J. 79, 247–259.

Keramidas, A., Moorhouse, A.J., Pierce, K.D., Schofield, P.R., Barry, P.H., 2002. Cation-selective mutations in the M2 domain of the inhibitory glycine receptor channel reveal determinants of

ion-charge selectivity. J. Gen. Physiol. 119, 393–410.

Kilby, K., Mathias, H., Boisvenue, L., Heisler, C., Jones, J.L., 2019. Micronutrient absorption and related outcomes in people with inflammatory bowel disease: A review. Nutrients. 11, 1388.

Kilpatrick, M.E., Trabolsi, B., Farid, Z., 1981. Levamisole compared to mebendazole in the treatment of *Ancylostoma duodenale* in Egypt. Trans. R. Soc. Trop. Med. Hyg. 75, 578–579.

Kim, W., Underwood, R.S., Greenwald, I., Shaye, D.D., 2018. OrthoList 2: a new comparative genomic analysis of human and *Caenorhabditis elegans* genes. Genetics 210, 445–461.

Kläger, S., Whitworth, J.A., Post, R.J., Chavasse, D.C., Downham, M.D., 1993. How long do the effects of ivermectin on adult *Onchocerca volvulus* persist? Trop. Med. Parasitol. Off. organ Dtsch. Tropenmedizinische Gesellschaft Dtsch. Gesellschaft fur Tech. Zusammenarbeit 44, 305–310.

Kletke, O., Sergeeva, O.A., Lorenz, P., Oberland, S., Meier, J.C., Hatt, H., Gisselmann, G., 2013. New insights in endogenous modulation of ligand-gated ion channels: histamine is an inverse agonist at strychnine sensitive glycine receptors. Eur. J. Pharmacol. 710, 59–66.

Kopp, S.R., Coleman, G.T., McCarthy, J.S., Kotze, A.C., 2008. Phenotypic characterization of two *Ancylostoma caninum* isolates with different susceptibilities to the anthelmintic pyrantel. Antimicrob. Agents Chemother. 52, 3980–3986.

Kopp, S.R., Kotze, A.C., McCarthy, J.S., Coleman, G.T., 2007. High-level pyrantel resistance in the hookworm *Ancylostoma caninum*. Vet. Parasitol. 143, 299–304.

Kotze, A.C., Clifford, S., O'grady, J., Behnke, J.M., McCarthy, J.S., 2004. An *in vitro* larval motility assay to determine anthelmintic sensitivity for human hookworm and *Strongyloides*

species. Am. J. Trop. Med. Hyg. 71, 608–616.

Kozuska, J.L., Paulsen, I.M., 2012. The Cys-loop pentameric ligand-gated ion channel receptors: 50 years on. Can. J. Physiol. Pharmacol. 90, 771–782.

Kracun, S., Harkness, P.C., Gibb, A.J., Millar, N.S., 2008. Influence of the M3–M4 intracellular domain upon nicotinic acetylcholine receptor assembly, targeting and function. Br. J. Pharmacol. 153, 1474–1484.

Krepel, H.P., Haring, T., Baeta, S., Polderman, A.M., 1993. Treatment of mixed *Oesophagostomum* and hookworm infection: effect of albendazole, pyrantel pamoate, levamisole and thiabendazole. Trans. R. Soc. Trop. Med. Hyg. 87, 87–89.

Krishna, D.R., Klotz, U., 1993. Determination of ivermectin in human plasma by high-performance liquid chromatography. Arzneimittelforschung. 43, 609–611.

Kubalek, E., Ralston, S., Lindstrom, J., Unwin, N., 1987. Location of subunits within the acetylcholine receptor by electron image analysis of tubular crystals from *Torpedo marmorata*. J. Cell Biol. 105, 9–18.

Kulke, D., Krücken, J., Welz, C., von Samson-Himmelstjerna, G., Harder, A., 2012. *In vivo* efficacy of the anthelmintic tribendimidine against the cestode *Hymenolepis microstoma* in a controlled laboratory trial. Acta Trop. 123, 78–84.

Labiano-Abello, N., Canese, J., Velazquez, M.E., Hawdon, J.M., Wilson, M.L., Hotez, P.J., 1999. Epidemiology of hookworm infection in Itagua, Paraguay: a cross sectional study. Mem. Inst. Oswaldo Cruz. 94, 583–586.

Lacey, E., 1988. The role of the cytoskeletal protein, tubulin, in the mode of action and mechanism

of drug resistance to benzimidazoles. Int. J. Parasitol. 18, 885–936.

Laing, R., Kikuchi, T., Martinelli, A., Tsai, I.J., Beech, R.N., Redman, E., Holroyd, N., Bartley, D.J., Beasley, H., Britton, C., Curran, D., Devaney, E., Gilabert, A., Hunt, M., Jackson, F., Johnston, S.L., Kryukov, I., Li, K., Morrison, A.A., Reid, A.J., Sargison, N., Saunders, G.I., Wasmuth, J.D., Wolstenholme, A., Berriman, M., Gilleard, J.S., Cotton, J.A., 2013. The genome and transcriptome of *Haemonchus contortus*, a key model parasite for drug and vaccine discovery. Genome Biol. 14, R88.

Langosch, D., Thomas, L., Betz, H., 1988. Conserved quaternary structure of ligand-gated ion channels: the postsynaptic glycine receptor is a pentamer. Proc. Natl. Acad. Sci. 85, 7394–7398.

Laughton, D.L., Lunt, G.G., Wolstenholme, A.J., 1997. Reporter gene constructs suggest that the *Caenorhabditis elegans* avermectin receptor β-subunit is expressed solely in the pharynx. J. Exp. Biol. 200, 1509–1514.

Lea, T.J., Usherwood, P.N.R., 1973a. Effect of ibotenic acid on chloride permeability of insect muscle-fibres. Comp. Gen. Pharmacol. 4, 351–363.

Lea, T.J., Usherwood, P.N.R., 1973b. The site of action of ibotenic acid and the identification of two populations of glutamate receptors on insect muscle-fibres. Comp. Gen. Pharmacol. 4, 333–350.

Leathwick, D.M., Miller, C.M., Sauermann, C.W., Candy, P.M., Ganesh, S., Fraser, K., Waghorn, T.S., 2016. The efficacy and plasma profiles of abamectin plus levamisole combination anthelmintics administered as oral and pour-on formulations to cattle. Vet. Parasitol. 227, 85–92.

Lee, A.Y.Y., Vlasuk, G.P., 2003. Recombinant nematode anticoagulant protein c2 and other inhibitors targeting blood coagulation factor VIIa/tissue factor. J. Intern. Med. 254, 313–321.

Lee, B.Y., Bacon, K.M., Bailey, R., Wiringa, A.E., Smith, K.J., 2011. The potential economic value of a hookworm vaccine. Vaccine. 29, 1201–1210.

Lewis, J.A., Wu, C.-H., Berg, H., Levine, J.H., 1980. The genetics of levamisole resistance in the nematode *Caenorhabditis elegans*. Genetics. 95, 905–928.

Li, B.W., Rush, A.C., Weil, G.J., 2014. High level expression of a glutamate-gated chloride channel gene in reproductive tissues of *Brugia malayi* may explain the sterilizing effect of ivermectin on filarial worms. Int. J. Parasitol. Drugs Drug Resist. 4, 71–76.

Li, S.X., Huang, S., Bren, N., Noridomi, K., Dellisanti, C.D., Sine, S.M., Chen, L., 2011. Ligand-binding domain of an α 7-nicotinic receptor chimera and its complex with agonist. Nat. Neurosci. 14, 1253-1259.

Li, Y., Bergeron, J.J., Luo, L., Ou, W.J., Thomas, D.Y., Kang, C.Y., 1996. Effects of inefficient cleavage of the signal sequence of HIV-1 gp 120 on its association with calnexin, folding, and intracellular transport. Proc. Natl. Acad. Sci. 93, 9606–9611.

Lifschitz, A., Lanusse, C., Alvarez, L., 2017. Host pharmacokinetics and drug accumulation of anthelmintics within target helminth parasites of ruminants. N. Z. Vet. J. 65, 176–184.

Lifschitz, A., Virkel, G., Sallovitz, J., Sutra, J.F., Galtier, P., Alvinerie, M., Lanusse, C., 2000. Comparative distribution of ivermectin and doramectin to parasite location tissues in cattle. Vet. Parasitol. 87, 327–338.

Limapichat, W., Lester, H.A., Dougherty, D.A., 2010. Chemical scale studies of the Phe-Pro

conserved motif in the cys loop of Cys loop receptors. J. Biol. Chem. 285, 8976–8984.

Link, C.D., 1995. Expression of human beta-amyloid peptide in transgenic *Caenorhabditis elegans*. Proc. Natl. Acad. Sci. 92, 9368–9372.

Link, C.D., Taft, A., Kapulkin, V., Duke, K., Kim, S., Fei, Q., Wood, D.E., Sahagan, B.G., 2003. Gene expression analysis in a transgenic *Caenorhabditis elegans* Alzheimer's disease model. Neurobiol. Aging 24, 397–413.

Lionel, N.D.W., Mirando, E.H., Nanayakkara, J.C., Soysa, P.E., 1969. Levamisole in the treatment of ascariasis in children. Br Med J 4, 340–341.

Liu, K.S., Sternberg, P.W., 1995. Sensory regulation of male mating behavior in *Caenorhabditis elegans*. Neuron. 14, 79–89.

Lloberas, M., Alvarez, L., Entrocasso, C., Virkel, G., Ballent, M., Mate, L., Lanusse, C., Lifschitz, A., 2013. Comparative tissue pharmacokinetics and efficacy of moxidectin, abamectin and ivermectin in lambs infected with resistant nematodes: Impact of drug treatments on parasite P-glycoprotein expression. Int. J. Parasitol. Drugs Drug Resist. 3, 20–27.

Lloberas, M., Alvarez, L., Entrocasso, C., Virkel, G., Lanusse, C., Lifschitz, A., 2012. Measurement of ivermectin concentrations in target worms and host gastrointestinal tissues: influence of the route of administration on the activity against resistant *Haemonchus contortus* in lambs. Exp. Parasitol. 131, 304–309.

Loukas, A., Prociv, P., 2001. Immune responses in hookworm infections. Clin. Microbiol. Rev. 14, 689–703.

Lummis, S.C.R., Beene, D.L., Lee, L.W., Lester, H.A., Broadhurst, R.W., Dougherty, D.A., 2005.

Cis–trans isomerization at a proline opens the pore of a neurotransmitter-gated ion channel. Nature. 438, 248–252.

Lynagh, T., Beech, R.N., Lalande, M.J., Keller, K., Cromer, B.A., Wolstenholme, A.J., Laube, B., 2015. Molecular basis for convergent evolution of glutamate recognition by pentameric ligand-gated ion channels. Sci. Rep. 5, 8558.

Lynagh, T., Cromer, B.A., Dufour, V., Laube, B., 2014. Comparative pharmacology of flatworm and roundworm glutamate-gated chloride channels: Implications for potential anthelmintics. Int. J. Parasitol. Drugs Drug Resist. 4, 244–255.

Lynagh, T., Webb, T.I., Dixon, C.L., Cromers, B.A., Lynch, J.W., 2011. Molecular determinants of ivermectin sensitivity at the glycine receptor chloride channel. J. Biol. Chem. 286, 43913–43924.

Mackenzie, C.D., Geary, T.G., Gerlach, J.A., 2003. Possible pathogenic pathways in the adverse clinical events seen following ivermectin administration to onchocerciasis patients. Filaria J. 2, S5.

Madden, D.R., 2002. The structure and function of glutamate receptor ion channels. Nat. Rev. Neurosci. 3, 91–101.

Martin, R.J., Buxton, S.K., Neveu, C., Charvet, C.L., Robertson, A.P., 2012. Emodepside and SL0-1 potassium channels: a review. Exp. Parasitol. 132, 40–46.

Martin, R.J., Clark, C.L., Trailovic, S.M., Robertson, A.P., 2004. Oxantel is an N-type (methyridine and nicotine) agonist not an L-type (levamisole and pyrantel) agonist: classification of cholinergic anthelmintics in *Ascaris*. Int. J. Parasitol. 34, 1083–1090.

Martin, R.J., Robertson, A.P., 2007. Mode of action of levamisole and pyrantel, anthelmintic resistance, E153 and Q57. Parasitology. 134, 1093–1104.

Martin, R.J., Valkanov, M.A., Dale, V.M.E., Robertson, A.P., Murray, I., 1996. Electrophysiology of *Ascaris* muscle and anti-nematodal drug action. Parasitology 113, S137–S156.

Martin, R.J., Verma, S., Levandoski, M., Clark, C.L., Qian, H., Stewart, M., Robertson, A.P., 2005. Drug resistance and neurotransmitter receptors of nematodes: recent studies on the mode of action of levamisole. Parasitology. 131, S71–S84.

Martínez-Valladares, M., Geldhof, P., Jonsson, N., Rojo-Vázquez, F.A., Skuce, P., 2012. *Teladorsagia circumcincta*: Molecular characterisation of the avr-14B subunit and its relatively minor role in ivermectin resistance. Int. J. Parasitol. Drugs Drug Resist. 2, 154–161.

Maté, L., Ballent, M., Cantón, C., Ceballos, L., Lifschitz, A., Lanusse, C., Alvarez, L., Liron, J.P., 2018. Assessment of P-glycoprotein gene expression in adult stage of *Haemonchus contortus in vivo* exposed to ivermectin. Vet. Parasitol. 264, 1–7.

Maxwell, C., Hussain, R., Nutman, T.B., Poindexter, R.W., Little, M.D., Schad, G.A., Ottesen, E.A., 1987. The clinical and immunologic responses of normal human volunteers to low dose hookworm (*Necator americanus*) infection. Am. J. Trop. Med. Hyg. 37, 126–134.

McCall, J.W., Guerrero, J., Roberts, R.E., Supakorndej, N., Mansour, A.E., Dzimianski, M.T., McCall, S.D., 2001. Further evidence of clinical prophylactic, retro-active (reach-back) and adulticidal activity of monthly administrations of ivermectin (Heartgard Plus™) in dogs experimentally infected with heartworms. Symposium. 1, 189-200.

McCrindle, C.M.E., Hay, I.T., Odendaal, J.S.J., Calitz, E.M., 1996. A primary health care approach to an outbreak of cutaneous larva migrans. J. S. Afr. Vet. Assoc. 67, 133–136.

McDiarmid, T.A., Au, V., Loewen, A.D., Liang, J., Mizumoto, K., Moerman, D.G., Rankin, C.H., 2018. CRISPR-Cas9 human gene replacement and phenomic characterization in *Caenorhabditis elegans* to understand the functional conservation of human genes and decipher variants of uncertain significance. Dis. Model. Mech. 11, dmm036517.

McFarland, J.W., 1982. Pyrantel, morantel and oxantel, in: Brinda, J.S., Lednicer, D. (Eds.), Chronicles of Drug Discovery. Wiley Interscience, New York. pp. 87.

McKay, J.P., Raizen, D.M., Gottschalk, A., Schafer, W.R., Avery, L., 2004. *eat-2* and *eat-18* are required for nicotinic neurotransmission in the *Caenorhabditis elegans* pharynx. Genetics. 166, 161–169.

McKellar, Q.A., Scott, E.W., 1990. The benzimidazole anthelmintic agents-a review. J. Vet. Pharmacol. Ther. 13, 223–247.

McKinnon, N.K., Bali, M., Akabas, M.H., 2012. Length and amino acid sequence of peptides substituted for the 5-HT3A receptor M3M4 loop may affect channel expression and desensitization. PLoS One. 7, e35563.

McMahon, J.E., 1979. Preliminary screening of antifilarial activity of levamisole and amodiaquine on *Wuchereria bancrofti*. Ann. Trop. Med. Parasitol. 73, 465–472.

Mealey, K.L., 2013. Ivermectin, in: Peterson, M.E., Talcott, P.A. (Eds.), Small Animal Toxicology. W.B. Saunders, St-Louis, Missouri. pp. 601–607.

Mealey, K.L., Bentjen, S.A., Gay, J.M., Cantor, G.H., 2001. Ivermectin sensitivity in collies is

associated with a deletion mutation of the *mdr1* gene. Pharmacogenet. Genomics 11, 727–733.

Mehlhorn, E., 2016. Worms of humans, in: Human Parasites: Diagnosis, Treatment, Prevention. Springer International Publishing AG, Switzerland, p. 218.

Meldal, B.H.M., Debenham, N.J., De Ley, P., De Ley, I.T., Vanfleteren, J.R., Vierstraete, A.R., Bert, W., Borgonie, G., Moens, T., Tyler, P.A., 2007. An improved molecular phylogeny of the Nematoda with special emphasis on marine taxa. Mol. Phylogenet. Evol. 42, 622–636.

Ménez, C., Alberich, M., Kansoh, D., Blanchard, A., Lespine, A., 2016. Acquired tolerance to ivermectin and moxidectin after drug selection pressure in the nematode *Caenorhabditis elegans*. Antimicrob. Agents Chemother. 60, 4809–4819.

Ménez, C., Sutra, J.F., Prichard, R., Lespine, A., 2012. Relative neurotoxicity of ivermectin and moxidectin in Mdr1ab (-/-) mice and effects on mammalian GABA(A) channel activity. PLoS Negl. Trop. Dis. 6, e1883.

Michael, B., Meinke, P.T., Shoop, W., 2001. Comparison of ivermectin, doramectin, selamectin, and eleven intermediates in a nematode larval development assay. J. Parasitol. 87, 692–696.

Millar, N.S., Gotti, C., 2009. Diversity of vertebrate nicotinic acetylcholine receptors. Neuropharmacology. 56, 237–246.

Miller, M.J., 1980. Use of levamisole in parasitic infections. Drugs. 20, 122–130.

Mitreva, M., Blaxter, M.L., Bird, D.M., McCarter, J.P., 2005. Comparative genomics of nematodes. TRENDS in Genetics. 21, 573-581.

Miyazawa, A., Fujiyoshi, Y., Unwin, N., 2003. Structure and gating mechanism of the

acetylcholine receptor pore. Nature. 423, 949–955.

Mongan, N.P., Jones, A.K., Smith, G.R., Sansom, M.S.P., Sattelle, D.B., 2002. Novel α7-like nicotinic acetylcholine receptor subunits in the nematode *Caenorhabditis elegans*. Protein Sci. 11, 1162–1171.

Montresor, A., Crompton, D.W.T., Gyorkos, T.W., Savioli, L., World Health Organization, 2002. Helminth control in school-age children: a guide for managers of control programmes. World Health Organization, Geneva. https://apps.who.int/iris/handle/10665/42473.

Moreno, Y., Nabhan, J.F., Solomon, J., MacKenzie, C.D., Geary, T.G., 2010. Ivermectin disrupts the function of the excretory- secretory apparatus in microfilariae of *Brugia malayi*. Proc. Natl. Acad. Sci. U. S. A. 107, 20120–20125.

Moser, W., Ali, S.M., Ame, S.M., Speich, B., Puchkov, M., Huwyler, J., Albonico, M., Hattendorf, J., Keiser, J., 2016. Efficacy and safety of oxantel pamoate in school-aged children infected with Trichuris trichiura on Pemba Island, Tanzania: a parallel, randomised, controlled, dose-ranging study. Lancet Infect. Dis. 16, 53-60.

Moser, W., Coulibaly, J.T., Ali, S.M., Ame, S.M., Amour, A.K., Yapi, R.B., Albonico, M., Puchkov, M., Huwyler, J., Hattendorf, J., 2017. Efficacy and safety of tribendimidine, tribendimidine plus ivermectin, tribendimidine plus oxantel pamoate, and albendazole plus oxantel pamoate against hookworm and concomitant soil-transmitted helminth infections in Tanzania and Côte d'Ivoire: a randomised, controlled, single-blinded, non-inferiority trial. Lancet Infect. Dis. 17, 1162–1171.

Mouzakis, J., Somboonwit, C., Lakshmi, S., Rumbak, M., Sinnott, J., Cherpelis, B., Keshishian, J., 2011. Levamisole induced necrosis of the skin and neutropenia following intranasal

cocaine use: a newly recognized syndrome. J. Drugs Dermatology JDD. 10, 1204–1207.

Ndyomugyenyi, R., Kabatereine, N., Olsen, A., Magnussen, P., 2008. Malaria and hookworm infections in relation to haemoglobin and serum ferritin levels in pregnancy in Masindi district, western Uganda. Trans. R. Soc. Trop. Med. Hyg. 102, 130–136.

Neff, M.W., Robertson, K.R., Wong, A.K., Safra, N., Broman, K.W., Slatkin, M., Mealey, K.L., Pedersen, N.C., 2004. Breed distribution and history of canine *mdr1-1Δ*, a pharmacogenetic mutation that marks the emergence of breeds from the collie lineage. Proc. Natl. Acad. Sci. 101, 11725–11730.

Nelson, M.E., Kuryatov, A., Choi, C.H., Zhou, Y., Lindstrom, J., 2003. Alternate stoichiometries of α4β2 nicotinic acetylcholine receptors. Mol. Pharmacol. 63, 332–341.

Neveu, C., Charvet, C.L., Fauvin, A., Cortet, J., Beech, R.N., Cabaret, J., 2010. Genetic diversity of levamisole receptor subunits in parasitic nematode species and abbreviated transcripts associated with resistance. Pharmacogenet. Genomics 20, 414–425.

Nielsen, H., Krogh, A., 1998. Prediction of signal peptides and signal anchors by a hidden Markov model. in Proc Int Conf Intell Syst Mol Biol.Ismb, 6, 122–130.

Njue, A.I., Hayashi, J., Kinne, L., Feng, X., Prichard, R.K., 2004. Mutations in the extracellular domains of glutamate-gated chloride channel α3 and β subunits from ivermectin-resistant *Cooperia oncophora* affect agonist sensitivity. J. Neurochem. 89, 1137–1147.

Njue, A.I., Prichard, R.K., 2004. Genetic variability of glutamate-gated chloride channel genes in ivermectin-susceptible and -resistant strains of *Cooperia oncophora*. Parasitology 129, 741–751.

Nolan, T.J., Lok, J.B., 2012. Macrocyclic lactones in the treatment and control of parasitism in small companion animals. Curr. Pharm. Biotechnol. 13, 1078–1094.

Norhayati, M., Fatmah, M.S., Yusof, S., Edariah, A.B., 2003. Intestinal parasitic infections in man: a review. Med. J. Malaysia 58, 296–305.

O'Connell, E.M., Mitchell, T., Papaiakovou, M., Pilotte, N., Lee, D., Weinberg, M., Sakulrak, P., Tongsukh, D., Oduro-Boateng, G., Harrison, S., 2018. *Ancylostoma ceylanicum* Hookworm in Myanmar Refugees, Thailand, 2012–2015. Emerg. Infect. Dis. 24, 1472.

O'neill, M.J., Murray, T.K., Lakics, V., Visanji, N.P., Duty, S., 2002. The role of neuronal nicotinic acetylcholine receptors in acute and chronic neurodegeneration. Curr. Drug Targets-CNS Neurol. Disord. 1, 399–411.

Ogata, A., Ando, H., Kubo, Y., Hiraga, K., 1984. Teratogenicity of thiabendazole in ICR mice. Food Chem. Toxicol. 22, 509–520.

Okulewicz, A., 2017. The impact of global climate change on the spread of parasitic nematodes. Ann. Parasitol. 63, 15–20.

Õmura, S., Crump, A., 2004. The life and times of ivermectin—a success story. Nat. Rev. Microbiol. 2, 984–989.

Ott, K.H., Kwagh, J.G., Stockton, G.W., Sidorov, V., Kakefuda, G., 1996. Rational molecular design and genetic engineering of herbicide resistant crops by structure modeling and site-directed mutagenesis of acetohydroxyacid synthase. J. Mol. Biol. 263, 359–368.

Ottesen, E.A., Campbell, W., 1994. Ivermectin in human medicine. J. Antimicrob. Chemother. 34, 195–203.

Page, S.W., 2008. Antiparasitic drugs. Small Anim. Clin. Pharmacol. 2, 198–260.

Paiement, J.P., Leger, C., Ribeiro, P., Prichard, R.K., 1999. *Haemonchus contortus*: effects of glutamate, ivermectin, and moxidectin on inulin uptake activity in unselected and ivermectin-selected adults. Exp. Parasitol. 92, 193–198.

Paradiso, K., Brehm, P., 1998. Long-term desensitization of nicotinic acetylcholine receptors is regulated via protein kinase A-mediated phosphorylation. J. Neurosci. 18, 9227–9237.

Paul, A.J., Tranquilli, W.J., Hutchens, D.E., 2000. Safety of moxidectin in avermectin-sensitive collies. Am. J. Vet. Res. 61, 482–483.

Pemberton, D.J., Franks, C.J., Walker, R.J., Holden-Dye, L., 2001. Characterization of glutamate-gated chloride channels in the pharynx of wild-type and mutant *Caenorhabditis elegans* delineates the role of the subunit GluCl-α2 in the function of the native receptor. Mol. Pharmacol. 59, 1037–1043.

Pettersen, E.F., Goddard, T.D., Huang, C.C., Couch, G.S., Greenblatt, D.M., Meng, E.C., Ferrin, T.E., 2004. UCSF Chimera—a visualization system for exploratory research and analysis. J. Comput. Chem. 25, 1605–1612.

Pirri, J.K., McPherson, A.D., Donnelly, J.L., Francis, M.M., Alkema, M.J., 2009. A tyramine-gated chloride channel coordinates distinct motor programs of a *Caenorhabditis elegans* escape response. Neuron. 62, 526–538.

Porta-de-la-Riva, M., Fontrodona, L., Villanueva, A., Cerón, J., 2012. Basic *Caenorhabditis elegans* methods: synchronization and observation. JoVE Journal Vis. Exp. e4019.

Portillo, V., Jagannathan, S., Wolstenholme, A.J., 2003. Distribution of glutamate-gated chloride

channel subunits in the parasitic nematode *Haemonchus contortus*. J. Comp. Neurol. 462, 213–222.

Posadas, I., López-Hernández, B., Ceña, V., 2013. Nicotinic receptors in neurodegeneration. Curr. Neuropharmacol. 11, 298–314.

Prichard, R., Ménez, C., Lespine, A., 2012. Moxidectin and the avermectins: consanguinity but not identity. Int. J. Parasitol. Drugs Drug Resist. 2, 134–153.

Prichard, R.K., Geary, T.G., 2019. Perspectives on the utility of moxidectin for the control of parasitic nematodes in the face of developing anthelmintic resistance. Int. J. Parasitol. Drugs Drug Resist. 10, 69–83.

Pritchett, D.B., Luddens, H., Seeburg, P.H., 1989. Type I and type II GABAA-benzodiazepine receptors produced in transfected cells. Science. 245, 1389–1392.

Prociv, P., 1998. Zoonotic hookworm infections (Ancylostomosis), in: Palmer, S.R., Soulsby, E.J.L., Simpson, D.I.H. (Ed.), Zoonoses (1st Edn). Oxford Medical Publications, Oxford, U.K. pp. 803–822.

Prociv, P., Croese, J., 1996. Human enteric infection with *Ancylostoma caninum*: hookworms reappraised in the light of a "new" zoonosis. Acta Trop. 62, 23–44.

Putrenko, I., Zakikhani, M., Dent, J.A., 2005. A family of acetylcholine-gated chloride channel subunits in *Caenorhabditis elegans*. J. Biol. Chem. 280, 6392–6398.

Qian, H., Martin, R.J., Robertson, A.P., 2006. Pharmacology of N-, L-, and B-subtypes of nematode nAChR resolved at the single-channel level in *Ascaris suum*. FASEB J. 20, 2606–2608.

Rajasekariah, G.R., Dhage, K.R., Deb, B.N., Bose, S., 1985. *Necator americanus* and *Ancylostoma ceylanicum*: development of protocols for dual infection in hamsters. Acta Trop. 42, 45–54.

Rao, V.T.S., Siddiqui, S.Z., Prichard, R.K., Forrester, S.G., 2009. A dopamine-gated ion channel (HcGGR3*) from *Haemonchus contortus* is expressed in the cervical papillae and is associated with macrocyclic lactone resistance. Mol. Biochem. Parasitol. 166, 54–61.

Rayes, D., De Rosa, M.J., Bartos, M., Bouzat, C., 2004. Molecular basis of the differential sensitivity of nematode and mammalian muscle to the anthelmintic agent levamisole. J. Biol. Chem. 279, 36372–36381.

Raymond, V., Mongan, N.P., Sattelle, D.B., 2000. Anthelmintic actions on homomer-forming nicotinic acetylcholine receptor subunits: Chicken α7 and ACR-16 from the nematode *Caenorhabditis elegans*. Neuroscience 101, 785–791.

Raza, A., Kopp, S.R., Bagnall, N.H., Jabbar, A., Kotze, A.C., 2016. Effects of *in vitro* exposure to ivermectin and levamisole on the expression patterns of ABC transporters in *Haemonchus contortus* larvae. Int. J. Parasitol. Drugs Drug Resist. 6, 103–115.

Reboul, J., Vaglio, P., Tzellas, N., Thierry-Mieg, N., Moore, T., Jackson, C., Shin-i, T., Kohara, Y., Thierry-Mieg, D., Thierry-Mieg, J., 2001. Open-reading-frame sequence tags (OSTs) support the existence of at least 17,300 genes in *C. elegans*. Nat. Genet. 27, 332–336.

Redman, E., Grillo, V., Saunders, G., Packard, E., Jackson, F., Berriman, M., Gilleard, J.S., 2008. Genetics of mating and sex determination in the parasitic nematode *Haemonchus contortus*. Genetics. 180, 1877–1887.

Redman, E., Sargison, N., Whitelaw, F., Jackson, F., Morrison, A., Bartley, D.J., Gilleard, J.S.,

2012. Introgression of ivermectin resistance genes into a susceptible *Haemonchus contortus* strain by multiple backcrossing. PLoS Pathog 8, e1002534.

Reichert, F., Pilger, D., Schuster, A., Lesshafft, H., de Oliveira, S.G., Ignatius, R., Feldmeier, H., 2018. Epidemiology and morbidity of hookworm-related cutaneous larva migrans (HrCLM): Results of a cohort study over a period of six months in a resource-poor community in Manaus, Brazil. PLoS Negl. Trop. Dis. 12, e0006662.

Ren, H.N., Yang, Y.Q., Cheng, B.Z., Guo, H.F., Yang, H.Z., Zhuang, Z.N., Zhang, C.W., Lu, X.Y., 1988. Toxicity of tribendimidin, a new anti-hookworm drug. Zhongguo ji sheng chong xue yu ji sheng chong bing za zhi= Chinese J. Parasitol. Parasit. Dis. 6, 199.

Reynoldson, J.A., Behnke, J.M., Pallant, L.J., Macnish, M.G., Gilbert, F., Giles, S., Spargo, R.J., Thompson, R.C.A., 1997. Failure of pyrantel in treatment of human hookworm infections (*Ancylostoma duodenale*) in the Kimberley region of north west Australia. Acta Trop. 68, 301–312.

Richard-Lenoble, D., Chandenier, J., Gaxotte, P., 2003. Ivermectin and filariasis. Fundam. Clin. Pharmacol. 17, 199–203.

Richards, J.C., Behnke, J.M., Duce, I.R., 1995. *In vitro* studies on the relative sensitivity to ivermectin of *Necator americanus* and *Ancylostoma ceylanicum*. Int. J. Parasitol. 25, 1185–1191.

Rienzo, M., Rocchi, A.R., Threatt, S.D., Dougherty, D.A., Lummis, S.C.R., 2016. Perturbation of critical prolines in *Gloeobacter violaceus* ligand-gated ion channel (GLIC) supports conserved gating motions among Cys-loop receptors. J. Biol. Chem. 291, 6272–6280.

Rim, H.J., Won, C.Y., Lee, S.I., Lim, J.K., 1975. Anthelmintic effect of oxantel pamoate and pyrantel pamoate suspension against intestinal nematode infestations. Korean J. Parasitol. 13, 97–101.

Roach, N.P., Sadowski, N., Alessi, A.F., Timp, W., Taylor, J., Kim, J.K., 2020. The full-length transcriptome of *C. elegans* using direct RNA sequencing. Genome Res. 30, 299–312.

Robertson, A.P., Clark, C.L., Burns, T.A., Thompson, D.P., Geary, T.G., Trailovic, S.M., Martin, R.J., 2002. Paraherquamide and 2-deoxy-paraherquamide distinguish cholinergic receptor subtypes in *Ascaris muscle*. J. Pharmacol. Exp. Ther. 302, 853–860.

Robertson, A.P., Puttachary, S., Buxton, S.K., Martin, R.J., 2015. Tribendimidine: mode of action and nAChR subtype selectivity in *Ascaris* and *Oesophagostomum*. PLoS Negl. Trop. Dis. 9.

Rosenmund, C., Stern-Bach, Y., Stevens, C.F., 1998. The tetrameric structure of a glutamate receptor channel. Science. 280, 1596–1599.

Rozen, S., Skaletsky, H., 2000. Primer3 on the WWW for general users and for biologist programmers, in: Krawetz, S., Misener, S. (Eds.) Bioinformatics Methods and Protocols: Methods in Molecular Biology. Humana Press, Totowa, New Jersey. pp. 365–386.

Rufener, L., Baur, R., Kaminsky, R., Mäser, P., Sigel, E., 2010. Monepantel allosterically activates DEG-3/DES-2 channels of the gastrointestinal nematode *Haemonchus contortus*. Mol. Pharmacol. 78, 895–902.

Rufener, L., Bedoni, N., Baur, R., Rey, S., Glauser, D.A., Bouvier, J., Beech, R., Sigel, E., Puoti, A., 2013. *acr-23* Encodes a monepantel-sensitive channel in *Caenorhabditis elegans*. PLoS Pathog. 9, e1003524.

Sakti, H., Nokes, C., Subagio Hertanto, W., Hendratno, S., Hall, A., Bundy, D.A.P., 1999. Evidence for an association between hookworm infection and cognitive function in Indonesian school children. Trop. Med. Int. Heal. 4, 322–334.

Šali, A., Blundell, T.L., 1993. Comparative protein modelling by satisfaction of spatial restraints. J. Mol. Biol. 234, 779–815.

Sanders, J.W., Goraleski, K.A., 2017. The hookworm blues: we still got 'em. Am. J. Trop. Med. Hyg. 97, 1277.

Sandground, J.H., 1939. Creeping eruption in the Netherland East Indies caused by the invasion of the larva of *Ancylostoma braziliense*. Geneeskd. Tijdschr. voor Ned. 79, 805–810.

Sangster, N.C., Bannan, S.C., Weiss, A.S., Nulf, S.C., Klein, R.D., Geary, T.G., 1999. *Haemonchus contortus*: sequence heterogeneity of internucleotide binding domains from p-glycoproteinsand an association with avermectin/milbemycin resistance. Exp. Parasitol. 91, 250–257.

Sasaki, T., Takagi, M., Yaguchi, T., Miyadoh, S., Okada, T., Koyama, M., 1992. A new anthelmintic cyclodepsipeptide, PF1022A. J. Antibiot. (Tokyo). 45, 692–697.

Scanlan, L.D., Lund, S.P., Coskun, S.H., Hanna, S.K., Johnson, M.E., Sims, C.M., Brignoni, K., Lapasset, P., Petersen, E.J., Elliott, J.T., Nelson, B.C., 2018. Counting *Caenorhabditis elegans*: protocol optimization and applications for population growth and toxicity studies in liquid medium. Sci. Rep. 8, 1–12.

Schimmel, A., Altreuther, G., Schroeder, I., Charles, S., Cruthers, L., Kok, D.J., Kraemer, F., Krieger, K.J., 2009. Efficacy of emodepside plus praziquantel tablets (Profender® tablets for

dogs) against mature and immature adult *Trichuris vulpis* infections in dogs. Parasitol. Res. 105, 17–22.

Schinkel, A. H., Smit, J. J., van Tellingen, O., Beijnen, J. H., Wagenaar, E., van Deemter, L., Mol, C. A., van der Valk, M. A., Robanus-Maandag, E. C., & te Riele, H. P., 1994. Disruption of the mouse *mdr1a* P-glycoprotein gene leads to a deficiency in the blood-brain barrier and to increased sensitivity to drugs. Cell. 77, 491–502.

Schuster, C.M., Ultsch, A., Schloss, P., Cox, J.A., Schmitt, B., Betz, H., 1991. Molecular cloning of an invertebrate glutamate receptor subunit expressed in *Drosophila* muscle. Science. 254, 112–114.

Schwarz, E.M., Hu, Y., Antoshechkin, I., Miller, M.M., Sternberg, P.W., Aroian, R. V, 2015. The genome and transcriptome of the zoonotic hookworm *Ancylostoma ceylanicum* identify infection-specific gene families. Nat. Genet. 47, 416.

Seguel, M., Gottdenker, N., 2017. The diversity and impact of hookworm infections in wildlife. Int. J. Parasitol. Parasites Wildl. 6, 177–194.

Shan, Q., Haddrill, J.L., Lynch, J.W., 2001. Ivermectin, an unconventional agonist of the glycine receptor chloride channel. J. Biol. Chem. 276, 12556–12564.

Shaye, D.D., Greenwald, I., 2011. OrthoList: a compendium of *C. elegans* genes with human orthologs. PLoS One. 6, e20085.

Sheriff, J.C., Kotze, A.C., Sangster, N.C., Hennessy, D.R., 2005. Effect of ivermectin on feeding by *Haemonchus contortus in vivo*. Vet. Parasitol. 128, 341–346.

Shoop, W.L., Eary, C.H., Michael, B.F., Haines, H.W., Seward, R.L., 1991. Anthelmintic activity

of paraherquamide in dogs. Vet. Parasitol. 40, 339–341.

Shoop, W.L., Mrozik, H., Fisher, M.H., 1995. Structure and activity of avermectins and milbemycins in animal health. Vet. Parasitol. 59, 139–156.

Simonis, N., Rual, J.-F., Carvunis, A.-R., Tasan, M., Lemmens, I., Hirozane-Kishikawa, T., Hao, T., Sahalie, J.M., Venkatesan, K., Gebreab, F., 2009. Empirically controlled mapping of the *Caenorhabditis elegans* protein-protein interactome network. Nat. Methods 6, 47–54.

Söderpalm, B., Lidö, H.H., Ericson, M., 2017. The glycine receptor—a functionally important primary brain target of ethanol. Alcohol. Clin. Exp. Res. 41, 1816–1830.

Somvanshi, V.S., Ellis, B.L., Hu, Y., Aroian, R. V, 2014. Nitazoxanide: nematicidal mode of action and drug combination studies. Mol. Biochem. Parasitol. 193, 1–8.

Soper, F.L., 1927. The relative egg-laying function of *Necator americanus* and *Ancylostoma duodenale*. Am. J. Epidemiol. 7, 542-560.

Soukhathammavong, P.A., Sayasone, S., Phongluxa, K., Xayaseng, V., Utzinger, J., Vounatsou, P., Hatz, C., Akkhavong, K., Keiser, J., Odermatt, P., 2012. Low efficacy of single-dose albendazole and mebendazole against hookworm and effect on concomitant helminth infection in Lao PDR. PLoS Negl. Trop. Dis. 6, e1417.

Sow, D., Soro, F., Javelle, E., Simon, F., Parola, P., Gautret, P., 2017. Epidemiological profile of cutaneous larva migrans in travelers returning to France between 2003 and 2015. Travel Med. Infect. Dis. 20, 61–64.

Speich, B., Ame, S.M., Ali, S.M., Alles, R., Huwyler, J., Hattendorf, J., Utzinger, J., Albonico, M., Keiser, J., 2014. Oxantel pamoate–albendazole for *Trichuris trichiura* infection. N. Engl.

J. Med. 370, 610–620.

Speich, B., Moser, W., Ali, S.M., Ame, S.M., Albonico, M., Hattendorf, J., Keiser, J., 2016. Efficacy and reinfection with soil-transmitted helminths 18-weeks post-treatment with albendazole-ivermectin, albendazole-mebendazole, albendazole-oxantel pamoate and mebendazole. Parasit. Vectors 9, 123.

Stefan, M.I., Le Novère, N., 2013. Cooperative binding. PLoS Comput. Biol. 9.

Steinmann, P., Utzinger, J., Du, Z.-W., Jiang, J.-Y., Chen, J.X., Hattendorf, J., Zhou, H., Zhou, X.-N., 2011. Efficacy of single-dose and triple-dose albendazole and mebendazole against soil-transmitted helminths and *Taenia* spp.: a randomized controlled trial. PLoS One 6, e25003.

Sterling, T., Irwin, J.J., 2015. ZINC 15 – Ligand discovery for everyone. J. Chem. Inf. Model. 55, 2324-2337.

Stoll, N.R., 1923. Investigations on the control of hookworm disease. XVIII. On the relation between the number of eggs found in human feces and the number of hookworms in the host. Amer. Jour. Hyg. 3, 156.

Stoltzfus, R.J., Chwaya, H.M., Tielsch, J.M., Schulze, K.J., Albonico, M., Savioli, L., 1997. Epidemiology of iron deficiency anemia in Zanzibari schoolchildren: the importance of hookworms. Am. J. Clin. Nutr. 65, 153–159.

Strange, K., 2006. An overview of *C. elegans* biology. In: *C. elegans*. Methods in molecular biology, vol 351. Humana Press, Totowa, New Jersey. pp. 1–11.

Strote, G., Wieland, S., Darge, K., Comley, J.C., 1990. *In vitro* assessment of the activity of

anthelmintic compounds on adults of *Onchocerca volvulus*. Acta Leiden. 59, 285–296.

Sutherland, I. A., D. L. Lee., 1990. A larval paralysis assay for the detection of thiabendazole resistance in trichostrongyles. Parasitology. 100, 131-135.

Swellengrebel, N.H., 1940. The efficient parasite. Science. 92, 465–469.

Takiguchi, Y., Mishima, H., Okuda, M., Terao, M., Aoki, A., Fukuda, R., 1980. Milbemycins, a new family of macrolide antibiotics: fermentation, isolation and physico-chemical properties. J. Antibiot. (Tokyo). 33, 1120–1127.

Taly, A., Corringer, P.J., Guedin, D., Lestage, P., Changeux, J.P., 2009. Nicotinic receptors: allosteric transitions and therapeutic targets in the nervous system. Nat. Rev. Drug Discov. 8, 733–750.

Tandon, V., Lyndem, L., Yadav, A.K., 1998. Hookworm infection: influence of ambient climatic factors on the development and hatching of eggs and development and survival of infective larvae. Parasitol. Int. 47, 177.

Tang, Y.T., Gao, X., Rosa, B.A., Abubucker, S., Hallsworth-Pepin, K., Martin, J., Tyagi, R., Heizer, E., Zhang, X., Bhonagiri-Palsikar, V., 2014. Genome of the human hookworm *Necator americanus*. Nat. Genet. 46, 261–269.

Tapia, L., Kuryatov, A., Lindstrom, J., 2007. Ca2+ permeability of the (α4) 3 (β2) 2 stoichiometry greatly exceeds that of (α4) 2 (β2) 3 human acetylcholine receptors. Mol. Pharmacol. 71, 769–776.

Tasneem, A., Iyer, L.M., Jakobsson, E., Aravind, L., 2005. Identification of the prokaryotic ligand-gated ion channels and their implications for the mechanisms and origins of animal Cys-loop

ion channels. Genome Biol. 6, R4.

Taylor, H.R., Greene, B.M., 1989. The status of ivermectin in the treatment of human onchocerciasis. Am. J. Trop. Med. Hyg. 41, 460–466.

The *C. elegans* Sequencing Consortium, 1998. Genome sequence of the nematode *C. elegans*: a platform for investigating biology. Science. 282, 2012–2018.

Thomas, H., 1979. The efficacy of amidantel, a new anthelmintic, on hookworms and ascarids in dogs. Tropenmed. Parasitol. 30, 404–408.

Thompson, A.J., Lester, H.A., Lummis, S.C.R., 2010. The structural basis of function in Cys-loop receptors. Q. Rev. Biophys. 43, 449–499.

Thompson, A.J., Lummis, S.C.R., 2003. A single ring of charged amino acids at one end of the pore can control ion selectivity in the 5-HT_3 receptor. Br. J. Pharmacol. 140, 359–365.

Thompson, O., Edgley, M., Strasbourger, P., Flibotte, S., Ewing, B., Adair, R., Au, V., Chaudhry, I., Fernando, L., Hutter, H., 2013. The million mutation project: a new approach to genetics in *Caenorhabditis elegans*. Genome Res. 23, 1749–1762.

Tikhonov, D.B., Magazanik, L.G., 2009. Origin and molecular evolution of ionotropic glutamate receptors. Neurosci. Behav. Physiol. 39, 763–773.

Tompkins, J.B., Stitt, L.E., Ardelli, B.F., 2010. *Brugia malayi*: *in vitro* effects of ivermectin and moxidectin on adults and microfilariae. Exp. Parasitol. 124, 394–402.

Ton, T.G.N., Mackenzie, C., Molyneux, D.H., 2015. The burden of mental health in lymphatic filariasis. Infect. Dis. poverty 4, 34.

Torres, J., Stevens, T.J., Samsó, M., 2003. Membrane proteins: the 'Wild West'of structural

biology. Trends Biochem. Sci. 28, 137–144.

Touroutine, D., Fox, R.M., Von Stetina, S.E., Burdina, A., Miller, D.M. 3rd, Richmond, J.E., 2005. *acr-16* encodes an essential subunit of the levamisole-resistant nicotinic receptor at the *Caenorhabditis elegans* neuromuscular junction. J. Biol. Chem. 280, 27013–27021.

Traub, R.J., 2013. *Ancylostoma ceylanicum*, a re-emerging but neglected parasitic zoonosis. Int. J. Parasitol. 43, 1009–1015.

Traub, R.J., Inpankaew, T., Sutthikornchai, C., Sukthana, Y., Thompson, R.C.A., 2008. PCR-based coprodiagnostic tools reveal dogs as reservoirs of zoonotic ancylostomiasis caused by *Ancylostoma ceylanicum* in temple communities in Bangkok. Vet. Parasitol. 155, 67–73.

Treinin, M., 2008. RIC-3 and nicotinic acetylcholine receptors: Biogenesis, properties, and diversity. Biotechnol. J. Healthc. Nutr. Technol. 3, 1539–1547.

Tritten, L., Braissant, O., Keiser, J., 2012a. Comparison of novel and existing tools for studying drug sensitivity against the hookworm *Ancylostoma ceylanicum in vitro*. Parasitology 139, 348–357.

Tritten, L., Nwosu, U., Vargas, M., Keiser, J., 2012b. *In vitro* and *in vivo* efficacy of tribendimidine and its metabolites alone and in combination against the hookworms *Heligmosomoides bakeri* and *Ancylostoma ceylanicum*. Acta Trop. 122, 101–107.

Tritten, L., Silbereisen, A., Keiser, J., 2011. *In vitro* and *in vivo* efficacy of monepantel (AAD 1566) against laboratory models of human intestinal nematode infections. PLoS Negl. Trop. Dis. 5, e1457.

Trott, O., Olson, A.J., 2010. AutoDock Vina: improving the speed and accuracy of docking with

a new scoring function, efficient optimization, and multithreading. J. Comput. Chem. 31, 455–461.

Turner, J.D., Tendongfor, N., Esum, M., Johnston, K.L., Langley, R.S., Ford, L., Faragher, B., Specht, S., Mand, S., Hoerauf, A., 2010. Macrofilaricidal activity after doxycycline only treatment of *Onchocerca volvulus* in an area of *Loa loa* co-endemicity: a randomized controlled trial. PLoS Negl. Trop. Dis. 4.

Turner M.J., Schaeffer J.M., 1989. Mode of action of ivermectin. In: Campbell, W.C. (ed) Ivermectin and Abamectin. Springer, New York, NY. pp. 73–88.

Unwin, N., 2005. Refined structure of the nicotinic acetylcholine receptor at 4 Å resolution. J. Mol. Biol. 346, 967–989.

Valera, S., Hussy, N., Evans, R.J., Adami, N., North, R.A., Surprenant, A., Buell, G., 1994. A new class of ligand-gated ion channel defined by P_{2X} receptor for extracellular ATP. Nature. 371, 516–519.

Vallés, A.S., Barrantes, F.J., 2012. Chaperoning α7 neuronal nicotinic acetylcholine receptors. Biochim. Biophys. Acta (BBA)-Biomembranes. 1818, 718–729.

Valley, C.C., Cembran, A., Perlmutter, J.D., Lewis, A.K., Labello, N.P., Gao, J., Sachs, J.N., 2012. The methionine-aromatic motif plays a unique role in stabilizing protein structure. J. Biol. Chem. 287, 34979–34991.

Van den Bossche, H., De Nollin, S., 1973. Effects of mebendazole on the absorption of low molecular weight nutrients by *Ascaris suum*. Int. J. Parasitol. 3, 401–407.

Vassilatis, D.K., Arena, J.P., Plasterk, R.H.A., Wilkinson, H.A., Schaeffer, J.M., Cully, D.F., Van

der Ploeg, L.H.T., 1997. Genetic and biochemical evidence for a novel avermectin-sensitive chloride channel in *Caenorhabditis elegans*. Isolation and characterization. J. Biol. Chem. 272, 33167–33174.

Velázquez-Flores, M. ángel, Salceda, R., 2011. Glycine receptor internalization by protein kinases activation. Synapse 65, 1231–1238.

Verweij, J.J., Brienen, E.A.T., Ziem, J., Yelifari, L., Polderman, A.M., Van Lieshout, L., 2007. Simultaneous detection and quantification of *Ancylostoma duodenale*, *Necator americanus*, and *Oesophagostomum bifurcum* in fecal samples using multiplex real-time PCR. Am. J. Trop. Med. Hyg. 77, 685–690.

Viguera, A.R., Serrano, L., 1995. Side-chain interactions between sulfur-containing amino acids and phenyalanine in alpha-helixes. Biochemistry. 34, 8771–8779.

Von Heijne, G., 1985. Signal sequences: the limits of variation. J. Mol. Biol. 184, 99–105.

Von Reuss, S.H., Bose, N., Srinivasan, J., Yim, J.J., Judkins, J.C., Sternberg, P.W., Schroeder, F.C., 2012. Comparative metabolomics reveals biogenesis of ascarosides, a modular library of small-molecule signals in *C. elegans*. J. Am. Chem. Soc. 134, 1817–1824.

Wagner, C.A., Friedrich, B., Setiawan, I., Lang, F., Bröer, S., 2000. The use of *Xenopus laevis* oocytes for the functional characterization of heterologously expressed membrane proteins. Cell. Physiol. Biochem. 10, 1–12.

Walker, M., Pion, S.D.S., Fang, H., Gardon, J., Kamgno, J., Basáñez, M.-G., Boussinesq, M., 2017. Macrofilaricidal efficacy of repeated doses of ivermectin for the treatment of river blindness. Clin. Infect. Dis. 65, 2026–2034.

Walter, P., Blobel, G., 1980. Purification of a membrane-associated protein complex required for protein translocation across the endoplasmic reticulum. Proc. Natl. Acad. Sci. 77, 7112–7116.

Wang, C., Huang, X.X., Zhang, Y.Q., Yen, Q.Y., Wen, Y., 1989. Efficacy of ivermectin in hookworms as examined in *Ancylostoma caninum* infections. J. Parasitol. 75, 373.

Wang, F., Imoto, K., 1992. Pore size and negative charge as structural determinants of permeability in the *Torpedo nicotinic* acetylcholine receptor channel. Proc. R. Soc. London. Ser. B Biol. Sci. 250, 11–17.

Ward, S., Carrel, J.S., 1979. Fertilization and sperm competition in the nematode *Caenorhabditis elegans*. Dev. Biol. 73, 304–321.

Waterston, R., Martin, C., Craxton, M., Huynh, C., Coulson, A., Hillier, L., Durbin, R., Green, P., Shownkeen, R., Halloran, N., 1992. A survey of expressed genes in *Caenorhabditis elegans*. Nat. Genet. 1, 114–123.

Weaver, H.J., Hawdon, J.M., Hoberg, E.P., 2010. Soil-transmitted helminthiases: implications of climate change and human behavior. Trends Parasitol. 26, 574–581.

Wei, K.-Y., Yan, Q., Tang, B., Yang, S.-M., Zhang, P.-B., Deng, M.-M., Lü, M.-H., 2017. Hookworm infection: a neglected cause of overt obscure gastrointestinal bleeding. Korean J. Parasitol. 55, 391.

Wess, J., 1996. Molecular biology of muscarinic acetylcholine receptors. Crit. Rev. Neurobiol. 10.

White, J.G., Southgate, E., Thomson, J.N., Brenner, S., 1986. The structure of the nervous system of the nematode *Caenorhabditis elegans*. Philos Trans R Soc L. B Biol Sci 314, 1–340.

Whittington, I.D., 1997. Reproduction and host-location among the parasitic Platyhelminthes. Int.

J. Parasitol. 27, 705–714.

Whitworth, J.A.G., Morgan, D., Maude, G.H., McNicholas, A.M., Taylor, D.W., 1991. A field study of the effect of ivermectin on intestinal helminths in man. Trans. R. Soc. Trop. Med. Hyg. 232–234.

Wiebe, V.J., 2015. Fenbendazole, in: Drug therapy for infectious diseases of the dog and cat. John Wiley & Sons Inc. Ames, Iowa. pp. 251.

Williamson, S.M., Robertson, A.P., Brown, L., Williams, T., Woods, D.J., Martin, R.J., Sattelle, D.B., Wolstenholme, A.J., 2009. The nicotinic acetylcholine receptors of the parasitic nematode *Ascaris suum*: formation of two distinct drug targets by varying the relative expression levels of two subunits. PLoS Pathog. 5.

Williamson, S.M., Storey, B., Howell, S., Harper, K.M., Kaplan, R.M., Wolstenholme, A.J., 2011. Candidate anthelmintic resistance-associated gene expression and sequence polymorphisms in a triple-resistant field isolate of *Haemonchus contortus*. Mol. Biochem. Parasitol. 180, 99–105.

Wishart, D.S., Knox, C., Guo, A.C., Shrivastava, S., Hassanali, M., Stothard, P., Chang, Z., Woolsey, J., 2006. DrugBank: a comprehensive resource for in silico drug discovery and exploration. Nucleic Acids Res. 34, D668–D672.

Witting, M., Ruttkies, C., Neumann, S., Schmitt-Kopplin, P., 2017. LipidFrag: Improving reliability of *in silico* fragmentation of lipids and application to the *Caenorhabditis elegans* lipidome. PLoS One 12, e0172311.

Witting, M., Schmitt-Kopplin, P., 2016. The *Caenorhabditis elegans* lipidome: A primer for lipid

analysis in *Caenorhabditis elegans*. Arch. Biochem. Biophys. 589, 27–37.

Wollweber, H., Niemers, E., Flucke, W., Andrews, P., Schulz, H.P., Thomas, H., 1979. Amidantel, a potent anthelminthic from a new chemical class. Arzneimittelforschung. 29, 31–32.

Wolstenholme, A.J., Maclean, M.J., Coates, R., McCoy, C.J., Reaves, B.J., 2016. How do the macrocyclic lactones kill filarial nematode larvae? Invertebr. Neurosci. 16, 7.

Wolstenholme, A.J., Rogers, A.T., 2005. Glutamate-gated chloride channels and the mode of action of the avermectin/milbemycin anthelmintics. Parasitology. 131, S85–S95.

Wood, J.S., 1982. Genetic effects of methyl benzimidazole-2-yl-carbamate on *Saccharomyces cerevisiae*. Mol. Cell. Biol. 2, 1064–1079.

World Health Organization, 2020. 2030 targets for soil-transmitted helminthiases control programmes. World Health Organization. https://apps.who.int/iris/handle/10665/330611.

World Health Organization, 2012. Soil-transmitted helminthiases: Eliminating soil-transmitted helmnthiases as a public health problem in children: Progress report 2001-2010 and strategic plan 2011-2020. https://apps.who.int/iris/handle/10665/44804.

Wotring, V.E., Chang, Y., Weiss, D.S., 1999. Permeability and single channel conductance of human homomeric ρ1 $GABA_C$ receptors. J. Physiol. 521, 327–336.

Wotring, V.E., Weiss, D.S., 2008. Charge scan reveals an extended region at the intracellular end of the GABA receptor pore that can influence ion selectivity. J. Gen. Physiol. 131, 87–97.

Xia, Y., Chu, W., Qi, Q., Xun, L., 2015. New insights into the QuikChangeTM process guide the use of Phusion DNA polymerase for site-directed mutagenesis. Nucleic Acids Res. 43, e12–e12.

Xiao, S.-H., Hui-Ming, W., Tanner, M., Utzinger, J., Chong, W., 2005. Tribendimidine: a promising, safe and broad-spectrum anthelmintic agent from China. Acta Trop. 94, 1–14.

Yadav, G., Ganguly, S., 2015. Structure activity relationship (SAR) study of benzimidazole scaffold for different biological activities: A mini-review. Eur. J. Med. Chem. 97, 419–443.

Yang, J., 1990. Ion permeation through 5-hydroxytryptamine-gated channels in neuroblastoma N18 cells. J. Gen. Physiol. 96, 1177–1198.

Yang, K., Han, X., 2016. Lipidomics: techniques, applications, and outcomes related to biomedical sciences. Trends Biochem. Sci. 41, 954–969.

Yang, Y.Q., Yang, H.Z., Ren, H.N., Cheng, B.Z., 1988. Histological and histochemical effects of tribendimidine on *Necator americanus*. Zhongguo yao li xue bao= Acta Pharmacol. Sin. 9, 264–267.

Yao, X., Song, F., Chen, F., Zhang, Y., Gu, J., Liu, S., Liu, Z., 2008. Amino acids within loops D, E and F of insect nicotinic acetylcholine receptor β subunits influence neonicotinoid selectivity. Insect Biochem. Mol. Biol. 38, 834–840.

Yates, D.M., Portillo, V., Wolstenholme, A.J., 2003. The avermectin receptors of *Haemonchus contortus* and *Caenorhabditis elegans*. Int. J. Parasitol. 33, 1183–1193.

Yates, D.M., Wolstenholme, A.J., 2004. An ivermectin-sensitive glutamate-gated chloride channel subunit from *Dirofilaria immitis*. Int. J. Parasitol. 34, 1075–1081.

Yoshimura, J., Ichikawa, K., Shoura, M.J., Artiles, K.L., Gabdank, I., Wahba, L., Smith, C.L., Edgley, M.L., Rougvie, A.E., Fire, A.Z., 2019. Recompleting the *Caenorhabditis elegans* genome. Genome Res. 29, 1009–1022.

Youssef, M.Y.M., Sadaka, H.A.H., Eissa, M.M., El-Ariny, A.F., 1995. Topical application of ivermectin for human ectoparasites. Am. J. Trop. Med. Hyg. 53, 652–653.

Yu, H., Li, M., Wang, W., Wang, X., 2016. High throughput screening technologies for ion channels. Acta Pharmacol. Sin. 37, 34–43.

Zaman, V., Lal, M., 1973. Treatment of *Wuchereria bancrofti* with levamisole. Trans. R. Soc. Trop. Med. Hyg. 67, 610.

Zheng, F., Robertson, A.P., Abongwa, M., Yu, E.W., Martin, R.J., 2016. The *Ascaris suum* nicotinic receptor, ACR-16, as a drug target: Four novel negative allosteric modulators from virtual screening. Int. J. Parasitol. Drugs Drug Resist. 6, 60–73.

Zimmermann, I., Dutzler, R., 2011. Ligand activation of the prokaryotic pentameric ligand-gated ion channel ELIC. PLoS Biol. 9, e1001101.

Zinser, E.W., Wolf, M.L., Alexander-Bowman, S.J., Thomas, E.M., Davis, J.P., Groppi, V.E., Lee, B.H., Thompson, D.P., Geary, T.G., 2002. Anthelmintic paraherquamides are cholinergic antagonists in gastrointestinal nematodes and mammals. J. Vet. Pharmacol. Ther. 25, 241–250.